ON THE DECARBONIZATION OF CHEMICAL AND ENERGY INDUSTRIES: POWER-TO-X DESIGN STRATEGIES

ANTONIO SÁNCHEZ GARCÍA

A dissertation submitted for the degree of

PhD IN CHEMICAL ENGINEERING

at the

UNIVERSIDAD DE SALAMANCA

VNiVERSiDAD D SALAMANCA

CAMPUS OF INTERNATIONAL EXCELLENCE

Academic advisor: Pastora Isabel Vega Cruz / Mariano Martín Martín

Programa de Doctorado en Ciencia y Tecnología Químicas

Departamento de Ingeniería Química y Textil

Universidad de Salamanca

October 2021

La **Dra. Pastora Isabel Vega Cruz**, Catedrática del Departamento de Informática y Automática de la Universidad de Salamanca y el **Dr. Mariano Martín Martín**, Profesor Titular de Universidad del Departamento de Ingeniería Química y Textil de la Universidad de Salamanca

Informan:

Que la memoria titulada: "On the decarbonization of chemical and energy industries: Power-to-X design strategies" que, para optar al Grado de Doctor en Ingeniería Química con Mención Internacional, presenta **D. Antonio Sánchez García** ha sido realizada bajo nuestra dirección dentro del Programa de Doctorado Ciencia y Tecnología Químicas (RD 99/2011) de la Universidad de Salamanca y que, considerando que constituye un trabajo de tesis.

Autorizan:

Su presentación ante la Escuela de Doctorado de la Universidad de Salamanca, mediante el formato de compendio de publicaciones.

Y para que conste a los efectos oportunos, firmo la presente en Salamanca, a 15 de octubre de 2021.

A mis padres

Nox praecessit dies autem adpropiavit abiciamus
ergo opera tenebrarum et induamur arma luis.
(La noche está avanzada. El día se avecina. Despojémenos pues
de las obras de las tinieblas y revistámonos de las armas de la luz).

— Biblia Vulgata-Latina, Romanos, 13:12.

ACKNOWLEDGMENTS

En primer lugar, a mis directores de tesis la Dra. Pastora Isabel Vega Cruz y el Dr. Mariano Martín Martín por darme la oportunidad de realizar mi tesis doctoral bajo su dirección, por su apoyo y sus consejos que han dirigido la tesis hacía lo que finalmente ha resultado.

A los miembros de mi grupo de investigación con quien he compartido este viaje de tesis, con el riesgo de dejarme a alguien, a Borja, Lidia, Edgar (¡a quien debo el formato de esta tesis!), Manuel y Guillermo. A los visitantes que tanto nos aportan, no solo desde un punto de vista académico, a Juan, Cesar, Salvador, Gabriel, Valentina, Thalles y Javier. Esta tesis se ha enriquecido de sus comentarios y apreciaciones, además de hacer mucho más fácil el arduo camino hasta aquí.

A los alumnos con los que he tenido el placer de colaborar durante este tiempo, y que esta tesis también lleva algo de ellos, a Luismi, Elena y Carlos.

Thanks to Prof. Qi Zhang for giving me the opportunity to visit him at the University of Minnesota and integrate me into his group. Thanks also to Andrew, Rishabh, Hanchu, Wei, and Che for your kind hosting in Minneapolis.

A los que formáis el laboratorio de investigación de la A0 y a todos los miembros del Departamento de Ingeniería Química y Textil, quiere nombrar, de nuevo, al Dr. Mariano Martín y al Dr. Carlos Costa, con los que he compartido más directamente mis tareas docentes en este tiempo. Al personal de la facultad con el que he tratado en estos años, muchas veces hacéis las cosas más fáciles a los que navegamos por las azarosas aguas de un doctorado.

En un ámbito más personal, a María que apareció en medio de este camino, gracias por tanto. A mis padres, esta tesis no hubiera sido posible sin su apoyo continuado durante tantos años.

Salamanca, 15 de Octubre de 2021

ABSTRACT

Nowadays, the concern on the sustainability is leading to an entire new economic system. This new paradigm affects all sectors such as agriculture, industry, financial sector, etc. Two of the most affected are the chemical industry and the energy system due to their current configuration and, these two sectors are particularly studied in this thesis. With regards to the chemical industry, electrochemical production is one of the most attractive methods to produce chemicals in a sustainable way leaving behind traditional non-renewable production. In this thesis, particular attention has been paid to the sustainable production of ammonia. Two different routes have been assessed, the first one uses water electrolysis and evaluates different air separation technologies depending on the scale, and the second one using biomass as feedstock. Using these electrochemical products, it is possible to build a new sustainable chemical industry. In this thesis, the synthesis of dimethyl carbonate (DMC) is proposed using renewable methanol, ammonia, and captured carbon dioxide. Regarding the energy sector, the introduction of renewable sources is essential to achieve the proposed goals. At this point, energy storage will be crucial to guarantee demand satisfaction due to the inherent fluctuations of solar and wind energies. This thesis is focused on the evaluation of chemicals as a potential form of storage or as energy carriers. The transformation of ammonia into power at process scale is studied providing the necessary results to implement this alternative at grid-scale. The design and operation of renewable-based facilities are to be addressed simultaneously including the location of the units due to the distributed renewable resources. An integrated system is proposed to use chemicals as energy carries for different energy applications in a region of Spain by calculating the optimal capacities and schedule and the optimal location of the facilities. In addition, the integration of different intermittent and non-intermittent renewable energies together with different storage technologies is performed from an economic and social perspective to meet a given power demand. All these proposed systems and tools contribute to create a future scenario in which chemical and energy sectors are transformed to be less impactful on the environment around us.

RESUMEN

Hoy en día, la preocupación por la sostenibilidad está dando lugar a todo un nuevo sistema económico. Este nuevo paradigma afecta a todos los sectores como la agricultura, la industria, el sector financiero, etc. Dos de los más afectados son la industria química y el sistema energético debido a su configuración actual y, estos dos sectores son particularmente estudiados en esta tesis. En cuanto a la industria química, la producción electroquímica es uno de los métodos más atractivos para producir productos químicos de forma sostenible dejando atrás la producción tradicional no renovable. En esta tesis se ha prestado especial atención a la producción sostenible de amoníaco. Se han evaluado dos rutas diferentes, la primera utiliza la electrólisis del agua y evalúa diferentes tecnologías de separación del aire en función de la escala, y la segunda utiliza la biomasa como materia prima. Utilizando estos productos electroquímicos, es posible construir una nueva industria química sostenible. En esta tesis se propone la síntesis de carbonato de dimetilo (DMC) utilizando metanol renovable, amoníaco y dióxido de carbono capturado. En cuanto al sector energético, la introducción de fuentes renovables es esencial para alcanzar los objetivos propuestos. En este punto, el almacenamiento de energía será crucial para garantizar la satisfacción de la demanda debido a las fluctuaciones inherentes a las energías solar y eólica. Esta tesis se centra en la evaluación de productos químicos como forma potencial de almacenamiento o como vectores de energía. Se estudia la transformación del amoníaco en electricidad a escala de proceso proporcionando los resultados necesarios para implementar esta alternativa a escala de red. El diseño y el funcionamiento de las instalaciones basadas en renovables se abordan simultáneamente, incluyendo la ubicación de las unidades debido a que los recursos renovables estan distribuidos. Se propone un sistema integrado para utilizar productos químicos como vectores energéticos para diferentes aplicaciones energéticas en una región de España, calculando las capacidades, la operación y la ubicación óptima de las instalaciones. Además, se realiza la integración de diferentes energías renovables intermitentes y no intermitentes junto con diferentes tecnologías de almacenamiento desde una perspectiva económica y social para satisfacer una determinada demanda eléctrica. Todos estos sistemas y herramientas propuestos contribuyen a crear un escenario futuro en el que los sectores químico y energético se transforman para ser menos impactantes en el medio ambiente que nos rodea.

PUBLICATIONS

This thesis is presented as a compendium of publications, where each of the chapters corresponds to a formal manuscript published in a scientific journal, or currently under review. The relation of manuscripts published or under review is detailed below:

Sánchez, A., & Martin, M. (2018). Scale up and scale down issues of renewable ammonia plants: Towards modular design. *Sustainable Production and Consumption*, *16*, 176–192. https://doi.org/10.1016/j.spc.2018.08.001

Sánchez, A., & Martín, M. (2018). Optimal renewable production of ammonia from water and air. *Journal of Cleaner Production*, *178*, 325–342. https://doi.org/10.1016/j.jclepro.2017.12.279

Sánchez, A., Gil, L. M., & Martín, M. (2019). Sustainable dmc production from co2 and renewable ammonia and methanol. *Journal of CO2 Utilization*, *33*, 521–531. https://doi.org/10.1016/j.jcou.2019.08.010

Sánchez, A., Martín, M., & Vega, P. (2019). Biomass based sustainable ammonia production: Digestion vs gasification. *ACS Sustainable Chemistry & Engineering*, *7*(11), 9995–10007. https://doi.org/10.1021/acssuschemeng.9b01158

Sánchez, A., Castellano, E., Martín, M., & Vega, P. (2021). Evaluating ammonia as green fuel for power generation: A thermo-chemical perspective. *Applied Energy*, *293*, 116956. https://doi.org/10.1016/j.apenergy.2021.116956

Sánchez, A., Martín, M., & Zhang, Q. (2021). Optimal design of sustainable power-to-fuels supply chains for seasonal energy storage. *Energy*, *234*, 121300. https://doi.org/10.1016/j.energy.2021.121300

Sánchez, A., Zhang, Q., Martín, M., & Vega, P. (Under Review). Towards a new renewable power system using energy storage: An economic and social analysis.

CONTENTS

LIST OF FIGURES

LIST OF TABLES

1

INTRODUCTION

1.1 current and urgent environmental issues

In 2015, United Nations Member States adopted the "2030 Agenda for Sustainable Development" targeting for a world that will be fairer, more prosperous, and more respectful to the environment (UN General Assembly, 2015). The 17 Sustainable Development Goals (SDG) (as shown in Figure 1.1) indicate the areas where urgent action is required by all countries. In these proposed goals, the main global environmental problems of the societies emerge and can be summarized in the following items (Iberdrola, 2021a):

Figure 1.1: Sustainable Development Goals by United Nations

- **Climate change mitigation and adaptation**: In their World Scientists' Warning to Humanity, Ripple et al. (2017) mentioned that a specially urgent issue is "the current trajectory of potentially catastrophic climate change due to the rising GHGs". The main culprits behind the rapid increase in greenhouse gas (GHG) emissions are the burning of fossil fuels, deforestation, and agricultural production. At the moment, carbon dioxide emissions are the primary global drivers of climate change. Since 1990, CO_2 emissions have increased by more than 60% involving a sharp rise in the global average temperature of more than 1°C above pre-industrial levels (Ritchie & Roser,

2020a). Important measures must be taken to mitigate the effects of climate change and to keep global temperature below 2ºC above pre-industrial levels as established in the Paris Agreement (United Nations, 2018).

- **Pollution problems and their effect on healt**: According to the World Health Organization (WHO), 90% of the population breathes polluted air and WHO's General Director called air pollution "a silent public health emergency" (Manisalidis et al., 2020). The six major air pollutants in society are: particle, ground-level ozone, carbon monoxide, sulfur oxides, nitrogen oxides, and lead. Contaminated water is also an important issue in this area. Lack of water sanitation affects around one third of the people in the world and is responsible for the spread of waterborne infections, as well as for the unsafe water for human consumption (Schwarzenbach et al., 2010). Access to safe and affordable water is one of the main goals of the UN, reducing releases of hazardous chemicals and materials into the water bodies and improving water and sanitation management.

- **Protecting the oceans**: Oceans are essential for human life. Despite their vast extension, oceans are threatened by different human activities. Climate change has led to an increase in the temperature of the sea surface, the rising concentration of atmospheric CO_2 leads to acidification of the oceans, the oxygen levels are fallen, fish stocks are declining, etc. (Landrigan et al., 2020). Ocean pollution is another major challenge for the conservation of this essential environment. Six of the major pollutants are: plastic waste, oil spills, manufactured chemicals, nutrients, mercury, and pesticides. A key objective is to reduce the land-based discharges which account for more than 80% of ocean pollution. A regulated and more sustainable fishing sector is also essential to achieve the UN's proposed targets.

- **The energy transition and renewables**: The UN states that an affordable, reliable, sustainable, and modern energy system must be ensured. Today, 940 million people (13% of the world's population) lack access to electricity, mainly concentrated in areas of Africa (in South Sudan or Chad less than 10% of the population has access to electricity). Additionally, 4-in-10 people do not have access to clean fuels for cooking, which involves a health risk due to indoor air pollution (Ritchie & Roser, 2020b). Therefore a significant effort should be made in this area. From a sustainable perspective, a high share of greenhouse gas emissions comes from the energy sector. Therefore, an efficient deployment of renewable energies is neces-

sary to reach the proposed goals. In 2019, around 25% of the global power production came from renewables, and, this percentage will be increased to around 70% in 2050 (BloombergNEF, 2020).

- **A sustainable food model**: Story et al. (2009) defined a sustainable food system as one that "provides healthy food to meet current food needs while maintaining healthy ecosystems that can also provide food for generations to come, with minimal negative impact to the environment; encourages local production and distribution infrastructures; makes nutritious food available, accessible, and affordable to all; is humane and just-protecting farmers and other workers, consumers, and communities". Nowadays, food and agriculture account for around 25% of the total GHG emissions, are responsible for about 70% of the total freshwater withdrawals, and are the primarily responsible for water eutrophication (Ritchie & Roser, 2020c). Therefore, changing the food model is essential to reach the proposed sustainable goals.
- **Protecting biodiversity**: Human activities such as land-use change and habitat fragmentation, overhunting, invasive species, or pollution are threatening earth ecosystems (Tilman et al., 2017). At this time, 27% of species are red listed by the International Union for Conservation of Nature. Around 50% of the earth's species are concentrated in about 1.4% of the land area, therefore, habitat loss and degradation is one of the most direct threats to biodiversity (Trew & Maclean, 2021). In the medium/long future, climate change could be one of the most significant threats. According to the predictions, a 14% of local species richness and 35% of suitable climate areas will be lost if global temperature rises to an average of 2^{o}C (Nunez et al., 2019).
- **Sustainable urban development and mobility**: Half of humanity, about 3.5 billion people, live in cities today, and, this is expected to increase to 5 billion by 2030. This situation poses a social and environmental sustainable challenge. Cities are a major emitter of greenhouse gases due to the high concentration of population, economic and social activities (Bibri & Krogstie, 2017). Therefore, efficient solutions should be adopted to ensure a sustainable development. Some measures could be: increasing the share of renewables, improving energy efficiency, introducing new green areas, developing a new intelligent and sustainable transport system, etc.
- **Hydric stress and water scarcity**: Liu et al. (2017) state that "water scarcity has become a major constraint to socio-economic development and a threat to livelihood in increasing parts of the world".

Today, 2.3 billion people live in water-stressed areas, and, two-thirds of the global population (around 4 billion people) live under severe water scarcity at least 1 month of the year (Mekonnen & Hoekstra, 2016). Increasing water efficiencies, mainly in crop production, or limiting the water consumption by river basin will be some of the most effective solutions to fight against this challenge.

- **Waste management**: The world produces around 2.01 billion of tonnes of municipal solid waste, of which at least 33% is not managed in an environmentally safe manner (The World Bank, 2021). The increase in the global population in the coming years will reach a value of 9.7 billion in 2050, leading to an increase in waste generated. Therefore, it is necessary and urgent to implement different policies using a circular economy strategy to mitigate this issue. For example, in the EU, the waste framework directive establishes a waste hierarchy in which the first option should be the prevention of the waste generation and the last resort, sending waste to landfill (European Council, 2008). These guidelines should be adopted in different areas such as plastic recycling, circular economy of electric batteries, management of municipal solid waste, etc.

The sustainable transformation of the world will affect all sectors of the current economic framework (Corporate Citizenship, 2016). It is necessary to adapt the existing system to achieve a fairer and more sustainable world in line with UN goals. The energy system must be adapted to provide an affordable and sustainable energy for all. National health systems and health care companies play a key role in achieving good health and well-being of the societies. Telecommunications and other technology companies should introduce new tools as artificial intelligence, Internet of things, information security, etc. to facilitate this global transition. Agriculture and fisheries are essential to reach the SDG 2, zero hunger, and these sectors must also be adapted following a sustainable criterion. The entire industrial sector should be transformed using more sustainable raw material, protecting land and marine environments, and avoiding pollution in all its activities. The financial sector should contribute by providing access to capital resources to facilitate this challenging transformation. Only through a joint effort of all sectors will it be possible to reach the highest levels of the proposed objectives. In this thesis, two sectors are particularly assessed: the chemical industry and the energy system.

1.2 towards a new green chemical industry

The chemical sector is one of the most energy-intense activities today. The chemical industry consumes about 28% of the industrial and 10% of the total final consumption of energy (Kätelhön et al., 2019). Additionally, it is also the largest industrial consumer of oil and gas, with 15% of the total primary demand of oil and 9% of the gas demand (Internacional Energy Agency, 2020). Some of the chemical processes have particularly significant energy consumption. For example, fertilizers production stands for about 1.2% of the world energy consumption, mainly concentrated in ammonia production (Andersson & Lundgren, 2014). In terms of emissions, about 880 Mt CO_2 are directly emitted from primary chemical production. Other pollutants such as sulfur dioxide, nitrogen dioxide or volatile organic compounds are also associated with activities of the traditional chemical sector. Therefore, an important boost to a new sustainable chemical industry is necessary to address the sustainability problem in this important sector.

All the guidelines towards a new sustainable chemical production are collected under the umbrella of "Green Chemistry" enunciated by Prof. Anastas. This term is defined as the "design of chemical products and processes to reduce or eliminate the use and generation of hazardous substances" (P. T. Anastas & Williamson, 1996). The conceptual framework to design new chemical products and processes is summarized in the twelve principles of green chemistry (as shown in Figure 1.2). From a product design perspective, there is a need to create new chemical products that are inherently safer but with the same functionalities or to design these chemicals for an innocuous degradation at the end of their function. From a process perspective, it is necessary to turn into the utilization of new renewable feedstocks, avoiding waste generation and increasing the energy efficiency of the process (P. Anastas & Eghbali, 2010).

One of the main policies to reduce greenhouse gas emissions is the decarbonization of the chemical industry (Oberthür et al., 2021). In the European Union, the increase in the price of CO_2 European emission allowances could be one of the main drivers towards decarbonization. To prevent the risk of carbon leakage and support the ambition of the EU on climate change mitigation reducing the carbon dioxide emissions, the European Commission has proposed the implementation of a carbon border adjustment mechanism. In Spain, the integrated national energy and climate plan states that the industrial sector must reduce its CO_2 emissions by 7Mt CO_2 in 2030 (Ministerio para la Transicion Ecologica y el Reto Demografico, 2020b). Additionally, the "Estrategia de descarbonizacion a largo plazo 2050" reduces the industrial CO_2 emissions from 72Mt CO_2 in 2020 to 7Mt CO_2 by 2050 (Ministerio para la Transicion Ecologica y el

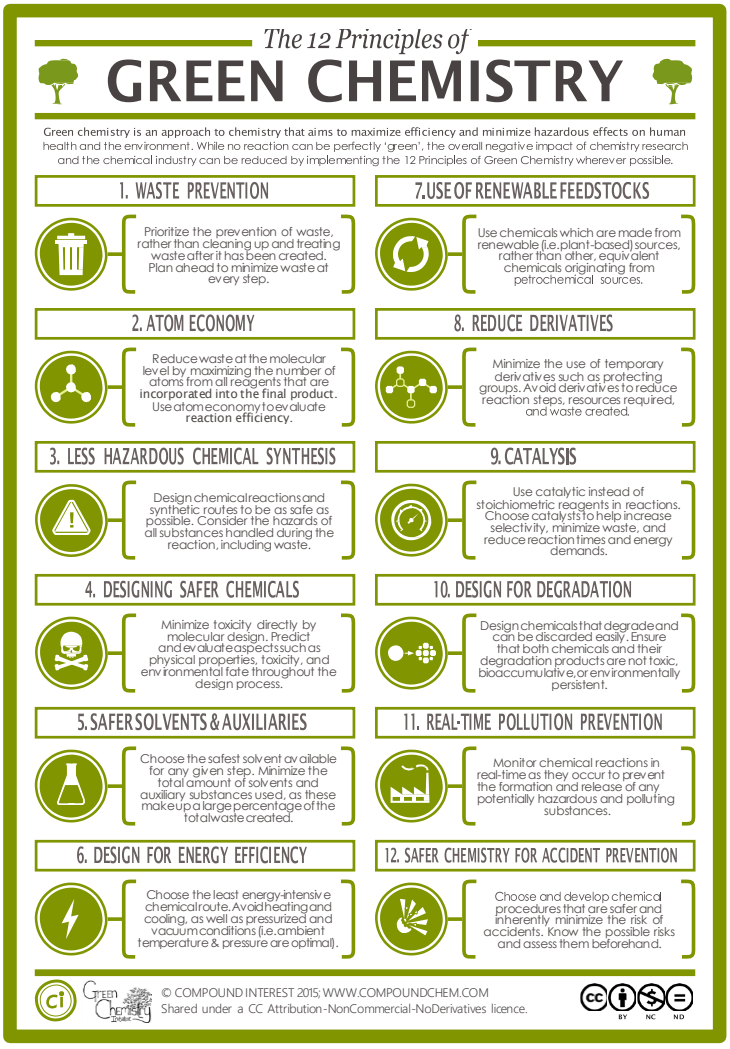

Figure 1.2: The 12 Principles of Green Chemistry (Compound Interest, 2015)

Reto Demografico, 2020a). Some of the solutions to achieve these goals in the chemical industry are: increasing the energy efficiency of processes, introducing carbon capture, storage, and utilization (CCSU) technologies, using new sustainable raw materials, or integrating renewable energies into the chemical sector (electrification).

Electrification could be the way to decarbonize the energy-intensive chemical industry (Schiffer & Manthiram, 2017). Particular attention needs to be paid to those chemicals with large production amounts and with high energy demand such as ammonia, ethylene, propylene, or methanol. The synthesis of ammonia using renewable energies through water elec-

trolysis is proposed to decarbonize the fertilizers production (Zhang et al., 2020). Recent projects plan to implement this technology on an industrial scale, for example, Iberdrola and Fertiberia are going to deploy a green hydrogen plant to feed the traditional ammonia Haber-Bosch process. The facility consists of 20 MW of water electrolysis combined with 100 MW of solar PV panels. The total investment is expected to be 150 M€ avoiding the emission of 48,000 tCO_2 per year (Iberdrola, 2021b). A step forward is the direct electrochemical ammonia synthesis by N_2 electroreduction (MacFarlane et al., 2020). At this point, the Haber-Bosch process is no longer required, however, in-depth research in this area is required to implement this technology on an industrial level, including scale-up studies in order to meet the current demand. Methanol is another chemical whose synthesis has been extensively studied. The first approximation to produce green methanol is, as in ammonia production, based on the combination of carbon dioxide and hydrogen from water electrolysis (Vázquez & Guillén-Gosálbez, 2021). Electrochemical conversion is also proposed for implementation over a long-term horizon (Albo et al., 2015). Several industrial projects have been planned to produce green methanol, for example, in Belgium with a 65MW electrolyzer to produce 44,000 t per year of methanol avoiding 140,000 t per year of CO_2 (Proman, 2020). Finally, the electrochemical synthesis of ethylene via CO_2 reduction is explored in multiple studies, but several breakthroughs are needed to make this competitive with current production alternatives (Pappijn et al., 2020).The synthesis of bulk chemicals using the electrochemical route is the first step in building a complete sustainable chemical industry. The methanol-to-olefins (MTO) process provides a link to produce basic chemicals from a sustainable resource as green methanol (Tian et al., 2015). From the same perspective, methanol-to-propylene (MTP) conversion is receiving attention due to the limited oil resources (Khanmohammadi et al., 2016). Targeting less hazardous and more degradable compounds, dimethyl carbonate (DMC) is an interesting alternative due to the wide range of applications to substitute traditional chemicals (Pyo et al., 2017). Different renewable processes based on the use of captured CO_2 have been proposed such as the direct synthesis using CO_2 and methanol or the production from urea (Kongpanna et al., 2015).

Carbon dioxide for these electrochemical processes can be obtained from different industrial sources or directly from the air using several carbon capture technologies (Bui et al., 2018). Capture in industrial sources could help mitigate CO_2 emissions in some sectors where decarbonization and electrification are difficult. Furthermore, the cost of carbon capture in these sources is cheaper than direct capture from the atmosphere. Direct atmospheric capture emerges as an option to mitigate distributed emission

sources where the installation of a capture technology during the release is difficult (Sanz-Pérez et al., 2016). Different technologies with different readiness levels (TRL) have been proposed to carry out this carbon capture such as amines, membranes, calcium carbonate looping, or ionic liquids.

Biomass has also been proposed as a source of chemicals in the context of a new system based on sustainability for moving away from petroleum products. (Tuck et al., 2012). Particularly, the use of residual biomass such as by-products from agricultural activities or food processing is attracting attention as a part of a circular economy strategy for the chemical industry. One of the first options analyzed is the synthesis of chemicals from carbohydrates. The production of ethanol (bioethanol) by fermentation is one of the most representative processes at industrial scale at present in this section. Current research has positioned ethanol as a chemical platform, for example, for the synthesis of olefins via dehydration (Cabrera Camacho et al., 2020). The US Department of Energy (DOE) establishes the top chemical opportunities to be produced from carbohydrates by 2004. This list is updated by Bozell and Petersen (2010) resulting in the following chemicals: ethanol, furans, glycerol and derivates, biohydrocarbons, lactic acid, succinic acid, hydroxypropionic acid/aldehyde, levulinic acid, sorbitol, and xylitol. The use of proteins from biomass is also proposed for the synthesis of platform chemicals. For example, the nonessential amino acid, L-arginine, can be transformed into 1,4 diaminobutane, the raw material for the synthesis of Nylon-4,6 (Könst et al., 2010). Another example is the utilization of glutamic acid for the synthesis of a wide range of products such as acrylonitrile or N-methylpyrrolidone (Lammens et al., 2011). For some of these biomass-based products, different industrial processes have been proposed, for example, for the synthesis of butadiene from biomass-derived furfural (Kuznetsov et al., 2020) or the integrated production of xylitol or sorbitol from switchgrass (Galán et al., 2021). Most of these chemical productions are based on the biochemical processing by fermentation of the carbohydrates and hydrolysis of the protein fraction. Another interesting alternative is the thermochemical route based on pyrolysis or gasification for the production of a syngas that can be used for chemical synthesis (Haro et al., 2014). The synthesis of methanol (Holmgren et al., 2012), ethanol (Martín & Grossmann, 2011), dimethyl ether (DME) (Haro et al., 2013) or different alcohols (Gupta et al., 2011) have been evaluated in the literature. Alternatively, syngas can also be obtained from different wet waste using anaerobic digestion which can be an interesting pathway to manage these residues but with a limited economic perspective (Hernández & Martín, 2016).

1.3 targeting a new sustainable energy system

The urgent requirement to decarbonize the energy system to meet the global sustainable goals is accelerating the transition to a new system based on renewable energy sources (RES). Currently, around 25% of the total power production is generated using renewables, mainly, hydroelectric power (about 15%) with only a small share of wind and solar (about 10%). However, the electricity sector is undergoing an unparalleled transformation towards sustainability. By 2050, BloombergNEF (2020) estimates that 69% of the total power production will be produced from RES with wind and solar accounting for 56% of the total electricity production. In terms of total primary energy supply, the share of renewables must rise from around 15% in 2015 to 66% by 2050 to meet global objectives (IRENA, 2018). In Europe, this energy transition is especially significant due to the commitment of the European member states to climate neutrality by 2050 (European Commission, 2021a). It is projected that, by 2050, 75% of total gross final energy consumption will come from renewables, and 97% of electricity will be generated from renewable sources (European Commission, 2012). These European guidelines are translated to the Spanish scenario where the different public strategies are adapted to target the achievement of the proposed objectives. Spanish decarbonization strategy (Estrategia de descarbonizacion a largo plazo 2050) states that 79% of the end-use energy must be renewable in the transport sector, 100% in the electric sector and 97% in the cooling and heating sector by 2050 (Ministerio para la Transicion Ecologica y el Reto Demografico, 2020a). A major boost to this transition will arrive in the next years with the funds from the European post-COVID recovery plan (NextGenerationEU) (European Commission, 2021b). In Spain, the recovery, transformation, and resilience plan includes a just and inclusive energy transition as one of the main goals with more than 6,300 M€ of planned investment. This includes the deployment of renewable technologies, the adaptation of the electricity grid, the hydrogen road-map, or the fair transition strategy (Gobierno de España, 2021).

The two main renewable energy sources to reach the objectives of a complete decarbonization of the electricity sector are solar (mainly photovoltaic) and wind. However, the increase of the share of these two RES is a challenge for the electricity system. With these technologies, power generation is completely dependent on the weather conditions in contrast to the traditional energy sources. Therefore, ensuring the balance between electricity production and demand on an hourly basis is one of the priorities in the design of the new electricity sector. A combination of different intermittent and non-intermittent renewable sources has been proposed. Bagheri et al. (2019) proposed the integration of biomass together with

wind and solar technologies, mitigating the high cost of electricity from the latter two sources. The combination of concentrated solar power (CSP) with different biomass (Vidal & Martín, 2015) or waste (de la Fuente & Martín, 2020) has also been proposed to reduce the variability associated with solar production. Hydroelectric power can also help mitigate the fluctuations of wind and solar due to better controllability of power generation, however, this source is also highly influenced by climatic conditions.

In a context with high penetration of renewable energy sources in the electricity system, energy storage will be key to guarantee demand satisfaction regardless of weather conditions. Different energy storage technologies have been proposed and can be grouped into four categories: mechanical, chemical, electrochemical, and electrical (Gür, 2018). The alternatives differ in the power rating and discharge times (as shown in Figure 1.3). Two of these technologies are currently available at a commercial scale: pumped-hydro and compressed air energy storage (CAES). Pumped-hydro is based on pumping water from a lower to a higher level when electricity demand is low and releasing this water to a turbine when electricity demand is high and generation is not enough. Today, pumped-hydro represents about 96% of the global installed storage capacity (Gür, 2018). The idea of CAES is to store compressed air during periods of low electricity demand in large underground cavities and release it through a turbine when electricity is

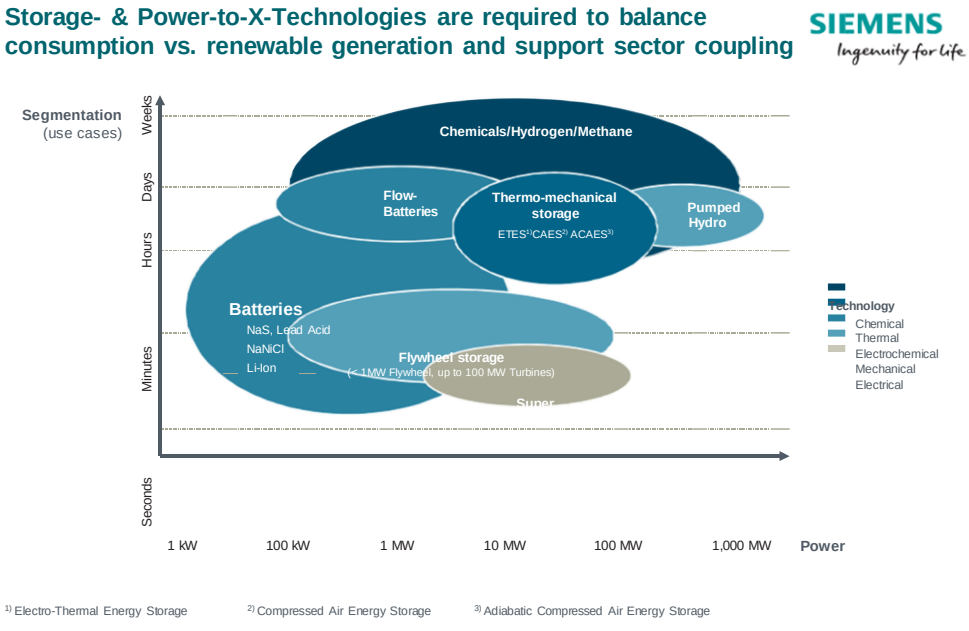

Figure 1.3: Storage technologies for different time horizon and power capacities (Simon, 2017)

Nevertheless, the most promising technologies for energy storage are still in the early stages of development. O. Schmidt et al. (2019) evaluate

different energy storage technologies and determine that the most promis-

ing alternatives are lithium-ion batteries for short-term storage horizons and hydrogen and its derivates for medium and long timescale (more than 700 hours). The use of batteries for different storage applications has been widely investigated (Diouf & Pode, 2015). At grid scale, batteries must meet the requirements of frequency regulation, peak shaving, integration with renewable energy sources, and power management (Chen et al., 2020). The use of batteries has also been proposed for residential use in the context of self-consumption. At this point, the trade-off between battery degradation (cost of replacement) and tariff policy (storing low price electricity) arises (Corengia & Torres, 2018).

The use of hydrogen and its derived products for grid storage applications has also been widely proposed (Pellow et al., 2015). The synthesis of these fuels has attracted attention due to the high energy density of these chemicals and the scalable and flexible behavior of this technology. Hydrogen is the first option analyzed within this alternative. It is a carbon-free fuel with a high gravimetric energy density. Two main options for producing hydrogen from renewable energies are available: water electrolysis or photocatalytic water splitting. The first one is more mature and is the most widespread option. Further research is needed to implement the second alternative (Guo et al., 2019). One of the main disadvantages of using hydrogen is the low volumetric energy density and the transport and storage conditions. Therefore, alternative options based on hydrogen production have been analyzed.

The transformation of hydrogen into methane, through CO_2 hydrogenation, is proposed to synthesize a gaseous fuel as methane with an energy density 3 times higher than hydrogen and with easy storage conditions (Davis & Martín, 2014). The existing infrastructure of natural gas, for example, the combined cycle facilities, can be used with this new synthetic fuel (Ghaib & Ben-Fares, 2018). Additionally, the use of hydrogen-based liquid fuels such as methanol (Matzen et al., 2015), dimethyl ether (DME) (Hankin & Shah, 2017) or ammonia (Allman et al., 2019) has also been evaluated. The use of these liquid chemicals is attractive due to the high volumetric energy density and the easy storage conditions. Ammonia is attracting a great deal of attention due to its carbon-free nature in the context of decarbonization. The environmental impact of the use of these fuels in the new energy system has been assessed in different works, for instance, for methane (Blanco et al., 2020), methanol (Zang et al., 2021) or ammonia (D'Angelo et al., 2021). All these chemical fuels are converted into power using the thermochemical (Verhelst et al., 2019) or the electrochemical (Siddiqui & Dincer, 2020) pathways.

Public support for these technologies is materialized, in the case of Spain, in the energy storage strategy (Ministerio para la Transicion Ecologica y

el Reto Demografico, 2021a). The Spain's current storage power capacity is around 8.3 GW which should be increased to about 30 GW by 2050 to meet the system requirements. The strategy introduces several measures in different areas such as the regulatory framework for energy storage, the introduction of energy storage in the electricity market, or the integration of energy storage with other sectors.

To complete a full transformation of the energy system, the heating and cooling and the transport sectors must be decarbonized. The heating and cooling industry has been introduced as one of the target sectors to be decarbonized due to the high importance in terms of energy consumption and associated emissions (Thomaßen et al., 2021). Electrification of the heating sector is proposed as the pathway towards sustainability, but significant uncertainties arise because this sector is difficult to decarbonize (Chaudry et al., 2015). Heat pumps emerge as the direct alternative to electrify the heating sector by providing a tool to reduce the use of natural gas as the main source of heating (Bellocchi et al., 2020). The use of H_2 is also proposed as a carrier to reduce the carbon footprint of heating generation (Sunny et al., 2020). An ongoing project in the UK is testing the transformation of the natural gas grid to distribute hydrogen in the city of Leeds. The aim is to provide a cost-effective route to zero-carbon heating at a domestic scale using a reliable and flexible supply of H_2 (Brandon & Kurban, 2017). Other energy carriers based on hydrogen have also been proposed as an effective solution targeting a carbon-free heating generation (J. Schmidt et al., 2019).

The transformation of the transport sector is also another challenge. The integration of renewable energies in this area is necessary to mitigate the important emissions of this sector (van der Zwaan et al., 2013). In the Spanish national scenario, the CO_2 emissions from the transport sector must be reduced from 87Mt in 2020 to only 2Mt by 2050. (Ministerio para la Transicion Ecologica y el Reto Demografico, 2020a). Direct electrification in the transport sector is particularly suitable for light-duty vehicles where this technology will be predominant in the future scenario. For an effective deployment of electric vehicles, a technically and economically competitive battery development is necessary (Li et al., 2019). The Spanish national government is promoting this sector through a Strategic Project for the Recovery and Economic Transformation (PERTE) of Electric and Connected Vehicles with more than 24,000 M€ of investment in this area (Ministerio de Industria, Comercio y Turismo, 2021). Synthetic fuels will play an important role in the future heavy road, air, or maritime transport sector. Different fuels have been suggested from two main sources: Power-to-X processes (such as those used in energy storage systems) and the use of biomass-based fuels (Stančin et al., 2020). Valente et al. (2021) evaluated the

use of hydrogen from different sources for heavy transport using planetary boundaries. The use of hydrogen and different derivate products (including liquid organic hydrogen carriers (LOHC)) for use in the maritime sector is analyzed by Van Hoecke et al. (2021). The use of biomass as a source of biofuels is also reviewed by dos Santos and Alencar (2020) including the Fischer-Tropsch synthesis.

Apart from the technical, economic, and environmental analysis of the energy transition, the social incidence is a significant challenge that should be also considered in the planning of the new energy system (Heras & Martín, 2020). The decommissioning of the traditional power plants based on, mainly, coal is reducing the job opportunities in rural areas where mining and the power industry are particularly significant (Carley & Konisky, 2020). Therefore, the planning of the new sustainable energy system should contribute to mitigating social inequalities between regions and reducing the social impact caused by the closure of traditional facilities. The energy transition can generate multiple employment opportunities during the different stages of the life of the facilities, increase local taxes in the regions where they are installed, etc. (Springer & Daue, 2020). The Spanish fair energy transition strategy (Ministerio para la Transicion Ecologica y el Reto Demografico, 2021b) gathers all the measurements to mitigate the social disturbances of the energy transition focusing on those areas where nuclear and coal power facilities are/were located.

1.4 the role of process system engineering

Process System Engineering (PSE) can be defined as "the scientific discipline of integrating scales and components describing the behavior of a physicochemical system, via mathematical modelling, data analytics, design, optimization and control" (Pistikopoulos et al., 2021). The scope of application of PSE is wide and includes areas as the chemical and biochemical industry, pharmaceutical, agrochemical, or food sector. PSE is a powerful tool to tackle problems of process synthesis and design, process analysis, process control, process optimization, etc. Therefore, PSE can significantly contribute to addressing the problems of a new sustainable chemical and energy system presented in the above sections.

1.4.1 *Modeling approach*

One of the first steps in tackling any problem from a PSE perspective is to model the presented issue. The modeling of the system is key for different operations as process synthesis and design, process operation,

or product design. An overview of the main modeling approaches is presented here based on the classification proposed by Martín and Grossmann (2012). The different models can be implemented on different software platforms as MATLAB©, Python, gPROMS©, GAMS©, Julia, ASPEN plus©, CHEMCAD©, ANSYS Fluent©, etc.

- **Short Cut Methods**: This approach is one of the most straightforward to represent physical systems. It is based on mass and energy balances, and is used in a wide range of applications such as heat exchangers or splitters. These kinds of models are also used in supply chain or process operation. One of the main limitations is the difficulty to model complex systems.

- **Mechanistic Models**: This modeling category uses a more detailed first principles approximation compared to the short-cut methods. These models are based on the underlying chemistry, physics, or biology that governs the behavior of the system. In this category, equilibrium models (Loeppert et al., 1995), kinetic models (Buzzi-Ferraris & Manenti, 2009), or phase equilibrium relationships (Brignole & Pereda, 2013) are included. The most rigorous models such as computational fluid dynamics (CFD) based on continuity, momentum, and energy equations also falls into this category (Anderson & Wendt, 1995).

- **Rules of thumb**: They provide the simplest approach to modeling a real system. Rules of thumb are based on operational data from the industry. These data are scarce and limited to the common range of operation, however, they reflect the actual operating conditions of the different units. Couper et al. (2005) and Hall (2012) collect several rules of thumb in the area of chemical engineering and Sadhukhan et al. (2014) for different biosystems.

- **Dimensionless analysis**: This approach provides the necessary tools to handle a large amount of experimental data in a simple way. From the experimental data, it is possible to create correlations of different dimensionless groups that determine the performance of the systems. Scale-up and down issues are captured in these models. A large number of applications have been proposed in different fields such as heat or mass transfer or fluid mechanics (Szirtes, 2007).

- **Surrogate models**: Surrogate modeling techniques create simple models using the data from rigorous ones. This is particularly important when the model developed to simulate the behavior of some units is too complex to be used in some applications such as process

operation or control. Queipo et al. (2005) defined the four stages to build a surrogate model: design of experiments (DOE), numerical simulations at sampling points for the previous step, construction of a surrogate model, and model validation. At this point, different kinds of surrogate models have been proposed. One of the simplest is the polynomial regression models in which the relationship between the variables is expressed using a polynomial (Montgomery et al., 2021). Kriging models combine computational efficiency with relatively small sampling data and have been used in sensitivity analysis and optimization (Quirante et al., 2015). Another example of surrogate models is an artificial neural network (ANN). This model tries to imitate the behavior of human neural networks in the brain. Different neurons are organized in layers that constitute the network (Himmelblau, 2000).

- **Experimental correlations**: The idea of experimental correlations is similar to that of surrogate models, however, the data, in this case, is provided from experimental results. One of the main challenges is that it is necessary to have a good data set, with all the variables involved in the phenomenon to create a good model for the unit. The range of applications of these correlations is limited by the experimental data. The main advantage of these kinds of models is the real data they represent.

1.4.2 *Mathematical programming*

Optimization of chemical and energy systems is a complex procedure. Several modeling approaches are necessary for the different systems and applications. These models can include linear or/and nonlinear equations, and continuous and/or discrete variables. This leads to different mathematical formulations of the problems explained throughout this section.

1.4.2.1 *Linear programming*

Bazaraa et al. (2008) defined linear programming (LP) as "the optimization (minimization or maximization) of a linear function while satisfying a set of linear equality and/or inequality constraints or restrictions". The linear programming problem can be expressed as follows (Grossmann, 2021):

$$\begin{aligned} \min \quad & Z = c^T x \\ \text{s.t.} \quad & Ax = b \\ & x \geq 0 \end{aligned} \tag{1.1}$$

where x is an n-vector, A is a mxn matrix, c is the n-vector of cost coefficients, and the right-hand side b is an m-vector.

Two main methods have been proposed to solve LP problems: the Simplex algorithm and interior-point methods. The Simplex method solves linear programming problems by exploring the extreme points each time improving the objective function (Bertsimas & Tsitsiklis, 1997). It is demonstrated that if a linear programming program in standard or canonical form has a finite optimal solution, then it has an optimal extreme point solution (Bazaraa et al., 2008). Interior point methods explore the interior of the feasible set combining the advantages of the Simplex method and of the ellipsoid algorithm (Bertsimas & Tsitsiklis, 1997). The Simplex method is more efficient for solving problems with thousands of variables and constraints, while interior-point performs better on very large scale and sparse problems (Grossmann, 2021). The most representative commercial solvers such as CPLEX (ILOG, 2009), Gurobi (Gurobi Optimization, 2021), or XPRESS (FICO, 2009) implement both methods.

A wide range of engineering problems has been formulated using linear programming. Some of them are blending problems, production scheduling, transportation problems, etc (Bazaraa et al., 2008; Sioshansi & Conejo, 2017).

1.4.2.2 *Nonlinear programming*

In a wide range of real-world problems, nonlinearities are necessary to model these systems. Therefore, an optimization problem that includes nonlinear constraints or objective function is called nonlinear programming (NLP) (Floudas, 1995).

$$\begin{aligned} \min \quad & f(x) \\ \text{s.t.} \quad & h(x) = 0 \\ & g(x) \leq 0 \\ & x \in X \subseteq \mathbb{R}^n \end{aligned} \tag{1.2}$$

where x is an n-vector, $f(x)$ is the objetive function of the problem, $h(x)$ is the set of equality constraints and $g(x)$ is the set of inequality constraints. Some of these functions are nonlinear.

For a constrained nonlinear problem (the most extended problem in an engineering perspective), the necessary conditions for a minimum at the point $\hat{x}$ in the NLP are given by the Karush-Kuhn-Tucker (KKT) conditions (Floudas, 1995). Let $\hat{x} \in X$ be a feasible solution of (1.2). Let also $f(x)$ and $g(x)$ be differentiable at $\hat{x}$ and $h(x)$ have continuous first partial derivatives at $\hat{x}$. If $\hat{x}$ is a local optimum of (1.2) and one of the constraints qualifications (linear independence, Slater, Kuhn-Tucker, or weak reverse convex) is satisfied, then there exist Lagrange multipliers such that:

$$\begin{aligned} &\nabla f(\hat{x}) + \lambda^T \nabla h(\hat{x}) + \mu^T \nabla g(\hat{x}) = 0 \\ &h(\hat{x}) = 0 \\ &g(\hat{x}) = 0 \\ &\mu_j g_j(\hat{x}) = 0 \quad j = 1, ..., p \\ &\mu_j \geq 0 \quad j = 1, ..., p \end{aligned} \tag{1.3}$$

If $f(x)$ is convex, the feasible region is convex and non-empty, then if there exists a local minimum at $\hat{x}$, then, $\hat{x}$ is a global minimum, the constraint qualification requirements is satisfied and the KKT conditions are necessary and sufficient for global minimum (Grossmann, 2021). Therefore, if an NLP is convex is not necessary to evaluate the second-order KKT conditions (information of the Hessian of the Lagrangean). Three different kinds of algorithms have been proposed to solve NLP problems: successive quadratic programming (SQP), reduced gradient algorithms, and interior point methods.

SQP algorithms are based on the solution of the quadratic program (equation 1.4) in each of the iterations to determine the value of the Newton step (d) and Lagrange multipliers (λ and μ) (Grossmann, 2021).

$$\begin{aligned} \min \quad & \nabla f(x^i)^T d + \frac{1}{2} d^T \nabla_{xx} L(x^i, \lambda^i, \mu^i) d \\ \text{s.t.} \quad & h(x^i) + \nabla h(x^i)^T d = 0 \\ & g(x^i) + \nabla g(x^i)^T d \leq 0 \end{aligned} \tag{1.4}$$

where the Lagrange function is given by:

$$L(x, \lambda, \mu) = f(x) + \sum_{j=1}^{m} \lambda_j h_j(x) + \sum_{j=1}^{r} \mu_j g_j(x) \tag{1.5}$$

Commercial solvers as SNOPT (Gill et al., 1997) or fmicon in MATLAB© (Mathworks, 2007) use these SQP algorithms (Biegler, 2010).

Reduced gradient methods consider a linear approximation of the constraints and eliminate variables to reduce the dimension of the problem

and, then, apply Newton's method. In each of the iterations, the reduced gradient is calculated, then the search direction and, finally, a line search is performed minimizing the objective function. Different commercial solvers as MINOS (Murtagh & Saunders, 1983) or CONOPT (Drud, 1996) are based on this algorithm.

Interior point methods reformulate the original NLP problem (eq.(1.2)) using the slack variables to replace inequalities by equalities and the log-barrier function to handle the non-negativity of the x variables.

$$\begin{aligned} \min \quad & f(x) - \alpha \sum_i ln(x_i) \\ \text{s.t.} \quad & r(x) = 0 \end{aligned} \tag{1.6}$$

Then, first-order KKT conditions are applied to this problem solving it using the Newton's method. This is, broadly speaking, the essence of the interior point methods used in commercial algorithms such as IPOPT (Wächter & Biegler, 2006) or KNITRO (Byrd et al., 2006).

Problems of optimal control, process design, structural design or water resources management have been solved using this perspective (Bazaraa et al., 2013; Sioshansi & Conejo, 2017).

1.4.2.3 *Mixed-integer linear programming*

The mixed-integer linear programming (MILP) models can be expressed as:

$$\begin{aligned} \min \quad & Z = a^T x + b^T y \\ \text{s.t.} \quad & Ax + By \leq d \\ & x \geq 0 \quad y \in \{0,1\}^m \end{aligned} \tag{1.7}$$

in which x are continuous variables and y are discrete variables, with binary as the most common case. In the MILP problems, there are no optimality conditions as the KKT in nonlinear programming. Different methods have been proposed to solve these kinds of problems: cutting planes, Benders decomposition, branch and bound search, and branch and cut methods (Grossmann, 2021).

Cutting planes consist of a sequence of LP problems in which different cutting planes are generated to cut-off the solution of the relaxed LP. They reduce the feasible region of the linear relaxation of the original problem excluding those solutions that are feasible in the linear relaxation but not in the original MILP problem (as shown in Figure 1.4).

Benders decomposition provides, in each iteration, a lower and an upper bound of the solution of the MILP problem. The upper bound is taken

the original MILPP.

We proceed in this section by first outlining how to generate cuts from a non-integer solution obtained from solving the linear relaxation of a pure-integer linear optimization problem. We then outline the iterative algorithm to generate cutting planes and demonstrate its use with an example.

Fig. 3.18 Geometrical representation of the feasible region of the linear relaxation of the Photovoltaic Panel-Repair Problem with cutting planes added

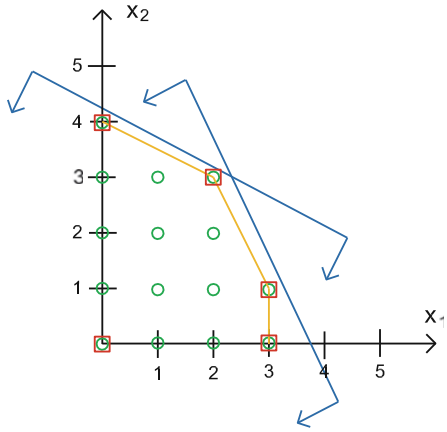

Figure 1.4: Schematic representation of the cutting planes algorithm. Blue lines represent the inequality constraints of the problem and yellow lines the cutting planes. x_1 and x_2 correspond to two integer variables (Sioshansi & Conejo, 2017).

3.6.1 *Generating Cutting Planes*

To derive a cutting plane, let us suppose that we solve the linear relaxation of a PILPP and obtain a solution, $\hat{x}$, which does not satisfy all of the integrality restrictions of the original PILPP. We further assume that the linear relaxation is converted to standard form (3.4) [3.10].

from a primal problem corresponding with the original problem where y-variables are fixed. The lower bound is provided by the master problem that is a linear programming derivated using the duality theory.

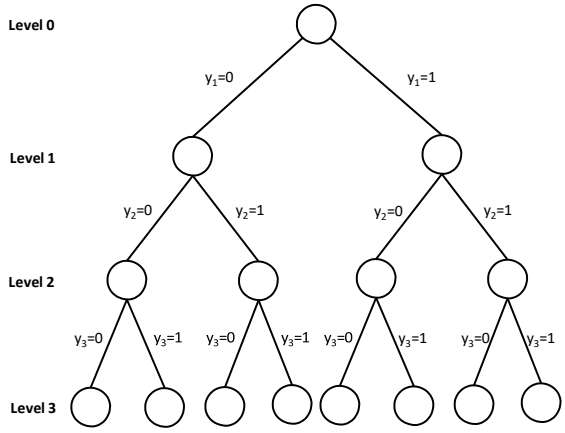

Figure 1.5: Binary tree for branch and bound search

Branch and bound methods are based on the enumeration of the 0-1 combinations in a binary tree. The first step is to solve the relaxation of the original problem. If the relaxation does not result in a 0-1 solution, the original root of the tree is divided, creating a set of subproblems at level 1. One of these subproblems is selected (fixing the binary variable of level 1) to solve the relaxed problem. If the solution is integer, the next

step is to return to the original subproblem set. If not, it is necessary to go deeper into the solution tree. To avoid the enumeration of all the possible candidates, fathoming rules are included (Floudas, 1995).

Finally, branch and cut methods combine branch and bound methods with cutting planes targeting a tighter lower bound. In the different nodes, the relaxation of the problem is solved. If the solution is not integer, the relaxing problem is solved by adding cutting planes in order to strengthen the lower bound (Grossmann, 2021). Today, branch and cut methods constitute the most successful method for solving integer programs (Conforti et al., 2014). This algorithm has been implemented in different commercial codes as CPLEX (ILOG, 2009) or Gurobi (Gurobi Optimization, 2021).

For large-scale optimization problems, it is necessary to decompose the original problem into smaller ones to get a solution in reasonable computational times. Based on the structure of the problem, different alternatives have been proposed as Lagrangean or Benders decomposition (Conforti et al., 2014).

Scheduling problems, transmission problems, supply chain, etc. have been solved using these methods.

1.4.2.4 *Mixed-integer nonlinear programming*

The general formulation of a mixed-integer nonlinear programming problem is as follows:

$$\begin{aligned} \min \quad & f(x,y) \\ \text{s.t.} \quad & h(x,y) = 0 \\ & g(x,y) \leq 0 \\ & x \in X \subseteq \Re^n \\ & y \in \{0,1\}^m \end{aligned} \tag{1.8}$$

where x represents a vector of continuous variables, y is the vector of binary variables, $h(x,y)$ and $g(x,y)$ denote the equality and inequality constraints respectively and, finally, $f(x)$ is the objective function. Different algorithms have been proposed to solve these kinds of optimization problems. Some of the are presented below.

Generalized Benders decomposition (GBD) is based on the generation of a lower and an upper bound in each iteration. The upper bound is calculated from a primal problem that is the original MINLP problem with fixed y variables. Its solution also provides information about the Lagrange multipliers associated with the equalities and inequalities constraints. The lower bound information is obtained from a master problem. The master

problem is obtained using the duality theory and, additionally to the lower bound, this level also provides information about the y variables to be fixed in the next iteration. The sequence of lower and upper bounds converge in a finite number of iteration (Geoffrion, 1972).

Outer approximation (OA), as in the GBD, generates a sequence of lower and upper bounds to the MINLP solution. The upper bound is provided solving the original problem fixing the value of the binary variables (primal problem). The lower bound is obtained from a master problem, where an outer approximation, that is, a linearization of the nonlinear objective and constraints function is performed around the primal solution. The master problem also provides the new combination of binary variables to be fixed in the next primal problem. The original OA is limited to inequality constraints and requires some convexity requirements of the objective and constraints functions (Duran & Grossmann, 1986). To include equality constraints, Kocis and Grossmann (1987) proposed a modification including equation relaxation. Finally, a penalty approach is used to include problems where the convexity conditions may not hold (Viswanathan & Grossmann, 1990). Fletcher and Leyffer (1994) generalized the OA changing the treatment of infeasibilities in the primal problem, formulating a new master problem that includes an original infeasible primal problem, and introducing a unified treatment of exact penalty functions.

Extended cutting plane (ECP) method proposed by Westerlund and Pettersson (1995) is an extension of the cutting plane algortihm to solve MILP. This method follows the same idea that outer aproximation, however, the NLP of the primal problem is replaced by a simple function evaluation. In this method, instead of linearizing all the nonlinear contraints, only the most violated contraint funtion is included in the master problem. ECP require more number of iterations to converge, however, can be more time efficient in those problems where the evaluation of the nonlinear program is hard.

Generalized cross decomposition (GCD) consists of two phases. Phase I includes a primal and a dual subproblem and phase II is the master problem. Additionally, a convergence test is also required. In phase I, the primal problem provides an upper bound of the solution and also Lagrange multipliers for the dual subproblem. The dual subproblem determines a lower bound of the optimal solution and provides a vector of binary variables y to be fixed in the primal problem. Both, the primal and the dual subproblems generate cuts for the master problem. The solution of the primal problem goes through a convergence test based on the multiplier values while the convergence test of the dual solution is based on the binary solution. If any of the convergence tests fails, the algorithm enters

into phase II. The idea is to reduce the number of times that the master problem is solved due to the computational requirements (Floudas, 1995).

Branch and bound is also applied to MINLP problems with a limited number of binary variables., otherwise, finding a solution is computationally expensive. In each of the nodes of the tree, a nonlinear problem is solved where a subset of binary variables is fixed (Grossmann, 2021).

Applications of MINLP emerges in areas such as design and scheduling problems, computer-aided molecular design or integrating design and control of chemical processes (Floudas, 1995).

1.5 structure of the thesis

This thesis is presented as a compendium of scientific articles. Therefore, each of the articles constitutes a chapter of this thesis where only minor formatting changes have been included with respect to the original publication. Supplementary information of each of the works has been attached as appendix of this thesis. The thesis work has been divided into four different parts:

- **Part I: Process design of sustainable ammonia production**: in this section, the attention is focused on the process design of compounds that can be used as bulk chemicals and also as energy storage/carriers. As mentioned above, different chemicals such as methane, methanol, ammonia, etc have been proposed. Ammonia is selected as the object of study for this thesis because is attracting attention due to its paramount properties and the lack of research in the green synthesis of this chemical. This section includes three chapters.
  - **Chapter 3: Optimal renewable production of ammonia from water and air**: this chapter includes an evaluation of the synthesis of green ammonia using renewable electricity from wind/-solar energy sources. At this point, an industrial perspective is used, therefore, nitrogen is produced using cryogenic distillation and hydrogen by water electrolysis.
  - **Chapter 4: Scale up and scale down issues of renewable ammonia plants: Towards modular design**: Distributed synthesis of chemicals using renewables from a modular perspective is attracting attention. In this chapter, a scale-up/down assessment of the synthesis of green ammonia is performed considering the influence of the modular structure on the performance of the units.

    - **Chapter 5: Biomass Based Sustainable Ammonia Production: Digestion vs Gasification**: The use of biomass as a source of chemicals is also envisaged in the new chemical industry. Chapter 5 presents a holistic approach to the production of ammonia from biomass by evaluating the thermochemical and biochemical route.

- **Part II: Transforming Power-to-X fuels into power**: in the previous section, the use of chemicals as energy storage alternatives or as energy carriers is proposed. Currently, research is focused on the different synthesis routes, however, the transformation of these fuels into power must also be evaluated, particularly, from a process perspective. Therefore, in this section, the aim is to determine the optimal transformation of green fuels into power to be used as grid storage infrastructure. One chapter is included in this section:
    - **Chapter 6: Evaluating ammonia as green fuel for power generation: A thermo-chemical perspective**: Ammonia is one of the most promising sustainable fuels, as it does not contain carbon. In this chapter, the thermochemical transformation of ammonia into power is evaluated considering all the stages involved.

- **Part III: Building a new chemical industry**: a complete transformation of the chemical industry is required to meet sustainable requirements and eliminate the use of oil as the main raw material. Therefore, it is necessary to create a new chemical sector based on electrochemical compounds and products derived from biomass as feedstock and trying to eliminate hazardous or non-degradable chemicals. This chapter includes:
    - **Chapter 7: Sustainable DMC production from CO_2 and renewable ammonia and methanol**: DMC is a chemical that is attracting attention because it is a safe reactant with low toxicity and bioaccumulation, fast biodegradability, and excellent solubility in water. Several applications have been proposed as solvents, fuel additive, electrolyte in ion-lithium batteries, etc. A sustainable production based on ammonia, methanol, and carbon dioxide is analyzed in this chapter.

- **Part IV: Operation of Power-to-X processes**: The operation of processes that use as raw material renewable electricity from solar and wind is a challenge due to the inherent fluctuations of these two resources. This fact is also key in determining the plant's capacities to meet a given demand. Therefore, an assessment of the operation

of the Power-to-X processes is required to be able to introduce these facilities in the current chemical and energy sectors. Two chapters are included in this section:

- **Chapter 8: Optimal design of sustainable power-to-fuels supply chains for seasonal energy storage**: Power-to-X fuel can be used to transform power, transportation, heating, etc. sector towards sustainability. In this chapter, an integrated supply chain and scheduling approach is followed to determine the optimal location of power-to-X facilities and also the best operation based on the available resources.
- **Chapter 9: Towards a New Renewable Power System using Energy Storage: an Economic and Social Analysis**: In this chapter, power production is analyzed by integrating different renewable intermittent and non-intermittent renewable sources together with energy storage. Particularly, the combination of wind, solar, and biomass with ion-lithium batteries, hydrogen and methane/ammonia is selected to evaluate an integrated facility ensuring demand satisfaction.

bibliography

Geoffrion, A. M. (1972). Generalized benders decomposition. *Journal of optimization theory and applications*, *10*(4), 237–260. https://doi.org/10.1007/BF00934810

Murtagh, B. A., & Saunders, M. A. (1983). *Minos 5.0 user's guide.* (tech. rep.). Stanford Univ CA Systems Optimization Lab.

Duran, M. A., & Grossmann, I. E. (1986). An outer-approximation algorithm for a class of mixed-integer nonlinear programs. *Mathematical programming*, *36*(3), 307–339. https://doi.org/10.1007/BF02592064

Kocis, G. R., & Grossmann, I. E. (1987). Relaxation strategy for the structural optimization of process flow sheets. *Industrial & engineering chemistry research*, *26*(9), 1869–1880. https://doi.org/10.1021/ie00069a026

Viswanathan, J., & Grossmann, I. (1990). A combined penalty function and outer-approximation method for minlp optimization. *Computers & Chemical Engineering*, *14*(7), 769–782. https://doi.org/10.1016/0098-1354(90)87085-4

Fletcher, R., & Leyffer, S. (1994). Solving mixed integer nonlinear programs by outer approximation. *Mathematical programming*, *66*(1), 327–349. https://doi.org/10.1007/BF01581153

Anderson, J. D., & Wendt, J. (1995). *Computational fluid dynamics* (Vol. 206). Springer.

Floudas, C. A. (1995). *Nonlinear and mixed-integer optimization: Fundamentals and applications*. Oxford University Press.

Loeppert, R. H., Schwab, A. P., & Goldberg, S. (1995). *Chemical equilibrium and reaction models*. Soil Science Society of America.

Westerlund, T., & Pettersson, F. (1995). An extended cutting plane method for solving convex minlp problems. *Computers & Chemical Engineering*, *19*, 131–136. https://doi.org/10.1016/0098-1354(95)87027-X

Anastas, P. T., & Williamson, T. C. (1996). *Green chemistry: Designing chemistry for the environment*. ACS Publications.

Drud, A. S. (1996). Conopt: A system for large scale nonlinear optimisation. *Reference manual for CONPOT subroutine library*.

Bertsimas, D., & Tsitsiklis, J. N. (1997). *Introduction to linear optimization* (Vol. 6). Athena Scientific Belmont, MA.

Gill, P. E., Murray, W., & Saunders, M. A. (1997). User's guide for snopt 5.3: A fortran package for large-scale nonlinear programming.

Himmelblau, D. M. (2000). Applications of artificial neural networks in chemical engineering. *Korean journal of chemical engineering*, *17*(4), 373–392. https://doi.org/10.1007/BF02706848

Couper, J. R., Penney, W. R., Fair, J. R., & Walas, S. M. (2005). *Chemical process equipment: Selection and design*. Gulf Professional Publishing.

Queipo, N. V., Haftka, R. T., Shyy, W., Goel, T., Vaidyanathan, R., & Kevin Tucker, P. (2005). Surrogate-based analysis and optimization. *Progress in Aerospace Sciences*, *41*(1), 1–28. https://doi.org/10.1016/j.paerosci.2005.02.001

Byrd, R. H., Nocedal, J., & Waltz, R. A. (2006). Knitro: An integrated package for nonlinear optimization. *Large-scale nonlinear optimization* (pp. 35–59). Springer.

Wächter, A., & Biegler, L. T. (2006). On the implementation of an interior-point filter line-search algorithm for large-scale nonlinear programming. *Mathematical programming*, *106*(1), 25–57. https://doi.org/10.1007/s10107-004-0559-y

Mathworks, T. (2007). Matlab optimization toolbox user's guide. *Math Work*.

Szirtes, T. (2007). *Applied dimensional analysis and modeling*. Butterworth-Heinemann.

Bazaraa, M. S., Jarvis, J. J., & Sherali, H. D. (2008). *Linear programming and network flows*. John Wiley & Sons.

European Council. (2008). Directive 2008/98/ec of the european parliament and of the council of 19 november 2008 on waste and repealing certain directives. *Official Journal of the European Union L*, *312*(3).

Buzzi-Ferraris, G., & Manenti, F. (2009). Kinetic models analysis. *Chemical Engineering Science*, *64*(5), 1061–1074. https://doi.org/10.1016/j.ces.2008.10.062

FICO. (2009). Xpress optimization suite. *Xpress-Optimizer, Reference manual, Fair Isaac Corporation*.

ILOG, I. (2009). V12. 1: User's manual for cplex. *International Business Machines Corporation*, *46*(53), 157.

Story, M., Hamm, M. W., & Wallinga, D. (2009). Food systems and public health: Linkages to achieve healthier diets and healthier communities. *Journal of Hunger & Environmental Nutrition*, *4*(3-4), 219–224. https://doi.org/10.1080/19320240903351463

Anastas, P., & Eghbali, N. (2010). Green chemistry: Principles and practice. *Chem. Soc. Rev.*, *39*, 301–312. https://doi.org/10.1039/B918763B

Biegler, L. T. (2010). *Nonlinear programming: Concepts, algorithms, and applications to chemical processes*. SIAM.

Bozell, J. J., & Petersen, G. R. (2010). Technology development for the production of biobased products from biorefinery carbohydrates—the us department of energy's "top 10" revisited. *Green Chem.*, *12*, 539–554. https://doi.org/10.1039/B922014C

Könst, P. M., Turras, P. M. C. C. D., Franssen, M. C. R., Scott, E. L., & Sanders, J. P. M. (2010). Stabilized and immobilized bacillus subtilis arginase for the biobased production of nitrogen-containing chemicals. *Advanced Synthesis & Catalysis*, *352*(9), 1493–1502. https://doi.org/10.1002/adsc.201000034

Schwarzenbach, R. P., Egli, T., Hofstetter, T. B., Von Gunten, U., & Wehrli, B. (2010). Global water pollution and human health. *Annual review of environment and resources*, *35*, 109–136. https://doi.org/10.1146/annurev-environ-100809-125342

Gupta, M., Smith, M. L., & Spivey, J. J. (2011). Heterogeneous catalytic conversion of dry syngas to ethanol and higher alcohols on cu-based catalysts. *ACS Catalysis*, *1*(6), 641–656. https://doi.org/10.1021/cs2001048

Lammens, T. M., Potting, J., Sanders, J. P. M., & De Boer, I. J. M. (2011). Environmental comparison of biobased chemicals from glutamic acid with their petrochemical equivalents. *Environmental Science & Technology*, *45*(19), 8521–8528. https://doi.org/10.1021/es201869e

Martín, M., & Grossmann, I. E. (2011). Energy optimization of bioethanol production via gasification of switchgrass. *AIChE Journal*, *57*(12), 3408–3428. https://doi.org/10.1002/aic.12544

European Commission. (2012). Energy: Roadmap 2050. Retrieved May 9, 2020, from https://ec.europa.eu/energy/sites/ener/files/documents/2012_energy_roadmap_2050_en_0.pdf

Hall, S. M. (2012). *Rules of thumb for chemical engineers*. Butterworth-Heinemann.

Holmgren, K. M., Berntsson, T., Andersson, E., & Rydberg, T. (2012). System aspects of biomass gasification with methanol synthesis – process concepts and energy analysis. *Energy*, *45*(1), 817–828. https://doi.org/10.1016/j.energy.2012.07.009

Martín, M., & Grossmann, I. E. (2012). Biopt: A library of models for optimization of biofuel production processes. In I. D. L. Bogle & M. Fairweather (Eds.), *22nd european symposium on computer aided process engineering* (pp. 16–20). Elsevier. https://doi.org/10.1016/B978-0-444-59519-5.50004-6

Tuck, C. O., Pérez, E., Horváth, I. T., Sheldon, R. A., & Poliakoff, M. (2012). Valorization of biomass: Deriving more value from waste. *Science*, *337*(6095), 695–699.

Bazaraa, M. S., Sherali, H. D., & Shetty, C. M. (2013). *Nonlinear programming: Theory and algorithms*. John Wiley & Sons.

Brignole, E. A., & Pereda, S. (2013). *Phase equilibrium engineering*. Newnes.

Haro, P., Ollero, P., Villanueva Perales, A., & Gómez-Barea, A. (2013). Thermochemical biorefinery based on dimethyl ether as intermediate: Technoeconomic assessment [Special Issue on Advances in sustainable biofuel production and use - XIX International Symposium on Alcohol Fuels - ISAF]. *Applied Energy*, *102*, 950–961. https://doi.org/10.1016/j.apenergy.2012.09.051

van der Zwaan, B., Keppo, I., & Johnsson, F. (2013). How to decarbonize the transport sector? *Energy Policy*, *61*, 562–573. https://doi.org/10.1016/j.enpol.2013.05.118

Andersson, J., & Lundgren, J. (2014). Techno-economic analysis of ammonia production via integrated biomass gasification. *Applied Energy*, *130*, 484–490. https://doi.org/10.1016/j.apenergy.2014.02.029

Conforti, M., Cornuéjols, G., Zambelli, G., et al. (2014). *Integer programming* (Vol. 271). Springer.

Davis, W., & Martín, M. (2014). Optimal year-round operation for methane production from co2 and water using wind and/or solar energy. *Journal of Cleaner Production*, *80*, 252–261. https://doi.org/10.1016/j.jclepro.2014.05.077

Haro, P., Villanueva Perales, Á. L., Arjona, R., & Ollero, P. (2014). Thermochemical biorefineries with multiproduction using a platform chemical. *Biofuels, Bioproducts and Biorefining*, *8*(2), 155–170. https://doi.org/10.1002/bbb.1465

Sadhukhan, J., Ng, K. S., & Hernandez, E. M. (2014). *Biorefineries and chemical processes: Design, integration and sustainability analysis*. John Wiley & Sons.

Albo, J., Alvarez-Guerra, M., Castaño, P., & Irabien, A. (2015). Towards the electrochemical conversion of carbon dioxide into methanol. *Green Chem.*, *17*, 2304–2324. https://doi.org/10.1039/C4GC02453B

Chaudry, M., Abeysekera, M., Hosseini, S. H. R., Jenkins, N., & Wu, J. (2015). Uncertainties in decarbonising heat in the uk. *Energy Policy*, *87*, 623–640. https://doi.org/10.1016/j.enpol.2015.07.019

Compound Interest. (2015). The twelve principles of green chemistry: What it is, & why it matters. Retrieved July 7, 2021, from https://www.compoundchem.com/2015/09/24/green-chemistry/

Diouf, B., & Pode, R. (2015). Potential of lithium-ion batteries in renewable energy. *Renewable Energy*, *76*, 375–380. https://doi.org/10.1016/j.renene.2014.11.058

Kongpanna, P., Pavarajarn, V., Gani, R., & Assabumrungrat, S. (2015). Techno-economic evaluation of different co2-based processes for dimethyl carbonate production. *Chemical Engineering Research and Design*, *93*, 496–510. https://doi.org/10.1016/j.cherd.2014.07.013

Matzen, M., Alhajji, M., & Demirel, Y. (2015). Chemical storage of wind energy by renewable methanol production: Feasibility analysis using a multi-criteria decision matrix. *Energy*, *93*, 343–353. https://doi.org/10.1016/j.energy.2015.09.043

Pellow, M. A., Emmott, C. J. M., Barnhart, C. J., & Benson, S. M. (2015). Hydrogen or batteries for grid storage? a net energy analysis. *Energy Environ. Sci.*, *8*, 1938–1952. https://doi.org/10.1039/C4EE04041D

Quirante, N., Javaloyes, J., & Caballero, J. A. (2015). Rigorous design of distillation columns using surrogate models based on kriging interpolation. *AIChE Journal*, *61*(7), 2169–2187. https://doi.org/10.1002/aic.14798

Tian, P., Wei, Y., Ye, M., & Liu, Z. (2015). Methanol to olefins (mto): From fundamentals to commercialization. *ACS Catalysis*, *5*(3), 1922–1938. https://doi.org/10.1021/acscatal.5b00007

UN General Assembly. (2015). Transforming our world: The 2030 agenda for sustainable development. *Division for Sustainable Development Goals: New York, NY, USA*.

Vidal, M., & Martín, M. (2015). Optimal coupling of a biomass based polygeneration system with a concentrated solar power facility for the constant production of electricity over a year. *Computers & Chemical Engineering*, *72*, 273–283. https://doi.org/10.1016/j.compchemeng.2013.11.006

Corporate Citizenship. (2016). Sdgs & sectors: A review of the business opportunities. *London (UK): Corporate Citizenship*.

Hernández, B., & Martín, M. (2016). Optimal process operation for biogas reforming to methanol: Effects of dry reforming and biogas compo-

sition. *Industrial & Engineering Chemistry Research*, *55*(23), 6677–6685. https://doi.org/10.1021/acs.iecr.6b01044

Khanmohammadi, M., Amani, S., Garmarudi, A. B., & Niaei, A. (2016). Methanol-to-propylene process: Perspective of the most important catalysts and their behavior. *Chinese Journal of Catalysis*, *37*(3), 325–339. https://doi.org/10.1016/S1872-2067(15)61031-2

Mekonnen, M. M., & Hoekstra, A. Y. (2016). Four billion people facing severe water scarcity. *Science advances*, *2*(2), e1500323. https://doi.org/10.1126/sciadv.1500323

Sanz-Pérez, E. S., Murdock, C. R., Didas, S. A., & Jones, C. W. (2016). Direct capture of co2 from ambient air. *Chemical Reviews*, *116*(19), 11840–11876. https://doi.org/10.1021/acs.chemrev.6b00173

Bibri, S. E., & Krogstie, J. (2017). Smart sustainable cities of the future: An extensive interdisciplinary literature review. *Sustainable Cities and Society*, *31*, 183–212. https://doi.org/10.1016/j.scs.2017.02.016

Brandon, N., & Kurban, Z. (2017). Clean energy and the hydrogen economy. *Philosophical Transactions of the Royal Society A: Mathematical, Physical and Engineering Sciences*, *375*(2098), 20160400. https://doi.org/10.1098/rsta.2016.0400

Hankin, A., & Shah, N. (2017). Process exploration and assessment for the production of methanol and dimethyl ether from carbon dioxide and water. *Sustainable Energy Fuels*, *1*, 1541–1556. https://doi.org/10.1039/C7SE00206H

Liu, J., Yang, H., Gosling, S. N., Kummu, M., Flörke, M., Pfister, S., Hanasaki, N., Wada, Y., Zhang, X., Zheng, C., Alcamo, J., & Oki, T. (2017). Water scarcity assessments in the past, present, and future. *Earth's Future*, *5*(6), 545–559. https://doi.org/10.1002/2016EF000518

Pyo, S.-H., Park, J. H., Chang, T.-S., & Hatti-Kaul, R. (2017). Dimethyl carbonate as a green chemical. *Current Opinion in Green and Sustainable Chemistry*, *5*, 61–66. https://doi.org/10.1016/j.cogsc.2017.03.012

Ripple, W. J., Wolf, C., Newsome, T. M., Galetti, M., Alamgir, M., Crist, E., Mahmoud, M. I., Laurance, W. F., & 15, 3. S. S. f. 1. C. (2017). World scientists' warning to humanity: A second notice. *BioScience*, *67*(12), 1026–1028. https://doi.org/10.1093/biosci/bix125

Schiffer, Z. J., & Manthiram, K. (2017). Electrification and decarbonization of the chemical industry. *Joule*, *1*(1), 10–14. https://doi.org/10.1016/j.joule.2017.07.008

Simon, E. (2017). Green ammonia. refuel kickoff meeting. Retrieved May 7, 2021, from https://arpa-e.energy.gov/sites/default/files/04c%20Denver-Green%20Ammonia-Siemens-final.pdf

Sioshansi, R., & Conejo, A. J. (2017). Optimization in engineering. *Cham: Springer International Publishing*, *120*.

Tilman, D., Clark, M., Williams, D. R., Kimmel, K., Polasky, S., & Packer, C. (2017). Future threats to biodiversity and pathways to their prevention. *Nature*, *546*(7656), 73–81. https://doi.org/10.1038/nature22900

Bui, M., Adjiman, C. S., Bardow, A., Anthony, E. J., Boston, A., Brown, S., Fennell, P. S., Fuss, S., Galindo, A., Hackett, L. A., Hallett, J. P., Herzog, H. J., Jackson, G., Kemper, J., Krevor, S., Maitland, G. C., Matuszewski, M., Metcalfe, I. S., Petit, C., … Mac Dowell, N. (2018). Carbon capture and storage (ccs): The way forward. *Energy Environ. Sci.*, *11*, 1062–1176. https://doi.org/10.1039/C7EE02342A

Corengia, M., & Torres, A. I. (2018). Effect of tariff policy and battery degradation on optimal energy storage. *Processes*, *6*(10), 204. https://doi.org/10.3390/pr6100204

Ghaib, K., & Ben-Fares, F.-Z. (2018). Power-to-methane: A state-of-the-art review. *Renewable and Sustainable Energy Reviews*, *81*, 433–446. https://doi.org/10.1016/j.rser.2017.08.004

Gür, T. M. (2018). Review of electrical energy storage technologies, materials and systems: Challenges and prospects for large-scale grid storage. *Energy Environ. Sci.*, *11*, 2696–2767. https://doi.org/10.1039/C8EE01419A

IRENA. (2018). Global energy transformation: A roadmap to 2050.

United Nations. (2018). The paris agreement. Retrieved May 7, 2020, from https://unfccc.int/process-and-meetings/the-paris-agreement/the-paris-agreement

Allman, A., Palys, M. J., & Daoutidis, P. (2019). Scheduling-informed optimal design of systems with time-varying operation: A wind-powered ammonia case study. *AIChE Journal*, *65*(7), e16434. https://doi.org/10.1002/aic.16434

Bagheri, M., Delbari, S. H., Pakzadmanesh, M., & Kennedy, C. A. (2019). City-integrated renewable energy design for low-carbon and climate-resilient communities. *Applied Energy*, *239*, 1212–1225. https://doi.org/10.1016/j.apenergy.2019.02.031

Guo, L., Chen, Y., Su, J., Liu, M., & Liu, Y. (2019). Obstacles of solar-powered photocatalytic water splitting for hydrogen production: A perspective from energy flow and mass flow. *Energy*, *172*, 1079–1086. https://doi.org/10.1016/j.energy.2019.02.050

Kätelhön, A., Meys, R., Deutz, S., Suh, S., & Bardow, A. (2019). Climate change mitigation potential of carbon capture and utilization in the chemical industry. *Proceedings of the National Academy of Sciences*, *116*(23), 11187–11194. https://doi.org/10.1073/pnas.1821029116

Li, Z., Khajepour, A., & Song, J. (2019). A comprehensive review of the key technologies for pure electric vehicles. *Energy*, *182*, 824–839. https://doi.org/10.1016/j.energy.2019.06.077

Nunez, S., Arets, E., Alkemade, R., Verwer, C., & Leemans, R. (2019). Assessing the impacts of climate change on biodiversity: Is below 2° c enough? *Climatic Change*, *154*(3), 351–365. https://doi.org/10.1007/s10584-019-02420-x

Schmidt, J., Gruber, K., Klingler, M., Klöckl, C., Ramirez Camargo, L., Regner, P., Turkovska, O., Wehrle, S., & Wetterlund, E. (2019). A new perspective on global renewable energy systems: Why trade in energy carriers matters. *Energy Environ. Sci.*, *12*, 2022–2029. https://doi.org/10.1039/C9EE00223E

Schmidt, O., Melchior, S., Hawkes, A., & Staffell, I. (2019). Projecting the future levelized cost of electricity storage technologies. *Joule*, *3*(1), 81–100. https://doi.org/10.1016/j.joule.2018.12.008

Verhelst, S., Turner, J. W., Sileghem, L., & Vancoillie, J. (2019). Methanol as a fuel for internal combustion engines. *Progress in Energy and Combustion Science*, *70*, 43–88. https://doi.org/10.1016/j.pecs.2018.10.001

Bartela, L. (2020). A hybrid energy storage system using compressed air and hydrogen as the energy carrier. *Energy*, *196*, 117088. https://doi.org/10.1016/j.energy.2020.117088

Bellocchi, S., Manno, M., Noussan, M., Prina, M. G., & Vellini, M. (2020). Electrification of transport and residential heating sectors in support of renewable penetration: Scenarios for the italian energy system. *Energy*, *196*, 117062. https://doi.org/10.1016/j.energy.2020.117062

Blanco, H., Codina, V., Laurent, A., Nijs, W., Maréchal, F., & Faaij, A. (2020). Life cycle assessment integration into energy system models: An application for power-to-methane in the eu. *Applied Energy*, *259*, 114160. https://doi.org/10.1016/j.apenergy.2019.114160

BloombergNEF. (2020). New energy outlook 2020. Retrieved December 1, 2020, from https://about.bnef.com/new-energy-outlook/

Cabrera Camacho, C. E., Alonso-Fariñas, B., Villanueva Perales, A. L., Vidal-Barrero, F., & Ollero, P. (2020). Techno-economic and life-cycle assessment of one-step production of 1,3-butadiene from bioethanol using reaction data under industrial operating conditions. *ACS Sustainable Chemistry & Engineering*, *8*(27), 10201–10211. https://doi.org/10.1021/acssuschemeng.0c02678

Carley, S., & Konisky, D. M. (2020). The justice and equity implications of the clean energy transition. *Nature Energy*, *5*(8), 569–577. https://doi.org/10.1038/s41560-020-0641-6

Chen, T., Jin, Y., Lv, H., Yang, A., Liu, M., Chen, B., Xie, Y., & Chen, Q. (2020). Applications of lithium-ion batteries in grid-scale energy storage systems. *Transactions of Tianjin University*, *26*(3), 208–217. https://doi.org/10.1007/s12209-020-00236-w

de la Fuente, E., & Martín, M. (2020). Site specific process design for hybrid csp-waste plants. *Computers & Chemical Engineering*, *135*, 106770. https://doi.org/10.1016/j.compchemeng.2020.106770

dos Santos, R. G., & Alencar, A. C. (2020). Biomass-derived syngas production via gasification process and its catalytic conversion into fuels by fischer tropsch synthesis: A review. *International Journal of Hydrogen Energy*, *45*(36), 18114–18132. https://doi.org/10.1016/j.ijhydene.2019.07.133

Heras, J., & Martín, M. (2020). Social issues in the energy transition: Effect on the design of the new power system. *Applied Energy*, *278*, 115654. https://doi.org/10.1016/j.apenergy.2020.115654

Internacional Energy Agency. (2020). Chemicals. Retrieved October 8, 2020, from https://www.iea.org/reports/chemicals

Kuznetsov, A., Kumar, G., Ardagh, M. A., Tsapatsis, M., Zhang, Q., & Dauenhauer, P. J. (2020). On the economics and process design of renewable butadiene from biomass-derived furfural. *ACS Sustainable Chemistry & Engineering*, *8*(8), 3273–3282. https://doi.org/10.1021/acssuschemeng.9b06881

Landrigan, P. J., Stegeman, J. J., Fleming, L. E., Allemand, D., Anderson, D. M., Backer, L. C., Brucker-Davis, F., Chevalier, N., Corra, L., Czerucka, D., et al. (2020). Human health and ocean pollution. *Annals of global health*, *86*(1). https://doi.org/10.5334/aogh.2831

MacFarlane, D. R., Cherepanov, P. V., Choi, J., Suryanto, B. H., Hodgetts, R. Y., Bakker, J. M., Ferrero Vallana, F. M., & Simonov, A. N. (2020). A roadmap to the ammonia economy. *Joule*, *4*(6), 1186–1205. https://doi.org/10.1016/j.joule.2020.04.004

Manisalidis, I., Stavropoulou, E., Stavropoulos, A., & Bezirtzoglou, E. (2020). Environmental and health impacts of air pollution: A review. *Frontiers in Public Health*, *8*, 14. https://doi.org/10.3389/fpubh.2020.00014

Ministerio para la Transicion Ecologica y el Reto Demografico. (2020a). Estrategia de descarbonizacion a largo plazo 2050. Retrieved June 7, 2020, from https://www.miteco.gob.es/es/prensa/documentoelp_tcm30-516109.pdf

Ministerio para la Transicion Ecologica y el Reto Demografico. (2020b). Plan nacional integrado de energía y clima (pniec) 2021-2030. Retrieved June 7, 2020, from https://www.miteco.gob.es/es/prensa/pniec.aspx

Pappijn, C., Reyniers, M.-F., Van Geem, K., et al. (2020). Challenges and opportunities of carbon capture and utilization: Electrochemical conversion of co2 to ethylene. *Frontiers In Chemical Engineering*, *8*.

Proman. (2020). Proman to build world's largest green methanol plant at north sea renewables hub. Retrieved December 10, 2020, from https://www.proman.org/news/proman-to-build-worlds-largest-green-methanol-plant-at-north-sea-renewables-hub/

Ritchie, H., & Roser, M. (2020a). Co2 and greenhouse gas emissions. *Our World in Data*. https://ourworldindata.org/co2-and-other-greenhouse-gas-emissions

Ritchie, H., & Roser, M. (2020b). Energy. *Our World in Data*. https://ourworldindata.org/energy

Ritchie, H., & Roser, M. (2020c). Environmental impacts of food production. *Our World in Data*. https://ourworldindata.org/environmental-impacts-of-food

Siddiqui, O., & Dincer, I. (2020). Experimental investigation of a sustainable integrated ammonia synthesis and fuel cell system. *Fuel*, *278*, 118300. https://doi.org/10.1016/j.fuel.2020.118300

Springer, N., & Daue, A. (2020). *Key economic benefits of renewable energy on public lands* (tech. rep.). Yale Center for Business and the Environment.

Stančin, H., Mikulčić, H., Wang, X., & Duić, N. (2020). A review on alternative fuels in future energy system. *Renewable and Sustainable Energy Reviews*, *128*, 109927. https://doi.org/10.1016/j.rser.2020.109927

Sunny, N., Mac Dowell, N., & Shah, N. (2020). What is needed to deliver carbon-neutral heat using hydrogen and ccs? *Energy Environ. Sci.*, *13*, 4204–4224. https://doi.org/10.1039/D0EE02016H

Zhang, H., Wang, L., Van herle, J., Maréchal, F., & Desideri, U. (2020). Techno-economic comparison of green ammonia production processes. *Applied Energy*, *259*, 114135. https://doi.org/10.1016/j.apenergy.2019.114135

D'Angelo, S. C., Cobo, S., Tulus, V., Nabera, A., Martín, A. J., Pérez-Ramírez, J., & Guillén-Gosálbez, G. (2021). Planetary boundaries analysis of low-carbon ammonia production routes. *ACS Sustainable Chemistry & Engineering*, *9*(29), 9740–9749. https://doi.org/10.1021/acssuschemeng.1c01915

European Commission. (2021a). 2050 long-term strategy. Retrieved May 8, 2020, from https://ec.europa.eu/clima/policies/strategies/2050_en

European Commission. (2021b). Recovery plan for europe. Retrieved May 10, 2020, from https://ec.europa.eu/info/strategy/recovery-plan-europe_en

Galán, G., Martín, M., & Grossmann, I. E. (2021). Integrated renewable production of sorbitol and xylitol from switchgrass. *Industrial & Engineering Chemistry Research*, *60*(15), 5558–5573. https://doi.org/10.1021/acs.iecr.1c00397

Gobierno de España. (2021). Plan de recuperación, tranformación y resiliencia. Retrieved June 7, 2021, from https://www.lamoncloa.gob.es/temas/fondos-recuperacion/Documents/30042021-Plan_Recuperacion_%20Transformacion_%20Resiliencia.pdf

Grossmann, I. E. (2021). *Advanced optimization for process systems engineering*. Cambridge University Press.

Gurobi Optimization. (2021). Gurobi Optimizer Reference Manual. https://www.gurobi.com

Iberdrola. (2021a). The big global environmental issues we need to resolve by 2030. Retrieved December 8, 2020, from https://www.iberdrola.com/environment/most-important-environmental-issues

Iberdrola. (2021b). Iberdrola builds the largest green hydrogen plant for industrial use in europe. Retrieved December 9, 2020, from https://www.iberdrola.com/about-us/lines-business/flagship-projects/puertollano-green-hydrogen-plant

Ministerio de Industria, Comercio y Turismo. (2021). Perte para el desarollo del vehiculo electrico y conectado. Retrieved June 7, 2021, from https://www.mincotur.gob.es/es-es/recuperacion-transformacion-resiliencia/Paginas/perte.aspx

Ministerio para la Transicion Ecologica y el Reto Demografico. (2021a). Estrategia de almacenamiento energetico. Retrieved June 7, 2021, from https://www.miteco.gob.es/es/prensa/ultimas-noticias/el-gobierno-aprueba-la-estrategia-de-almacenamiento-energ%C3%A9tico-clave-para-garantizar-la-seguridad-del-suministro-y-precios-m%C3%A1s-bajos-de-la-energ/tcm:30-522653

Ministerio para la Transicion Ecologica y el Reto Demografico. (2021b). Transicion justa. Retrieved May 8, 2021, from https://www.miteco.gob.es/es/transicion-justa/default.aspx

Montgomery, D. C., Peck, E. A., & Vining, G. G. (2021). *Introduction to linear regression analysis*. John Wiley & Sons.

Oberthür, S., Khandekar, G., & Wyns, T. (2021). Global governance for the decarbonization of energy intensive industries: Great potential underexploited. *Earth System Governance*, *8*, 100072. https://doi.org/10.1016/j.esg.2020.100072

Pistikopoulos, E. N., Barbosa-Povoa, A., Lee, J. H., Misener, R., Mitsos, A., Reklaitis, G. V., Venkatasubramanian, V., You, F., & Gani, R. (2021). Process systems engineering – the generation next? *Computers &*

Chemical Engineering, *147*, 107252. https://doi.org/10.1016/j.compchemeng.2021.107252

The World Bank. (2021). Trends in solid waste management. https://datatopics.worldbank.org/what-a-waste/trends_in_solid_waste_management.html

Thomaßen, G., Kavvadias, K., & Jiménez Navarro, J. P. (2021). The decarbonisation of the eu heating sector through electrification: A parametric analysis. *Energy Policy*, *148*, 111929. https://doi.org/10.1016/j.enpol.2020.111929

Trew, B. T., & Maclean, I. M. D. (2021). Vulnerability of global biodiversity hotspots to climate change. *Global Ecology and Biogeography*, *30*(4), 768–783. https://doi.org/10.1111/geb.13272

Valente, A., Tulus, V., Galán-Martín, Á., Huijbregts, M. A. J., & Guillén-Gosálbez, G. (2021). The role of hydrogen in heavy transport to operate within planetary boundaries. *Sustainable Energy Fuels*, *5*, 4637–4649. https://doi.org/10.1039/D1SE00790D

Van Hoecke, L., Laffineur, L., Campe, R., Perreault, P., Verbruggen, S. W., & Lenaerts, S. (2021). Challenges in the use of hydrogen for maritime applications. *Energy Environ. Sci.*, *14*, 815–843. https://doi.org/10.1039/D0EE01545H

Vázquez, D., & Guillén-Gosálbez, G. (2021). Process design within planetary boundaries: Application to co2 based methanol production. *Chemical Engineering Science*, *246*, 116891. https://doi.org/10.1016/j.ces.2021.116891

Zang, G., Sun, P., Elgowainy, A., & Wang, M. (2021). Technoeconomic and life cycle analysis of synthetic methanol production from hydrogen and industrial byproduct co2. *Environmental Science & Technology*, *55*(8), 5248–5257. https://doi.org/10.1021/acs.est.0c08237

2

OBJECTIVES

The main objective of this thesis is the assessment of Power-to-X processes, particularly focusing on Power-to-Ammonia, to decarbonize the chemical industry, replacing the traditional production of different bulk chemicals, and the energy sector, where Power-to-X alternatives could be used as an energy carrier for different applications and as an energy storage system to address fluctuations of variable renewable resources in the new power system. The specific objectives of the thesis can be summarized as follow:

- To evaluate the sustainable production of ammonia using renewable electricity via water electrolysis on an industrial scale. The goal is to determine the optimal operating conditions of the process and the economic performance of this system in order to substitute the traditional non-renewable production.
- To perform a scale-up/down study of the synthesis of renewable ammonia by water electrolysis. An electrolyzer is a modular unit that can be easily adapted to different production capacities. However, for air separation, different technologies are proposed depending on the flow requirements. A techno-economic comparison of these technologies is carried out for different production capacities considering power from renewable sources.
- To determine the potential of using biomass as a resource for green ammonia production. The use of biomass as a source of chemicals is widely proposed (as presented in the introduction). A holistic evaluation is required considering thermochemical and biochemical technologies in biomass processing.
- If ammonia or other chemicals are used as an energy storage system in power production, it is necessary to evaluate the transformation of these chemicals into power. In particular, this thesis focuses on the transformation of ammonia into power through its combustion (thermochemical route). With this evaluation, the technical performance and the cost of electricity for this storage alternative are determined to provide powerful tools to implement this storage technology in real applications.

- To propose new chemical processes to build a new chemical industry based on the principles of green chemistry. More specifically, the synthesis of dimethyl carbonate (DMC) is studied in this thesis using renewable chemicals produced with green hydrogen and carbon dioxide.

- When renewable energies are used as the feedstock of chemical processes, two main questions arise: the location of the facilities due to the distribution of wind/solar resources and the operation of these facilities due to the inherent fluctuations of the variable renewable energies. The objective is, therefore, to integrate these two perspectives. In particular, the synthesis of energy carriers for different energy applications is analyzed by considering the distribution of these fuels (supply chain) and design and operation of the facilities (design and scheduling). Methodologies to solve these kinds of large-scale problems have been also evaluated in this thesis.

- To determine the optimal operation of an integrated facility where different intermittent and non-intermittent renewables and energy storage technologies are considered to guarantee demand satisfaction. The cost of electricity will be calculated when the storage alternatives are introduced for different locations. In parallel, a social perspective of the energy transition is also required to mitigate the social disturbances generated. At this point, this thesis also addresses the problem of how to measure this social impact in a concrete way.

Part I

PROCESS DESIGN OF SUSTAINABLE AMMONIA PRODUCTION

3

OPTIMAL RENEWABLE PRODUCTION OF AMMONIA FROM WATER AND AIR

abstract

In this work a production facility of ammonia has been evaluated using air and water as raw materials. Nitrogen is obtained from air separation using a Linde's double column. Hydrogen is produced from water splitting using solar, photovoltaic, or wind energy. Next, hydrogen and oxygen are purified to remove water and traces of chemicals. Finally, ammonia is synthesized in a three bed packed reactor. Two cooling designs were considered, indirect and direct cooling. The ammonia is recovered by condensation using the cold air. The process is simulated developing surrogate models for each of the units involved with special attention to the electrolyzer, Linde's column, synthesis reactor and ammonia recovery. In particular, the multibed reactor is modeled rigorously off line to validate the conversions and its operation. The full process is formulated as an MINLP problem. Solar energy and indirect cooling are selected for the production of ammonia. However, the high cost of panels results in high investment capital, over 1500M€, but promising production cost of ammonia, 1.35 €/kg.

Keywords: Air, Ammonia, Hydrogen, Process Optimization, Solar Energy, Water, Wind Energy

resumen

En este trabajo se ha evaluado una instalación de producción de amoníaco utilizando aire y agua como materias primas. El nitrógeno se obtiene a partir de la separación del aire utilizando una doble columna de Linde. El hidrógeno se produce a partir de la rotura del agua utilizando energía solar fotovoltaica o eólica. A continuación, el hidrógeno y el oxígeno se purifican para eliminar el agua y los restos de sustancias químicas. Por último, el amoníaco se sintetiza en un reactor de tres lechos. Se han considerado dos diseños de refrigeración, indirecta y directa. El amoníaco se recupera por condensación utilizando el aire frío. El proceso se simula desarrollando modelos surrogados para cada una de las unidades implicadas, con especial atención al electrolizador, la columna de Linde, el reactor de síntesis y la recuperación de amoníaco. En particular, el reactor multilecho se modela rigurosamente fuera del programa principal para validar las conversiones y su funcionamiento. El proceso completo se formula como un problema MINLP. Para la producción de amoníaco se selecciona la energía solar y la refrigeración indirecta. Sin embargo, el elevado coste de los paneles se traduce en un alto capital de inversión, más de 1500M€, pero un prometedor coste de producción de amoníaco, 1,35€/kg.

Palabras Clave: Aire, Amoniaco, Hidrógeno, Optimización de procesos, Energía solar, Agua, Energía eólica

3.1 introduction

The increasing demand of energy and current concerns on sustainability are supporting the development of technologies which use solar radiance, wind and biomass. While biomass is a carbon source and thus, it can be considered as a source of chemicals, the use of wind and solar energy is typically devoted to the production of electricity. One of the main features of renewable sources of energy is their variability across regions and over time. In particular, renewable sources such as solar and wind constitute a major challenge due to their availability during the day and during the year. In order for the facilities based on these resources to operate under steady state, storage systems, supplementary sources of energy or a combination of some of them are needed. Weekman (2010) and Yuan and Chen (2012) presented overviews regarding the integration possibilities as a perspective for the future combination of different sources of energy. There have been several attempts to design processes that mitigate the effect of that variability. For instance, the use of molten salts to store solar energy for several hours so that concentrated solar plants can operate continuously during a day (L. Martín & Martín, 2013). Alternatively, it is possible to store solar and wind energy in the form of chemicals, i.e methane, for its further use when needed. Davis and Martín (2014b) evaluated the production of methane from CO_2 using wind energy over a year. Solar or wind based facilities on their own cannot maintain the production level without combining different energy sources, but the high cost of the power island of the facilities mitigates the investment in idle chemical units overtime (Davis & Martín, 2014a). The advantage of producing chemicals directly out of the renewable energy is that they can be stored and used downstream on a continuous basis

Ammonia is another interesting product not only because it can be used to store solar or wind energy but also as hydrogen carrier for the so-call hydrogen economy (Agrawal et al., 2005). The production of ammonia is an example of the fact that the chemical industry is unique in its possibilities to develop alternative routes to the same final product, even using different raw materials. Ammonia was first recovered from the coal gas industry. The increase in the demand for ammonia as a result of its use to produce nitric acid presented a new paradigm. In order not to use Chile saltpeter, saving it for the fertilizers industry, Frederic Kulmann evaluated the oxidation of ammonia over platinum. Years later, Haber and Bosch designed the process to produce ammonia from hydrogen and nitrogen. However, ammonia can be also produced from nitrogen and hydrogen directly (Ernst et al., 1925).

The source of hydrogen is natural gas in 60%-70% of the facilities (Appl, 2011). Hydrogen has been produced using renewable energy since 1923 (Haldane, 1924). However, the development was not pursued any further again until the 70's, when photovoltaic systems attracted the attention (Bockris, 1975). Thirty years later, the use of solar and wind energy received attention again within the research community and several studies were presented that evaluated the production of hydrogen from solar (Levene et al., 2005) and wind energy (Levene et al., 2006). The results showed that for hydrogen to be competitive, cheaper power was needed. Recently, life cycle assessment studies have also been developed to compare renewable technologies for the production of hydrogen. The use of biomethane reforming was the one presenting the lowest impact (Hajjaji et al., 2013), but water electrolysis was not included in the study. Finally, Ozbilen et al. (2012) evaluated water splitting using thermochemical cycles to decide on the steps. Bhandari et al. (2014) concluded that water electrolysis is one of the most promising alternatives from the environmental point of view, as long as power is renewable. The comparison between the use of solar or wind to produce power has also been presented from several points of view. Xydis (2013) used an exergy analysis, while Davis and Martín (2014a) only focused on the economics of the system that produced hydrogen to be used to capture CO_2 by producing methane.

The other major raw material is nitrogen. Traditional processes use air directly, since the hydrogen source is a hydrocarbon. Alternatively, it that can be obtained from air separation. Air separation is a mature technology that has received renewed attention lately due to its large power consumption and the possibility of operating them during off-peak hours. Recent papers evaluate the operation of such plants considering the variability in the electricity price (Mitra et al., 2012) and even considering cryostorage of energy (Zhang et al., 2015).

The use of electrolytic hydrogen together with nitrogen for the production of ammonia is not entirely new. Fauser process (Ernst et al., 1925) already worked under these principia for the production of ammonia from air and water. The difference today is the use of renewable resources to provide for the energy required to obtain hydrogen and nitrogen and the possibility of storage them for regulating the production capacity in absence of energy and/or high electricity prices. Recently, some modelling effort has been reported in the production of ammonia. A simulated based optimization approach has been used to analyze the production of ammonia (Flórez-Orrego & de Oliveira Junior, 2017). Tock et al. (2015) produced an analysis where biomass was used together with natural gas to improve the sustainability of current ammonia processes. Furthermore, distributed production of ammonia has also been evaluated using solar

energy for agricultural purposes (Du et al., 2015). Other studies just focus on the synthesis loop (Penkuhn & Tsatsaronis, 2017). Finally, air and water electrolysis using wind energy were considered under a simulation based approach but with no analysis of the energy source (Matzen et al., 2015), or just providing a description of the process using wind energy in the context of targeting a more sustainable agricultural system (Pfromm, 2017).

In this work, the monthly operation of an integrated facility for the production of ammonia from water and air is optimized using renewable sources of energy providing a technoeconomic analysis of the process that includes the energy consumption of compressors and electrolyzer and the cost of the units involved. The facility consists of four stages: power collection, air separation, water electrolysis and ammonia synthesis. The energy required for the system is provided either using solar or wind energy. Detail turbines power curves and panel performance as well as a three bed ammonia synthesis reactor with indirect or direct cooling are considered to evaluate the optimal feed to each reactor bed improving heat integration within the reactor. The work is organized as follows. Section 3.2 describes the process diagram. Section 3.3 presents the modelling effort. Section 3.3 also shows the optimization procedure to determine the energy required and the operating conditions of the units, including the air separation column, the compressors, the ammonia synthesis reactor with its flows, temperature and pressure and the ammonia recovery stage. Section 3.4 presents the raw material and energy requirements, the selection of energy source and reactor design and the monthly production capacity. Finally, in 3.5 some conclusions are discussed.

3.2 ammonia production

The process starts with the technologies that transform solar and wind energy into power. The use of onshore wind turbines or photovoltaic (PV) panels is considered in this work.

3.2.1 *Production of hydrogen*

An electrolyzer system is used to split water into hydrogen and oxygen. Two gas streams are produced containing mainly hydrogen and oxygen respectively. Both exit the electrolyzer saturated with water and with traces of the other species. Most of the water can be removed by condensation. In case of the oxygen stream, after condensation, final dehydration is carried out using an adsorbent bed. Finally, it is compressed for storage. The hydrogen stream is to be further processed to remove the oxygen traces,

using a deoxygenation reactor, and final dehydration using zeolites. Finally, it can be compressed or mixed with the other reactant (Davis & Martín, 2014b).

3.2.2 *Production of nitrogen*

The production of nitrogen is part of the air separation business. It is a well established technology by using the Linde's double column, suitable for large capacities. This process is highly energy intense (Mitra et al., 2012). Argon is assumed that is not separated.

3.2.3 *Ammonia synthesis*

The ammonia synthesis stage consists of the so-called synthesis loop. The gases are compressed and heated to the optimal conditions before entering the reactor. Two designs are tested. The first one is a direct cooling three bed reactor. In this case, fresh syngas is used to cool down the gas stream that exits each of the catalytic beds. The ratio of syngas to be fed after each bed is computed as part of the solution. The second reactor is simpler. It generates steam to cool down the product gas from each of the beads before being fed to the next one. In both cases, the stream leaving the reactor is cooled down to condense the ammonia. The unreacted gases are recycled. Figure 3.1 shows a scheme of the process.

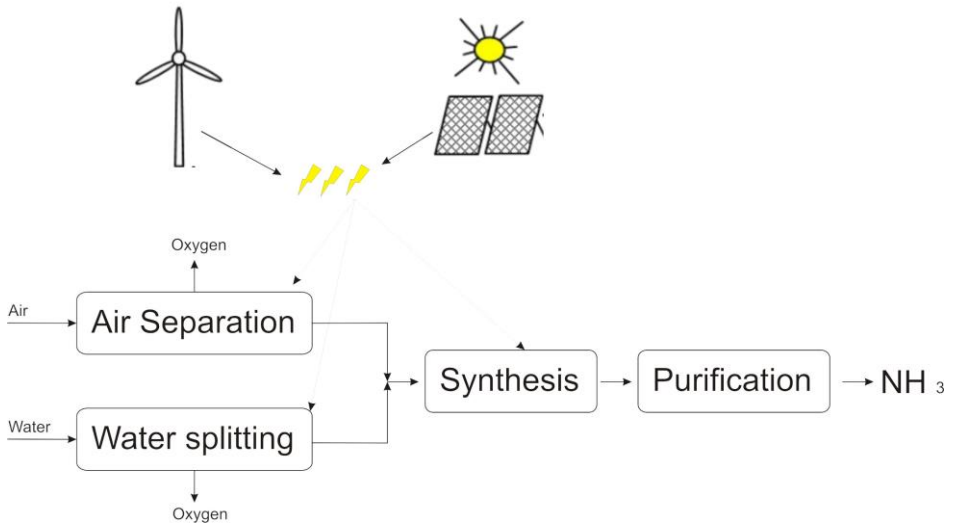

Figure 3.1: Process flowsheet

3.3 modelling

Process optimization requires realistic thermodynamics for the results to be useful. The process is modeled using an equation based approach including mass and energy balances applied to all the species involved (N_2, O_2, H_2O, H_2, NH_3, Ar), thermodynamic and chemical equilibria, chemical kinetics, rules of thumb and experimental data (M. Martín, 2016). While process simulators include the proper thermodynamics, equation based optimization needs to include those features. Surrogate models are developed from rigorous simulations in CHEMCAD© to evaluate the performance of units such as two-phase valves in the distillation of air as well as to compute the k coefficients used to model compressors. The complex kinetics and structure of the ammonia converter is not available in commercial software. The model for the reactor involves chemical equilibria, heat transfer and pressure drop. Although including all of them in the optimization model through a rigorous kinetic model could be an option, it is more efficient for optimization purposes to develop a detailed model in MATLAB© and use the results as bounds to the temperature and yields within the equation based process design in GAMS© that includes mass and energy balances and chemical equilibrium. For simplicity, the entire flowsheet is divided into three pieces that will be presented before the modelling assumptions are described.

3.3.1 *Energy Sources*

In this section, the assumptions and models for the units that collect the energy, solar or wind, and transform it into power are described.

3.3.1.1 *Wind Turbine power*

de la Cruz and Martín (2016) characterized a number of wind turbines from the SAM software package (NREL, 2013). Based onthat study, eq.3.1 is used to model the power curve of the turbine Nordex N100-2500. It has a P_{nom} equal to 2,500 kW. The characteristic parameters a and m are 8.226 m/s and 0.806 s/m respectively.

$$P_{turbine} = \frac{P_{nom}}{1 + e^{(-(v-a)m)}} \tag{3.1}$$

The power provided by the wind farm is that given by the number of units installed and the wind velocity (v) at each time period.

3.3.1.2 *Solar panel installation*

Each PV panel typically provides 1 kWp per 8 m^2 (Maaßen et al., 2011) with installation costs ranging from 1,700 to 4,000 $/kWp (Goodrich et al., 2012). The efficiency of the panels, ω, is assumed to be 25%. The power produced from the solar field is computed using the solar incidence, I, as per eq.3.2.

$$P_{panel} = \frac{0.75}{24} A_{panel}(m^2) I \left(\frac{kWh}{m^2 d}\right) \omega \tag{3.2}$$

3.3.2 *Hydrogen production and purification*

Figure 3.2 shows the water splitting section of the facility.

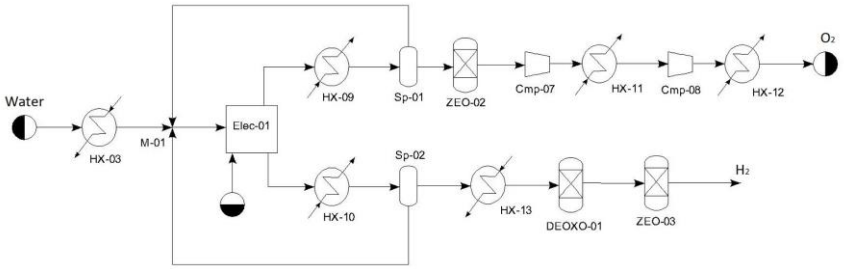

Figure 3.2: Water splitting section of the ammonia production facility

Electrolyzer. The reaction taking place in the electrolyzer is given by equation 3.3, where water is split into oxygen and hydrogen, using a solution of 25% of KOH as the electrolyte. The reaction takes place at 80 °C and 5 bar, generating 0.0124 kg H_2/s (NEL Hydrogen, 2012) per electrolyzer.

$$2H_2O \rightarrow 2H_2 + O_2 \tag{3.3}$$

The power required is 53.15 kWh/kg H_2 (Ivy, 2004). The composition of the hydrogen stream is assumed to be 99.9% H_2 and the rest oxygen on a dry basis. The oxygen rich stream contains 99.5% O_2 and the rest hydrogen on a dry basis. Apart from electricity, the other raw material is water, which is consumed not only by the reaction, but also accompanying the gas phases saturating them. The mass balances to the electrolyzer

are performed based on the stoichiometry of reaction 3.3, its conversion, assumed to be 90%, and the purity of the streams as discussed above.

Water condensation. This stage is modeled assuming that the gas is cooled to 25 °C and remains saturated at that temperature. Thus, the water that exceeds saturation condenses. Antoine correlation is used to compute the water within the gas phase (Sinnott, 2014). The energy involved is computed by an energy balance to the heat exchanger accounting for the amount of water condensed. A flash is located after the cooling to separate the liquid water and the saturated gas phase. The amount of water that the gas phase can drag is computed using eqs.3.4-3.7, where $M_{w,i}$ represent the molar mass of species i.

$$p_{sat-atm} = e^{\left(A - \frac{B}{C+T}\right)} \tag{3.4}$$

$$p_{v-atm} = \phi p_{sat-atm} \tag{3.5}$$

$$y = \frac{M_{w,water}\, p_{v-atm}}{M_{w,drygas}\,(p_{air} - p_{v-atm})} \tag{3.6}$$

$$fc_{water} = fc_{drygas}\, y \tag{3.7}$$

Compressor Design. All the compressors in the flowsheet are considered to behave as polytrophic. Equations 3.8 and 3.9 are used to compute the final temperature (T_{out}) and work (W) involved at each compression state. Based on rules of thumb, the efficiency, η, is 0.85 and k is obtained using an off-line simulation of the compressor in CHEMCAD© resulting in 1.4 (Couper et al., 2005), with T in °C and P in bar.

$$T_{out} = T_{in} + (T_{in} + 273.15)\left[\left(\frac{P_{out}}{P_{in}}\right)^{\frac{k-1}{k}} - 1\right]\frac{1}{\eta_s} \tag{3.8}$$

$$W_{Comp} = \frac{8.314 Fk (T_{in} + 273.15)}{M_W (k-1)}\frac{1}{\eta_s}\left[\left(\frac{P_{out}}{P_{in}}\right)^{\frac{k-1}{k}} - 1\right] \tag{3.9}$$

On the one hand, the stream consisting mainly of oxygen is compressed in a three stage compression system with a maximum compression ratio of 5. This compression system includes intercooling and a dehydration stage using zeolites after the first compression, to store and sell the produced oxygen. On the other hand, the hydrogen stream is compressed to 5 bar so as to adjust the pressure to the requirements of the deoxo reactor. After the deoxygenation, the stream is dehydrated.

Zeolite dehydration. Molecular sieves of zeolites are used to dehydrate the gas phases. The removal efficiency of water is assumed to be 99.97%. While the dehydration of oxygen takes place after the first compression stage at a moderate temperature, the dehydration of the hydrogen stream

is postponed until after the deoxo reactor, due to the production of a small amount of water when the traces of oxygen are removed. This process operates at 90 ^{o}C and 5 bar.

Deoxo reaction. This reaction is used to eliminate the traces of oxygen in the stream of hydrogen by generating water by consuming a small fraction of hydrogen. A conversion equal to 99.7% is assumed and it is recommended to operate at 90 ^{o}C (Davis & Martín, 2014b). The reaction is given by eq.3.10. The mass balance to the reactor is performed based on the stoichiometry of the reaction and using the conversion. Due to the small amount of hydrogen in the stream, the energy balance is neglected.

$$2H_2 + O_2 \rightarrow 2H_2O \tag{3.10}$$

3.3.3 *Air separation*

Fig.3.3 shows the section of the facility corresponding with the separation of air. Air is separated into nitrogen and oxygen using a double Linde's column. For it to operate, the air is cooled down to 80-100 K. Apart from the use of the cold streams from the distillation column, part of the cooling is due to the expansion of the gas in a valve. Therefore, the gas is compressed up to around 210 bar. The compression process is similar to the one presented above in the production of hydrogen and oxygen. In a first stage the air is compressed in a two stage compression system with inter cooling avoiding condensation so that the pressure reaches 6 bar, the operating pressure of the zeolite that is used to dehydrate atmospheric air. Each compression is modeled using eqs.3.8-3.9 as before. The zeolite is assumed to remove the air humidity completely. It operates at 305 K and 6 bar, thus after compression the air is cooled down to this temperature. After the zeolite, the air is further compressed to a pressure between 190 bar and 210 bar. Each compression stage cannot surpass a pressure ratio of 5. The final pressure is left as variable.

Once compressed, the air is cooled down first to 305 K in HX7. Next, before feeding the air to the columns two stages are carried out. First, heat exchanger 8 uses cold nitrogen and oxygen to cooldown the compressed air. Nitrogen will be around 77 K and the oxygen stream around 90 K. To make sure that there is no temperature cross, ΔT_{min} of 3 K is established in this heat exchanger. Furthermore, it is assumed that the final temperatures for nitrogen and oxygen are the same. In a second step air is used as heating utility for the reboiler of the high pressure section of the column. Finally, a valve is responsible for the final cooling in the expansion and allows partial liquefaction of the stream. The final pressure is the operating one at the high pressure section of Linde's double column. The liquid fraction, j, is

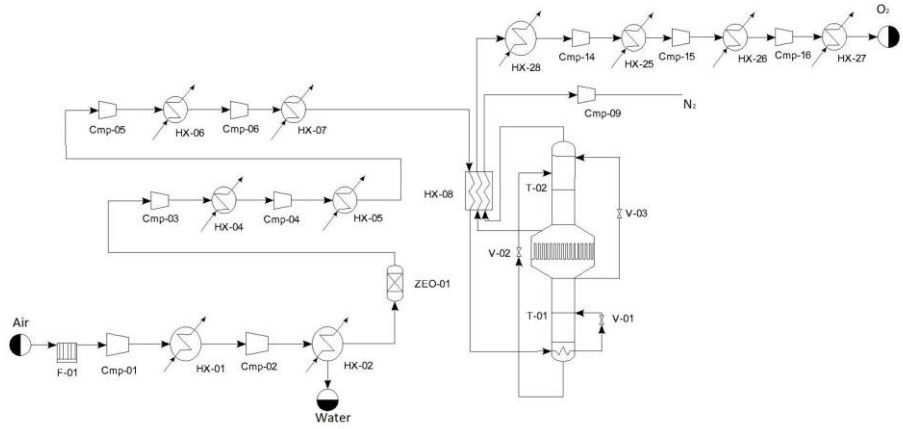

Figure 3.3: Air separation section

computed by developing a surrogate model using CHEMCAD© with SRK as thermodynamic model. The expansion is simulated for a number of initial temperatures, T_{in}, from 90 to 120 K, initial pressures, P_{in}, from 190 to 210 bar, and final pressures, P_{out}, from 5 to 6 bar, since it is the typical operating pressure of the high pressure section of Linde's double column, eq.3.11 shows the correlation for j:

$$j = 1.825723 - 0.009841 T_{in}(K) + 0.023034 \frac{P_{out}(\text{mmHg})}{760} - 0.000267 \frac{P_{in}(\text{mmHg})}{760} \tag{3.11}$$

For all surrogate models, a comparison between the experimental data and the simulated ones were compared to validate them before use. For the sake of the length of the work, those figures are not shown but fittings with R's above 0.99 are found. Similarly another correlation, eq.3.12, is developed to estimate the outlet temperature (T_{out}):

$$T_{out}(K) = 83.876892 + 2.477150 \frac{P_{out}(\text{mmHg})}{760} \tag{3.12}$$

This partially liquid stream is fed to the column. The flows across the column are assumed to be constant.

High pressure column. Fig.3.4 shows the scheme of the flows across the lower part of Linde's column. A mass balance to the feed tray is as follows.

$$L_2' = L_2 + jF \tag{3.13}$$

$$V_2 = V_2' + (1 - j)F \tag{3.14}$$

Where j is the liquefied fraction in the feed to the column computed using eq.3.11. Now, a global mass balance and a balance to the components is performed. For the bottoms, the composition of the residue is fixed based on typical operation of these types of towers (Bhunya, 2014) to be 61.28% N_2, 37.30% O_2 and 1.42% Ar.

$$V_2' + R_2 = L_2' \tag{3.15}$$

For the distillate of the high pressure column, the mass balance is as follows:

$$V_2 = D_2 + L_2 \tag{3.16}$$

The composition of the distillate is assumed to be 99% of nitrogen and 1% free between oxygen and argon. The energy balance to the reboiler is compute as eq.3.17:

$$V_2' \sum_i^i y_{R2} \lambda_i = Q_{Reb} \tag{3.17}$$

In this equation, λ_i s the vaporization latent heat of species i. The molar fractions, y_i, are determined as those in equilibrium with the liquid product. The operating range of pressures is from 5 to 6 bar. For simplicity an average pressure of 5.5 bar is assumed to compute the composition of the stream. Simulating this equilibrium with CHEMCAD© using SKR as thermodynamic package y_i becomes 82.5% of nitrogen, 16.7% of oxygen and 0.8% of argon. The temperature of the stream leaving the columns ($T_{Bot,HP}$) is computed using a surrogate model as a function of the pressure, since Antoine correlations did not represent the phenomena at low temperatures. Thus:

$$T_{\text{Bot,HP}}(K) = 2.4917 \frac{P_{\text{Bot,HP}}(\text{mmHg})}{760} + 85.4157 \tag{3.18}$$

To ensure that no temperature cross occurs in this heat exchanger, a $\Delta T_{min} > 3$ is defined at both ends of the reboiler. The condenser of the high pressure column provides the energy for the reboiler of the low pressure column.

Low pressure column. Fig.3.5 shows the detail of the flows entering, exiting and across the upper part of Linde's column. The temperature of the distillate of the high pressure column ($T_{Cond,HP}$) is given by the following correlation as a function of the pressure within the range of 5-6 bar, eq.3.19. A composition of 99% of nitrogen and 1% oxygen is assumed in this stream to develop the surrogate models.

$$T_{\text{Cond,HP}}(K) = 2.3580 \frac{P_{\text{Cond,HP}}(\text{mmHg})}{760} + 82.5169 \tag{3.19}$$

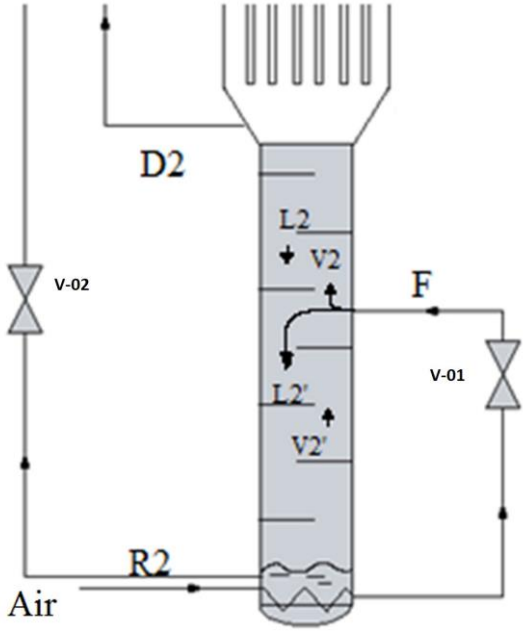

Figure 3.4: Flows across the high pressure column

The energy balance to the condenser of the high pressure columns is given as in eq. (20).

$$|\dot{Q}_{CD,HP}| = V_2 \sum_i x^i_{D2} \lambda_i \tag{3.20}$$

The energy balances to the condenser-reboiler couple both columns and determine the flows. The only residue produced from Linde's column comes actually out of the low pressure column. Therefore, the composition (x^i_{R1}) is fixed to be 95% O_2, 3% Ar and 2% N_2.

$$\dot{Q}_{CD,HP} = |\dot{Q}_{CA,LP}| = L'_1 \sum_i x^i_{R1} \lambda_i \tag{3.21}$$

Similarly, a correlation is developed to compute the temperature of the bottoms of the column ($T_{Bot,LP}$) as a function of the operating pressure within the range of 1-2 bar as follows:

$$T_{Bot,LP}(K) = 7.0864 \frac{P_{Bot,LP}(mmHg)}{760} + 83.0096 \tag{3.22}$$

To ensure a sufficient temperature gradient, constraint 3.23 is added:

$$T_{Bot,LP}(K) + 3 \leq T_{Cond,HP}(K) \tag{3.23}$$

For the distillate of the low pressure column, the same procedure as before is used to develop a correlation between the temperature and the pressure. The composition is assumed to be basically nitrogen, 99.6% and the rest argon.

$$T_{\text{Cond,LP}}(K) = 6.3300\frac{P_{\text{Cond,LP}}(\text{mmHg})}{760} + 71.5645 \tag{3.24}$$

This column is fed by the residue of the high pressure column as main feed and the distillate of the high pressure section as reflux. Both streams from the high pressure column are expanded resulting in the partial liquefaction of the streams. The fraction of the feed liquefied is defined as g, while the fraction of the reflux that liquefies is referred to as i. The flows across the column are assumed constant. Thus, the balances across the column are as follows:

$$L_1 = iD_2 \tag{3.25}$$

$$L_1' = iD_2 + gR_2 \tag{3.26}$$

$$V_1 + (1-i)D_2 = D_1 \tag{3.27}$$

$$V_1' = L_1' - R_1 \tag{3.28}$$

$$V_1' = V_1 - (1-g)R_1 \tag{3.29}$$

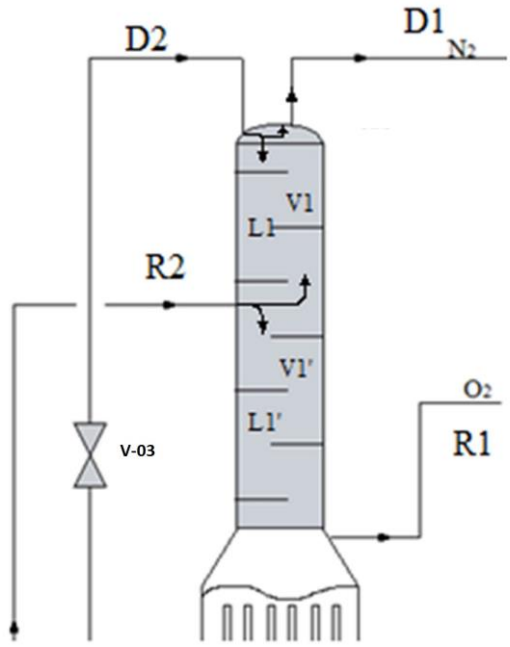

Figure 3.5: Flows across the low pressure column

To predict i and g, the expansion valves are modeled by developing surrogate models as before. It turned out that good fitting was found between the liquefied fraction and the inlet and outlet pressures to the valves. The range is 5-6 bar as inlet pressure and 1-2 bar for the final pressure. Thus, for the main column feed, the expansion is modeled to determine the liquefied fraction, g, and the temperature. Thus, g is computed by eq.3.30:

$$g = 0.901759 - 0.027181 \frac{P_{in}(\text{mmHg})}{760} + 0.059806 \frac{P_{out}(\text{mmHg})}{760} \tag{3.30}$$

And the final temperature of the valve exit is computed using eq.3.31:

$$T_{out}(K) = 74.014389 + 0.066153 \frac{P_{in}(\text{mmHg})}{760} + 6.535790 \frac{P_{out}(\text{mmHg})}{760} \tag{3.31}$$

Similarly, for the valve that feeds the reflux to the top on the low pressure column, the liquefied fraction is computed as per eq.3.32:

$$i = 0.903162 - 0.028452 \frac{P_{in}(\text{mmHg})}{760} + 0.060316 \frac{P_{out}(\text{mmHg})}{760} \tag{3.32}$$

And the temperature is computed as per eq.3.33:

$$T_{out}(K) = 71.509474 + 6.330243 \frac{P_{out}(\text{mmHg})}{760} \tag{3.33}$$

3.3.4 *Ammonia synthesis*

The ammonia synthesis loop starts with mixing the unreacted gases with fresh hydrogen and nitrogen. A constraint is imposed so that the molar flow of hydrogen is larger or equal to that given by the stoichiometry of the reaction but lower than 3.2 times that of nitrogen.

$$N_2 + 3H_2 \rightleftharpoons NH_3 \tag{3.34}$$

The next step is the multistage compression system with intercooling. Typically the operating pressure at the reactor ranges from 100 to 1000 bar and 400-500 ^{o}C. Therefore, a three stage compression system is suggested. Two reactor cooling technologies are evaluated:

Direct cooling: The fresh syngas is divided into three so that a fraction

of the total feed is fed to each of the catalytic beds. The gas fed to each

of the beds must be at least at 400 °C. Preheating is considered using the stream exiting the reactor. In this way, the energy is integrated within the reactor system. Thus, the total flow rate of product is split into three streams to preheat the feeds to each of the three beds. Next, the hot gas stream exiting the first bed is cooled down using fresh syngas and fed to the second bed. The final temperature of the gases exiting each of the beds is constraint to 460-500 °C, according to the detailed simulation in MATLAB©, that is presented below. The fresh syngas can have been preheated or not. Similarly, for the third bed of the reactor, the feed has been cooled down to around 400 °C using fresh syngas, see Fig.3.6. ΔT_{min} of 3 °C has been imposed to avoid temperature cross. Stream mixing is modeled as adiabatic mixture of gases.

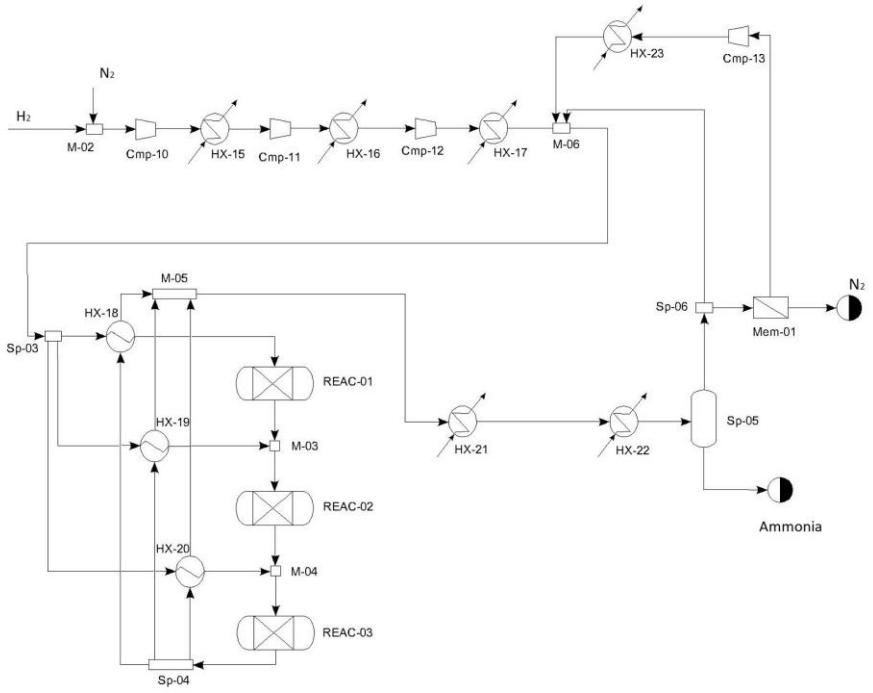

Figure 3.6: Reactor system with direct cooling

Each bed is assumed to be an equilibrium reactor. However, literature shows that at the end of the bed the equilibrium conversion is not reached (Appl, 1999). Therefore, the final temperature is computed by an energy balance where the conversion has been computed by a rigorous model to a three bed reactor performed in MATLAB©. Thus, the equilibrium is imposed as an upper bound for the concentration after each bed from eq.3.35-3.37 (Hougen et al., 1954):

$$P_i = \frac{n_i}{n_T} P_T \qquad \forall i \in \{NH_3, N_2, H_2\} \tag{3.35}$$

$$K_p = \frac{P_{NH_3}}{P_{N_2}^{0.5} P_{H_2}^{1.5}} = \frac{\left(\frac{n_{NH_3}}{n_T} P_T\right)}{\left(\frac{n_{N_2}}{n_T} P_T\right)^{0.5} \left(\frac{n_{H_2}}{n_T} P_T\right)^{1.5}} = \frac{n_T \; n_{NH_3}}{P_T \, n_{N_2}^{0.5} \, n_{H_2}^{1.5}} \tag{3.36}$$

$$log_{10}(K_p) = \frac{2250.322}{T} - 0.85430 - 1.51049 \log_{10} T - 2.58987 \cdot 10^{-4} T + 1.48961 \cdot 10^{-7} T^2 \tag{3.37}$$

Both reactors used the same catalyst, characterized by a particle size (d_p) of 2.5 mm and a particle density of 2200 kg/m^3 (Araujo & Skogestad, 2008). Ideal gases is assumed and the viscosity and thermal conductivity and heat capacity are computed as follows:

$$k_{syngas} = \sum_{i=1}^{N} \frac{x_i k_i}{\sum_j x_j \theta_{ij}} \tag{3.38}$$

$$\theta_{ij} = \frac{1}{\sqrt{8}} \left(1 + \frac{M_i}{M_j}\right)^{-\frac{1}{2}} \left[1 + \left(\frac{\mu_i}{\mu_j}\right)^{\frac{1}{2}} \left(\frac{M_j}{M_i}\right)^{\frac{1}{4}}\right]^2 \tag{3.39}$$

$$Cp_{syngas} = \sum_{i=1}^{N} x_i Cp_i \tag{3.40}$$

where M are the molecular weights, m the species viscosity and Cp the heat capacity. The kinetics of the reaction is given by Dyson and Simon (1968).

$$r = 3 k_{reac} \left[K_p^2 a_{N_2} \left(\frac{a_{H_2}^3}{a_{NH_3}^2}\right)^{\alpha} - \left(\frac{a_{NH_3}^2}{a_{H_2}^3}\right)^{1-\alpha} \right] \Phi\Omega \tag{3.41}$$

where

$$k_{reac} = 8.849 \cdot 10^{14} e^{-\left(\frac{40765}{1.988 T}\right)} \tag{3.42}$$

$$\alpha = 0.5 \tag{3.43}$$

$$a_i = y_i \gamma_i P \tag{3.44}$$

$$\gamma_{H_2} = exp\left(e^{-3.8402 T^{0.125} + 0.541}\right) P - e$$

$$-0.1263T^{0.5}-15.98\,P^2$$

$$+300\left(e^{-0.011901T-5.941}\right)\left(e^{-P/300}-1\right) \tag{3.45}$$

$$\gamma_{N_2}=0.93431737+0.3101804\cdot10^{-3}T+0.295896\cdot10^{-3}P$$
$$-0.2707279\cdot10^{-6}T^2+0.4775207\cdot10^{-6}P^2 \tag{3.46}$$

$$\gamma_{NH_3} = 0.1438996 + 0.2028538 \cdot 10^{-2} T - 0.4487672 \cdot 10^{-3} P^3 - 0.1142945 \cdot 10^{-5} T^2 + 0.2761216 \cdot 10^{-6} P^2 \quad (3.47)$$

$$\Phi = b_0 + b_1 T + b_2 \eta + b_3 T^2 + b_4 \eta^2 + b_5 T^3 + b_6 \eta^3 \quad (3.48)$$

$$\eta = \frac{F^0_{N_2} - F_{N_2}}{F^0_{N_2}} \quad (3.49)$$

And the catalytic activity (Ω) equal to 1 (Appl, 2011). Table 3.1 shows the coefficients for the effectiveness factor (Φ) correlation as a function of the operating pressure.

Table 3.1: Coefficients for eq.3.48

P (atm)	b_0	b_1	b_2	b_3	b_4	b_5	b_6
150	-17.539096	0.07697849	6.900548	-1.082790E-04	-26.42469	4.927648E-08	38.93727
225	-8.2125534	0.03774149	6.190112	-5.354571E-05	-20.86963	2.379142E-08	27.88403
300	-4.6757259	0.02354872	4.687353	-3.463308E-05	-11.28031	1.540881E-08	10.46627

For the heat transfer there are two contributions, the transfer in a pipe and when the gas is flowing through the catalyst bed (Leva et al., 1948). For the pipes use Dittus-Boelter equations are used as follows (Holman, 2009):

$$Nu = 0.023 Re^{0.8} Pr^{0.4} \quad (3.50)$$

$$Nu = \frac{hD}{k} \quad (3.51)$$

$$Re = \frac{DG}{\mu} \quad (3.52)$$

$$Pr = \frac{C_p \mu}{k} \quad (3.53)$$

$$h = 3.5 \frac{k}{D} e^{-4.6 \frac{D_p}{D}} \frac{D_p G}{\mu} \quad (3.54)$$

$$D = \frac{4 \text{ Area}}{\text{Wetted Perimeter}} \quad (3.55)$$

The reactor that is modeled to evaluate the performance and yield is represented by Fig.3.7. The feed goes along the reactor and is heated up using the hot product gas before being fed to the different beds. The beds operate adiabatically and the gas product is cooled down with fresh syngas.

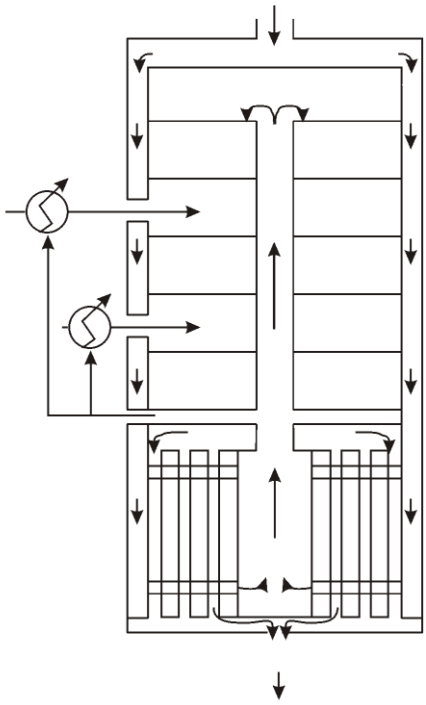

Figure 3.7: Scheme of the direct cooling three bed reactor

The mass balance to each of the beds is written as follows.

$$\frac{dX}{dz} = \frac{rA_t}{F_{H_2}^0} \tag{3.56}$$

$$F_{H_2} = F_{H_2}^0(1 - X) \tag{3.57}$$

$$F_{N_2} = F_{N_2}^0 - \frac{F_{H_2}^0 X}{3} \tag{3.58}$$

$$F_{NH_3} = F_{NH_3}^0 - \frac{2F_{H_2}^0 X}{3} \tag{3.59}$$

$$A_t = \frac{Q}{v} = \frac{\rho_{ini}\dot{m}_{ini}}{v} \tag{3.60}$$

$$v = 0.4 \quad m/s \tag{3.61}$$

$$\frac{R_{in}}{R_{out}} = 0.25 \tag{3.62}$$

The heat transfer is divided into four terms including heat transfer to the rising gas, from the bed, heat of reaction and flow energy (Gaines, 1977).

Heat transfer to the rising gas:

$$dQ_{central} = -UdA_t(T - T_{central}) = \dot{m}_{bed1}C_p dT_{central}$$
$$\frac{dT_{central}}{dz} = \frac{-UL(T - T_{central})}{\dot{m}_{bed1}C_p} \quad (3.63)$$

$$dA_t = Ldz \quad (3.64)$$

$$\frac{1}{U} = \frac{1}{h_{bed}} + \frac{1}{h_{central}} + \frac{D_{central}^{out} \log\left(\frac{D_{central}^{out}}{D_{central}^{in}}\right)}{2k_{stainlessteel}} + \text{Fouling} \quad (3.65)$$

$$k_{stainlessteel} = 21.4 \quad W/mK \quad (3.66)$$

$$\text{Fouling} = 0.001 \quad m^2K/W \quad (3.67)$$

$$e = 0.07D_{central}^{out} \quad (3.68)$$

Heat transfer from the bed:

$$dQ_{external} = \frac{k_{isolation}dA_t(T - T_{ext})}{\delta} = \dot{m}_{bed1}C_p dT_{ext}$$
$$\frac{dT_{ext}}{dz} = \frac{k_{isolation}L'(T - T_{ext})}{\dot{m}_{bed1}C_p\,\delta} \quad (3.69)$$

$$dA_t = L'dz \quad (3.70)$$

$$k_{isolation} = 0.05 \quad W/mK \quad (3.71)$$

$$\delta = 0.1 \ m \quad (3.72)$$

Heat of reaction:

$$dQ_{reaction} = \frac{2}{3}|\Delta H_r|F_{H_2}^0 dX \quad (3.73)$$

Energy of flow:

$$dQ_{gases} = \dot{m}C_p dT \quad (3.74)$$

The total heat balance is given as follows:

$$dQ_{gases} + dQ_{reaction} + dQ_{ext} + dQ_{central} = 0 \quad (3.75)$$

$$-\dot{m}C_p\frac{dT}{dT} + \frac{2}{3}|\Delta H_r|F_{H_2}^0\frac{dX}{dX} - \dot{m}_{bed1}C_p\frac{dT_{ext}}{dT_{ext}} - \dot{m}_{bed1}C_p\frac{dT_{central}}{dT_{central}} \quad (3.76)$$

$$\frac{dT}{dz} = \frac{-\dot{m}C_p \frac{dz}{3} + |\Delta H_r| F_{H_2} \frac{dz}{3} - \dot{m}_{bed1} C_p \frac{dz}{3} - \dot{m}_{bed1} C_p \frac{dz}{3}}{\dot{m} C_p} \tag{3.77}$$

$$\frac{dT}{dz} = \frac{1}{3} \frac{2}{\dot{m} C_p} \left| \Delta H_r | F^0_{H_2} \frac{dX}{dz} - \dot{m}_{bed1} C_p \frac{dT_{ext}}{dz} - \dot{m}_{bed1} C_p \frac{dT_{central}}{dz} \right| \tag{3.78}$$

Finally, the pressure drop across the bed can be computed using Ergun's equation as follows:

$$\frac{dP}{dz} = -150\frac{(1-\epsilon)^2 \mu v_{gas}}{\epsilon^3 dp^2} - 1.75\frac{(1-\epsilon)}{\epsilon^3}\frac{\rho_g v_{as}^2}{d_p} \tag{3.79}$$

where ϵ is the bed porosity. Pressure drop turns out to be at most 2 bar, therefore for the flowsheet optimization we neglect it (See Supplementary material).

Indirect cooling: In this case the operation of the reactor is simpler since after heating up the feed using the hot product gases, the entire flow is fed one bed after the other. At each bed the conversion is validated using a detailed model in MATLAB© off-line, since the equilibrium conversion cannot be reached (Appl, 1999). The stream product of each bed is cooled down producing steam. The feed temperature to each bed is variable but around 400 °C and the exit also variable from 460 to 500 °C. Fig.3.8 shows the scheme of indirect cooling section of the flowsheet.

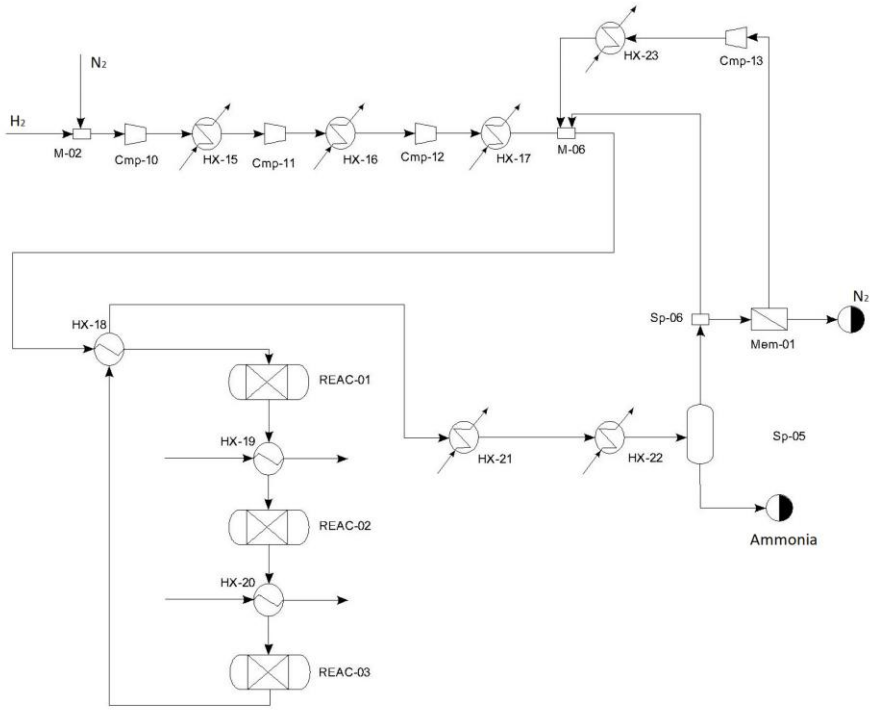

Figure 3.8: Scheme of the reactor for process flowsheeting

The actual reactor modeled in MATLAB© is presented in Fig.3.9. The model is similar to that of the previous reactor, eqs.3.56-3.79. But in this

case the energy balance has been modified since there is no central flow and no central transfer due to geometry of this reactor. Thus, eqs.3.80-3.81 are used (Elnashaie et al., 1988):

$$dQ_{external} = -\frac{k_{isolation} dA_t (T - T_{ext})}{\delta} = \dot{m}_{bed1} C_p dT_{ext} \qquad (3.80)$$

$$\Rightarrow \frac{dT_{ext}}{dz} = -\frac{k_{isolation} L' (T - T_{ext})}{\dot{m}_{bed1} C_p \delta}$$

$$dQ_{central} = 0 \qquad (3.81)$$

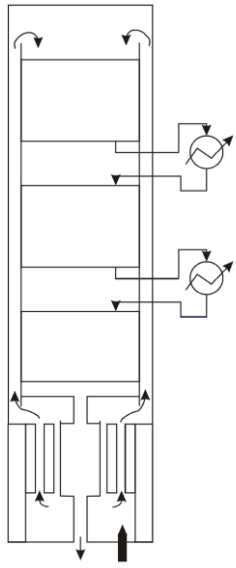

Figure 3.9: Scheme of the reactor

The stream exiting the reactor is cooled down to recover the ammonia by condensation. The condensation is performed following two steps of cooling. First, the heat has been used to preheat the feed to the beds. Next, cooling water is used. To determine the ammonia condensation in HX21 a surrogate model is developed as a function of the operating pressure for a final temperature of 25 °C.

$$\beta_{NH_3} = 0.025860989 + 0.001428067 \frac{P(\text{mmHg})}{760} \qquad (3.82)$$

Finally, to improve the recovery, the cold streams from the distillation tower are used as refrigerant. The separation achieved is computed using a surrogate model developed from running a flash calculation in

CHEMCAD©. Thus, the recovery in the liquid phase as a function of the pressure and temperature is correlated as follows.

$$\sigma_{NH_3} = 2.063269676 + 0.000163965\frac{P(\text{mmHg})}{760} - 3.49979\ 10^{-5}T(K) \tag{3.83}$$

$$\sigma_{H_2} = -0.005616112 + 4.0769\ 10^{-6}\frac{P(\text{mmHg})}{760} + 2.28468\ 10^{-5}T(K) \tag{3.84}$$

$$\sigma_{N_2} = -0.008053425 + 9.08758\ 10^{-6}\frac{P(\text{mmHg})}{760} + 3.49979\ 10^{-5}T(K) \tag{3.85}$$

Thus, a mass balance to the flash determines the recycle gas and the product as follows.

Liquid:

$$m_{i,out} = \sigma_i m_{i,in} \tag{3.86}$$

Gas:

$$m_{i,out} = (1 - \sigma_i)m_{i,in} \tag{3.87}$$

A purge is allowed to remove the impurities and avoid building up. The optimization decides the amount to be purged before recycling the unreacted gases back to the reactor system. The purge stream contains valuable hydrogen. Therefore, a membrane is located to recover it from the purge and recycle it. It is capable of recovering 85% of the hydrogen and, together with it, 10% of the other gases also go through the membrane (Air Products, 2016; Membrane Technology and Research, 2016).

3.3.5 *Solution procedure*

The framework involves all the models for the units described along Section 3.3 and consists of about 1500 equations and inequalities and approximately the same number of variables. It is formulated as a MINLP in GAMS© with two binary variables, one per reactor design, and two alternative energy sources determined by integer variables on the number of solar panels and wind turbines required. The problem is decomposed by solving two relaxed NLPs, one per reactor design, and with the integer variables of the energy sources relaxed to continuous. The production rate, 300 t/d, results in the need for a large number of either solar panels or wind turbines, reducing the error of approximating these integer variables

by continuous ones. The complexity in the operation of the three bed reactors is solved by developing a rigorous kinetic model in MATLAB©. The results in the temperature and conversions after each bed are used as bounds for the optimization of the process. Next, the splitting fractions of the flow that feed the reactor are updated in MATLAB© and run again to validate the temperature and conversion bounds are imposed in GAMS©. The objective function consists of a simplified production cost where the power is provided by the PV panels (Photovoltaic Software, 2017) or the wind turbines (de la Cruz & Martín, 2016). The profiles of the solar and wind energy are taken from Davis and Martín (2014a):

$$Z = F_{NH_3} - \frac{0.33}{\tau} n_{panel}\left(P_{panel}C_{panel} + A_{panel}C_{area}\right) + n_{turbine}P_{nom}C_{turbine} - \frac{1}{3600}\left(C^{op}_{turbine}P_{nominal}n_{turbine}\right) \tag{3.88}$$

$$P \geq n_{panel}P_{panel} + n_{turbine}P_{turbine} \tag{3.89}$$

$$P_{turbine} = \frac{P_{nom}}{1 + e^{(-(v-a)m)}} \tag{3.90}$$

$$a = 8.226 \tag{3.91}$$

$$m = 0.805 \tag{3.92}$$

$$P_{panel} = \frac{0.75}{24} A_{panel}(m^2) I \frac{kWh}{m^2 d} \omega \tag{3.93}$$

$$\omega = 0.25 \tag{3.94}$$

$$A = 1.66 \quad m^2 \tag{3.95}$$

$$\tau = \text{seconds in a year} \tag{3.96}$$

C_{panel} is assumed to be 1080 €/kW$_p$ (IREA, 2012), C_{area} is fixed to 7 €/m^2 (Goodrich et al., 2012), $C_{turbine}$ is 1600 €/kW and $C^{o}_{turbine}$ is 0.015 €/kWh (Davis & Martín, 2014a, 2014b).

The main decision variables are the operating pressures of the two distillation columns, the amount of hydrogen to be produced, the ratio nitrogen to hydrogen fed to the synthesis section, the operating pressure and temperature at the converter, the splitting fractions that define the feed to each bed of the synthesis reactor, the operating conditions of the ammonia recovery section, the ammonia recovery temperature and the purge.

Each NLP is solved following a multistart optimization procedure with

CONOPT 3.0 as preferred solver on a monthly basis. To achieve the total production capacity, 300 t/d, once selected the best power technology on a monthly basis, the production profile is recomputed following the resource

availability. Hourly operation is out of the scope of this work, but the results on the energy consumption, the needs for raw materials and the economic analysis is valuable for a more detailed analysis of the operation of the plant.

3.4 results and discussion

3.4.1 *Plant design and operation*

In this section the operation of both plants, the one with a reactor that uses indirect cooling and the one that uses direct cooling are described. Both have a production capacity of 300 t/d of ammonia. PV panels are selected over wind turbines by the optimization because of the allocation of the case of study, region in the South of Europe where solar incidence is high and even though wind velocity is not low, is not enough to be selected as energy source. Note that the framework presented is general and therefore it can be run in a different allocation with wind and solar data to see the selected technology for that region.

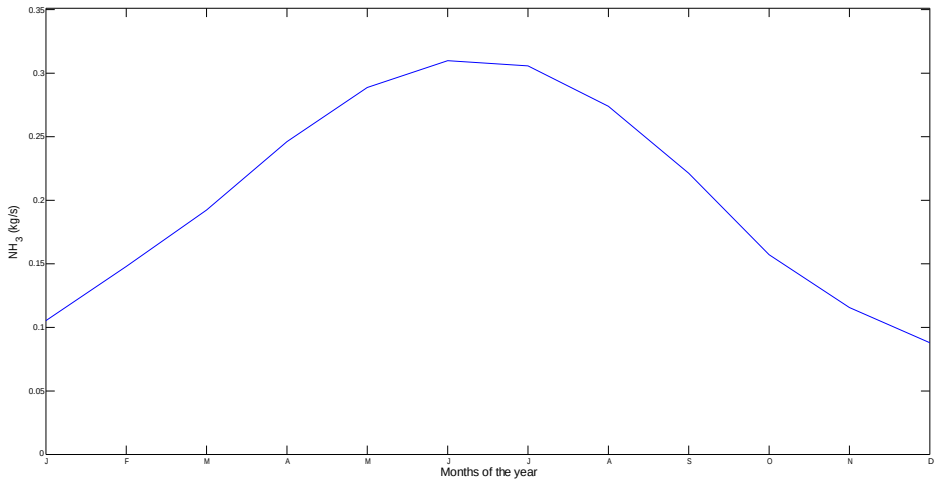

Figure 3.10: Ammonia production profile over time

In the case of the direct cooling reactor, Fig.3.10 shows the production profile over time using solar panels as power source. The plant required 2.9 million PV panels with the current efficiency. The high cost of the panels result in the fact that they operate continuously at full capacity while the chemical plant will absorb the variation in the energy availability. Table 3.2 shows the main operating conditions of the major units.

Table 3.2: Main operating variables of major units in direct cooling

Unit	Pressure (bar)	Temperature (K)	
Distillation Column LP	1	77.9/90.1	
Distillation Column HP	6	96.7/100.3	
Synthesis Reactor. BI	168	673.0-768.7	
Synthesis Reactor. BII	168	717.4-769.9	
Synthesis Reactor. BIII	168	715.3-770.7	
Initial Splitter	168	298.0	To B1: 0.61 To B2: 0.15 To B3: 0.24
Recycle Streams	168	770.7	To B1: 0.64 To B2: 0.16 To B3: 0.20
Purge Fraction	168	240.0	0.5
Ammonia Recovery			0.92

Tables 3.3-3.5 show the composition and operating conditions of major streams across the flowsheet. The low pressure section of Linde's column operates at 1 bar, while the high pressure operates at 6 bar. The reactor is suggested to operate at 168 bar. This is the main energy consumption source for the chemical section of the process, with the exception of the electrolyzer. The gases must be compressed to the operating pressure and it has to come at the expense of the renewable power produced, which is expensive. 61% of the syngas is fed to the first bed of the reactor, while 15% goes to the second and 24% to the third. The hot product gas is split into three to heat up the fed to the beds. The split fraction is similar to the other one for the feed syngas. 64% of the hot product gas is used to heat up the feed to the first bed, 16% to the second and the rest to heat up the fed to the last bed. The reactor ammonia profile can be seen in Fig.3.11. After each bed the dilution of the gas shifts the equilibrium to the raw materials allowing the system to achieve a different equilibrium after the following catalytic bed. Fig.3.12 presents the conversion profile over the length of each of the beds. The actual conversion per bed is low. Figures A.1-A.4 in the Supplementary Material show the temperature and pressure drop profiles across the three beds.

The beds are larger descending along the reactor. The higher ammonia concentration fed to each of the beds the deeper bed needed to reach the conversion. Thus, the first bed is 1.4m deep, the second one 3.1m and the

Table 3.3: Main operating variables of the air separation section (Direct and indirect cooling)

	Air Raw Material	Double Column			Final N_2	Final O_2
	In	In	Out	Out	Out	Out
T(K)	292.0	98.74	77.89	90.10	214.7	298.0
P(atm)	1	6	1	1	5	125
	kmol/s	kmol/s			kmol/s	kmol/s
Water	0.006	0	0	0	0	0
Oxygen	0.088	0.088	0	0.088	0	0.088
Nitrogen	0.328	0.328	0.326	0.002	0.326	0.002
Argon	0.004	0.004	0.001	0.003	0.001	0.003
Hydrogen	0	0	0	0	0	0
Ammonia	0	0	0	0	0	0
Total	0.426	0.42	0.327	0.093	0.0327	0.093

Table 3.4: Main operating variables of the water splitting section (Direct and indirect cooling)

	Water Raw Material	Electrolyzer			Final H_2	Final O_2
	In	In	Out	Out	Out	Out
T(K)	292.0	353.0	353.0	353.0	363.0	298.0
P(atm)	5	5	5	5	5	125
	kmol/s	kmol/s			kmol/s	kmol/s
Water	0.411	0.472	0.022	0.043	0	0
Oxygen	0	0	0.212	0	0	0.212
Nitrogen	0	0	0	0	0	0
Argon	0	0	0	0	0	0
Hydrogen	0	0	0.001	0.424	0.423	0.001
Ammonia	0	0	0	0	0	0
Total	0.411	0.472	0.235	0.467	0.423	0.213

last one 5.7 m. The cross sectional area is 1.88 m^2 resulting in the need for 2846 kg, 6456 kg and 11710 kg of catalyst respectively. 92% of the ammonia produced is recovered. The unreacted gases contain an inert that must be removed to avoid build up. 50% of the recycle is purged but the hydrogen is recovered using a membrane, see Table 3.2.

Table 3.5: Main operating parameters for the ammonia synthesis (Direct cooling)

	Ammonia Reactor		Ammonia Separator		Final Purge Gas
	In	In	Out	Out	Out
T(K)	298.0	441.2	240.0	240.0	240.0
P(atm)	168	168	168	168	168
	kmol/s		kmol/s		kmol/s
Water	0	0	0	0	0
Oxygen	0	0	0	0	0
Nitrogen	0.602	0.498	0.498	0.001	0.221
Argon	0.003	0.003	0.003	0	0.001
Hydrogen	1.806	1.495	1.495	0.001	0.111
Ammonia	0.011	0.218	0.019	0.199	0.008
Total	2.422	2.214	2.015	0.201	0.341

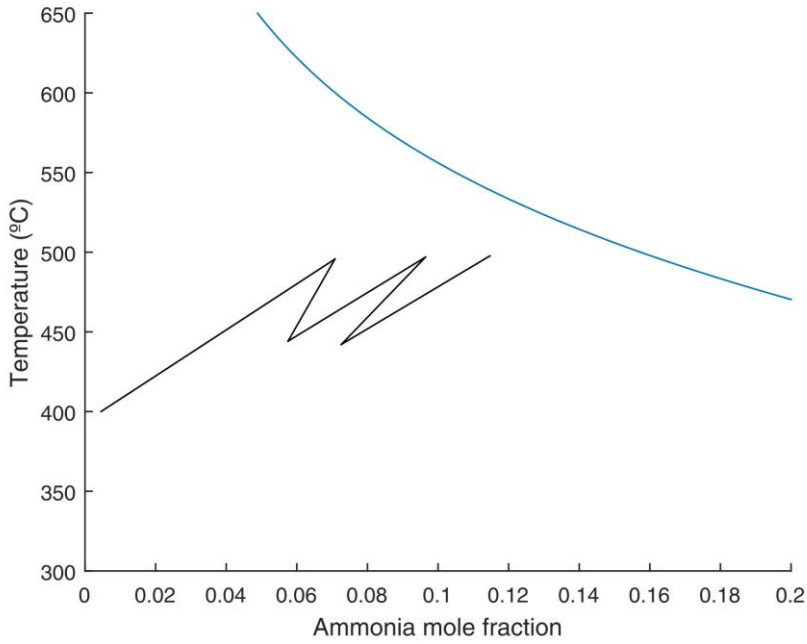

Figure 3.11: Ammonia concentration across the direct cooling reactor

Similarly, the operating profile of the plant using indirect cooling follows that of the solar availability, see Fig.3.10. In this case, there is no gas dilution

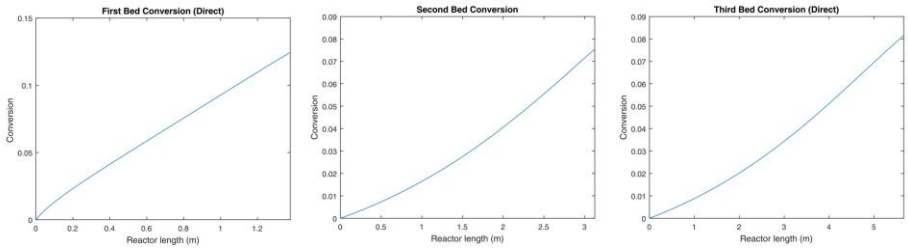

Figure 3.12: Conversion profiles in the three beds of the direct cooling reactor

since cooling water is used to refrigerate the reactor, there is no dilution of the gas stream after each bed, see Fig.3.13, resulting in the fact that the conversion at each of the beds is smaller, see Fig.3.14, compared to the direct cooling version of the reactor. Figures A.5-A.7 in the supplementary material show the temperature and pressure drop profiles across the three beds. Table 3.6 shows the main operating conditions of the major pieces of equipment and Tables 3.3, 3.4, and 3.7 show the details of major streams across the flowsheet. They are similar to the previous case not only for the distillation column, which is to be expected, but also for the reactor, 168 bar. In this case the beds depths are 1.5 m, 1.9 m and 3.2 m respectively. The beds are shorter than in the previous case, but with a larger cross sectional area, 3 m^2. Thus the catalyst weights are 5224 kg, 6371 kg and 10755 kg respectively. Similarly to the use of indirect cooling, 91% of the ammonia produced is recovered. 50% of the unreacted gases are purged but a membrane is used to recover hydrogen out of this stream, see Table 3.6.

Table 3.6: Main operating conditions at major units in indirect cooling

Unit	Pressure (bar)	Temperature (K)	
Distillation Column LP	1	77.9/90.1	
Distillation Column HP	6	96.7/100.3	
Synthesis Reactor. BI	168	673.0-760.7	
Synthesis Reactor. BII	168	729.4-758.7	
Synthesis Reactor. BIII	168	731.3-767.8	
Purge Fraction	168	240.0	0.5
Ammonia Recovery			0.91

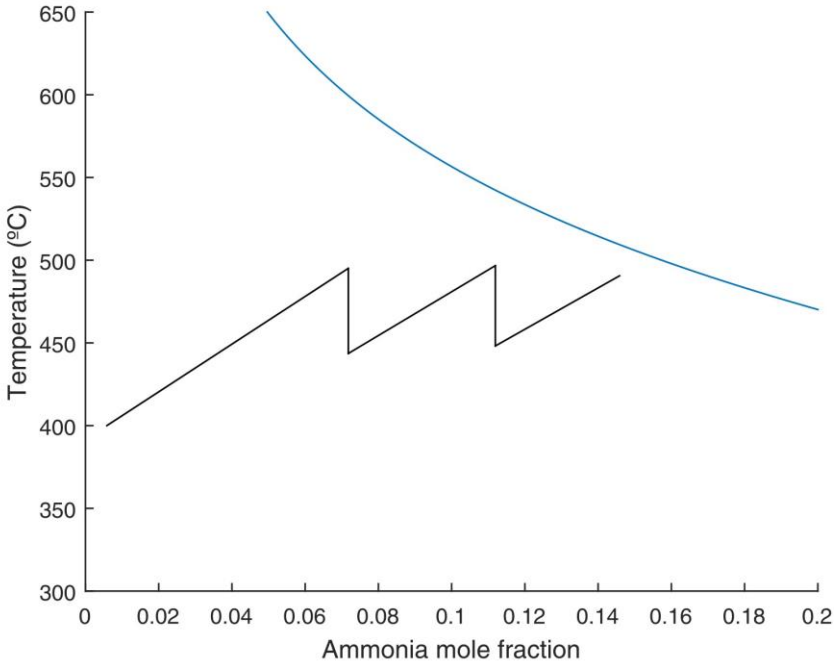

Figure 3.13: Temperature and ammonia profiles along the indirect cooling reactor

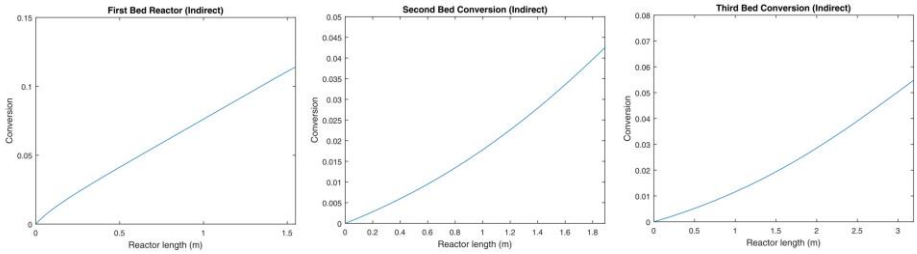

Figure 3.14: Conversion at each of the reactor beds. Indirect cooling

Due to the volatility in the price of the PV pannels and wind turbines and the expected decrease over time, Figs.3.15 and 3.16 show a sensitivity analysis to determine the selection of the energy source as a function of the cost and the energy availability. This Fig.3.15 shows, for four cases, low to high wind velocity and low to high solar incidence the Pareto curves that determine the limit in the relative costs of the pannels and the turbines for a particular technology to be selected. Furthermore, Fig.3.16 shows, for current technology costs, the pareto curve on the relative availability of solar or wind for that resource to be selected.

Table 3.7: Main operating parameters for the ammonia synthesis (Indirect cooling).

	Ammonia Reactor		Ammonia Separator		Final Purge Gas
	In	In	Out	Out	Out
T(K)	298.0	378.7	240.0	240.0	240.0
P(atm)	168	168	168	168	168
	kmol/s		kmol/s		kmol/s
Water	0	0	0	0	0
Oxygen	0	0	0	0	0
Nitrogen	0.602	0.498	0.498	0.001	0.221
Argon	0.003	0.003	0.003	0	0.001
Hydrogen	1.806	1.495	1.495	0.001	0.111
Ammonia	0.011	0.218	0.019	0.199	0.008
Total	2.422	2.214	2.015	0.201	0.341

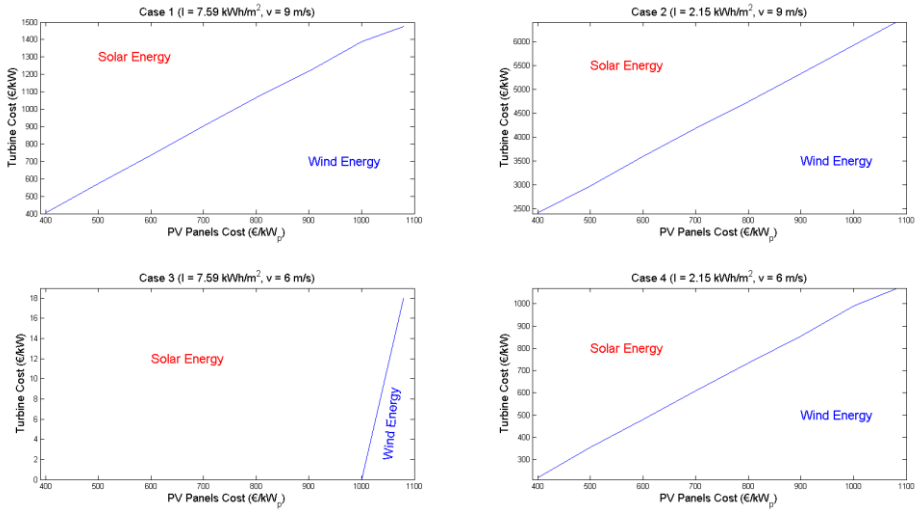

Figure 3.15: Pareto curves for PV panels and turbines cost

3.4.2 *Investment and production costs*

The evaluation of the investment cost is based on the use of the factorial method presented by Sinnott (2014). It relies on the estimation of the unit costs. The correlations developed by Almena and Martín (2016) are used, most of them based on the information from the Matche web page

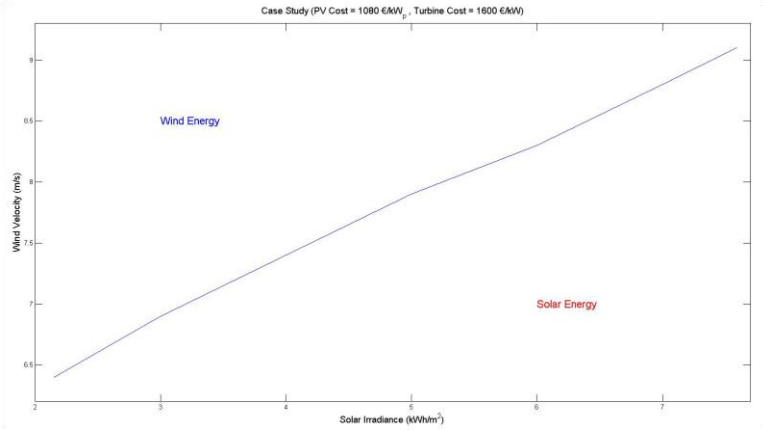

Figure 3.16: Pareto curve for solar incidence versus wind velocity for current costs of panels and turbines

(McNulty et al., 2014), while Goodrich et al. (2012) is the reference for the solar panel cost and Saur (2008) for the electrolyzers. Because of the particularities of these facilities, the factorial method is used to estimate the cost of the chemical section of the plant. Next, the estimation of the solar panel section is added. Figs.3.17 and 3.18 show the breakdown of the investment cost for the different units for direct and indirect cooling respectively. In the case of direct cooling, the chemical section of the plant represents 53% of the investment in equipment. For the indirect cooling technology, the chemical plant represents 47%. In both cases the electrolyser is the largest contribution with at least 60% of the chemical plant costs. The direct cooling type plant shows a slightly lower investment cost, 1518 M€ vs. 1552 M€ and the difference comes from the chemical section of the facility, 733 M€ vs. 699 M€, the rest, 819 M€ correspond to the cost in solar PV panels.

The operating costs are computed considering fixed and variable costs. The variable costs involve raw materials, where the oxygen produced is assumed to be an asset of the process at 21 €/t, utilities, mostly cooling water, and other materials, 5% of maintenance. The fixed costs include maintenance, labour, insurances, fees, and administrative costs, amortization, insurance and others. Labor is estimated based on salaries for the employees of the facility in Spain.

Lab costs are estimated as 25% of labour, supervision as 20% of labour, general costs ad 50% of labour, amortization is computed assuming 30 yr of life spam for the chemical units and 32.5 for solar panels, insurance is 1% of fixed capital, the units costs, fees correspond to another 1% of fixed capital (Sinnott, 2014). For the direct case, the production costs adds up to 146 M€/yr, resulting in a production cost of ammonia of 1.35 €/kg. In this

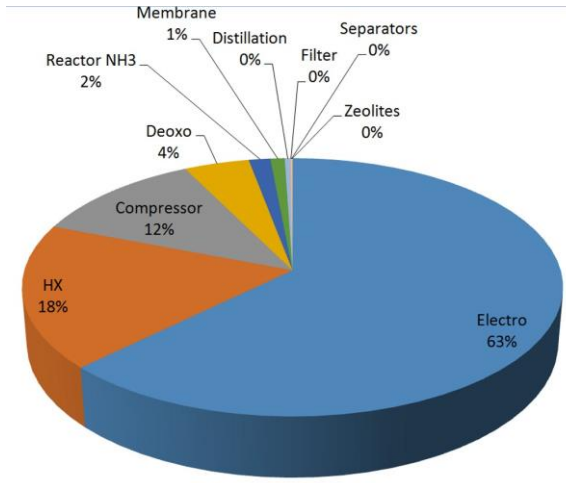

Figure 3.17: Equipment cost breakdown: Direct cooling

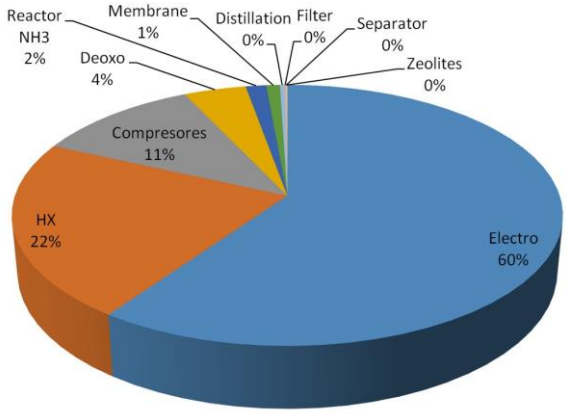

Figure 3.18: Break down of units costs: Indirect cooling

case steam is generated to cooldown the reactor which also improves the sustainability of the process and represent another asset for the process. For the indirect cooling case the production costs are 3% higher, around 148 M€/yr resulting in a production cost of 1.38 €/kg. Both systems show similar economics within the error of estimation. Current cost of ammonia depends on the country but is within the rage of 0.1-0.3 €/kg (Boulamanti & Moya, 2017) but values in the range of $0.5-0.6/kg are reported lately in the US (Pfromm, 2017). Therefore, much work must still to be done to reduce solar panels and electrolyzers cost.

Over the next years it is expected that the panels cost decreases. Therefore, a sensitivity analysis on the production cost of ammonia with the cost of the panels is presented in Fig.3.19 for direct and indirect cooling.

The investment cost is linear with ammonia production cost from current panel cost of 1050 €/kW to values of 300 €/kW. Furthermore, recent results show that panel's efficiency is also expected to reach values of 40%. Thus, Fig.3.19 shows the effects of the expected increase in the efficiency on the final cost of ammonia. The price is still above the current fossil based ammonia but it is getting closer with savings of 10-30 % as the efficiency increases up to 40 %. Further improvements in the efficiency of the panels, probably up to 60-65 %, are needed to reach current reported prices of ammonia.

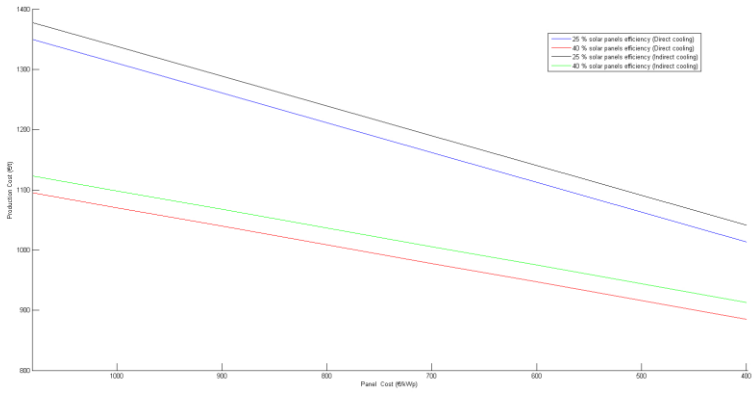

Figure 3.19: Effect of panels cost on ammonia production cost: Direct cooling and Indirect cooling

3.5 conclusions

In this work an ammonia plant is designed using renewable power sources. The main decision variables are the energy source, solar or wind, and the reactor structure. The operating conditions are optimized at major units such as air distillation, ammonia synthesis reactor and ammonia purification. Surrogate models for all the units are developed based on first principles and detailed simulation using process simulators, CHEMCAD©, for air distillation, or a detailed MATLAB© simulation for the two reactor structures so that the energy is optimally integrated within the direct cooling reactor system.

Solar energy is suggested for the location with the disadvantage of the large area required for solar panels. However, the decision between the uses of direct or indirect cooling is not easy being direct cooling slight better in economic analysis, lower investment and production costs, both

dominated by the cost of the solar field representing about 50% of the investment.

This analysis provides basic process information such as operating conditions and energy flows aswell as process economics that are the starting point for the evaluation of the effect of resource uncertainty and detail solar and wind profiles over time.

nomenclature

A_{panel}	Area per panel (m^2/panel)
A_t	Cross sectional area (m^2)
A	Antoine equation parameter
a	Turbine fitting parameter (m/s)
a_i	Activity of component i (atm)
B	Antoine equation parameter
b_i	Effectiveness factor constant
C	Antoine equation parameter
Cp_i	Heat capacity of component i (kJ/kmol K)
C_{panel}	Solar panel cost (€/kW_p)
C_{area}	Area cost (€/m^2)
$C_{turbine}$	Turbine cost (€/kW)
$C_{turbine}^{op}$	Turbine operational cost (€/kWh)
D	Diameter (m)
D_p	Particle size (m)
D_2	Distillate flow in the high pressure column (kmol/s)
e	Steel thickness (m)
F	Total flow rate (Feed flow rate) (kg/s)
F_i	Molar flow rate of component i (kmol/s)
fc	Flow rate (kg/s)
G	mass velocity (kg/m^2 s)
g	Liquid fraction in the valve V-2 output
h	Convection heat transfer coefficient (W/m^2 K)
I	Solar Radiation (kWh/m^2 d)
i	Liquid fraction in the valve V-3 output
j	Liquid fraction in the valve V-01 output

K_p	Equilibrium constant (1/atm)
k	Polytrophic coefficient
k_{reac}	Rate constant (kmol/m^3 hr)
k_i	Thermal conductivity of component i (W/m K)
$M_{w,i}$	Molar mass of species i (kg/kmol)
L	Length of the circumference (m)
L_1'	Rectifying section liquid flow in the low pressure column (kmol/s)
L_1	Stripping section liquid flow in the low pressure column (kmol/s)
L_2'	Rectifying section liquid flow in the high pressure column (kmol/s)
L_2	Stripping section liquid flow in the high pressure column (kmol/s)
m	Turbine fitting parameter (s/m)
Nu	Nusselt Number
n_{H_2}	Hydrogen moles (kmol)
n_{N_2}	Nitrogen moles (kmol)
n_{NH_3}	Ammonia moles (kmol)
n_T	Total moles (kmol)
n_{panel}	Number of solar panels
$n_{turbine}$	Number of turbines
P	Pressure (mmHg)
$P_{Bot,HP}$	Bottom pressure in the high pressure column (mmHg)
$P_{Cond,HP}$	Distillate pressure in the high pressure column (mmHg)
$P_{Bot,LP}$	Bottom pressure in the low pressure column (mmHg)
$P_{Cond,LP}$	Distillate pressure in the low pressure column (mmHg)
$P_{turbine}$	Power generated by a turbine (kW)
P_{nom}	Nominal power of the selected turbine (kW)
P_{panel}	Power generated by a solar panel (kW)

$p_{sat_a tm}$	Vapor saturation pressure (mmHg)
$p_{v_a tm}$	Vapor pressure (mmHg)
P_T	Total pressure (atm)
P_{NH_3}	Ammonia partial pressure (atm)
P_{H_2}	Hydrogen partial pressure (atm)
P_{N_2}	Nitrogen partial pressure (atm)
Pr	Prandtl Number
Q	Volume flow (m3/s)
Q_{reb}	Heat flow in the high pressure column reboiler (kJ/s)
$Q_{CD,HP}$	Heat flow in high pressure condenser (kJ/s)
$Q_{CA,LP}$	Heat flow in low pressure reboiler (kJ/s)
Q_i	Heat terms (kJ/s)
R	Radius (m)
R_2	Bottom flow in the high pressure column (kmol/s)
Re	Reynolds Number
r	Reaction rate (kmol/m^3 hr)
T	Temperature (K)
$T_{Bot,HP}$	Bottom temperature in the high pressure column (K)
$T_{Cond,HP}$	Distillate temperature in the high pressure column (K)
$T_{Bot,LP}$	Bottom temperature in the low pressure column (K)
$T_{Cond,LP}$	Distillate temperature in the low pressure column (K)
U	Global heat transfer coefficient (W/m^2 K)
V_1	Rectifying section vapor flow in the low pressure column (kmol/s)
V_1	Stripping section vapor flow in the low pressure column (kmol/s)
V_2	Rectifying section vapor flow in the high pressure column (kmol/s)
V_2	Stripping section vapor flow in the high pressure column (kmol/s)
v	Wind velocity (m/s)
X	Conversion
x_{R1}	Liquid molar concentration in

	the low pressure reboiler
x^{i}_{D2}	Liquid molar concentration in the high pressure distillate
y	Absolute humidity (kg of water vapor per kg of dry gas)
y^{i}_{R2}	Gas molar concentration in the high pressure column reboiler
Z	objective function

Symbols

ω	Solar panel efficiency
ϕ	Relative humidity
η_s	Compressor efficiency
λ_i	Vaporization latent heat of species i (kJ/kg)
Φ	Effectiveness factor
α	Kinetic parameter
Ω	catalytic activity
γ_i	Fugacity coefficient of component i
η	Nitrogen conversion
μ_i	Viscosity of component i (Pa s)
ΔH_r	Reaction heat (kJ/mol)
ϵ	Catalytic porosity
ρ	Density (kg/m^3)
δ	Isolation thickness (m)
β_i	Separation yield in HX21
σ_i	Separation yield in HX22
τ	Conversion factor between hour and seconds

acknowledgments

The authors would like to acknowledge Salamanca Research for optimization software licenses. The authors acknowledge the TCUE fellowship from Fundación Universidad - Empresa USAL 2016 to Mr. A. Sánchez and MINECO grant DPI2015-67341-C2-1-R. As acknowledges the FPU grant from MECD.

bibliography

Haldane, J. B. S. (1924). *Daedalus; or, science and the future: A paper read to the heretics, cambridge, on february 4th, 1923*. Kegan Paul, Trench.

Ernst, F. A., Reed, F. C., & Edwards, W. L. (1925). A direct synthetic ammonia plant. *Industrial & Engineering Chemistry*, *17*(8), 775–788. https://doi.org/10.1021/ie50188a002

Leva, M., Weintraub, M., Grummer, M., & Clark, E. L. (1948). Cooling of gases through packed tubes. *Industrial & Engineering Chemistry*, *40*(4), 747–752. https://doi.org/10.1021/ie50460a042

Hougen, O., Watson, K., & Ragatz, R. (1954). Chemical process principles, part i, john willey & sons. *Inc., New York*.

Dyson, D. C., & Simon, J. M. (1968). Kinetic expression with diffusion correction for ammonia synthesis on industrial catalyst. *Industrial & Engineering Chemistry Fundamentals*, *7*(4), 605–610. https://doi.org/10.1021/i160028a013

Bockris, J. (1975). Energy: The solar-hydrogen alternative. *New York*.

Gaines, L. D. (1977). Optimal temperatures for ammonia synthesis converters. *Industrial & Engineering Chemistry Process Design and Development*, *16*(3), 381–389. https://doi.org/10.1021/i260063a024

Elnashaie, S. S., Abashar, M. E., & Al-Ubaid, A. S. (1988). Simulation and optimization of an industrial ammonia reactor. *Industrial & Engineering Chemistry Research*, *27*(11), 2015–2022. https://doi.org/10.1021/ie00083a010

Appl, M. (1999). Ammonia: Priciples & industrial practice.

Ivy, J. (2004). *Summary of electrolytic hydrogen production: Milestone completion report* (tech. rep.). National Renewable Energy Lab., Golden, CO (US).

Agrawal, R., Offutt, M., & Ramage, M. P. (2005). Hydrogen economy - an opportunity for chemical engineers? *AIChE Journal*, *51*(6), 1582–1589. https://doi.org/10.1002/aic.10561

Couper, J. R., Penney, W. R., Fair, J. R., & Walas, S. M. (2005). *Chemical process equipment: Selection and design*. Gulf Professional Publishing.

Levene, J., Mann, M., Margolis, R., & Milbrandt, A. (2005). An analysis of hydrogen production from renewable electricity sources. Retrieved March 8, 2020, from https://www.nrel.gov/docs/fy05osti/37612.pdf

Levene, J., Kroposki, B., & Sverdrup, G. (2006). Wind energy and production of hydrogen and electricity — opportunities for renewable hydrogen. Retrieved March 7, 2020, from https://www.nrel.gov/docs/fy06osti/39534.pdf

Araujo, A., & Skogestad, S. (2008). Control structure design for the ammonia synthesis process. *Computers & Chemical Engineering*, *32*(12), 2920–2932. https://doi.org/10.1016/j.compchemeng.2008.03.001

Saur, G. (2008). *Wind-to-hydrogen project: Electrolyzer capital cost study* (tech. rep.). National Renewable Energy Lab.(NREL), Golden, CO (United States).

Holman, J. (2009). Heat transfer.

Weekman, V. W. (2010). Gazing into an energy crystal ball. *Chemical Engineering Progress*, *106*(6), 23–27.

Appl, M. (2011). Ammonia, 2. production processes. *Ullmann's encyclopedia of industrial chemistry*.

Maaßen, M., Rübsamen, M., & Perez, A. (2011). Photovoltaic solar energy in spain seminar papers in international finance and economics. seminar paper 4/2011.

Goodrich, A., James, T., & Woodhouse, M. (2012). *Residential, commercial, and utility-scale photovoltaic (pv) system prices in the united states: Current drivers and cost-reduction opportunities* (tech. rep.). National Renewable Energy Lab.(NREL), Golden, CO (United States).

IREA. (2012). Renewable energy technologies: Cost analysis series. *Concentrating solar power*, *4*(5).

Mitra, S., Grossmann, I. E., Pinto, J. M., & Arora, N. (2012). Optimal production planning under time-sensitive electricity prices for continuous power-intensive processes. *Computers and Chemical Engineering*, *38*, 171–184. https://doi.org/10.1016/j.compchemeng.2011.09.019

NEL Hydrogen. (2012). Technical data. Retrieved January 7, 2017, from https://www.nel-hydrogen.com/home/?pid=75

Ozbilen, A., Dincer, I., & Rosen, M. A. (2012). Life cycle assessment of hydrogen production via thermochemical water splitting using multi-step cu–cl cycles. *Journal of Cleaner Production*, *33*, 202–216. https://doi.org/10.1016/j.jclepro.2012.03.035

Yuan, Z., & Chen, B. (2012). Process synthesis for addressing the sustainable energy systems and environmental issues. *AIChE Journal*, *58*(11), 3370–3389. https://doi.org/10.1002/aic.13914

Hajjaji, N., Pons, M.-N., Renaudin, V., & Houas, A. (2013). Comparative life cycle assessment of eight alternatives for hydrogen production from renewable and fossil feedstock. *Journal of Cleaner Production*, *44*, 177–189. https://doi.org/10.1016/j.jclepro.2012.11.043

Martín, L., & Martín, M. (2013). Optimal year-round operation of a concentrated solar energy plant in the south of europe. *Applied Thermal Engineering*, *59*(1), 627–633. https://doi.org/10.1016/j.applthermaleng.2013.06.031

NREL. (2013). System advisor model (sam). Retrieved March 7, 2020, from https://sam.nrel.gov/

Xydis, G. (2013). On the exergetic capacity factor of a wind - solar power generation system. *Journal of Cleaner Production*, *47*, 437–445. https://doi.org/10.1016/j.jclepro.2012.07.014

Bhandari, R., Trudewind, C. A., & Zapp, P. (2014). Life cycle assessment of hydrogen production via electrolysis – a review. *Journal of Cleaner Production*, *85*, 151–163. https://doi.org/10.1016/j.jclepro.2013.07.048

Bhunya, D. K. (2014). *Simulation study of cryogenic air separation unit using aspen hysys at rourkela steel plant* (Doctoral dissertation).

Davis, W., & Martín, M. (2014a). Optimal year-round operation for methane production from co2 and water using wind and/or solar energy. *Journal of Cleaner Production*, *80*, 252–261. https://doi.org/10.1016/j.jclepro.2014.05.077

Davis, W., & Martín, M. (2014b). Optimal year-round operation for methane production from co2 and water using wind energy. *Energy*, *69*, 497–505. https://doi.org/10.1016/j.energy.2014.03.043

McNulty, T., Story, P., Creason, A., & Scott, E. (2014). Matche (2014) cost estimates,index of process equipment. Retrieved December 1, 2020, from http://www.matche.com/equipcost/EquipmentIndex.html

Sinnott, R. (2014). *Chemical engineering design* (Vol. 6). Elsevier.

Du, Z., Denkenberger, D., & Pearce, J. (2015). Solar photovoltaic powered on-site ammonia production for nitrogen fertilization. *Solar Energy*, *122*, 562–568. https://doi.org/10.1016/j.solener.2015.09.035

Matzen, M., Alhajji, M., & Demirel, Y. (2015). Chemical storage of wind energy by renewable methanol production: Feasibility analysis using a multi-criteria decision matrix. *Energy*, *93*, 343–353. https://doi.org/10.1016/j.energy.2015.09.043

Tock, L., Maréchal, F., & Perrenoud, M. (2015). Thermo-environomic evaluation of the ammonia production. *The Canadian Journal of Chemical Engineering*, *93*(2), 356–362. https://doi.org/10.1002/cjce.22126

Zhang, Q., Grossmann, I. E., Heuberger, C. F., Sundaramoorthy, A., & Pinto, J. M. (2015). Air separation with cryogenic energy storage: Optimal scheduling considering electric energy and reserve markets. *AIChE Journal*, *61*(5), 1547–1558. https://doi.org/10.1002/aic.14730

Air Products. (2016). Prism® membrane systems for ammonia plants... tell me more. Retrieved May 7, 2017, from https://www.airproducts.no / wp - content / uploads / 2016 / 06 / Membrane - Systems - For - Ammonia-Plants.pdf

Almena, A., & Martín, M. (2016). Technoeconomic analysis of the production of epichlorohydrin from glycerol. *Industrial & Engineering*

Chemistry Research, *55*(12), 3226–3238. https://doi.org/10.1021/acs.iecr.5b02555

de la Cruz, V., & Martín, M. (2016). Characterization and optimal site matching of wind turbines: Effects on the economics of synthetic methane production. *Journal of Cleaner Production*, *133*, 1302–1311. https://doi.org/10.1016/j.jclepro.2016.06.019

Martín, M. (2016). *Industrial chemical process analysis and design*. Elsevier.

Membrane Technology and Research. (2016). Hydrogen recovery from ammonia plant purge gas. Retrieved May 7, 2017, from www.mtrinc.com/pdf_print/refinery_and_syngas/MTR_Brochure_Hydrogen_Recovery_from_Ammonia_Plant_Purge_Gas.pdf

Boulamanti, A., & Moya, J. A. (2017). Production costs of the chemical industry in the eu and other countries: Ammonia, methanol and light olefins. *Renewable and Sustainable Energy Reviews*, *68*, 1205–1212. https://doi.org/10.1016/j.rser.2016.02.021

Flórez-Orrego, D., & de Oliveira Junior, S. (2017). Modeling and optimization of an industrial ammonia synthesis unit: An exergy approach. *Energy*, *137*, 234–250. https://doi.org/10.1016/j.energy.2017.06.157

Penkuhn, M., & Tsatsaronis, G. (2017). Comparison of different ammonia synthesis loop configurations with the aid of advanced exergy analysis. *Energy*, *137*, 854–864. https://doi.org/10.1016/j.energy.2017.02.175

Pfromm, P. H. (2017). Towards sustainable agriculture: Fossil-free ammonia. *Journal of Renewable and Sustainable Energy*, *9*(3), 034702. https://doi.org/10.1063/1.4985090

Photovoltaic Software. (2017). How to calculate the annual solar energy output of a photovoltaic system? Retrieved May 7, 2020, from https://photovoltaic- software.com/principle- ressources/how-calculate-solar-energy-power-pv-systems

4

SCALE UP AND SCALE DOWN ISSUES OF RENEWABLE AMMONIA PLANTS: TOWARDS MODULAR DESIGN

abstract

In this work, the scale-up and down of a renewable-based ammonia facility has been evaluated. Nitrogen is obtained from air separation. Three technologies have been compared, membrane separation, pressure swing adsorption and a Linde's double column. Hydrogen is produced from water splitting using solar, photovoltaic, or wind energy. Finally, ammonia is synthesized in a three bed packed reactor. Two reactor designs were evaluated, direct and indirect cooling. The process is optimized by solving an NLP for each reactor design and nitrogen technology combination and for several production capacities, evaluating the operating and investment costs resulting from the need to use a number of parallel units. The production capacity defines the best technology depending on its characteristics. The results show that for very low production membranes are recommended, medium capacities should be produced using PSA while large require the use of distillation. The actual transition points have been computed. The high costs of panels and electrolyzers mitigate the issues related to duplicating small units. The expected decrease in the cost of both will result in competitive renewable ammonia production costs. Correlations for the investment and production costs as a function of the scale have been developed.

Keywords: Air, Ammonia, Modular design, Scale up, Solar and wind energy, Water

resumen

En este trabajo se ha evaluado el escalado de una instalación de amoníaco renovable. El nitrógeno se obtiene a partir de la separación del aire. Se han comparado tres tecnologías, la separación por membranas, la adsorción a presión y la doble columna de Linde. El hidrógeno se produce a partir de la rotura del agua mediante energía solar fotovoltaica o eólica. Por último, el amoníaco se sintetiza en un reactor de tres lechos. Se evaluaron dos diseños de reactor, con refrigeración directa e indirecta. El proceso se optimiza resolviendo un NLP para cada diseño de reactor y combinación de tecnología de nitrógeno y para varias capacidades de producción, evaluando los costes de explotación e inversión derivados de la necesidad de utilizar varias unidades paralelas. La capacidad de producción define la mejor tecnología en función de sus características. Los resultados muestran que para producciones muy bajas se recomiendan las membranas, las capacidades medias deben producirse utilizando PSA mientras que las grandes requieren el uso de la destilación. Se han calculado los puntos de transición reales. Los elevados costes de los paneles y los electrolizadores mitigan los problemas relacionados con la duplicación de las unidades pequeñas. La disminución prevista del coste de ambos dará lugar a unos costes de producción de amoníaco renovable competitivos. Se han desarrollado correlaciones para los costes de inversión y producción en función de la escala.

Palabras Clave: Aire, Amoníaco, Diseño modular, Escalado, Energía solar y eólica, Agua

4.1 introduction

Renewable sources of energy such as biomass, solar, wind or geothermal, just to mention some of the most widely extended,are characterized by a highly distributed production across regions (EPA, 2017). Total renewable energy available is more than enough to provide for society needs, but the traditional production paradigm is changing. Economies of scale have featured current industry and its infrastructures based on large production complexes (i.e Dow, Exxonmobil or BASF hubs). The well-known six tenths rule has extensively been used in the chemical industry to scale up or down the cost of technologies (Douglas, 1988). However, distributed production does not follow this rule. Distributed production also corresponds to the production at small scales (Pepermans et al., 2005). This new production scheme results in the use of a number of individual units so that the cost is no longer a continuous function. The step forward is modularization of chemical plants. The plants will be built in the form of modulus that are easily assembled at any place to make the most of distributed resources (Baldea et al., 2017). The advantages of these plants are straightforward, easy and quick deployment and low investment risk to exploit resources even in remote places. However, the disadvantages must be also considered including the environmental impact of the transportation of the plants and of the products (EPA, 2017).

In this context, the production of ammonia is a good example of the use of renewable power to obtain a basic chemical that is used as a raw material for a number of industries, including fertilizers, explosives and plastics. Large ammonia plants based on fossil resources dominate industry (Appl, 2011). Alternatively, nitrogen and hydrogen can be produced from renewable sources (Sánchez & Martín, 2018). The economy of renewable based chemicals are heavily affected by distributed generation. Renewable hydrogen can be obtained from biomass (Martín & Grossmann, 2011) or using solar (Levene et al., 2005; Davis & Martín, 2014b) or wind energy (Levene et al., 2006; Davis & Martín, 2014a) through water splitting. Air separation to produce nitrogen is a mature process too. The technology used to separate air into its components depends on the scale and the purity (Ivanova & Lewis, 2012). Large scale production is typically carried out using Linde's double column. Non cryogenic separations require less capital investment. According to the leaflets of the air separation industry, technologies like pressure swing adsorption or membranes can be used for smaller production capacities, below 500 t/d of oxygen. On the other hand, cryogenic air separation units (ASUs) become cost effective above 200–300 t/d and are more efficient above 500 t/d all the way to 2000 t/d (Matheson, 2018; Messer, 2018), see Fig.4.1. However, the purities

of the products are jeopardized resulting in losing an important asset, selling oxygen as byproduct. Finally, ammonia synthesis is carried out in converters characterized by their energy integrated structures since the yield to ammonia is limited by equilibrium.

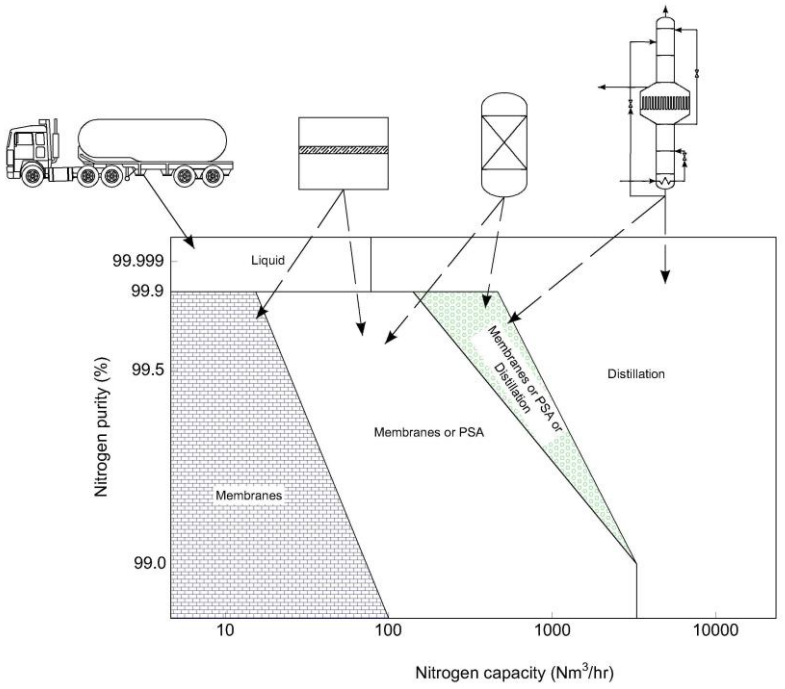

Figure 4.1: State of the art of air separation technologies

In this work, a process level analysis for the optimal use of distributed sources of energy at various scales applied to the production of ammonia is performed. The scale-up and down of facilities is evaluated selecting the proper technology for each of the three sections of the plant, evaluating the technologies and their economics. The facility consists of four stages: power collection, considering wind turbines or solar PV panels, air separation for which membranes, PSA or distillation technologies are evaluated, water electrolysis and ammonia synthesis evaluating two reactor designs. The work is organized as follows. Section 4.2 describes the process flowsheet. Section 4.3 presents the modeling effort of the membranes and PSA. Section 4.4 shows the optimization procedure to determine the energy required and the major operating conditions of the units, including the air separation (Distillation, membranes or PSA), the compressors, the ammonia synthesis reactor with its flows, temperature and pressure and the ammonia recovery stage. Section 4.5 presents some results of the operation, the raw materials

and energy requirements, the production and capital cost for scaling-up or down considering modular or non-modular design and a sensitivity analysis on the prices of PV panels or wind turbines. Finally, in Section 4.6, some conclusions are drawn.

4.2 ammonia production

The process starts with the technologies that transform solar and wind energy into power. We consider for this work the use of onshore wind turbines or photovoltaic (PV) panels.

4.2.1 *Production of hydrogen*

An electrolyzer system is used to split water into hydrogen and oxygen. Two gas streams are produced containing mainly hydrogen and oxygen respectively. Both exit the electrolyzer saturated with water and with traces of the other species. Most of the water can be removed by condensation. In case of the oxygen stream, after condensation, final dehydration is carried out using an adsorbent bed. Finally, it is compressed for storage. The hydrogen stream is to be further processed to remove the oxygen traces, using a deoxygenation reactor, and final dehydration using zeolites (Davis & Martín, 2014b). Finally, it can be compressed or mixed with the nitrogen.

4.2.2 *Production of nitrogen*

The production of nitrogen is part of the air separation portfolio of operations in the air separation business. The use of three alternatives is considered: (i) PSA systems for the production of nitrogen, and a byproduct stream rich in oxygen, (ii) membrane separation, producing a permeate and a reject rich in oxygen and (iii) the Linde's double column, suitable for large capacities as presented in previous paper (Sánchez & Martín, 2018). It is assumed that Ar is not recovered.

4.2.3 *Ammonia synthesis*

The ammonia synthesis stage is widely known as the synthesis loop where the gases are mixed and prepared to be fed to a multibed reactor operating at high pressure. The particular thermodynamics of the ammonia synthesis reaction results in the need to operate in a multibed structure with intercooling (Appl, 1999). Cooling can be achieved either by using cold fresh syngas by means of a more integrated scheme, or by using com-

pressed water producing steam. Thus, direct or indirect reactor designs are considered respectively as a function of the cooling technology. Ammonia is typically recovered by condensation and the unreacted gases must be recovered due to the high production costs of nitrogen and hydrogen. Fig.4.2 shows a general scheme of the process.

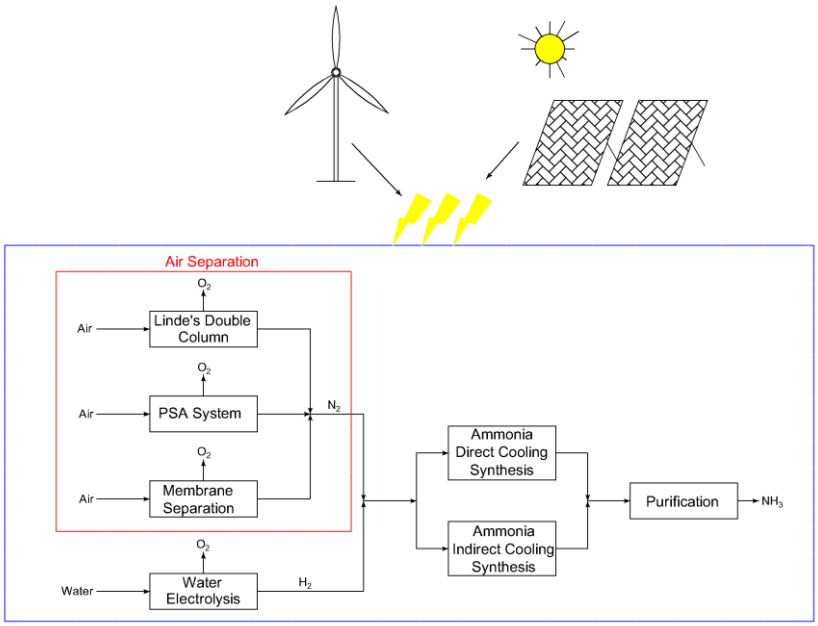

Figure 4.2: Process flowsheet

4.3 modelling

This section is focused on presenting the main modeling features of the PSA systems and the membranes and refers the reader to a previous paper (Sánchez & Martín, 2018) for the details on the modeling of the Linde's column, the electrolysis section and the ammonia synthesis loop. For these three sections only a brief description is provided.

4.3.1 *Power sources modeling*

In this section, the assumptions and models for the units that collect the energy, solar or wind, and transform it into power are provided.

4.3.1.1 *Wind turbine power*

A particular wind turbine, the Nordex N100-2500, from the SAM software package (NREL, 2013) is selected. Based on de la Cruz and Martín (2016), Eq.4.1 is used to model the power curve of the turbine with P_{nom} equal to 2500 kW and the characteristic parameters a and m equal to 8.226 m/s and 0.806 s/m respectively.

$$P_{turbine} = \frac{P_{nom}}{1 + e^{(-(v-a)m)}} \tag{4.1}$$

The power provided by the wind farm is that given by the number of units installed and the wind velocity at each time period.

4.3.1.2 *Solar panel installation*

The power produced from the solar field is computed using the solar incidence, I, as given in Eq.4.2. The efficiency of the panels, ω, is assumed to be 25%. It is assumed that each PV panel provides 1 kW_p per 8 m^2 (Maaßen et al., 2011) with an installation cost of 1600 €/kW_p (Goodrich et al., 2012).

$$P_{panel} = \frac{0.75}{24} A_{panel}(m^2) I \left(\frac{kWh}{m^2 d}\right) \omega \tag{4.2}$$

4.3.2 *Hydrogen production and purification*

Hydrogen is produced by water electrolysis using a liquid electrolyte operating at 80 °C and 5 bar. The power consumption of the electrolyzer ascends up to 53.15 kWh/kg H_2 (Ivy, 2004). Three electrolyzer capacities have been considered: 0–100 Nm^3/h for membranes based ammonia plant, 0–500 Nm^3/h for PSA and 0–800 Nm^3/h for distillation (Godula-Jopek, 2015). The actual number of electrolyzers is a function of their capacity. The purity of both streams, oxygen and hydrogen is high. However, to avoid issues in the ammonia synthesis stage, traces of oxygen will be removed from the hydrogen stream using a deoxo reactor, operating at 90 °C, and consuming a small amount of hydrogen to turn oxygen back into water. Finally, the stream is dehydrated before mixing it with nitrogen. The oxygen stream is dehydrated and compressed and cooled for storage. First principles models are developed to evaluate each unit, from Antoine correlations for humidity calculations, mass and energy balances,

experimental conversion for the deoxo reactor and rules of thumb for the

dehydration of the streams. All the compressors are modeled assuming polytropic compression, an efficiency of 85% and a polytropic coefficient of 1.4 based on rules of thumb (Couper et al., 2005).

4.3.3 *Air separation*

4.3.3.1 *Linde's double column*

The operation of the column is simulated using surrogate models based on rigorous thermodynamic computations using process simulators, CHEMCAD ©. The gas is compressed up to around 200 bar. The actual pressure is a process variable. Before feeding the column, the cold oxygen and nitrogen product streams are used for the final cooling of the compressed air. Next, the air is used as heating agent in the reboiler of the high pressure column. Subsequently, the air is expanded down to 5–6 bar. The final pressure is a variable. The stream is separated in the high pressure column so that the bottoms, a stream rich in oxygen will be used as feed for the low pressure column while the top is used as the reflux of the low pressure column. Both product streams from the high pressure column are expanded to 1–2 bar and fed to the low pressure column. The liquid fractions after each expansion are correlated as a function of the operating pressure and temperature using detail simulations in CHEMCAD©. Both columns are coupled by the condenser–reboiler of the high and low pressure columns respectively. The energy required by the reboiler is provided by the condenser on the high pressure column. From the top of the low pressure column nitrogen is obtained for further synthesis. From the bottoms, mainly oxygen and argon are recovered. The model details can be found in (Sánchez & Martín, 2018). Fig.4.3 shows the section of the facility corresponding with the separation of air.

4.3.3.2 *Membrane separation*

In Fig.4.4, the nitrogen generation section using membrane technology is presented. Air is compressed up to 6–25 bar. The adsorbent bed (ZEO-01) reduces the moisture of the gases. The use of an adsorbent bed and the selection of the appropriate inlet membrane temperature prevents from water condensation within the membrane, a fact that damages the membranes (Häring, 2008). The models of all these units are developed as previously based on first principles, Antoine correlations for humidity calculations, assuming polytropic compression and mass and energy balances. In the literature, it is possible to find different kind of materials for air separation

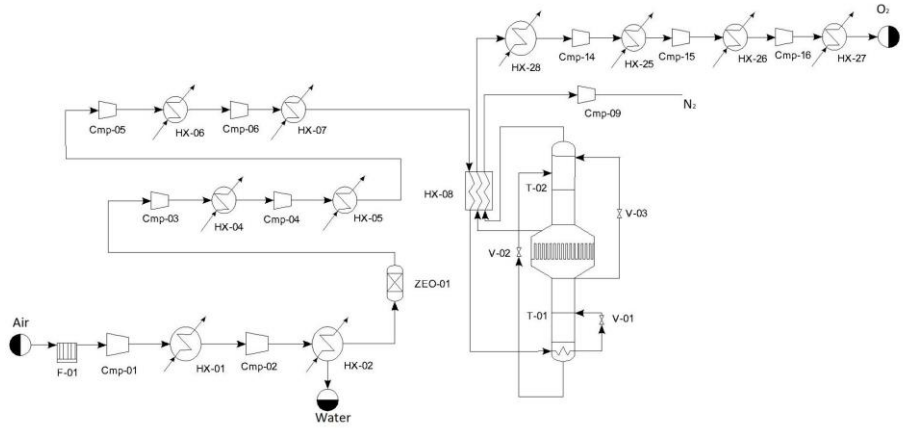

Figure 4.3: Air separation section

membranes, for example, polysulfone hollow fiber membranes (Lababidi, 2000) or carbon molecular sieves membranes (Campo et al., 2010).

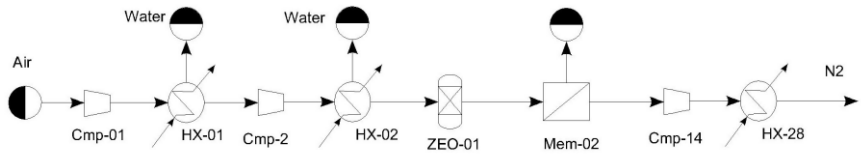

Figure 4.4: Nitrogen section of the ammonia production facility using air separation membranes

To model the membrane itself, a parameter estimation approach is used to develop a correlation using industrial data from the literature. Specifically, two membrane sizes have been considered. A large one, with a nitrogen flowrate interval between 16 and 516 Nm^3/h (Air Liquide, 2017), and a smaller one, with an operating range between 8 and 145 Nm^3/h (Air Liquide, 2016). With these data, two regression models are developed for each membrane. The first one is used to estimate the inlet air flow and the second one computes the outlet flow of a high purity nitrogen stream. According to the data, the variables are the membrane pressure and the nitrogen product purity. The pressure in the reject side is assumed to be constant across the membrane, pressure drop is neglected. However, the pressure in the permeate side is taken to be constant and equal to 1 bar (atmospheric pressure) (Baker, 2012).

Eqs.4.3–4.4 show the models for the high capacity membrane.

$$F_{out}(Nm^3/h) = -27168 + 27.622P(psig) + 547.7Purity(\%) + 0.000144\,(P(psig))^2 - 2.761\,(Purity(\%))^2 - 0.27408P(psig)Purity(\%) \tag{4.3}$$

$$F_{in}(Nm^3/h) = -44595 + 33.650P(psig) + 903Purity(\%) + 0.000169\,(P(psig))^2 - 4.572\,(Purity(\%))^2 - 0.32331P(psig)Purity(\%) \tag{4.4}$$

Similarly, the surrogates for the small scale membrane are given by Eqs.4.5–4.6:

$$F_{out}(Nm^3/h) = -8772 + 7.791P(psig) + 177.0Purity(\%) + 0.000053\,(P(psig))^2 - 0.893\,(Purity(\%))^2 - 0.07735P(psig)Purity(\%) \tag{4.5}$$

$$F_{in}(Nm^3/h) = -14260 + 9.492P(psig) + 288.8Purity(\%) + 0.000020\,(P(psig))^2 - 1.463\,(Purity(\%))^2 - 0.09118P(psig)Purity(\%) \tag{4.6}$$

An oxygen-enriched stream is produced in the permeate side containing about 35% oxygen (Air Liquide, 2016).

4.3.3.3 *PSA systems*

Fig.4.5 shows the section of the facility devoted to produce nitrogen from air. In this technology, only two components are taken into account for the calculations, nitrogen and oxygen. Feed air is compressed to 6–10 bar before the adsorbers. The typical adsorbents in the nitrogen generation from air are Carbon Molecular Sieves (CMS). The equilibrium relationship of the oxygen and nitrogen on CMS do not differ particularly, but the main different lies on the diffusion velocity of both components inside CMS pores (Häring, 2008). Other impurities present in the inlet PSA stream, such as remaining water, are absorbed by the CMS. At least, two PSA units are required to operate in parallel to secure continuous operation downstream (while one vessel is producing nitrogen (adsorption step),

the second one is in the purge step). The final compression is needed to adjust the pressure of the produced nitrogen to the ammonia synthesis loop. Units such as heat exchangers and compressors are modeled as discussed above, based on mass and energy balances, polytropic behavior and Antoine correlations.

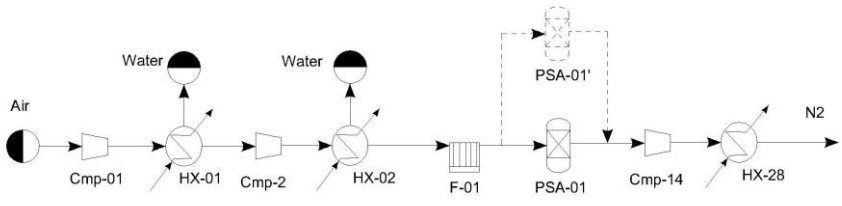

Figure 4.5: Nitrogen production section by PSA

The operation of typical adsorption bed process is based on cycles. In general, different types of cycles are designed according to the final purpose (Ruthven & Farooq, 1990). In this case study, attention is only focused on the adsorption step. The following assumptions are considered to develop the adsorption model (Agarwal et al., 2009; Mofarahi et al., 2009):

- The system is considered isothermal.
- The total pressure remains constant during the high pressure adsorption step. Pressure drops are neglected.
- The flow inside the bed is modeling following the axial dispersed plug flow model.
- The equilibrium relationship for the two components considered are assumed linear.
- Mass transfer is represented by a linear driving force (LDF) expression.
- Ideal gas behavior is assumed for all gases.

Based on these considerations, the adsorption step is described by Eqs.4.7–4.16. In this set, the following variables have been defined: C_i is the gas phase concentration for each component (mol/m^3), C is the total gas concentration (mol/m^3), u is the gas velocity inside the bed (m/s), q_i is the solid phase concentration in the CMS for component i (mol/m^3), q_i^* is the equilibrium solid phase concentration for each component (mol/m^3) and F_i is the flowrate for each component (mol/s). The necessaries parameters to the equations are: ϵ is the bed porosity, k_i is the effective mass transfer coefficient for each component (s^{-1}), K_i is the equilibrium constant

for the adsorption of the component i and A_t is the bed cross-sectional area (m^2). The values of these parameters are in Table 1.

Component mass balance (Eq.4.7):

$$\frac{\partial C_i}{\partial t} + \frac{\partial (uC_i)}{\partial z} - D_L \frac{\partial^2 C_i}{\partial z^2} + \frac{(1-\epsilon)}{\epsilon} \frac{\partial q_i}{\partial t} = 0 \tag{4.7}$$

Overall mass balance (Eq.4.8):

$$\frac{\partial (uC)}{\partial z} + \frac{(1-\epsilon)}{\epsilon} \sum_i \frac{\partial q_i}{\partial t} = 0 \tag{4.8}$$

Mass transfer rate based on linear driving force (LDF) (Eq.4.9):

$$\frac{\partial q_i}{\partial t} = k_i (q_i^* - q_i) \tag{4.9}$$

Adsorption equilibrium relationship (assumed linear relationship) (Eq.4.10):

$$q_i^* = K_i C_i \tag{4.10}$$

Boundary conditions (where v_0 is the inlet bed velocity) (Eqs.4.11–4.14):

$$D_L \frac{\partial C_i}{\partial z}\bigg|_{z=0} = -v_0 \left(C_i|_{z=0^-} - C_i|_{z=0} \right) \tag{4.11}$$

$$\frac{\partial C_i}{\partial z}\bigg|_{z=L} \tag{4.12}$$

$$u|_{z=0} = v_0 \tag{4.13}$$

$$\frac{\partial u}{\partial z}\bigg|_{z=L} \tag{4.14}$$

Mole Flux (Eq.4.15):

$$\frac{\partial F_i}{\partial t} \equiv \frac{\partial C_t}{\partial t} u \epsilon A \tag{4.15}$$

Initial conditions (Eq.4.16):

$$C_i = 0 \quad ; \quad q_i = 0 \quad ; \quad F_i = 0 \tag{4.16}$$

In this work, the following parameters are used for the simulation (see Table 4.1):

The PSA mathematical model is solved using the software gPROMS© with the Centered Finite Difference Method (CFDM) for discretization.

To predict the nitrogen mole flux produced from the PSA system, a surrogate model is developed based on the rigorous model presented above. The nitrogen flow is computed as a function of the operating

Table 4.1: Parameters in PSA simulation (Raghavan & Ruthven, 1985; Sadeghzadeh Ahari et al., 2006)

D_L (m^2/s)	4.876E-4
ε	0.4
k_A (s^{-1})	4.471E-3
k_B (s^{-1})	7.620E-3
K_A	9.35
K_B	9.35
L (m)	3.5
R (m)	0.425

pressure and temperature and the inlet velocity. The final nitrogen purity is fixed to 99.3%. The range for the variables is 6–10 bar for the pressure, 293–308 K for the temperature and 0.1–0.3 m/s for the inlet velocity. Eq.4.17 shows good fitting with the detailed simulation results.

$$\begin{aligned} F_{N_2}^{Out}(mol/s) &= 8.3335 + 0.6755P(bar) - 0.0700T(K) \\ &+ 17.94v_0(m/s) + 0.00134\,(P(bar))^2 + 0.000137\,(T(K))^2 \\ &-10.182(v_0(m/s))^2 - 0.002110P(bar)T(K) \\ &+ 2.0621P(bar)v_0(m/s) - 0.04524T(K)v_0(m/s) \end{aligned} \tag{4.17}$$

4.3.4 *Ammonia synthesis*

The ammonia synthesis loop starts with mixing the unreacted gases with fresh hydrogen and nitrogen. A constraint is imposed so that the molar flow of hydrogen is larger or equal to that given by the stoichiometry of the reaction, but lower than 3.2 times that of nitrogen.

$$N_2 + 3H_2 \rightleftharpoons NH_3 \tag{4.18}$$

The next step is the multistage compression system with intercooling. Typically the operating pressure at the reactor ranges from 100 to 1000 bar and 673–773 K. Therefore, a three stage compression system is suggested. Next, two reactor cooling technologies are considered. The details of the models can be seen in Sánchez and Martín (2018). Here, only a brief description of the operation is presented.

Direct cooling: A three bed reactor is used. There is a trade-off between the thermodynamics and the kinetics. The feed to each bed should be around 673 K. The complexities in removing the heat generated in the reaction results in the need to operate adiabatically and avoid the temperatures above 773 K. Even though the reaction is limited by the equilibrium, typically it cannot be reached (Appl, 1999). The stream exiting each bed is cooled down back of around 673 K using fresh syngas. Thus, the fresh syngas is split into three. The product from the last bed is used to heat up the feed to all the beds in case it is necessary. A detail model in MATLAB© including kinetics, heat transfer and pressure drop is used to provide bounds to the mass and energy balances used to model it for optimization purposes. ΔT_{min} of 3 K has been imposed to avoid temperature cross. Stream mixing is modeled as adiabatic mixture of gases.

Indirect cooling: The operation of the reactor is simpler. The product gas from each bed is cooled down using compressed water. Again, equilibrium is not reached at each bed and a detailed MATLAB© simulation is used to provide bounds for the conversion and the operating temperatures.

Ammonia is recovered by condensation. A two-stage cooling process is performed. First, the hot stream is used to preheat the feed to the beds. Next, cooling water is used. To determine the amount of ammonia condensed a surrogate model is developed from rigorous simulations in CHEMCAD© as a function of the operating pressure for a final temperature of 298 K.

$$\beta_{NH_3} = 0.025860989 + \frac{P(\text{mmHg})}{760} \quad (4.19)$$
$$0.001428067$$

Finally, to increase the recovery, the cold streams from the distillation tower are used as cooling agent. The separation achieved is computed using a surrogate model developed from running a flash calculation in CHEMCAD©. Thus, the recovery in the liquid phase as a function of the pressure and temperature is correlated as follows.

$$\sigma_{NH_3} = 2.063269676 + 0.000163965\frac{P(\text{mmHg})}{760} - 3.49979\ 10^{-5}T(K) \quad (4.20)$$

$$\sigma_{H_2} = -0.005616112 + 4.0769\ 10^{-6}\frac{P(\text{mmHg})}{760} + 2.28468\ 10^{-5}T(K) \quad (4.21)$$

$$\sigma_{N_2} = -0.008053425 + 9.08758\ 10^{-6}\frac{P(\text{mmHg})}{760} + 3.49979\ 10^{-5}T(K) \quad (4.22)$$

Thus, a mass balance to the flash determines the recycle gas and the product as follows:

Liquid:

$$m_{i,out} = \sigma_i m_{i,in} \tag{4.23}$$

Gas:

$$m_{i,out} = (1 - \sigma_i) m_{i,in} \tag{4.24}$$

A purge is allowed to remove the impurities and avoid building up. The optimization decides the amount to be purged before recycling the unreacted gases back to the reactor system. The purge stream contains valuable hydrogen. Therefore, a membrane is located to recover it from the purge and recycle it. It is capable of recovering 85% of the hydrogen and, together with it, 10% of the other gases also go through the membrane (Air Products, 2016; Membrane Technology and Research, 2016).

4.4 methodology

4.4.1 *MINLP solution procedure*

The problem is formulated as an MINLP in GAMS© with seven binary variables, one per reactor design, one per air separation technology and the other ones for the energy source to select among solar panel and wind turbines. The problem is decomposed by solving six relaxed NLP, one for each combination between the two different reactor design (direct and indirect cooling) and the three alternative for air separation (membranes, PSA and distillation), where the number of turbines and panels are relaxed as continuous variables.

The problem formulated in the previous section, approximately 1500 equations and inequalities in the distillation case and 1000 equations and inequalities in the membranes or PSA case, is solved using the objective function described in Eqs.4.25–4.33. The objective function consists of a simplified production cost, where the power is provided by PV panels (Photovoltaic Software, 2017) or wind turbines (de la Cruz & Martín, 2016) and the ammonia price is assumed equal to 1 €/kmol. The profiles of the solar and wind energy are taken from Davis and Martín (2014a) for an allocation in the south of Spain.

$$Z = F_{NH_3} - \frac{0.33}{\tau} n_{panel} \left(P_{panel} C_{panel} + A_{panel} C_{area} \right) + n_{turbine} P_{nom} C_{turbine} - \frac{1}{3600} \left(C^{op}_{turbine} P_{nominal} n_{turbine} \right) \quad (4.25)$$

$$P \geq n_{panel} P_{panel} + n_{turbine} P_{turbine} \quad (4.26)$$

$$P_{turbine} = \frac{P_{nom}}{1 + e^{(-(v-a)m)}} \quad (4.27)$$

$$a = 8.226 \quad (4.28)$$

$$m = 0.805 \quad (4.29)$$

$$P_{panel} = \frac{0.75}{24} A_{panel} (m^2) I \frac{kWh}{m^2 d} \omega \quad (4.30)$$

$$\omega = 0.25 \quad (4.31)$$

$$A = 1.66 \quad m^2 \quad (4.32)$$

$$\tau = \text{seconds in a year} \quad (4.33)$$

C_{panel} is assumed to be 1080 €/kWp (International Renewable Energy Agency, 2012), C_{area} is fixed to 7 €/m^2 (Goodrich et al., 2012), $C_{turbine}$ is 1600 €/kW and $C^{op}_{turbine}$ is 0.015 €/kWh (Davis & Martín, 2014a). The NLP is solved on a monthly basis using a multistart optimization approach with CONOPT 3.0 as the main solver. To achieve the total production capacity, once the best technology is selected on a monthly basis, the production profile is recomputed following the solar/wind availability.

To scale up/down, the formulated problem is solved for different ammonia production capacities within the range of operation of the various technologies. In particular, the transitions when the maximum capacity of one unit, either membranes or PSA systems, is reached, are studied comparing the operation of that section and rest of the facility before and after the second unit is required. While the operation of the nitrogen production section may be discontinuous in the change from one unit to the use of the second one, and the operating conditions change with the scale, the rest of the plant behaves smoothly, the energy and mass flows scale proportionally and the intensive variables remain constant in the scale up (Martín & Grossmann, 2017). A compressor after the membrane/PSA is used to maintain downstream operation. The optimization results at various scales are used to develop correlations to predict the operating conditions as a function of the production capacity. These results will be

used to size units for the cost estimation purposes.

4.4.2 *Cost estimation procedure*

Scaling up-Scaling down the investment cost is a complex process. First, the capital cost of the different units involved was correlated as a function of a characteristic variable, such as the exchange area of the heat exchangers. This scaling variable is directly related to the mass or energy flows involved in that particular unit. However, for the operation of the membranes or the PSA systems, there is no such proportionality, but to achieve certain purity and flows, the operating conditions must change. With a single unit (membrane or PSA) it is possible to produce a wide range of purities and flows. However, a change in the operating conditions of the unit is required. In Table 4.2, the scaling variable and the operational range is presented for all units involved in the plant. The latter is only considered in the unit that presents a maximum/minimum size. This affects the cost estimation. If the scaling variables exceed the limits, the unit must be duplicated. For this section, the scale up/scale down requires special attention. While in the rest of the plant, when a scaled up or down is carried out, the operating conditions are the same and, only a proportional change in the mass and energy flows in the different units happens. However, in the nitrogen production section using membranes or PSA systems, the operating conditions can change. Proportional scale up of the mass and energy flows in this section does not hold. To determine the mass and energy flows, a surrogate model is developed from the results of the optimization of a number of production capacities to be used in the scale up or down without running multiple optimization cases for all the capacities studied. These correlations relate the operating variables in this section, such as heat flows and work, to the outlet flow from the membrane or PSA that already scales proportionally like rest of the plant. Thus, with the nitrogen flow and the correlations developed it is possible to determine the operating conditions within the nitrogen section, evaluate the scale up or down and size the units.

The factorial method is applied to estimate the total investment cost. To compute the equipment cost, the correlations developed by Almena and Martín (2016) are used. The electrolyzer cost is taken from Saur and Ramsden (2011), the PSA adsorbent cost from NETL (2013) and the membrane cost from Air Products (2018). The first case distinguishes between modular units, PSA and membranes, and the rest. Membranes and PSA are estimated as individual modulus with a limited operating range of production capacities. Note that their operating conditions are not scalable. Once the maximum capacity is reached the unit must be duplicated. The rest of the units are scaled using the correlations in by Almena and Martín (2016). Again, when the maximum production capacity is reached, a second

Table 4.2: Procedure of scaling equipment

Equipment	Scaling variable	Range
Compressors	Power	-
Deoxo	H_2	-
Distillation Tower	Rectifying section vapor flow	-
Electrolyzer	H_2 flow	Mem or Small Mem: 0–100 Nm^3/h PSA: 0–300 Nm^3/h Distillation: 0–800 Nm^3/h
Filter	Inlet flow	-
Ammonia Mem	Ammonia total flow	-
Ammonia Reactor	Ammonia total flow	-
G-L Separators	Out flow, P and T	-
Heat Exchanger	Area	0–2000 m^2
Mem	N_2 flow	0.445–1.905 mol/s
Small Mem	N_2 flow	0.203–0.543 mol/s
PSA	N_2 flow	1.508–6.697 mol/s
ZEO	Inlet flow, P and T	-

unit is required. However, the operating conditions are constant in the scale-up/down but for the ones linked to the PSA and membrane systems. Alternatively, modular design for the entire facility is also evaluated. In modular design, PSA as well as membrane technologies are designed as individual units. The rest of the units such as compressors, reactors or heat exchangers are designed for the maximum flows corresponding with the maximum outlet nitrogen capacity in one membrane or PSA. Thus, when the maximum capacity is surpassed, the total plant must be duplicated (one new module is necessary). Then, economies of scale are partially lost. The energy collection units are adapted to the desired production.

The method to compute the operating cost includes variable and fixed costs (Sinnott, 2014). Within variable costs, raw materials are included. The oxygen that it is produced during the cryogenic distillation or electrolysis is considered as an asset of the process with a price of 21 €/t. However, the rejection from PSA and membrane systems cannot be sold for profit. Utilities, mostly cooling water and steam, and other materials are also included within the variable costs.

The fixed costs include maintenance, labor, laboratory, amortization, insurances, taxes and other items. Maintenance cost is estimated as 5% of fixed capital for the chemical equipment. A maintenance cost of 15 €/kW year for solar panels and 32 €/kW year for wind turbines is assumed (NREL, 2016). Labor is estimated based on equation provided for Green and Southard (2019). Lab, supervision and general costs are estimated as 25%, 20% and 50% of labor, respectively. Linear amortization is computed assuming a 32.5 years of life spam for solar panels, 20 years for wind turbine (NREL, 2016) and 30 years for chemical units. Insurances and taxes are estimated as 1% of fixed capital each of them.

4.5 results and discussion

The allocation of the plant is the same as in the previous work, the South of Spain characterize by high solar incidence and small regions of high wind velocities (Sánchez & Martín, 2018).

4.5.1 *Key operating parameters*

The main operation conditions in the facility are summarized in Tables 4.3–4.5. In Table 4.3, the membranes temperature and pressure for a fixed capacity production of ammonia are presented. The temperature and the pressure change when the nitrogen demand changes to maintain the purity. The small membrane can produce a nitrogen flux between 0.203 and 0.543 moles of N_2 per second. This translates into an ammonia production capacity (with only one membrane) in the range of 0.051–0.495 moles NH_3/s for the ammonia direct cooling reactor and 0.086–0.572 moles NH_3/s for the indirect one. In this range, the membrane conditions are adjusted, within the range presented in the previous Section 4.3.3.2, to produce the nitrogen flow needed for ammonia synthesis loop. In the case of the smaller membrane, the nitrogen production range is within 0.445–1.905 moles N_2/s and the ammonia intervals are in 0.111–1.737 moles NH_3/s for direct cooling and 0.119–2.020 moles NH_3/s for indirect cooling. The rest of variables in the facility remain constant through the different capacities. The ammonia reactor conditions are the same in both membranes. The indirect cooling reactor operates at a higher pressure, and with the same fed flow to the synthesis loop, resulting in a higher ammonia production (around a 9%).

When the PSA system is used to produce nitrogen, see Table 4.4, the inlet velocity, operating pressure and temperature for PSA unit are the major operating variables. As in the case of the use of membranes, the

Table 4.3: Main operating variables of the air separation section (Direct and indirect cooling)

	Units	Mem Small		Mem	
		Direct	Indirect	Direct	Indirect
NH_3 Flowrate	moles/s	0.334	0.361	0.835	0.910
Nitrogen Purity		0.993	0.993	0.993	0.993
Membrane Temperature	K	308	308	308	308
Membrane Pressure Reject	atm	18.0019	17.1737	13.584	12.899
Membrane Pressure Permeate	atm	1	1	1	1
Synthesis Reactor BI Pressure	atm	152.3	207.53	152.3	207.53
Synthesis Reactor BI Temperature	K	673–773	673–773	673–713	673–773
Synthesis Reactor BII Pressure	atm	152.3	207.53	152.3	207.53
Synthesis Reactor BII Temperature	K	713–773	713–773	713–773	713–773
Synthesis Reactor BIII Pressure	atm	152.3	207.53	152.3	207.53
Synthesis Reactor BIII Temperature	K	713–773	713–773	713–773	713–773
Initial Splitter to B1		0.76	-	0.76	-
Initial Splitter to B2		0.11	-	0.11	-
Initial Splitter to B3		0.13	-	0.13	-
Ammonia Recovery Temperature	K	260	260	260	260
Ammonia Purity		>99%	>99%	>99%	>99%
Total gas purge fraction		0.12	0.11	0.12	0.11

results presented in the table correspond to the ammonia capacity showed. The range of capacities for one PSA unit is within 1.508–6.967 moles N_2/s, corresponding with an ammonia production range of 0.376–6.354 moles NH_3/s in the ammonia direct reactor and 0.384–7.389 moles NH_3/s for indirect cooling. The ammonia synthesis conditions are similar to those presented in the previous technology. In both cases, a purge is necessary to avoid building up inert components. The gas purge fraction presented is referred to the total flow of gases from the ammonia gas–liquid separator.

Finally, the largest ammonia capacity is achieved using cryogenic distillation in the nitrogen production section. The main operating results are showed in Table 4.5. The ammonia rate presented in this technology is significantly higher than in the previous cases. In the distillation section, the high pressure column operates at 6 bar and the low pressure one at

Table 4.4: Principal operating variables in ammonia facility producing nitrogen by PSA

	Units	PSA	
		Direct	Indirect
NH_3 Flowrate	moles/s	3.34	3.642
Nitrogen Purity		0.993	0.993
PSA inlet velocity	m/s	0.255	0.236
PSA Temperature	K	293	293
PSA Pressure	atm	6	6
Synthesis Reactor BI Pressure	atm	152.3	210.07
Synthesis Reactor BI Temperature	K	673–773	673–773
Synthesis Reactor BII Pressure	atm	152.3	210.07
Synthesis Reactor BII Temperature	K	713–773	713–773
Synthesis Reactor BIII Pressure	atm	152.3	210.07
Synthesis Reactor BIII Temperature	K	713–773	713–773
Initial Splitter to B1		0.76	-
Initial Splitter to B2		0.11	-
Initial Splitter to B3		0.13	-
Ammonia Recovery Temperature	K	260	260
Ammonia Purity		>99%	>99%
Total gas purge fraction		0.12	0.11

1 bar. No argon recovery is considered in this study. In this technology, a production range is not presented due to the easy scale up-scale down for the distillation and the large dimensions necessary for this kind of equipment that limits the modular development. The lower production capacity is selected for the smaller feasible tray distillation column, that with a diameter of 3 ft (Couper et al., 2005). In this case, both reactor designs present the same operating pressure but differ in the inlet/outlet temperatures in the reactor bed. Also in this case, the ammonia production flowrate is similar in both reactor alternatives.

Note that cryogenic separation requires the higher operating pressure and therefore, a larger consumption of power is expected compared to the use of membranes and PSA.

Table 4.5: Major operation conditions in distillation based ammonia plants

	Units	Distillation	
		Direct	Indirect
NH_3 Flowrate	moles/s	201	201
Nitrogen Purity		>99.3%	>99.3%
High Pressure Air Distillation Column	atm	6	6
Low Pressure Air Distillation Column	atm	1	1
Synthesis Reactor BI Pressure	atm	168.01	168.01
Synthesis Reactor BI Temperature	K	673–768.7	673–760.7
Synthesis Reactor BII Pressure	atm	168.01	168.01
Synthesis Reactor BII Temperature	K	717.4–769.9	729.4–758.67
Synthesis Reactor BIII Pressure	atm	168.01	168.01
Synthesis Reactor BIII Temperature	K	715.3–770.7	731.38–767.78
Initial Splitter to B1		0.61	-
Initial Splitter to B2		0.15	-
Initial Splitter to B3		0.24	-
Ammonia Recovery Temperature	K	240	240
Ammonia Purity		>99%	>99%
Total gas purge fraction		0.17	0.17

Regarding the energy source, PV panels are selected for this case of study according to the solar irradiance and wind velocity profiles of the particular allocation. The results presented below use solar photovoltaic panels as power collection devices. The only exception corresponds to the sensitivity analysis presented at the end of this study where both energy sources, wind and solar, have been evaluated. This is expected for an allocation in the south of Spain. In a previous work, a sensitivity analysis has been performed to show the optimum energy source taking account the weather conditions. A future scenario with a reduced price for solar panels and wind turbines is also presented (Sánchez & Martín, 2018).

4.5.2 *Scale up results*

In this section, the effect of the scale on the production and investment cost of ammonia production facilities is presented. The results are divided

into 4 subsections. First, the profiles of the capital costs as a function of the capacity of nitrogen. Next, nitrogen production section is integrated with the entire facility to present the comparison of the costs for the two cooling technologies considered for the reactor design. This comparison assumes individual scale up of any unit, meaning that as the production capacity increases, the size required by the unit determines its number and cost. However, current trends are in line with building "modular facilities". In this case, each modulus must be bought as such within a range of production capacities. Thus, the scale up is no longer evaluated per unit, but per modulus. This modular cost is used only for membrane and PSA technologies since distillation columns are not expected to be used for modular design. The production of ammonia requires chemical and power collecting units. In a third section, the contribution to these sections to the investment is shown. Finally, a sensitivity analysis is presented focused on the cost of the PV panels and wind turbines. Development of these technologies is expected to reduce their cost in the near future and that has an impact on the production and investment costs of ammonia.

4.5.2.1 *Nitrogen production*

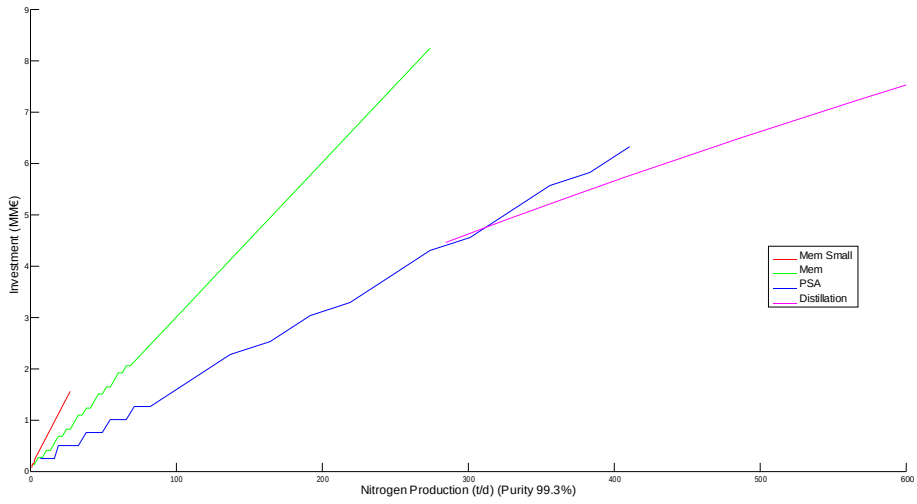

Figure 4.6: Investment for different nitrogen technologies

Fig.4.6 shows the chemical equipment investment cost for the production of nitrogen from air for ammonia synthesis purposes. Note that energy collecting units, PV panel costs, are not included. A purity of 99.3% is fixed based on previous studies (Sánchez & Martín, 2018). Two membrane sizes, PSA and distillation technologies are shown. The production cost is

also correlated to the investment, due to amortization (see cost estimation procedure section). The rules of thumb specify that the tray towers are suited for diameters above about 3 ft (Couper et al., 2005). With the minimum nitrogen flow considered, the first distillation column (high pressure) presents a diameter of 0.768 m and the second tower (low pressure) a diameter of 0.955 m, both in accordance with the previous rules. Based on these results, the maximum capacity for an ammonia plant using small membranes is fixed to 10 t NH_3 per day, which corresponds to around 20 membranes working in parallel. In the case of the ammonia facility working with large capacity membranes, the operation range is established in the range of 0.69–100 t NH_3 per day, requiring about 60 membranes. When PSA systems are used, the ammonia capacity varies between 2.4–150 t NH_3 per day, a bit more that the cutting point shown in Fig.4.6 with the distillation. For this maximum capacity, around 25 units (50 adsorption beds) are necessary. The use of the distillation begins, approximately, when this alternative is still competitive. The nitrogen production from cryogenic methods presents a lower capital cost than the one of the PSA for a production capacity around 10000 Nm^3/h (300 t/day), results that can be validated in the literature (Baker, 2012). The first pattern that is interesting to point out is the curvature of the entire set of data. As the production capacity increases, the general trend goes closer to the 6 tenths rule. However, this rule does not hold true for each of the individual technologies. From the smallest production capacity, membrane technologies scale almost lineally. In particular, for large membranes, steps can be seen as the production capacity of each membrane is reached and another membrane is required. Similarly for PSA systems, the steps are wider and local minima in production costs can be found. Once a new PSA system is required, as its full capacity is used, there is a small decrease in the investment per unit produced. Steps turn into waves for production capacities over 100 tons per day. In the comparison, it is seen that only for very small sizes membranes are more economic than PSA systems. The use of distillation is beginning to be interesting over 300 tons per day. It is seen that even at sizes where distillation columns can already be used, distillation takes some additional capacity for it to become competitive with PSA systems.

4.5.2.2 *Direct vs indirect*

When nitrogen production is integrated with hydrogen production and ammonia synthesis, the costs for panels and regular units mitigate the trends seen in Fig.4.6 due to the larger energy demand required by cryogenic separation units. Figures for small scale (Fig.4.7) and for the general

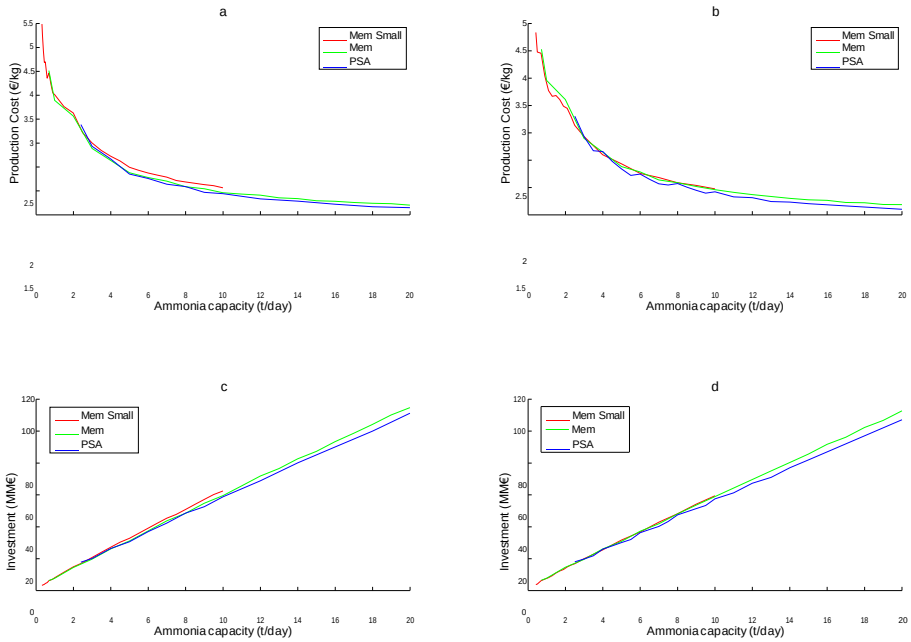

Figure 4.7: Production Cost and Investment for small scale alternatives technologies (a: Direct cooling production cost, b: Indirect cooling production cost, c: Direct cooling investment, d: Indirect cooling investment)

trend (Fig.4.8) are presented. The general trend in the production cost is of a power law, decreasing the production cost with the capacity. In general, direct cooling is more expensive at small scale. This is in part due to the fact that no additional profit is obtained from producing steam in the reactor and the complex cooling scheme. The difference is larger at very small scales, and it is mitigated over a production capacity of 10 t/day. At small production capacities, below 20 t/day, the possibility of using small membranes, membranes and PSA is based on their feasible processing rates. Very small capacities require the use of membranes, below 2.5 t/day. Larger membranes are more economic when they can be used and remain competitive with PSA systems for a range of production capacities. For production capacities between 2.5 and 10 t/day, Fig.4.7 a and b, the competition between PSA and membranes is tough and, for indirect cooling, Fig.4.7 b, it is highly dependent on the actual production capacity required. PSA are more suited for larger sizes. Over 10 t/d the ammonia production cost goes below 2 €/kg. As the production capacity increases, Fig.4.8 a and b for direct and indirect cooling respectively, PSA becomes the preferred technology even when distillation columns can be used, about 60 t/day. An interesting result is that the production cost is the minimum for production capacities of around 150 t/day using PSA systems. In cryogenic separation units, the large energy needed to operate them, results in the fact that the

investment in PV solar panels is high. This is a critical step because the

more competitive behavior of the use of distillation columns compared to PSA systems observed in Fig.4.6 is lost when energy collecting units are included in that analysis due to the high cost they represent. This point is really interesting because the use of renewable energy sources in chemical process is, nowadays, directly related to the distributed production and the need to provide renewable energy competitively (Reese et al., 2016). If the use of small production capacities is attractive in terms of investment and production costs, the integration of renewable energies within traditional process will be a promising alternative, because one of the difficulties is the use of large amounts of solar or wind energy.

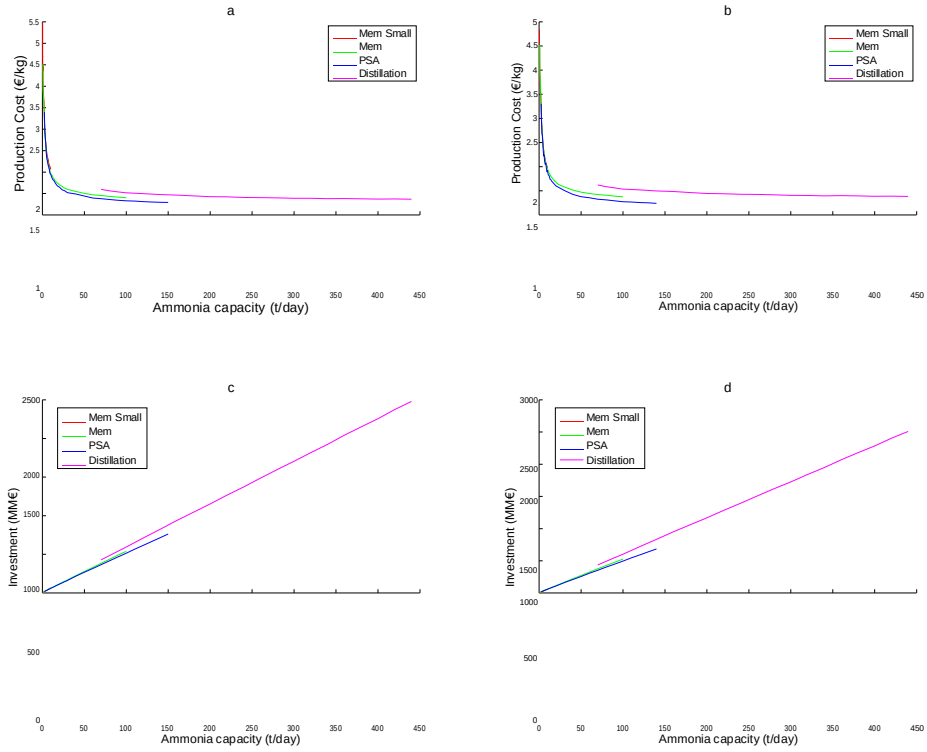

Figure 4.8: Production Cost and Investment for all nitrogen technologies (a: Direct cooling production cost, b: Indirect cooling production cost, c: Direct cooling investment, d: Indirect cooling investment)

In terms of investment, the analysis is again divided between small scale and the general trend. Fig.4.7 c and c for direct and indirect cooling respectively, presents the investment cost for production capacities below 20 t/day. It is seen that the investment increases almost linearly and curves for larger production capacities (Fig.4.8 c and d). More importantly, a more detailed view shows the steps resulting from the need to add new units in parallel as the production capacity increases. This fact is more important for PSA that membranes. PSA becomes the cheaper alternative over 10

t/y for both direct and indirect cooling. In general, indirect cooling is 2% cheaper than direct cooling due to the complex cooling structure for the reactor. Larger production capacities require the use of distillation columns, Fig.4.8 c and d for direct and indirect cooling respectively. It looks as if PSA

system could be more interesting even for larger production capacities, but the number of units required becomes challenging to operate.

4.5.2.3 *Modular design*

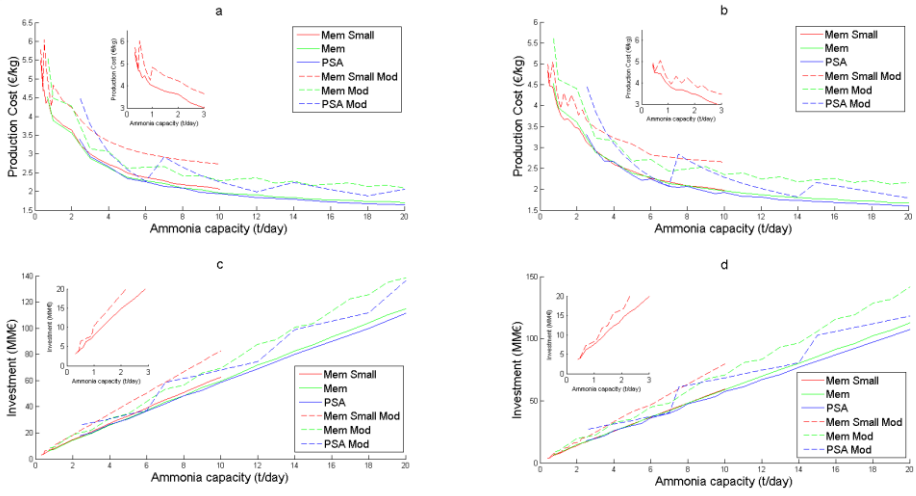

Figure 4.9: Production Cost and Investment comparison between modular and non-modular design (a: Direct cooling production cost, b: Indirect cooling production cost, c: Direct cooling investment, d: Indirect cooling investment)

The distributed availability of solar energy and the also distributed use of fertilizers make modular design an interesting trend in the chemical industry. This fact is changing the paradigm of the production since smaller facilities are being designed, but most importantly, they are being built as sets for assembly reducing the economy risk involved in investing large sums on novel technologies. In Fig.4.9, the production costs for small capacities, using (a) direct cooling and (b) indirect cooling, are presented. The most important feature in these figures is the comparison between the modular design with the unit by unit scale up is the discontinuity in the cost when modular designs are considered. In general modular is more expensive that unit by unit design. However, the flexibility behind the use of a modular facility provides an advantage that is difficult to quantify in two ways. First, the modular can be shipped from one location to another to serve different markets or make the most of a seasonal resource. Second, the modules are independent and the financial risk is minimized. Modular design however also presents drawbacks. There are particular sizes for which the production costs show local minimum. For instance, PSA modular can be as competitive as any other technology for capacities

of 6 and 7 t/d for indirect and direct cooling, respectively. Those should the targeted sizes to be used. Furthermore, due to those minima the selection among modular membrane vs modular PSA is not an easy decision but it highly depends on the production capacity required. These results are interesting from a decision making standpoint since trade-offs can be found in supply chain studies using this information.

While the production cost shows a power law profile, the investment cost, Fig.4.9, c for direct and d for indirect cooling reactor systems, increases almost linearly, but for the waves as a result of the addition of a new module to increase the production capacity. As in the case of the production cost, the modular design shows that depending on the capacity, PSA or modular membranes can be the technology of choice, in particular below a production capacity of 10 t/day.

4.5.2.4 *Power collection vs production*

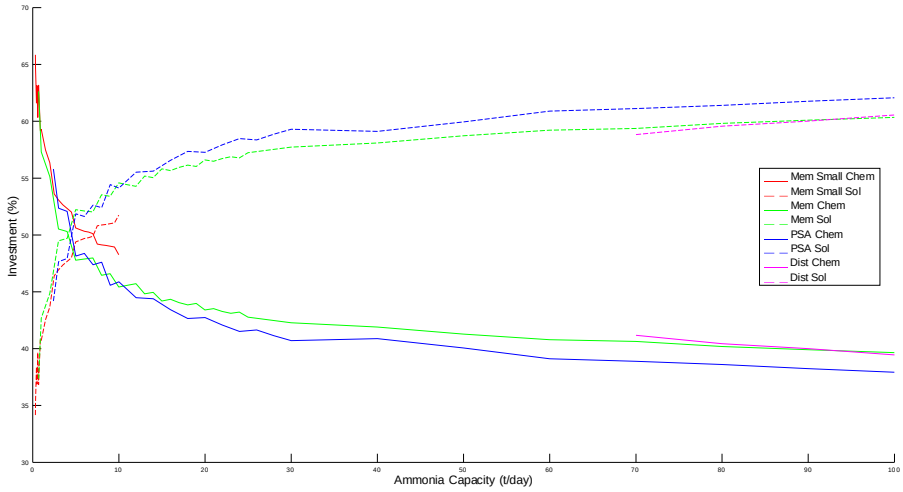

Figure 4.10: Solar vs Chemical equipment investment

In previous papers for the production of chemicals using electrolysis, rather appealing results are presented. Typically, the power production section of the facility represents 94% of the investment in units (Davis & Martín, 2014a, 2014b). In Fig.4.10, the contribution of the power and the chemical units to the cost is presented for direct cooling alternatives, the most promising and for the sake of the length of the work. This trend is rather similar for large production capacities, where for the use of membranes, distillation or PSA systems, the solar panels represent above 60% of the equipment cost. However, this trend changes for small production

capacities. Below 5 t/day the contribution of the power collecting units represents below 50% of the investment in equipment. For very small capacities, the chemical units can reach 70% of the investment required in units. For production capacities below 20 t/d it is possible to see the steps associated to the need for additional units. Although a general trend can be established, the fluctuations can be key to decide on the best technology to use.

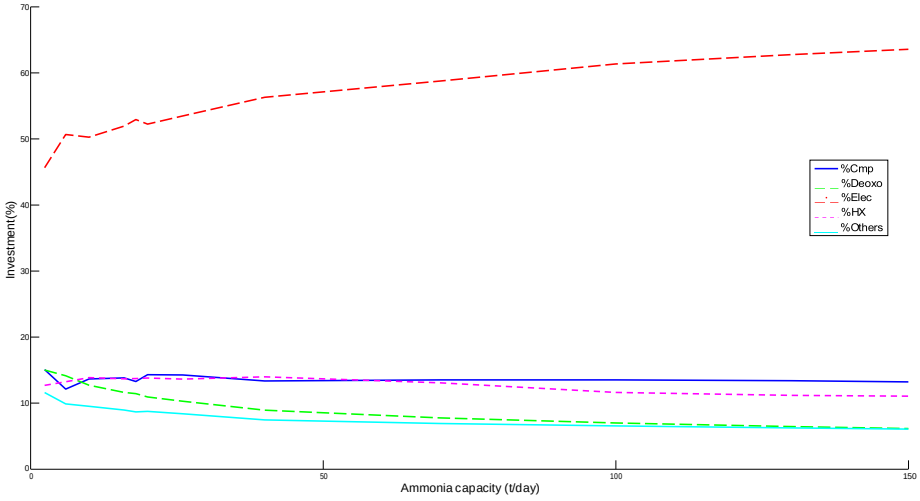

Figure 4.11: Chemical equipment investment evolution for different capacities

If only the chemical equipment is considered, Fig.4.11 shows the breakdown of the investment results for the case of the PSA system as an example. The largest share by far is due to the electrolyzer, a share that increases with the production capacity due to the need for a 3 to 1 ratio of hydrogen to nitrogen. This is also due to the fact that the equation to estimate the cost of the electrolyzers does not present economics of scale, but the cost increases linearly with the capacity achieving this high share of the equipment cost. An electrolyzer capital cost reduction is expected in the next years (Hinkley et al., 2016).Apart from the electrolyzers, the contribution of the rest of the units decreases with the production capacity due to the economies of scale associated with the cost estimation of these units, mainly compressors and heat exchangers. Finally, Fig.4.12 shows the breakdown of the contribution to the cost of the different chemical units for various technologies and production capacities. The share of the electrolyzer is more important when the capacity is larger. Economies of scale reduce the contribution to the total cost of units such as the deoxo reactor, while the increased demand for hydrogen and results in large

electrolysis sections. In large capacities, heat exchangers and compressors represent the highest items after electrolysis.

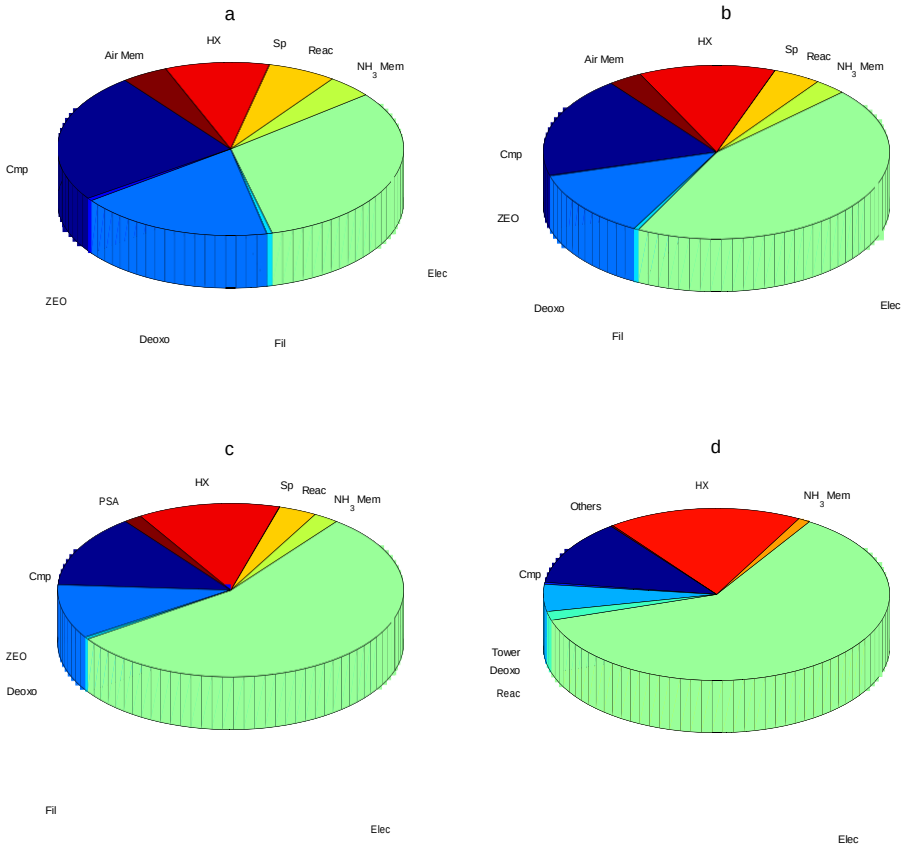

Figure 4.12: Equipment cost breakdown: Different capacities and different technologies (a: Small Membrane (1 t NH_3/day), b: Membrane (10 t NH_3/day), c: PSA (30 t NH_3/day), d: Distillation (200 t NH_3/day))

4.5.2.5 *PV prices: sensitivity analysis*

Maturity makes technologies cheaper. Numerous studies in the literature evaluate the effect of future expected costs for PV panels or wind turbines on the use of renewable energy (Heuberger et al., 2017). With the current costs for solar and wind energy collecting technologies, the cost for renewable ammonia is above that from traditional resources. For the case of direct cooling in the ammonia synthesis reactor, Figs.4.13 and 4.14 present the production and investment costs and the estimates over the next 30 years. In fact, the scale has an interesting effect decreasing the cost from 5.5 €/kg down to around 1.5 almost for any technology. Distillation achieves the lowest production cost around 1.4 €/kg for large plants. The profile follows a potential law in general for all cases. However,

discontinuities can be seen for very small capacities finding local minima as the production capacity increase. By 2050, almost 90% reduction in the PV panel cost (Fraunhofer & Energiewende, 2015) and around 23% in the wind

turbines (International Renewable Energy Agency, 2012) is expected. Using this prediction, Fig.4.13 (a-d) for small and large membranes, PSA and distillation columns respectively, it is possible to see savings larger than 25% of the production costs with very promising values even below 1 €/kg for the largest production capacities of membranes, PSA and distillation technologies. With this level of savings it is not only that renewable ammonia becomes attractive but also competitive with traditional technologies. In all cases, the plant that uses wind turbines as energy source is more expensive is terms of production cost for the availability energy in the allocation of the case of study since turbines are becoming mature and they are already reaching the mature cost.

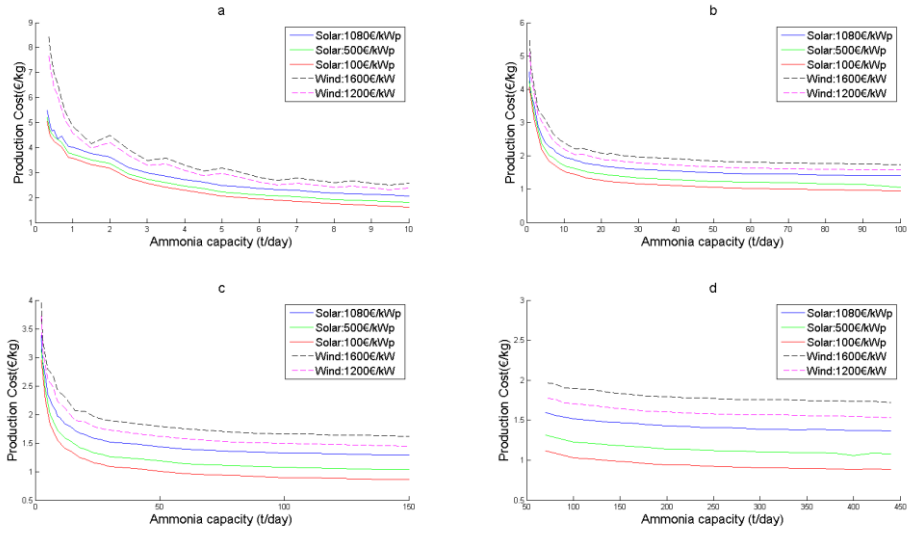

Figure 4.13: Production Cost: PV Panels Price Sensitivity Analysis (a: Small Membrane, b: Membrane, c: PSA, d: Distillation)

Fig.4.14 shows the investment cost of the facilities for the four technologies used in nitrogen production, namely, small membranes, membranes, PSA and distillation columns. The large share of the solar field on the investment cost results in major savings if the cost of PV panels reach the levels expected in the Roadmap 2050 with total investment cost half current prices (Fraunhofer & Energiewende, 2015). Taking into account that the PV panels represented over 60% of the total investment as, the results shown in Fig. 4.15 are straightforward. Furthermore, especially in Fig.4.14 a, c and d, discontinuities can be seen in spite of the general lineal trend. These discontinuities provide a certain economy of scale. Wind turbines capital cost present more impact on the total investment, in particular, when a small membrane is used due to the large energy that it is possible to obtain

with only one turbine (with a highest cost per equipment). In Fig.4.14 a, waves appear, when a new turbines are necessary.

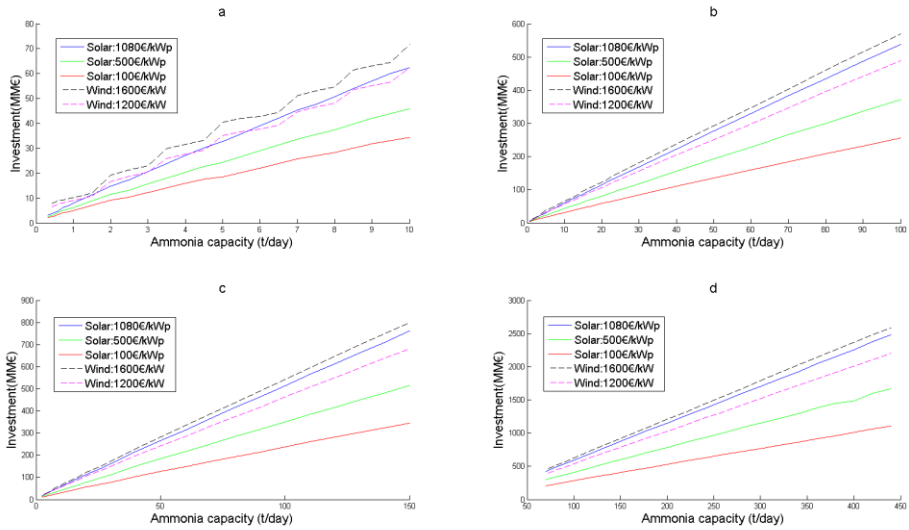

Figure 4.14: Investment: PV Panels Price Sensitivity Analysis (a: Small Membrane, b: Membrane, c: PSA, d: Distillation)

A regression study has been performed to obtain different correlations that represent the production cost or the capital cost versus the ammonia capacity. A typical power regression model (Eq.4.34) is selected for production cost adjust. In the case of capital cost, a linear model, Eq.4.35, is chosen.

$$C_{prod}(€/kg) = b \cdot (q(t/day))^d \tag{4.34}$$

$$I(\text{MM€}) = j \cdot (q(t/day)) + h \tag{4.35}$$

In Tables 4.6 and 4.7, the fitting parameters are presented for two cases: with a PV panels price of 1080 €/kW$_p$ and with 100 €/kW$_p$, the two extreme cases in the energy source selected.

The above equations present a good fitting between the different variables. The average absolute error in all cases is about 1%–10%.

The changes in the PV panel prices affect decisively to the investment distribution. If a price of 1080 €/kW$_p$ is used, as it is shown in Fig.4.10, the panels investment represents a high percent, increasing with the ammonia capacity. However, if the price falls 100 €/kW$_p$ (Fig. 4.15), the photovoltaic investment only represents around a 10%–20% of the total plant capital cost. The chemical equipment investment always dominates the total investment.

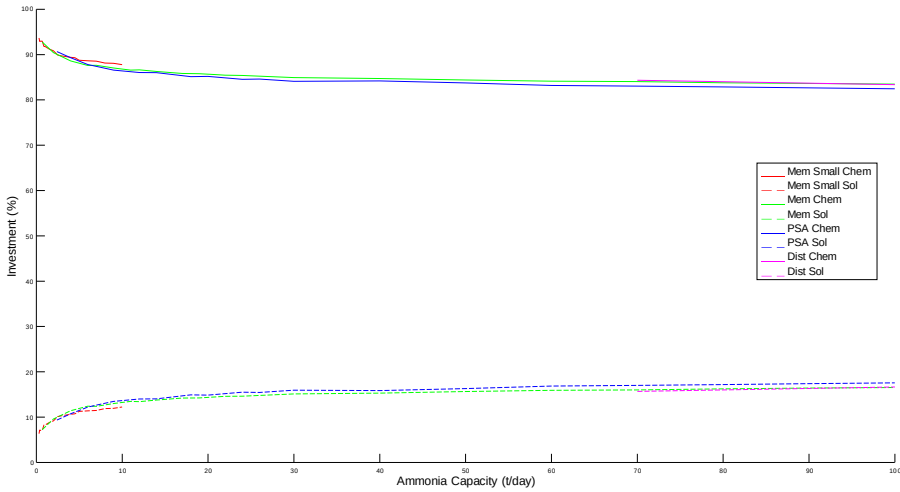

Figure 4.15: Solar vs Chemical Equipment Investment (PV panels price = 100 €/kW$_p$)

Table 4.6: Cost production fitting parameters

	b		d	
	1080 €/kW_p	100 €/kW_p	1080 €/kW_p	100 €/kW_p
Small Membrane	3.955697	3.550717	-0.276696	-0.324149
Membrane	3.596221	3.21486	-0.234141	-0.288366
PSA	3.238858	2.905003	-0.202753	-0.261971
Distillation	2.204004	1.788228	-0.080172	-0.118267

Table 4.7: Investment fitting parameters

	b		d	
	1080 €/kW_p	100 €/kW_p	1080 €/kW_p	100 €/kW_p
Small Membrane	6.174132	3.343221	1.69189	1.862363
Membrane	5.363789	2.525733	6.342758	6.87237
PSA	5.040767	2.267622	8.717249	9.379684
Distillation	5.543095	2.421744	41.411212	42.130757

4.6 conclusions

In this work, a scale up/down study for the production of renewable based ammonia has been developed considering three technologies, namely

small and large membranes, PSA systems and distillation columns for nitrogen production, two energy collecting technologies, PV panels and wind turbines and two synthesis reactors, direct and indirect cooling. Modular and unit by unit scale up are considered.

A number of trade-offs are seen in the results. While membranes are suitable for very small production capacities, PSA system for medium and distillation column for large, PSA systems are competitive across scales, but the large number of units required can be a drawback to pursue this technology that requires lower operating pressure than distillation columns. Modular designs are only efficient and competitive when full capacity is used, however are versatile in their operation. The large energy consumption has larger impact in the investment of large facilities, where energy collecting units represent 60% of the production costs. However, smaller capacities investment cost is governed by chemical units. Finally, the expected decrease in PV panels is far larger than that of wind turbines, representing 90% savings and very promising production costs for ammonia below 1 €/kg. These saving can reduce the investment cost by half in the near future.

Ammonia production supply chain must include these findings for a better allocation of the facilities and exploitation of resources while serving the communities.

nomenclature

A_{panel}	Area per panel (m^2/panel)
A_t	Cross sectional area (m^2)
a	Turbine fitting parameter (m/s)
b	Cost Production fitting parameter
C_{panel}	Solar panel cost (€/kW_p)
C_{area}	Area cost (€/m^2)
$C_{turbine}$	Turbine cost (€/kW)
$C^{op}_{turbine}$	Turbine operational cost (€/kWh)
C	Total gas phase concentration (mol/m^3)
C_i	Gas phase concentration of component i (mol/m^3)
d	Cost Production fitting parameter
D_L	Diffusion coefficient (m^2/s)
F	Total flow rate (Feed flow rate) (kg/s)
F_i	Molar flow rate of component i (kmol/s)

k_i	Effective mass transfer coefficient for component i s^{-1}
K_i	Adsorption equilibrium constant for component i
h	Investment fitting parameter
I	Solar radiation (kWh/m^2 d)
j	Investment fitting parameter
L	Total bed length (m)
m	Turbine fitting parameter (s/m)
n_{panel}	Number of solar panels
$n_{turbine}$	Number of turbines
P	Pressure (mmHg)
$P_{turbine}$	Power generated by a turbine (kW)
P_{nom}	Nominal power of the selected turbine (kW)
P_{panel}	Power generated by a solar panel (kW)
q_i	Solid phase concentration of component i (mol/m^3)
q_i^*	Equilibrium solid phase concentration of component I (mol/m^3)
R	Radius (m)
T	Temperature (K)
u	Gas velocity (m/s)
v	Wind velocity (m/s)
z	Space variable (m)
Z	objective function

Symbols

ω	Solar panel efficiency
ϵ	Porosity
β_i	Separation yield in HX21
σ_i	Separation yield in HX22

acknowledgments

The authors would like to acknowledge Salamanca Research for optimization software licenses. The authors acknowledge the FPU, Spain grant (FPU16/06212) from MECD, Spain to Mr. A. Sánchez and MINECO, Spain grant DPI2015-67341-C2-1-R.

bibliography

Raghavan, N. S., & Ruthven, D. M. (1985). Pressure swing adsorption. part iii: Numerical simulation of a kinetically controlled bulk gas separation. *AIChE Journal*, *31*(12), 2017–2025. https://doi.org/10.1002/aic.690311211

Douglas, M. J. (1988). *Conceptual design of chemical processes*. McGrawHill.

Ruthven, D., & Farooq, S. (1990). Air separation by pressure swing adsorption. *Gas Separation & Purification*, *4*(3), 141–148. https://doi.org/10.1016/0950-4214(90)80016-E

Appl, M. (1999). Ammonia: Priciples & industrial practice.

Lababidi, H. (2000). Air separation by polysulfone hollow fibre membrane permeators in series: Experimental and simulation results. *Chemical Engineering Research and Design*, *78*(8), 1066–1076. https://doi.org/10.1205/026387600528337

Ivy, J. (2004). *Summary of electrolytic hydrogen production: Milestone completion report* (tech. rep.). National Renewable Energy Lab., Golden, CO (US).

Couper, J. R., Penney, W. R., Fair, J. R., & Walas, S. M. (2005). *Chemical process equipment: Selection and design*. Gulf Professional Publishing.

Levene, J., Mann, M., Margolis, R., & Milbrandt, A. (2005). An analysis of hydrogen production from renewable electricity sources. Retrieved March 7, 2020, from https://www.nrel.gov/docs/fy05osti/37612.pdf

Pepermans, G., Driesen, J., Haeseldonckx, D., Belmans, R., & D'haeseleer, W. (2005). Distributed generation: Definition, benefits and issues. *Energy Policy*, *33*(6), 787–798. https://doi.org/10.1016/j.enpol.2003.10.004

Levene, J., Kroposki, B., & Sverdrup, G. (2006). Wind energy and production of hydrogen and electricity — opportunities for renewable hydrogen. Retrieved March 7, 2020, from https://www.nrel.gov/docs/fy06osti/39534.pdf

Sadeghzadeh Ahari, J., Pakseresht, S., Mahdyarfar, M., Shokri, S., Zamani, Y., Nakhaei pour, A., & Naderi, F. (2006). Predictive dynamic model of air separation by pressure swing adsorption. *Chemical Engineering & Technology*, *29*(1), 50–58. https://doi.org/10.1002/ceat.200500226

Häring, H. (2008). The air gases nitrogen, oxygen and argon. *Industrial Gases Processing*, 9–109.

Agarwal, A., Biegler, L. T., & Zitney, S. E. (2009). Simulation and optimization of pressure swing adsorption systems using reduced-order modeling. *Industrial & Engineering Chemistry Research*, *48*(5), 2327–2343. https://doi.org/10.1021/ie071416p

Mofarahi, M., Towfighi, J., & Fathi, L. (2009). Oxygen separation from air by four-bed pressure swing adsorption. *Industrial & Engineering Chemistry Research*, *48*(11), 5439–5444. https://doi.org/10.1021/ie801805k

Campo, M., Magalhães, F., & Mendes, A. (2010). Separation of nitrogen from air by carbon molecular sieve membranes. *Journal of Membrane Science*, *350*(1), 139–147. https://doi.org/10.1016/j.memsci.2009.12.021

Appl, M. (2011). Ammonia, 2. production processes. *Ullmann's encyclopedia of industrial chemistry*.

Maaßen, M., Rübsamen, M., & Perez, A. (2011). Photovoltaic solar energy in spain seminar papers in international finance and economics. seminar paper 4/2011.

Martín, M., & Grossmann, I. E. (2011). Energy optimization of hydrogen production from lignocellulosic biomass [Energy Systems Engineering]. *Computers & Chemical Engineering*, *35*(9), 1798–1806. https://doi.org/10.1016/j.compchemeng.2011.03.002

Saur, G., & Ramsden, T. (2011). *Wind electrolysis: Hydrogen cost optimization* (tech. rep.). National Renewable Energy Lab.(NREL), Golden, CO (United States).

Baker, R. W. (2012). *Membrane technology and applications*. John Wiley & Sons.

Goodrich, A., James, T., & Woodhouse, M. (2012). *Residential, commercial, and utility-scale photovoltaic (pv) system prices in the united states: Current drivers and cost-reduction opportunities* (tech. rep.). National Renewable Energy Lab.(NREL), Golden, CO (United States).

International Renewable Energy Agency. (2012). Renewable energy technologies: Cost analysis series.

Ivanova, S., & Lewis, R. (2012). Producing nitrogen via pressure swing adsorption. *Chemical Engineering Progress*, *108*(6), 38–42.

NETL. (2013). Pre-combustion membranes. appendix b: Carbon dioxide capture technology sheets.

NREL. (2013). System advisor model (sam). Retrieved March 7, 2020, from https://sam.nrel.gov/

Davis, W., & Martín, M. (2014a). Optimal year-round operation for methane production from co2 and water using wind and/or solar energy. *Journal of Cleaner Production*, *80*, 252–261. https://doi.org/10.1016/j.jclepro.2014.05.077

Davis, W., & Martín, M. (2014b). Optimal year-round operation for methane production from co2 and water using wind energy. *Energy*, *69*, 497–505. https://doi.org/10.1016/j.energy.2014.03.043

Sinnott, R. (2014). *Chemical engineering design* (Vol. 6). Elsevier.

Fraunhofer, I., & Energiewende, A. (2015). Current and future cost of photovoltaics. long-term scenarios for market development, system prices and lcoe of utility-scale pv systems. *Agora Energiewende*, *82*.

Godula-Jopek, A. (2015). *Hydrogen production: By electrolysis*. John Wiley & Sons.

Air Liquide. (2016). 4240 air separation membrane.

Air Products. (2016). Prism® membrane systems for ammonia plants... tell me more. Retrieved May 7, 2017, from https://www.airproducts.no/wp-content/uploads/2016/06/Membrane-Systems-For-Ammonia-Plants.pdf

Almena, A., & Martín, M. (2016). Technoeconomic analysis of the production of epichlorohydrin from glycerol. *Industrial & Engineering Chemistry Research*, *55*(12), 3226–3238. https://doi.org/10.1021/acs.iecr.5b02555

de la Cruz, V., & Martín, M. (2016). Characterization and optimal site matching of wind turbines: Effects on the economics of synthetic methane production. *Journal of Cleaner Production*, *133*, 1302–1311. https://doi.org/10.1016/j.jclepro.2016.06.019

Hinkley, J., Hayward, J., McNaughton, R., Gillespie, R., Matsumoto, A., Watt, M., & Lovegrove, K. (2016). Cost assessment of hydrogen production from pv and electrolysis. *Report to ARENA as part of Solar Fuels Roadmap, Project A-3018*, 1–4.

Membrane Technology and Research. (2016). Hydrogen recovery from ammonia plant purge gas. Retrieved May 7, 2017, from www.mtrinc.com/pdf_print/refinery_and_syngas/MTR_Brochure_Hydrogen_Recovery_from_Ammonia_Plant_Purge_Gas.pdf

NREL. (2016). Distributed generation energy technology operations and maintenance costs. Retrieved March 7, 2020, from https://www.nrel.gov/analysis/tech-cost-om-dg.html

Reese, M., Marquart, C., Malmali, M., Wagner, K., Buchanan, E., McCormick, A., & Cussler, E. L. (2016). Performance of a small-scale haber process. *Industrial & Engineering Chemistry Research*, *55*(13), 3742–3750. https://doi.org/10.1021/acs.iecr.5b04909

Air Liquide. (2017). 4640 air separation membrane.

Baldea, M., Edgar, T. F., Stanley, B. L., & Kiss, A. A. (2017). Modular manufacturing processes: Status, challenges, and opportunities. *AIChE Journal*, *63*(10), 4262–4272. https://doi.org/10.1002/aic.15872

EPA. (2017). Distributed generation of electricity and its environmental impacts. Retrieved May 8, 2020, from https://www.epa.gov/energy/distributed-generation-electricity-and-its-environmental-impacts

Heuberger, C. F., Rubin, E. S., Staffell, I., Shah, N., & Mac Dowell, N. (2017). Power capacity expansion planning considering endogenous technology cost learning. *Applied Energy*, *204*, 831–845. https://doi.org/10.1016/j.apenergy.2017.07.075

Martín, M., & Grossmann, I. E. (2017). Optimal integration of a self sustained algae based facility with solar and/or wind energy. *Journal of Cleaner Production*, *145*, 336–347. https://doi.org/10.1016/j.jclepro.2017.01.051

Photovoltaic Software. (2017). How to calculate the annual solar energy output of a photovoltaic system? Retrieved May 7, 2020, from https://photovoltaic- software.com/principle- ressources/how-calculate-solar-energy-power-pv-systems

Air Products. (2018). Prism membrane resource cente. Retrieved May 7, 2017, from https://www.airproducts.com/products/gases/supply-options/prism-membranes/prism-membrane

Matheson. (2018). Atmospheric gases are produced using a process known as air separation. Retrieved May 7, 2020, from https://www.mathesongas.com/engineering/onsite-gas-production/air-separation

Messer. (2018). Gases in road tankers and storage tanks. Retrieved May 7, 2020, from https://www.messergroup.com/gases-in-high-quantities

Sánchez, A., & Martín, M. (2018). Optimal renewable production of ammonia from water and air. *Journal of Cleaner Production*, *178*, 325–342. https://doi.org/10.1016/j.jclepro.2017.12.279

Green, D. W., & Southard, M. Z. (2019). *Perry's chemical engineers' handbook*. McGraw-Hill Education.

5

BIOMASS BASED SUSTAINABLE AMMONIA PRODUCTION: DIGESTION VS GASIFICATION

abstract

The synthesis of ammonia is one of the most important chemical processes in the world. The Haber-Bosch process has predominantly been used to synthesize ammonia over the last decades. However, it uses coal or natural gas as raw materials. In this work, the path to produce ammonia from biomass has been evaluated and optimized. Thermochemical and biochemical routes have been compared. Three alternative gasification technologies have been considered together with anaerobic digestion. For the reforming stage, two alternatives have been compared: autothermal and steam reforming. Finally, ammonia is synthesized in a multibed reactor with two different configurations: direct or indirect cooling. The problem is formulated as a mixed integer nonlinear program but solved as a set of 14 nonlinear programs. Indirect gasifier followed by steam methane reforming and direct cooling ammonia reactor is the path that presents the best performance with an ammonia production cost of about 380 €/t. The biochemical route shows worse results to ammonia due to the low yield to biogas and, therefore, to ammonia.

Keywords: Ammonia, Biomass, Digestion, Gasification, Process design

resumen

La síntesis de amoníaco es uno de los procesos químicos más importantes del mundo. El proceso Haber-Bosch se ha utilizado de manera predominante para sintetizar amoníaco en las últimas décadas. Sin embargo, este proceso utiliza carbón o gas natural como materia prima. En este trabajo se ha evaluado y optimizado la ruta para producir amoníaco a partir de biomasa. Se han comparado las rutas termoquímica y bioquímica. Se han considerado tres tecnologías alternativas de gasificación junto con la digestión anaeróbia. Para la etapa de reformado, se han comparado dos alternativas: el reformado autotérmico y el reformado con vapor. Por último, el amoníaco se sintetiza en un reactor multicapa con dos configuraciones diferentes: refrigeración directa o indirecta. El problema se formula como un programa mixto entero no lineal pero se resuelve como un conjunto de 14 problemas no lineales. El gasificador indirecto seguido del reformado de metano con vapor y el reactor de amoníaco con enfriamiento directo es el camino que presenta el mejor rendimiento con un coste de producción de amoníaco de unos 380 €/t. La ruta bioquímica muestra peores resultados en la producción de amoníaco debido al bajo rendimiento a biogás y, por tanto, a amoníaco.

Palabras clave: Amoníaco, Biomasa, Digestión, Gasificación, Diseño de procesos

5.1 introduction

Ammonia is one the most important chemicals worldwide with a production of about 200 million tons per year, the second largest production for any chemical (Giddey et al., 2017). Around 85% of the ammonia production is devoted to synthesize a wide range of fertilizers: urea, ammonium nitrate, ammonium sulfate, etc. The demand of fertilizers is expected to increase following the growth in global population and, therefore, in food demand (Gilbert et al., 2014). The forecasts foresee that the global ammonia production capacity could reach 237 million tons by 2020 (Andersson & Lundgren, 2014). Ammonia production is gaining attention due to the possibility of using it as a means to store energy or as a hydrogen carrier. Different alternatives are being studied to convert ammonia into energy with high efficiency such as internal combustion engines, PEM fuel cells after ammonia cracking, or solid oxide fuel cells (Giddey et al., 2017).

The current production processes use, mainly, natural gas or coal as raw material (Appl, 2011). However, these production schemes present high levels of greenhouse gas emissions. Coal based ammonia releases 3.4 tons of greenhouse carbon dioxide per ton of ammonia; meanwhile, in the production of natural gas based ammonia, the levels of emissions are on the order of 2.7 tons of greenhouse carbon dioxide per ton (Morgan et al., 2017). "Decarbonization"of the chemical industry is necessary to mitigate the effects of climate change and to meet the goals of international agreements. For example, the Paris agreement establishes that the increase in global temperature must be below 2 °C during this century (United Nations, 2018). Another feature of the current processes is the high energy requirements. Around 1-2% of the global energy is consumed in the ammonia synthesis (Baltrusaitis, 2017).

Alternative ammonia production processes are being developed following three pathways. The first one consists of producing hydrogen from water via electrolysis, separating air components to obtain nitrogen and synthesizing ammonia following the well-established Haber-Bosch process (Malmali et al., 2018; Sánchez & Martín, 2018a). Different air separation technologies have been studied depending on the production capacity (Sánchez & Martín, 2018b). The power needed for the entire process can be supplied using renewable resources or combining it with the power grid (Allman et al., 2019). A pilot plant using a wind turbine to generate power, electrolysis to produce hydrogen and pressure swing adsorption to produce nitrogen is being operated in Minnesota, U.S. (Reese et al., 2016). Another method to produce ammonia from renewable resources is its direct electrochemical formation. In this case, ammonia is synthesized in an electrolytic cell using nitrogen and hydrogen (or directly water).

This method allows a better integration with variable renewable energies such as wind or solar (Bicer & Dincer, 2017). However, it is still under development and further research is required (Giddey et al., 2017). The last alternative to produce renewable ammonia uses biomass as raw material. In this alternative, two main processes have been proposed: ammonia production from biomass digestion or ammonia production from biomass gasification (Tunå et al., 2014). The production of ammonia from biomass via gasification has been reported in the literature presenting competitive costs and environmental performances (Tock et al., 2015; Arora et al., 2016, 2017; Paixão et al., 2018; Demirhan et al., 2019). For example, Tock et al. (2015) carried out an economic and environmental evaluation of the process. Arora et al. (2016) simulated the process at small scale in ASPEN Plus©. In both cases, indirect gasification was considered. So far, no systematic analysis of biomass to ammonia following different transformation paths has been presented in the literature.

In this work, a systematic process level framework has been developed to optimize and evaluate the different paths of ammonia production from biomass. In the gasification section, three different gasifier configurations have been evaluated: indirect gasification, direct gasification with O_2/steam, and direct gasification with air (or enriched air) and steam. The biochemical route via anaerobic digestion has also been analyzed. In the hydrocarbon reforming stage, autothermal reforming and steam methane reforming have been compared. Finally, for the synthesis of ammonia, two types of reactors have been considered: multibed reactor with direct or indirect cooling. The rest of the paper is organized as follows: The Process Description section describes the process flowsheet and the alternatives to produce ammonia from biomass. The Process Model section shows the modeling approach for each unit of the flowsheet. The Solution Procedure section presents the objective function, the solution, and the cost estimation procedures. The Results section comments on the results. First, the main operating variables for the different processes and a simplified environmental index computing the carbon dioxide emissions associated with the processes, and finally the economic analysis for each alternative. A sensitivity analysis for the biomass price is also presented. Subsequently, a scale up/ down study is shown for the most promising alternatives selected in the economic analysis. Finally, in the Conclusions section, some conclusions are drawn.

5.2 process description

The biomass selected for this work is switchgrass, with a large potential as a bioenergy crop (Monti, 2012). The switchgrass composition (in dry and ash free basis) used in this work can be seen in Table 5.1. The biomass flow rate for all cases of study presented in this work is fixed to 18 kg/s (0.6 MMt/year).

Table 5.1: Ultimate Analysis for the Switchgrass (Phyllis, 2012)

Ultimate analysis	% dry and ash free
C	49.12
H	6.13
N	0.6
S	0.11
O	43.51

In the case of gasification, dry switchgrass is used with a moisture content of 8.16% (% biomass as received) and an ash content of 4.59% (% dry biomass). For the digestion, wet switchgrass is employed. The features of the switchgrass for digestion are shown in the Supporting Information.

In Figure 5.1, a block flow diagram for the proposed superstructure is shown. Three gasifier designs have been evaluated for the gasification stage. Indirect gasification uses one chamber for the gasification where the biomass and the steam are fed. The char is burnt in a combustor to obtain the heat necessary for the gasification step. Direct gasification uses one single unit. Oxygen and steam are fed together with biomass. Finally, direct gasification with air and steam is also evaluated. The gasifier is fed with air or enriched air instead of oxygen as a gasifying agent.

The raw syngas generated in the gasifiers is cleaned up to remove, mainly, particles and hydrogen sulfide. To remove the fine particles dragged by the raw syngas, a filter is set up just after the gasification section. The H_2S is removed using a bed of ZnO. After that, the gases are fed to the reformer. In this unit, methane and other high hydrocarbons are transformed into hydrogen, carbon monoxide, or carbon dioxide and water. Two different reformer technologies have been evaluated: steam methane reforming (SMR) and autothermal reforming (ATR). In the first one, only steam is fed to the reformer, and the heat is supplied burning a fuel gas in a separated chamber. In the second one, together with the steam, air is supplied. A

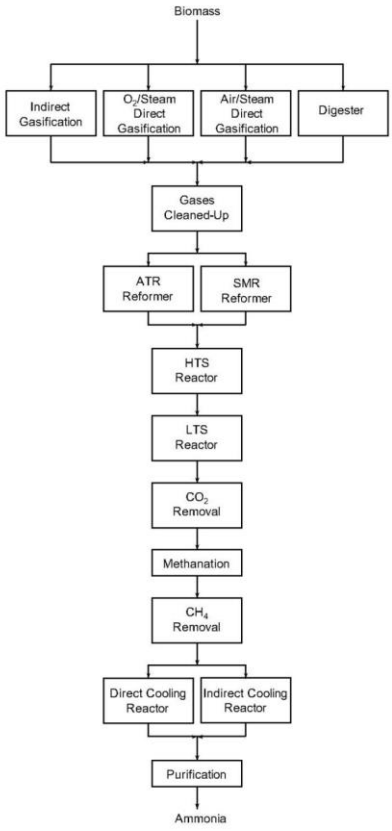

Figure 5.1: Simplified process superstructure for ammonia production from biomass

fraction of the inlet hydrocarbons is combusted with oxygen delivering the heat necessary for the process.

To reach the hydrogen concentration in the gas stream needed for the synthesis of ammonia, the water gas shift conversion technology is selected. A two temperature level shift is proposed. The first one operates at high temperature (high temperature shift, HTS), while the second one operates at low temperature (low temperature shift, LTS). After that, the CO_2 and other components present in smaller amounts in the stream are removed in an adsorption bed of activated carbon. CO_2 can be a raw material, for example, to produce and additional renewable methane via hydrogenation (Davis & Martín, 2014).

Carbon monoxide poisons the catalyst used in ammonia synthesis. For this reason, its concentration must be reduced considerably. A methanation reactor is used where the traces of CO and CO_2 are transformed into

methane. Next, another activated carbon bed is used to remove the traces. After this treatment, the gas stream is ready for synthesis (Appl, 1999).

The ammonia synthesis loop starts by compressing the inlet stream up to the reaction pressure. Then, the fresh and the recycled gases are mixed. Two different reactor configurations have been studied: direct and indirect cooling. In the first one, the inlet stream is used to directly cool down the outlet stream from the reactor beds. In the second one, the heat generated at each catalytic bed is withdrawn, generating steam in external heat exchangers. The ammonia synthesis is limited by the equilibrium. After the reactor, ammonia is condensed from the unreacted gases. A fraction of these unreacted gases is purged to avoid impurities build-up. The hydrogen in the purge stream is recovered to reduce the ammonia production costs using a membrane.

In the case of using biomass digestion, a few differences have been introduced in the flowsheet. The biogas from the digester is not filtered, because no particles are expected to be present. Furthermore, its lower temperature compared to the raw syngas makes cooling down before compression not needed. And finally, the heat exchanger before the reformer (HX7) is replaced by a furnace because it is not possible to heat up the gases to about 800-900 K with steam or with other stream of the facility. The further processing of the digestate is out of the scope of this work, as it has been previously studied (Martín-Hernández et al., 2018), and no additional revenue or credit is assumed from it.

5.3 process model

The entire flowsheet has been modeled using an equation based approach. Here, only a brief description is presented. More information about the models has been provided in the Supporting Information.

The indirect gasification (Figure 5.2 A) consists of two chambers. The raw syngas composition obtained in the gasifier is computed using the correlations taken from Phillips et al. (2007). In the combustion chamber, a total combustion is considered, and therefore, it is possible to determine the outlet temperature and composition by performing mass and energy balances. The performance of the O_2/steam direct gasification (Figure 5.2 B) is computed using the correlations from Dutta and Phillips (2009). Finally, for the air/steam direct gasifier (Figure 5.2 C), empirical correlations are developed to predict the gas composition, based on data from a pilot plant (Campoy et al., 2008; Campoy et al., 2009) as a function of the gasifier temperature, the steam to biomass ratio, the oxygen percentage, and the

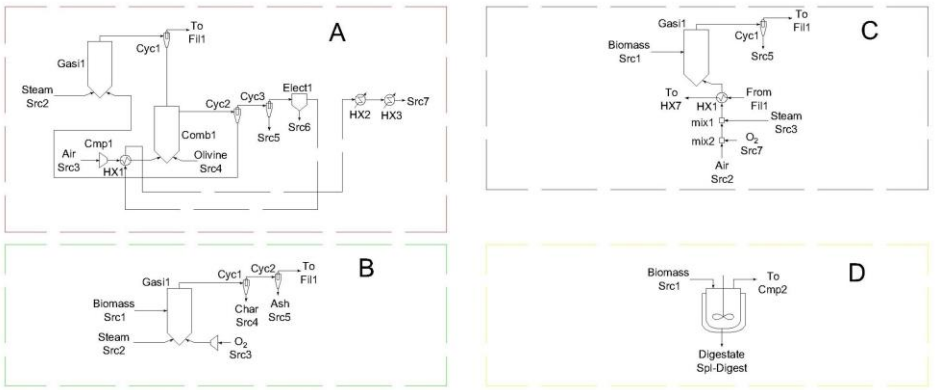

Figure 5.2: Process flow diagram for the gasification/digestion section in the facility: (A) indirect gasification, (B) O_2/steam direct gasification, (C) air/steam direct gasification, (D) anaerobic digestion

equivalent ratio. The model for the air/steam gasifier includes the yield correlations, the mass and energy balances, and some empirical parameters.

The digester has been modeled according to León and Martín (2016). The biomass experimental data required for the model are presented in the Supporting Information.

The next step is the gas clean-up. The particles from the gasification section are separated using a cyclone, while the traces of hydrogen sulfide are removed using a bed of ZnO, eq.5.1. Complete removal is considered.

$$H_2S + ZnO \rightarrow H_2O + ZnS \tag{5.1}$$

Two kinds of reformer reactors have been considered: autothermal reforming (ATR) and steam methane reforming (SMR). Both reformers are modeled as equilibrium and adiabatic systems. Two main equilibrium reactions take place: the decomposition of methane and the water gas shift reaction (WGSR). Furthermore, all high hydrocarbons are transformed to carbon dioxide and hydrogen inside the reformers (Aasberg-Petersen et al., 2003).

$$C_nH_m + nH_2O \rightarrow nCO + \left(n + \frac{m}{2}\right) H_2 \tag{5.2}$$

$$CH_4 + H_2O \rightleftharpoons 3H_2 + CO \tag{5.3}$$

$$CO + H_2O \rightleftharpoons H_2 + CO_2 \tag{5.4}$$

After the reforming stage, a two-step shift conversion is chosen to increase the amount of hydrogen in the stream. Both steps are modeled as equilibrium and adiabatic reactors. The final temperatures are in the range 573-773 K for the first one (high temperature) and 453-533 K for the second

one (low temperature). After the WGSR reactors, the carbon dioxide is removed from the stream using a bed of activated carbon. Because of the high poisoning effect of the CO on the ammonia catalyst, its concentration must be reduced below 10 ppm. CO and CO_2 methanation is carried out. The methanation reactor is adiabatic. Finally, the traces of methane are removed using an adsorption bed. The yields of the adsorption bed are taken on the basis of experimental results, and they can be found in the Supporting Information.

The final stage is the ammonia synthesis (Figure 5.3). Before being introduced in the reactor, the inlet gases are compressed up to the synthesis pressure. Two reactor configurations have been considered: direct and indirect cooling. The detailed model for these reactors is presented in Sánchez and Martín (2018a). In both cases, a rigorous model is solved in MATLAB© to provide accurate bounds to a simple model based on non-equilibrium mass balances and adiabatic energy balances used for the optimization of the flowsheet. The ammonia separation is carried out through condensation. Surrogate models were created to compute the amount of ammonia and other gases separated in the condensation. In the ammonia loop, a membrane is set up in the recycle stream to recover the hydrogen. Industrial data describe the membrane operation (Air Products, 2016; Membrane Technology and Research, 2016).

5.4 solution procedure

The problem is formulated as a mixed integer nonlinear problem (MINLP) with eight binary variables to select the gasification/digestion technology (indirect gasification, direct gasification with oxygen/steam, direct gasification with air/ steam, or digestion), the reformer alternative (autothermal reforming or steam methane reforming), and the ammonia reactor configuration (direct or indirect cooling). The problem is relaxed to solve 14 nonlinear problems (NLPs) for the different combinations between the technologies. In the case of direct gasification with air/steam, only autothermal reforming has been considered.

A simplified profit equation is used as the objective function (eq5.5). Since each of the problems corresponds to an NLP where the flowsheet is fixed, the capital costs do not have an influence on the operating conditions, and therefore, they are not included in the objective function.

$$\begin{aligned} obj = {} & F_{NH_3}C_{NH_3} - W_{total}C_{elect} - C_{steam}F_{steam} \\ & - C_{cooling\ water}F_{cooling\ water} - C_{O_2}F_{O_2} - C_{N_2}F_{N_2} \\ & - C_{biomass}F_{biomass} - C_{olivine}F_{olivine} \end{aligned} \tag{5.5}$$

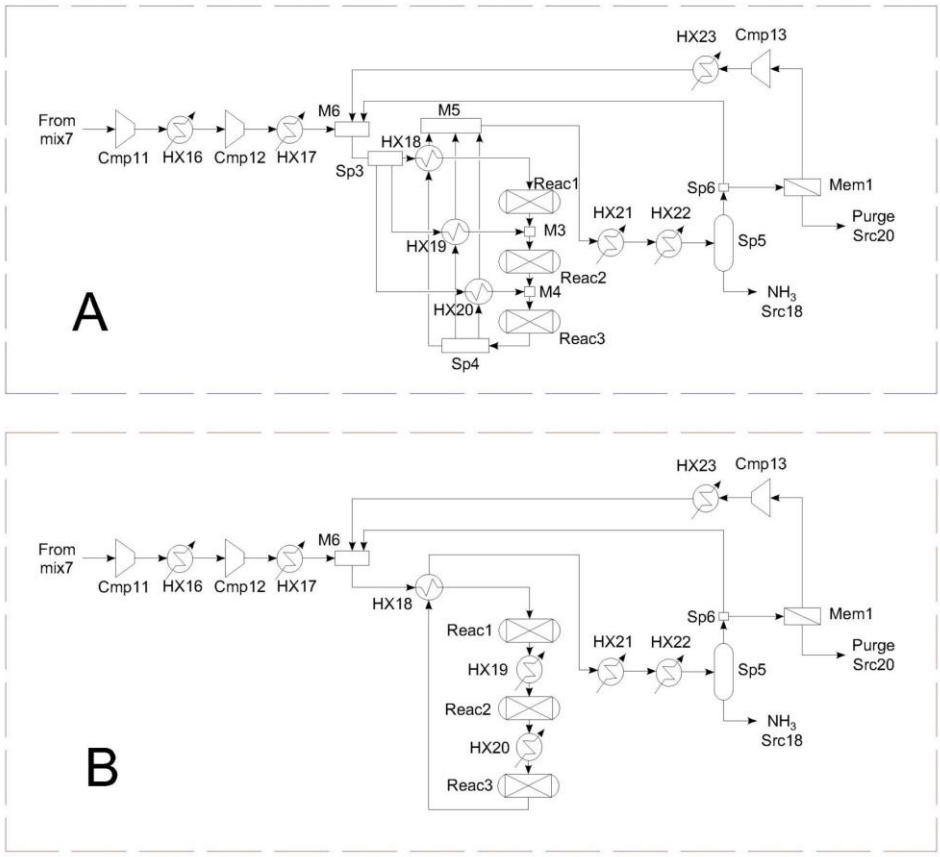

Figure 5.3: Process flow diagram for the ammonia synthesis section: (A) direct cooling reactor, (B) indirect cooling reactor

where the meaning of the different variables and the values of the cost for the different terms involved are presented in Table 5.2.

The problem formulated in the modeling section consists of 2200-3500 equations and 2400-4000 variables depending on the combination of technologies. It is solved in GAMS© using a multistart optimization approach with CONOPT 3.0 as the preferred solver. The decision variables in the optimization problem are the operating conditions of the units involved in the flowsheet, for instance, the amount of oxygen/steam fed to the gasifier, the temperature in the gasifier units, the pressure in the different reactors, the amount of air/steam fed to the reformers, the pressure in the ammonia synthesis loop, as well as the feed temperature and split ratio to each bed.

For the optimal operation of the different alternatives, capital and operating costs have been estimated using the factorial method (Sinnott, 2014).To estimate the equipment cost, correlations (Almena & Martín, 2016) and

Table 5.2: Symbols and Costs for the Objective Function

Symbol	Variable	Value	Source
F_{NH_3}	ammonia production		
C_{NH_3}	ammonia cost	0.5 €/kg	Pfromm (2017)
W_{total}	total power		
C_{elect}	electricity price	7.87 cent €/kWh	Statista (2018)
F_{steam}	steam needed		
C_{steam}	steam cost	2.2 €/GJ	Yang and You (2018)
$F_{cooling\ water}$	cooling water needs		
$C_{cooling\ water}$	cooling water cost	4.58 €/kt	Yang and You (2018)
F_{O_2}	oxygen demand		
C_{O_2}	oxygen price	0.021 €/kg	Noureldin et al. (2014)
F_{N_2}	nitrogen demand		
C_{N_2}	nitrogen price	0.037 €/kg	Elishav et al. (2017)
$F_{biomass}$	inlet biomass		
$C_{biomass}$	biomass cost	58.75 €/dry tonne	Dalle Ave and Adams (2018)
$F_{olivine}$	inlet olivine		
$C_{olivine}$	olivine cost	275 €/kg	Tan et al. (2017)

literature data have been employed. For details of specific units and costs, we refer the reader to the Supporting Information.

5.5 results

5.5.1 *Main Operating Variables*

The main operating conditions for the facility are summarized in Tables 5.3-5.5. In Tables 5.3 and 5.4, a brief overview of the conditions for all gasification based processes is shown. The main components of the gas flow exiting the gasifier are carbon monoxide, carbon dioxide, hydrogen, and methane. The concentrations for these species are presented in Table 5.3. In the SMR reformer, it is necessary to burn a fraction of the raw syngas from the gasifier to supply the heat necessary in the reformer. A trade-off is presented between the reformer conversion and the yield. To increase the conversion, a larger supply of heat is needed, resulting in the consumption of a larger fraction of the inlet gas and reducing the yield to hydrogen. For this reason, a lower methane conversion in the SMR

Table 5.3: Main Operating Conditions for the Gasifier Section

		Gasifier	Combustor	Gasifier out (molar % dry N_2 free)			
		T_{out} (K)	T_{out} (K)	% H_2	% CH_4	% CO	% CO_2
1	Ind+ATR+Dir	1287.04	1358.55	33.92	12.38	41.37	9.28
2	Ind+ATR+Ind	1287.04	1358.55	33.92	12.38	41.37	9.28
3	Ind+SMR+Dir	1287.04	1358.55	33.92	12.38	41.37	9.28
4	Ind+SMR+Ind	1287.04	1358.55	33.92	12.38	41.37	9.28
5	Dir+ATR+Dir	1236.60	29.13	14.87	23.23	29.87	
6	Dir+ATR+Ind	1236.60		29.13	14.87	23.23	29.87
7	Dir+SMR+Dir	1241.66		27.84	14.75	25.43	28.73
8	Dir+SMR+Ind	1255.22		21.31	14.01	35.92	23.40
9	Air+ATR+Dir	1038.29		34.37	10.59	36.11	13.49
10	Air+ATR+Ind	1038.49		34.81	10.30	38.72	11.02

reformer is recommended compared to the ATR. In Table 5.4, the percent of combusted stream is presented together with the methane reformer conversion.

Table 5.4: Operating Variables in Gasification Based Processes

		Combustor	Reformer			Ammonia	
		% split	P (bar)	T_{out} (K)	X_{CH_4} (%)	P (bar)	F NH_3 (kg/s)
1	Ind+ATR+Dir		20.0	1265.22	99.2	125.0	9.95
2	Ind+ATR+Ind		20.0	1265.04	99.2	125.0	9.93
3	Ind+SMR+Dir	13.8	20.0	1137.99	71.7	125.0	9.69
4	Ind+SMR+Ind	13.8	20.0	1137.96	71.7	125.0	9.69
5	Dir+ATR+Dir		20.0	1160.08	98.2	125.0	8.65
6	Dir+ATR+Ind		20.0	1159.26	98.2	125.0	8.65
7	Dir+SMR+Dir	6.2	20.0	1073.00	62.4	125.0	8.48
8	Dir+SMR+Ind	11.0	20.0	1116.87	71.8	125.0	8.12
9	Air+ATR+Dir		20.0	1122.59	75.5	126.3	8.70
10	Air+ATR+Ind		20.0	1200.45	96.5	155.2	7.72

For the indirect processes (processes 1-4), the gasifier presents the same conditions independently of the reformer technology or the reactor configuration; see Table 5.3. Up to 13% of the gas from the gasifier is burned to

supply heat when using SMR. The final ammonia production is higher in the indirect gasifier processes due to the larger yield to hydrogen in the gasification step as it is shown in Table 5.3. The reformer performance is better in the SMR showing a larger production of hydrogen. However, after the WGS reactors, the hydrogen concentration is higher in the autothermal reforming processes, and therefore, the final ammonia production is also larger (see Table 5.4). Note that the operating pressure is fixed to the bound, since there is a trade-off between the cost for compression and the experimental operating limits.

In the oxygen/steam direct gasification processes (processes 5-8), a significant increase in the percentage of carbon dioxide is shown with respect to the indirect gasification. Therefore, a reduction in the ammonia production capacity takes place when direct gasification is employed.

Table 5.5: Main Operating Conditions for Digestion Processes

		Digester out (molar %)			Combustor	Reformer			Ammonia	
		% CH_4	% CO_2	% H_2O	% split	P (bar)	T_{out} (K)	X_{CH_4} (%)	P (bar)	F NH_3 (kg/s)
11	Dig+ATR+Dir	55.94	25.28	15.74	5.01	20.0	1093.54	90.4	154.8	1.58
12	Dig+ATR+Ind	55.94	25.28	15.74	5.01	20.0	1093.12	90.3	152.3	1.58
13	Dig+SMR+Dir	56.87	25.27	15.73	40.16	20.0	1133.76	89.8	125.0	1.92
14	Dig+SMR+Ind	56.87	25.27	15.73	40.16	20.0	1133.65	89.8	125.0	1.81

Finally, the air/steam gasification (processes 9 and 10) shows an ammonia production in the same levels as the oxygen/steam direct gasifier (see Table 5.4) because the flows of the stream in air/steam processes are quite similar to the oxygen/steam ones. For the operation of the gasifier, a steam to biomass ratio (S/B) of 0.334, an oxygen percentage of the enriched air (OP) of 0.4, and an equivalent ratio (ER) of 0.207 are selected.

In the digester based processes, the main conditions are shown in Table 5.5. In this case, the outlet gases from the digester present a higher content of methane, followed by carbon dioxide and water. Hydrogen is not directly produced in the digester. The biogas must be reformed into syngas. In this flowsheet, there is no heat source to heat up the feed to the reformer. Therefore, the heat is supplied by burning a fraction of the biogas. In the case of using the ATR, only a small fraction is required (about 5%). However, for the SMR based processes, a larger fraction of gas, around 40%, is needed to operate the heat exchanger and the reactor itself.

Comparing Tables 5.4 and 5.5, it is possible to see that, for the same biomass flow rate, the amount of ammonia is significantly lower in the case of biomass digestion compared to its gasification. This fact is due to the high amount of water or other components in the inlet biomass that

cannot be transformed into biogas. For this case of study, around 80% of the inlet mass goes to the digestate and only 20% forms the biogas.

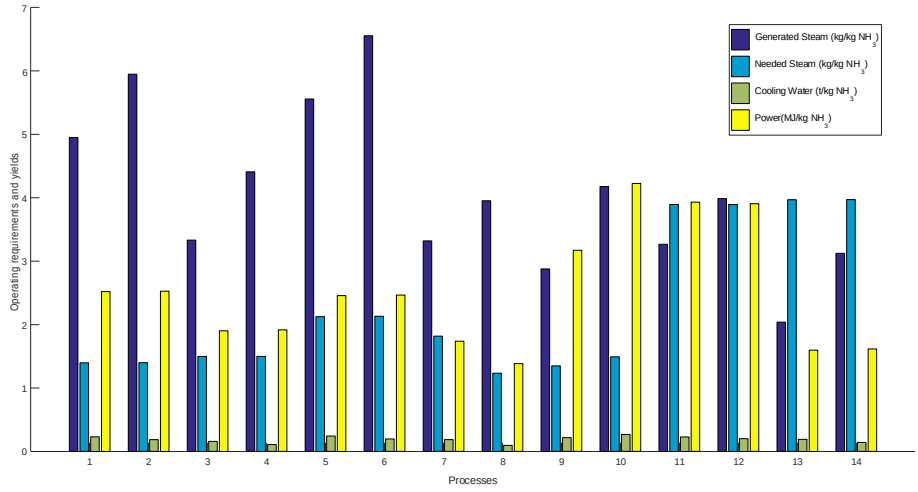

Figure 5.4: Steam, cooling water, and power consumption for different alternatives

In Figure 5.4, the steam (generated and consumed), cooling water, and power consumption for the different process alternatives are shown. In the processes that use indirect cooling reactors (odd numbers in Figure 5.4), the amount of steam generated is higher because it is possible to produce it between reactor beds. However, when using direct cooling configurations, no steam is generated but heat exchangers are not needed either. When using digestion, this trend also holds. For the steam requirements, the processes that use biogas digestion present higher consumption than the gasifier ones. Around 1-2 kg of steam/kg of ammonia are needed in the gasification processes versus about 4 kg of steam/kg of ammonia in the digestion ones. The cooling water usage in all processes is around 0.2 t of cooling water/kg of ammonia. As a general trend, indirect cooling processes present a lower cooling water usage. In addition, processes using SMR also use less water than the ATR alternatives. Finally, power consumption is a key parameter for the process profitability. Figure 5.4 shows that the processing using ATR is more energy intense than the correspondent SMR processes. The reason behind this is that, in spite of burning a fraction of the fed stream to provide energy for the SMR, the amount of ammonia produced is approximately the same as the ATR designs (a bit lower in the gasifier processes and a bit higher in the digester processes). For example, in the indirect gasifier and direct cooling ammonia reactor, the change from ATR to SMR reduces the ammonia production by

2.6%. However, a fraction of the raw syngas is split, sending 13.8% to the combustor. It is possible to achieve almost the same production capacity processing a smaller flow of gases. Thus, the power consumption at the compressors is lower, resulting in lower total energy consumption per kilogram of ammonia. This fact is especially clear when using digestion. In the SMR, about 40% of the stream is sent to the combustor. Due to this, mainly, the energy requirements per kg of ammonia decrease by 60%.

5.5.2 *Environmental Evaluation*

Using the mass and energy balances, a simplified environmental evaluation of each process has been performed following the methodology proposed Martín (2016). In this metric, REPSIM, the operating parameters are translated as CO_2 emissions generated or mitigated.

For the purpose of this work, the inlet biomass is assumed to generate CO_2 emissions due to collection, transportation, etc., of 87.5 kg of CO_2/t of dry switchgrass (Kumar & Sokhansanj, 2007). The other two raw materials, oxygen and nitrogen, present carbon dioxide emission values of 556 and 171 g of CO_2/Nm^3, respectively (Natural Resources Canada, 2008). The emissions related to the power involved in the processes are taken into account using a factor of 0.832 kg of CO_2/kWh (Martín, 2016). The cooling water for the process is computed using the energy requirement for water supply and distribution. Then, the carbon footprint is calculated using the energy to CO_2 factor. The cooling needs correspond to 7775 kWh/Mgal (Hernández & Martín, 2016). Finally, the contribution of the steam used to CO_2 emissions is according to the energy required to produce it. Thus, the carbon emissions are calculated using the same energy to CO_2 factor as in the case of the power consumed.

Apart from these contributions, the carbon dioxide generated in processing the switchgrass is released because in the synthesis of ammonia no carbon source is necessary. Therefore, the carbon dioxide from biomass must also be added to the previous one. However, this carbon dioxide is biogenic; namely, it comes from biomass and it is later consumed by the growing biomass and no additional CO_2 is released to the atmosphere (Arora et al., 2016). In general, in the literature, this CO_2 contribution is neglected in the environmental analysis. In this study, two different values for the released CO_2 are computed, one considering the biogenic carbon dioxide emissions and another one without it. As it was said previously, the carbon dioxide generated in the process could be integrated with other technologies to produce other interesting chemicals or fuels, for example, methanol (Martín & Grossmann, 2017) or methane (Davis & Martín, 2014).

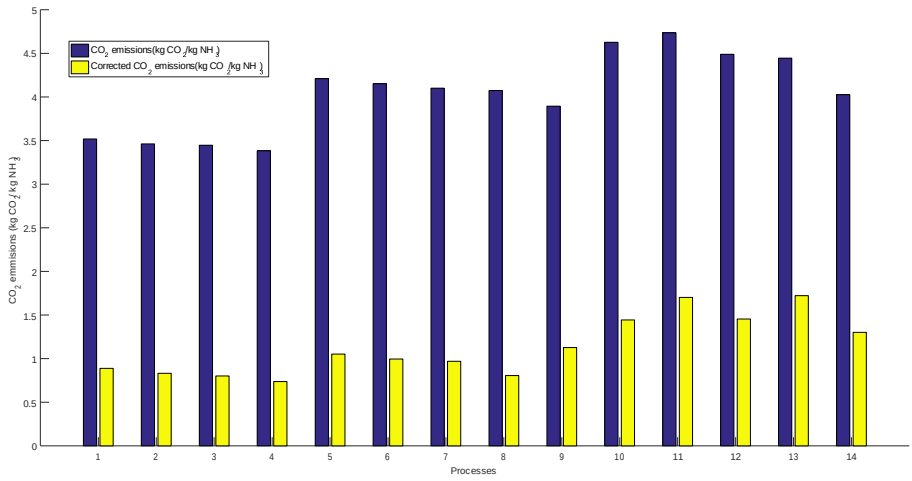

Figure 5.5: Carbon dioxide emissions for different alternatives

In Figure 5.5, the results for this environmental index are shown. These results show the amount of carbon dioxide generated per kg of ammonia produced. The blue columns represent the total CO_2 emissions and the yellow ones the emissions without the biogenic carbon dioxide. If the biogenic carbon dioxide is not neglected, the level of emissions is quite similar to that of the actual processes (about 3-4 kg of CO_2/ kg of NH_3) (Morgan et al., 2017). However, discounting this contribution, a reduction of up to 80% can be obtained.

In terms of the comparison among process alternatives, the indirect gasifier based processes have the lowest level of emissions. As it was shown before, these processes present low cooling water usage and high levels of generated steam, and also, no pure oxygen or nitrogen is required. These facts result in a better environmental performance for the indirect gasifier based processes.

At the other end, digestion based processes show the highest level of carbon dioxide generation. These processes are highly energy intensive, and in general, the steam generated in the facility cannot provide for their needs. For this reason, the environmental index is worse.

5.5.3 *Investment and Production Costs*

In Figure 5.6, a summary of the capital costs for the process alternatives can be seen. The production capacity for each facility is also shown (red line). The investment is higher for the gasification based processes than in the case of the digestion based ones. However, the ammonia production

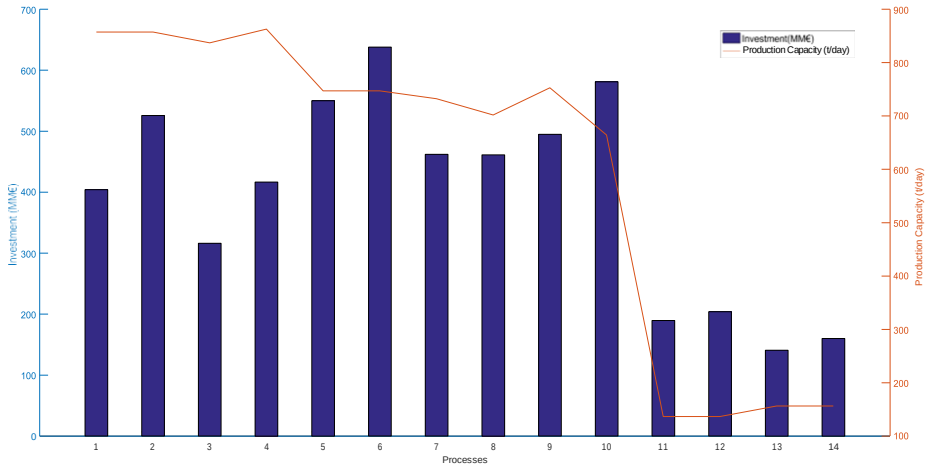

Figure 5.6: Investment cost for different alternatives

capacity is higher using gasification, for the same biomass feed. As a general trend, the configurations using an indirect cooling reactor present a higher investment than the direct ones. The main reason is that in indirect cooling it is necessary to invest in heat exchangers for the operation of the reactor. These heat exchangers generate steam at a cost. Comparing the two reformer alternatives, the investment costs when using the SMR are lower than in the case of using the ATR. The explanation is that, when the SMR reformer is used, a fraction of the inlet stream is burnt to produce the heat necessary. For this reason, the downstream units are smaller as well as their cost. In the gasifier alternatives, the indirect gasifier shows a smaller investment compared to the direct counterparts (steam/air or steam/oxygen).

In Figure 5.7, the production costs for the different alternatives are shown. The ammonia production capacities for the different alternatives are also shown in the figure (red line). The range of production cost for the ammonia from biomass is between 390 €/t (process 3, indirect gasifier with SMR and direct cooling reaction) and 1284 €/t (process 12, digester with ATR and indirect cooling reactor). The indirect gasifier alternatives show lower costs than the direct ones. In general, the indirect gasifier presents high ammonia production and lower capital cost than the direct ones (see the Supporting Information). Between SMR and ATR, SMR processes show higher yield than those using ATR. In SMR, the ammonia production capacity is similar to the ATR processes but the investment is significantly lower than that for ATR. For the direct versus indirect cooling configurations, the trade-off between steam production and heat exchanger investment is resolved in favor of the direct cooling alternatives.

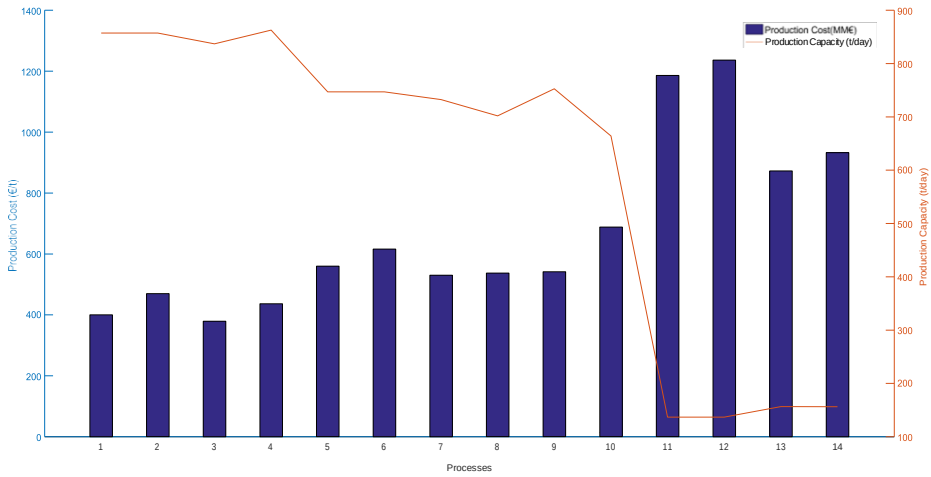

Figure 5.7: Production cost for different alternatives

The decrease in the need for stream due to the internal production does not mitigate the increase in the amortization due to the capital cost of the additional heat exchangers. The production costs for the digestion processes are higher than the gasification ones. As it was explained before, a large amount of inlet biomass is not converted in biogas and forms the digestate. The digestate in this work is not treated, and for this reason, no economical profit has been computed. A commercial use of the digestate could reduce the production cost for the ammonia, but further investigation is required to evaluate the necessary investment for these new treatments, the impact in the production cost, and the market of the fertilizer. Therefore, the most promising alternative, in economic terms, is the combination of indirect gasifier with SMR reformer and direct cooling ammonia reactor.

In Figure 5.8, a sample of the distribution of the equipment cost has been presented. Only the ATR and direct cooling reactor are shown for the three gasifiers and the digester for comparison. The main contributors in the investment are heat exchangers, gasifier, compressors, and the ammonia synthesis reactor. The heat exchangers can represent more than 50% of the total investment of the facility. Direct alternatives present a lower heat exchanger contribution, as is expected according to the reasoning presented above.

In the indirect gasifier based processes, the heat exchangers show the larger contribution. In the other gasifier technologies, it is the gasifier itself which presents the largest share in the capital cost. As was explained before (see the Supporting Information), the indirect gasifier presents a lower investment cost, and this is reflected in the capital cost distribution.

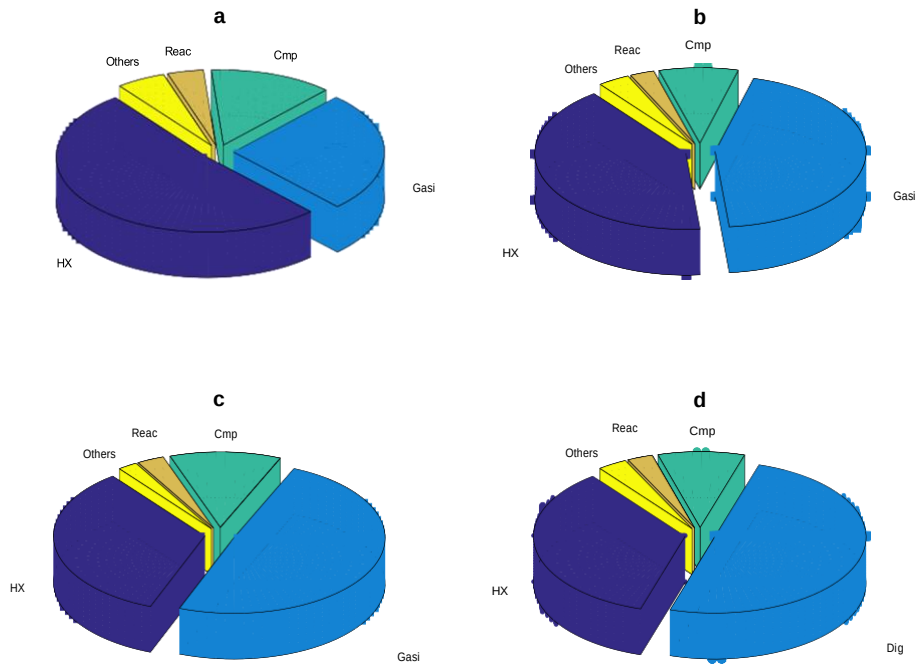

Figure 5.8: Equipment investment breakdown for some of the proposed alternatives [(a) indirect gasifier + ATR reforming + direct cooling; (b) O_2/ steam direct gasifier + ATR reforming + direct cooling; (c) air/steam direct gasifier + ATR reforming + direct cooling; (d) digester + ATR reforming + direct cooling]

In the digester, about 50% of the total investment is represented by the digester. Figure 5.9 shows the cost distribution.

The most significant item in the cost analysis breakdown is the capital charges associated with the initial investment. It is followed by raw material, mainly the inlet biomass, the maintenance cost, and the utilities item. The cost distribution is quite similar for all of the cases presented in the figure.

5.5.4 *Sensitivity Analysis*

For the previous analysis, a price of biomass equal to 58.75 €/dry tonne is used (Dalle Ave & Adams, 2018). However, there is large variability in the biomass price. A lot of factors affect the switchgrass production cost, for example, fertilizer prices, transportation cost, growth yield, etc (Khanna et al., 2008). Therefore, a sensitivity analysis is carried out to evaluate the influence of the cost of biomass in the ammonia production cost. The most promising processes for each gasification and digestion technology have been selected for the analysis. Namely, indirect gasifier with SMR and

direct cooling, oxygen/steam direct gasifier with SMR and direct cooling,

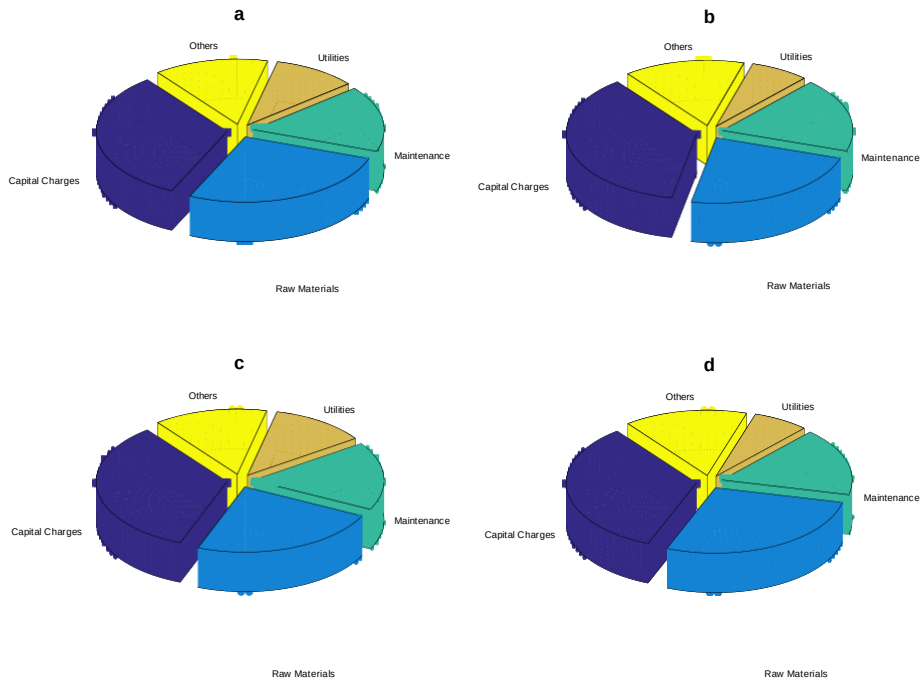

Figure 5.9: Operating cost breakdown for some of the proposed alternatives [(a) indirect gasifier + ATR reforming + direct cooling; (b) O_2/steam direct gasifier + ATR reforming + direct cooling; (c) air/steam direct gasifier + ATR reforming + direct cooling; (d) digester + ATR reforming + direct cooling]

air/steam direct gasifier with ATR and direct cooling, and digester with SMR and direct cooling reactor.

In the sensitivity analysis, a range in the biomass prices between 30 €/dry tonne and 100 €/dry tonne has been evaluated taking into account the variability presented in the literature for the switchgrass production cost (Khanna et al., 2008; Witzel & Finger, 2016) The results are shown in Figure 5.10. For the indirect gasification with SMR and direct cooling reactor, the ammonia production cost ranges between 325 and 450 €/t. The production costs using direct gasification with either air/steam or oxygen/steam are quite similar, both in the range 470-625 €/t. The digester based processes, as it is expected, present higher production costs in the range 725-1100 €/t. A linear trend relates the production cost with the biomass prices. The slope is higher in the digester due to the different moisture content between the switchgrass for gasification and that for digestion.

The actual cost of the ammonia is in the range of $500-600 per tonne of ammonia (Pfromm, 2017) with a strong dependency of the fossil fuel cost fluctuations (Allman & Daoutidis, 2018). The calculated production cost of

ammonia from biomass can be competitive for some technologies with the current production technology.

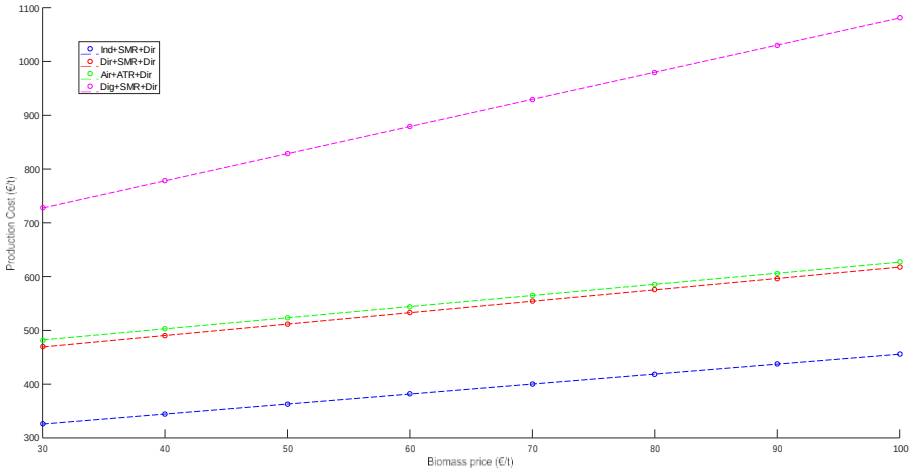

Figure 5.10: Sensitivity analysis for the biomass price

5.5.5 *Scale up/Scale down*

The economics of scale present a high influence in the production cost and the investment in chemical plants. Traditionally, large chemical production complexes have been installed. However, this trend is slowly changing to new alternative processes based on resource availability (Pepermans et al., 2005). Distributed production in chemical facilities presents a strong link with modular design (Baldea et al., 2017). The methodology to scale up or down the chemical process was described in Sánchez and Martín (2018b).

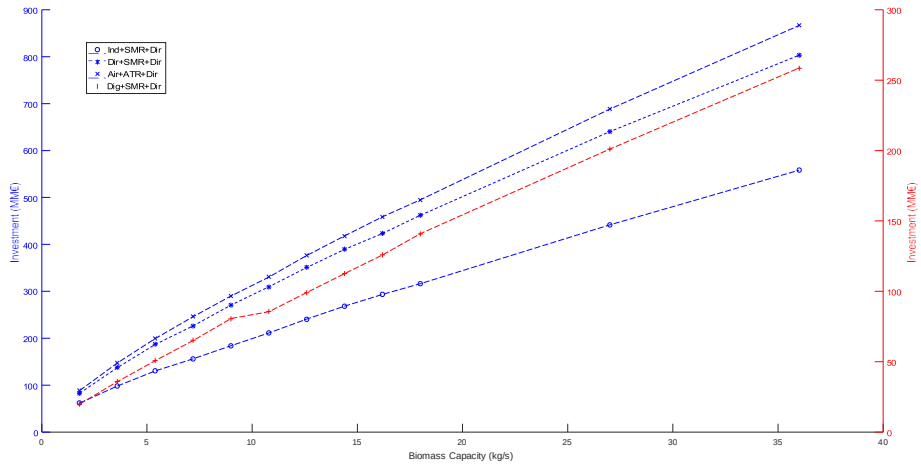

Figure 5.11: Scale up and down for the investment

For biomass based ammonia processes, the investment and production costs have been evaluated for different biomass processing rates to assess the influence of the production capacity in these two parameters. Figure 5.11 shows the total investment for different production capacities for the four most promising different alternatives according to the previous analysis: indirect gasifier with SMR and direct reactor, direct gasifier with SMR and direct ammonia reactor, air/steam gasifier plus ATR and direct cooling reactor, and, finally, digester combined with SMR and direct reactor. The scale index for the gasifier processes is around 0.75, a little different compared to the classical six-tenth rule. However, the power index for the case of the digestion is about 0.85. Therefore, the digestion based processes present smaller economies of scale with respect to the gasification based ones. Note that the digester represents a high share in the investment (see Figure 5.8), and it is an equipment without economies of scale, affecting the scale up/down behavior of the entire process.

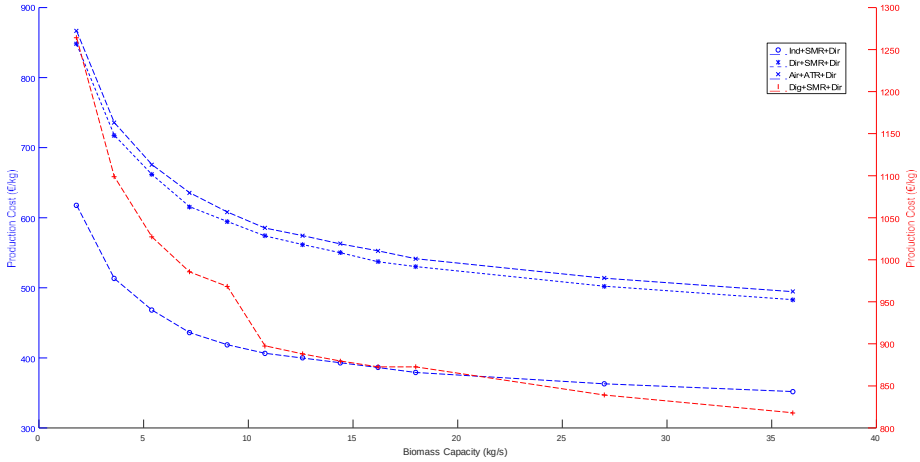

Figure 5.12: Operating cost for different inlet biomass capacities

For the production cost, Figure 5.12 presents the influence of the biomass capacity in the ammonia production costs. For the smaller capacities, the ammonia cost is around 600-900 €/t for the gasification based processes, about a 60% of the increase with respect to the base case. In the case of biomass digestion, the cost for smaller capacities surpasses the level of 1000 €/t, showing an increase of around 45% with respect to the base case. Smoother trends are obtained for the gasifier processes due to the need for additional reactors as they become filled in the digester based processes.

5.6 conclusions

In this work, the synthesis of ammonia from biomass has been systematically evaluated. Different alternatives for gasification, reforming, and ammonia synthesis reactors have been compared. The main decision variables for the process are determined in the optimization procedure, for example, the working temperature in the gasifier, the amount of steam fed to the reformers, the water gas shift operating conditions, or the ammonia synthesis pressure. The economic results show that the combination of indirect gasifier with steam methane reforming and direct cooling reactor is recommended for the biomass to ammonia process. This alternative presents a production cost of about 380 €/t, competitive with the actual production processes, and an investment of approximately 316 MM€. This process also shows a good environmental performance regarding the processes analyzed. In the digestion processes, the production cost increases up to 900-1200 €/t. The high amount of digestate determines the economic performance of this technology.

A sensitivity analysis of the effect of biomass price is carried out. The digestion processes are strongly affected by this price. Finally, a scale up/down study is presented to analyze the economies of scale in biomass to ammonia processes.

nomenclature

C_{NH_3}	Ammonia cost (€/kg)
C_{elect}	Electricity price (cent €/kWh)
C_{steam}	Steam cost (€/GJ)
$C_{cooling\ water}$	Cooling water price (€/kt)
C_{O_2}	Oxygen price (€/kg)
C_{N_2}	Cost for nitrogen gas (€/kg)
$C_{biomass}$	Biomass price (€/dry t)
$C_{olivine}$	Olivine cost (€/kg)
F_{NH_3}	Final ammonia production (kg/s)
F_{steam}	Total steam needed in the facility (GJ/s)
$F_{cooling\ water}$	Total amount of cooling water in the plant (kt/s)
F_{O_2}	Oxygen total flow (kg/s)
F_{N_2}	Nitrogen inlet flow (kg/s)
$F_{biomass}$	Biomass flow as raw material (dry t/s)

$F_{olivine}$	Total inlet flow of olivine (kg/s)
W_{total}	Total power in the facility (kWh)

acknowledgments

The authors would like to acknowledge Salamanca Research for optimization software licenses. The authors acknowledge the FPU, Spain grant (FPU16/06212) from MECD, Spain to Mr. A. Sánchez and MINECO, Spain grant DPI2015-67341-C2-1-R.

bibliography

Appl, M. (1999). Ammonia: Priciples & industrial practice.

Aasberg-Petersen, K., Christensen, T. S., Stub Nielsen, C., & Dybkjær, I. (2003). Recent developments in autothermal reforming and prereforming for synthesis gas production in gtl applications [Advances in C1 Chemistry in the Year 2002]. *Fuel Processing Technology*, *83*(1), 253–261. https://doi.org/10.1016/S0378-3820(03)00073-0

Pepermans, G., Driesen, J., Haeseldonckx, D., Belmans, R., & D'haeseleer, W. (2005). Distributed generation: Definition, benefits and issues. *Energy Policy*, *33*(6), 787–798. https://doi.org/10.1016/j.enpol.2003.10.004

Kumar, A., & Sokhansanj, S. (2007). Switchgrass (panicum vigratum, l.) delivery to a biorefinery using integrated biomass supply analysis and logistics (ibsal) model. *Bioresource Technology*, *98*(5), 1033–1044. https://doi.org/10.1016/j.biortech.2006.04.027

Phillips, S., Aden, A., Jechura, J., Dayton, D., & Eggeman, T. (2007). *Thermochemical ethanol via indirect gasification and mixed alcohol synthesis of lignocellulosic biomass* (tech. rep.). National Renewable Energy Lab.(NREL), Golden, CO (United States).

Campoy, M., Gómez-Barea, A., Villanueva, A. L., & Ollero, P. (2008). Air-steam gasification of biomass in a fluidized bed under simulated autothermal and adiabatic conditions. *Industrial & Engineering Chemistry Research*, *47*(16), 5957–5965. https://doi.org/10.1021/ie800220t

Khanna, M., Dhungana, B., & Clifton-Brown, J. (2008). Costs of producing miscanthus and switchgrass for bioenergy in illinois. *Biomass and Bioenergy*, *32*(6), 482–493. https://doi.org/10.1016/j.biombioe.2007.11.003

Natural Resources Canada. (2008). Appendix b: Co2 emission factors. Retrieved May 7, 2020, from https://www.nrcan.gc.ca/energy-

efficiency/energy-efficiency-industry/energy-management-industry/energy-benchmarking-industry/benchmarking-guides/5171

Campoy, M., Gómez-Barea, A., Vidal, F. B., & Ollero, P. (2009). Air-steam gasification of biomass in a fluidised bed: Process optimisation by enriched air. *Fuel Processing Technology*, *90*(5), 677–685. https://doi.org/10.1016/j.fuproc.2008.12.007

Dutta, A., & Phillips, S. D. (2009). *Thermochemical ethanol via direct gasification and mixed alcohol synthesis of lignocellulosic biomass* (tech. rep.). National Renewable Energy Lab.(NREL), Golden, CO (United States).

Appl, M. (2011). Ammonia, 2. production processes. *Ullmann's encyclopedia of industrial chemistry*.

Monti, A. (2012). *Switchgrass: A valuable biomass crop for energy*. Springer Science & Business Media.

Phyllis, E. (2012). Database for biomass and waste. *Energy Research Centre of the Netherlands*.

Andersson, J., & Lundgren, J. (2014). Techno-economic analysis of ammonia production via integrated biomass gasification. *Applied Energy*, *130*, 484–490. https://doi.org/10.1016/j.apenergy.2014.02.029

Davis, W., & Martín, M. (2014). Optimal year-round operation for methane production from co2 and water using wind and/or solar energy. *Journal of Cleaner Production*, *80*, 252–261. https://doi.org/10.1016/j.jclepro.2014.05.077

Gilbert, P., Alexander, S., Thornley, P., & Brammer, J. (2014). Assessing economically viable carbon reductions for the production of ammonia from biomass gasification. *Journal of Cleaner Production*, *64*, 581–589. https://doi.org/10.1016/j.jclepro.2013.09.011

Noureldin, M. M. B., Elbashir, N. O., & El-Halwagi, M. M. (2014). Optimization and selection of reforming approaches for syngas generation from natural/shale gas. *Industrial & Engineering Chemistry Research*, *53*(5), 1841–1855. https://doi.org/10.1021/ie402382w

Sinnott, R. (2014). *Chemical engineering design* (Vol. 6). Elsevier.

Tunå, P., Hulteberg, C., & Ahlgren, S. (2014). Techno-economic assessment of nonfossil ammonia production. *Environmental Progress & Sustainable Energy*, *33*(4), 1290–1297. https://doi.org/10.1002/ep.11886

Tock, L., Maréchal, F., & Perrenoud, M. (2015). Thermo-environomic evaluation of the ammonia production. *The Canadian Journal of Chemical Engineering*, *93*(2), 356–362. https://doi.org/10.1002/cjce.22126

Air Products. (2016). Prism® membrane systems for ammonia plants... tell me more. Retrieved May 7, 2017, from https://www.airproducts.no / wp - content / uploads / 2016 / 06 / Membrane - Systems - For - Ammonia-Plants.pdf

Almena, A., & Martín, M. (2016). Technoeconomic analysis of the production of epichlorohydrin from glycerol. *Industrial & Engineering Chemistry Research*, *55*(12), 3226–3238. https://doi.org/10.1021/acs.iecr.5b02555

Arora, P., Hoadley, A. F., Mahajani, S. M., & Ganesh, A. (2016). Small-scale ammonia production from biomass: A techno-enviro-economic perspective. *Industrial & Engineering Chemistry Research*, *55*(22), 6422–6434. https://doi.org/10.1021/acs.iecr.5b04937

Hernández, B., & Martín, M. (2016). Optimal process operation for biogas reforming to methanol: Effects of dry reforming and biogas composition. *Industrial & Engineering Chemistry Research*, *55*(23), 6677–6685. https://doi.org/10.1021/acs.iecr.6b01044

León, E., & Martín, M. (2016). Optimal production of power in a combined cycle from manure based biogas. *Energy Conversion and Management*, *114*, 89–99. https://doi.org/10.1016/j.enconman.2016.02.002

Martín, M. (2016). Repsim metric for design of sustainable renewable based fuel and power production processes. *Energy*, *114*, 833–845. https://doi.org/10.1016/j.energy.2016.08.031

Membrane Technology and Research. (2016). Hydrogen recovery from ammonia plant purge gas. Retrieved May 7, 2017, from www.mtrinc.com/pdf_print/refinery_and_syngas/MTR_Brochure_Hydrogen_Recovery_from_Ammonia_Plant_Purge_Gas.pdf

Reese, M., Marquart, C., Malmali, M., Wagner, K., Buchanan, E., McCormick, A., & Cussler, E. L. (2016). Performance of a small-scale haber process. *Industrial & Engineering Chemistry Research*, *55*(13), 3742–3750. https://doi.org/10.1021/acs.iecr.5b04909

Witzel, C.-P., & Finger, R. (2016). Economic evaluation of miscanthus production – a review. *Renewable and Sustainable Energy Reviews*, *53*, 681–696. https://doi.org/10.1016/j.rser.2015.08.063

Arora, P., Hoadley, A. F., Mahajani, S. M., & Ganesh, A. (2017). Multi-objective optimization of biomass based ammonia production - potential and perspective in different countries. *Journal of Cleaner Production*, *148*, 363–374. https://doi.org/10.1016/j.jclepro.2017.01.148

Baldea, M., Edgar, T. F., Stanley, B. L., & Kiss, A. A. (2017). Modular manufacturing processes: Status, challenges, and opportunities. *AIChE Journal*, *63*(10), 4262–4272. https://doi.org/10.1002/aic.15872

Baltrusaitis, J. (2017). Sustainable ammonia production. *ACS Sustainable Chemistry & Engineering*, *5*(11), 9527–9527. https://doi.org/10.1021/acssuschemeng.7b03719

Bicer, Y., & Dincer, I. (2017). Assessment of a sustainable electrochemical ammonia production system using photoelectrochemically

produced hydrogen under concentrated sunlight. *ACS Sustainable Chemistry & Engineering*, *5*(9), 8035–8043. https://doi.org/10.1021/acssuschemeng.7b01638

Elishav, O., Tvil, G., Mosevitzky, B., Lewin, D., Shter, G. E., & Grader, G. S. (2017). The nitrogen economy: The feasibility of using nitrogen-based alternative fuels. *Energy Procedia*, *135*, 3–13. https://doi.org/10.1016/j.egypro.2017.09.482

Giddey, S., Badwal, S. P. S., Munnings, C., & Dolan, M. (2017). Ammonia as a renewable energy transportation media. *ACS Sustainable Chemistry & Engineering*, *5*(11), 10231–10239. https://doi.org/10.1021/acssuschemeng.7b02219

Martín, M., & Grossmann, I. E. (2017). Towards zero co2 emissions in the production of methanol from switchgrass. co2 to methanol. *Computers & Chemical Engineering*, *105*, 308–316. https://doi.org/10.1016/j.compchemeng.2016.11.030

Morgan, E. R., Manwell, J. F., & McGowan, J. G. (2017). Sustainable ammonia production from u.s. offshore wind farms: A techno-economic review. *ACS Sustainable Chemistry & Engineering*, *5*(11), 9554–9567. https://doi.org/10.1021/acssuschemeng.7b02070

Pfromm, P. H. (2017). Towards sustainable agriculture: Fossil-free ammonia. *Journal of Renewable and Sustainable Energy*, *9*(3), 034702. https://doi.org/10.1063/1.4985090

Tan, E. C. D., Snowden-Swan, L. J., Talmadge, M., Dutta, A., Jones, S., Ramasamy, K. K., Gray, M., Dagle, R., Padmaperuma, A., Gerber, M., Sahir, A. H., Tao, L., & Zhang, Y. (2017). Comparative techno-economic analysis and process design for indirect liquefaction pathways to distillate-range fuels via biomass-derived oxygenated intermediates upgrading. *Biofuels, Bioproducts and Biorefining*, *11*(1), 41–66. https://doi.org/10.1002/bbb.1710

Allman, A., & Daoutidis, P. (2018). Optimal scheduling for wind-powered ammonia generation: Effects of key design parameters. *Chemical Engineering Research and Design*, *131*, 5–15. https://doi.org/10.1016/j.cherd.2017.10.010

Dalle Ave, G., & Adams, T. A. (2018). Techno-economic comparison of acetone-butanol-ethanol fermentation using various extractants. *Energy Conversion and Management*, *156*, 288–300. https://doi.org/10.1016/j.enconman.2017.11.020

Malmali, M., Reese, M., McCormick, A. V., & Cussler, E. L. (2018). Converting wind energy to ammonia at lower pressure. *ACS Sustainable Chemistry & Engineering*, *6*(1), 827–834. https://doi.org/10.1021/acssuschemeng.7b03159

Martín-Hernández, E., Sampat, A. M., Zavala, V. M., & Martín, M. (2018). Optimal integrated facility for waste processing. *Chemical Engineering Research and Design*, *131*, 160–182. https://doi.org/10.1016/j.cherd.2017.11.042

Paixão, V. P., Secchi, A. R., & Melo, P. A. (2018). Preliminary design of a municipal solid waste biorefinery for environmentally friendly nh3 production. *Industrial & Engineering Chemistry Research*, *57*(45), 15437–15449. https://doi.org/10.1021/acs.iecr.8b02927

Sánchez, A., & Martín, M. (2018a). Optimal renewable production of ammonia from water and air. *Journal of Cleaner Production*, *178*, 325–342. https://doi.org/10.1016/j.jclepro.2017.12.279

Sánchez, A., & Martín, M. (2018b). Scale up and scale down issues of renewable ammonia plants: Towards modular design. *Sustainable Production and Consumption*, *16*, 176–192. https://doi.org/10.1016/j.spc.2018.08.001

Statista. (2018). Prices of electricity for the industry in spain from 2008 to 2017 (in euro cents per kilowatt hour). Retrieved May 7, 2020, from https://www.statista.com/statistics/595813/electricity-industry-price-spain/

United Nations. (2018). The paris agreement. Retrieved May 7, 2020, from https://unfccc.int/process-and-meetings/the-paris-agreement/the-paris-agreement

Yang, M., & You, F. (2018). Modular methanol manufacturing from shale gas: Techno-economic and environmental analyses of conventional large-scale production versus small-scale distributed, modular processing. *AIChE Journal*, *64*(2), 495–510. https://doi.org/10.1002/aic.15958

Allman, A., Palys, M. J., & Daoutidis, P. (2019). Scheduling-informed optimal design of systems with time-varying operation: A wind-powered ammonia case study. *AIChE Journal*, *65*(7), e16434. https://doi.org/10.1002/aic.16434

Demirhan, C. D., Tso, W. W., Powell, J. B., & Pistikopoulos, E. N. (2019). Sustainable ammonia production through process synthesis and global optimization. *AIChE Journal*, *65*(7), e16498. https://doi.org/10.1002/aic.16498

Part II

TRANSFORMING POWER-TO-X FUELS INTO POWER

6

EVALUATING AMMONIA AS GREEN FUEL FOR POWER GENERATION: A THERMO-CHEMICAL PERSPECTIVE

abstract

Energy storage will be necessary for a future power system with high penetration of renewable sources, mainly, wind and solar, to ensure the stability of the grid. In this context, power-to-chemicals is a promising concept for a medium/long-term storage horizon and a wide range of capacities. Within this alternative, ammonia rises as one of the fuels with the highest potential in a scenario targeting decarbonization. The first step is the production of ammonia using renewable energy sources, followed by its transformation into energy. This second area requires a deeper analysis at process scale in order to introduce this technology into the future power system. In this work, an assessment of an ammonia-based power plant is presented, focusing on the thermo-chemical route. A combined cycle is evaluated, considering different gas clean-up technologies to recover valuable components and comply with environmental restrictions. As a result, the total efficiency of the power facility reaches about 40%, limited by the maximum temperature allowed in the gas turbine. The influence of the price of ammonia is also evaluated due to the paramount importance of this parameter. The production cost ranges from 0.2 to 0.6 €/kWh, with the lowest level corresponding to a scenario in which there is a significant reduction in the cost of renewable power generation and electrolysis technology. Therefore, the feasibility of the use of ammonia as an energy storage alternative is demonstrated, providing a powerful platform for the implementation of a power grid with high penetration of fluctuating sources.

Keywords: Ammonia Combustion, Energy Storage, Green Ammonia, Power-to-X, Power Generation, Renewable Fuels

resumen

El almacenamiento de energía será necesario en un futuro sistema eléctrico con alta penetración de fuentes renovables, principalmente, eólica y solar, para garantizar la estabilidad de la red. En este contexto, la conversión de energía en productos químicos es un concepto prometedor para un horizonte de almacenamiento a medio/largo plazo y una amplia gama de capacidades. Dentro de esta alternativa, el amoníaco se erige como uno de los combustibles con mayor potencial en un escenario orientado a la descarbonización. El primer paso es la producción de amoníaco utilizando fuentes de energía renovables, seguido de su transformación en energía. Esta segunda área requiere un análisis más profundo a escala de proceso para poder introducir esta tecnología en el futuro sistema eléctrico. En este trabajo, se presenta la evaluación de una central eléctrica basada en el amoníaco, centrándose en la ruta termoquímica. Se evalúa un ciclo combinado, considerando diferentes tecnologías de limpieza de gases para recuperar componentes valiosos y cumplir con las restricciones medioambientales. Como resultado, la eficiencia total de la instalación eléctrica alcanza alrededor del 40%, limitada por la temperatura máxima permitida en la turbina de gas. También se evalúa la influencia del precio del amoníaco debido a la importancia primordial de este parámetro. El coste de producción oscila entre 0,2 y 0,6 €/kWh, correspondiendo el nivel más bajo a un escenario en el que se produce una reducción significativa del coste de la generación de energía renovable y de la tecnología de electrólisis. Por lo tanto, se demuestra la viabilidad del uso del amoníaco como alternativa de almacenamiento de energía, proporcionando una potente plataforma para la implementación de una red eléctrica con alta penetración de fuentes fluctuantes.

Palabras clave: Combustión de amoníaco, Almacenamiento de energía, Amoníaco verde, Power-to-X, Producción eléctrica, Combustibles renovables

6.1 introduction

An increase in the share of renewable energy sources (RES) is expected in the coming years to meet the global sustainable goals (UN General Assembly, 2015). Current predictions indicate that, in 2050, 69% of the power will be produced from RES, being wind and solar the two main sources with 56% of the total share (BloombergNEF, 2020). The penetration is not homogeneous across the different territories. The deepest and fastest energy transition will take place in Europe, where 74% of the power will be generated using PV panels and wind turbines by 2050. The main challenges of an energy system with high penetration of these RES are the random variability of the solar/wind resources and the imbalance between power generation and electricity consumption. Therefore, a combination of intermittent and non-intermittent RES and different storage technologies is required to ensure the robustness of the grid (Child et al., 2019). Hence, different energy storage technologies have been proposed to mitigate the fluctuations in power production (Gür, 2018; Frate et al., 2021). For a day/week/month/seasonal storage, power-to-chemicals alternatives are receiving attention due to the high energy density of these fuels, the possibility of easy storage and transportation of these products, and the scalable and flexible behavior of this storage alternative.

Hydrogen has been proposed as one of the key elements in the next energy system for grid-scale storage (Pellow et al., 2015; Y. Zhang et al., 2019), and also for transportation (Ehrenstein et al., 2020). A major boost to the hydrogen economy is expected in the coming years, mainly in Europe, where the post-COVID European Green Deal introduces the goal of making the old continent the first climate-neutral territory by 2050 (van Renssen, 2020). The European hydrogen strategy foresees a cumulative investment in renewable hydrogen up to €470 billion by 2050 (European Commission, 2020). At this point, the development of a competitive electrolysis technology is crucial for the implementation of this path (Mohammadi & Mehrpooya, 2018). To convert H_2 into power, fuel cells are the most extended technology (C. Zhang et al., 2020). However, one of the main challenges is the temporary storage of hydrogen. Several options have been proposed, for example, high-pressure gas tanks (Götz et al., 2016) or metal hydrides (Heras & Martín, 2021). In addition, different hydrogen-based derived products have been proposed which are easier to store and transport. Methane received attention due to the existing infrastructure to distribute natural gas. This hydrogen carrier can be produced through methanation using H_2 and CO_2 (Davis & Martín, 2014; Sternberg & Bardow, 2016). Other carbon-based carriers as methanol (Daggash et al., 2018; Al-Qahtani et al., 2020) or DME (Martín, 2016; Dieterich et al., 2020) have also been

evaluated. Moreover, different technologies have been proposed to convert these fuels into power, for instance, gas turbines or fuel cells (L. Wang et al., 2020).

In particular, one of the hydrogen carriers that is attracting more attention is ammonia since it is a high energy density fuel, with simple storage and with no CO_2 associated emissions (Fúnez Guerra et al., 2020; Cesaro et al., 2021; Palys et al., 2021). Some safety issues have been reported on the use of ammonia as fuel (Di Sarli et al., 2017), however, industrial experience with this chemical turns ammonia into a safe fuel with risks and hazards similar to others such as gasoline or LPG (MacFarlane et al., 2020). Several works have analyzed the synthesis of ammonia using renewable power (G. Wang et al., 2017; Allman & Daoutidis, 2018; Sánchez & Martín, 2018a). After its production, the next stage is to transform it into power when renewable generation is low (Valera-Medina et al., 2018). Two main options are proposed: technologies based on ammonia fuel cells (electro-chemical) and combustion (thermo-chemical). Siddiqui and Dincer (2020) conducted an experimental evaluation of an integrated system, in which, ammonia is synthesized on-site and used directly in a fuel cell. Furthermore, different hydrogen/ammonia blends have also been evaluated to improve the performance of the system (Siddiqui et al., 2020). In this area, Jeerh et al. (2021) review the different fuel cell technologies in which ammonia can be used as fuel. Solid oxide fuel cells (SOFC) rise, to date, as the most promising alternative in ammonia fuel cells. Regarding combustion, Kobayashi et al. (2019) summarized the main experimental advances in ammonia combustion in recent years. Different ammonia/methane (Valera-Medina et al., 2017) and ammonia/hydrogen (Valera-Medina et al., 2019) blends have been proposed as fuel mixtures for gas turbines to overcome the challenges in ammonia combustion. A thermodynamic analysis of an ammonia-fueled gas turbine is presented by Keller et al. (2020). Furthermore, ammonia-based internal combustion engines have also been proposed to be used in transportation applications (Mounaïm-Rousselle & Brequigny, 2020). Lastly, some authors proposed an integration of both methods to produce power from ammonia (Ezzat & Dincer, 2020). However, most of these analyses are experimental and only evaluate the major unit of the ammonia-to-power process. Therefore, an analysis at process scale is required to assess the entire transformation of ammonia into power including the preparation of the raw materials, the transformation into power, and the subsequent treatments, in order to ensure the economic and environmental feasibility of the process. With these studies, it is possible to evaluate the performance of the entire facility, determining the total energy efficiency of the process and the cost of the electricity for the different technologies. These assessments are mandatory

to be able to introduce these technologies in real applications and, to the best of our knowledge, no specific research in this area is available in the literature.

In this work, a process level analysis of the production of power from ammonia using the thermo-chemical path is presented. Particularly, a combined cycle is analyzed using a fuel blend consisting on ammonia and hydrogen. The decomposition of the ammonia to produce the necessary hydrogen is also evaluated in this work. Additionally, different gas cleanup technologies have also been examined. The process superstructure is optimized to determine the optimal path and operating conditions of the ammonia-to-power transformation. After the optimization, some additional sensitivity and scale up studies are carried out to evaluate the technical performance of the process and the economics of this new power generation alternative.

6.2 process description

The process of converting ammonia into power is divided into four main sections: fuel mixture preparation, combined cycle (gas and steam turbines), gas clean-up, and N_2/Ar separation (as shown in Figure 6.1). In the first section, the fuel mixture is prepared according to the features required by the combustion of ammonia. As it has been previously mentioned, ammonia is a relatively unreacted fuel and, therefore, a mixture of hydrogen and ammonia is used in this work as a feed for the combined cycle. This mixture is selected versus other alternatives, such as the ammonia/methane blends, in order to maintain the carbon-free power generation using ammonia. Particularly, a blend of 70% of ammonia and 30% of hydrogen is selected in this work to overcome the ignition and burning velocity issues of the combustion of ammonia alone (Valera-Medina et al., 2019). To produce the necessary hydrogen, ammonia decomposition is employed to be able to operate the facility with ammonia alone as feedstock. To decompose ammonia, a catalytic membrane reactor is set up. Inside the reactor, ammonia is broken down into nitrogen and hydrogen, the two initial constituents, and hydrogen is recovered in the same unit using an appropriate membrane (Chiuta et al., 2013; Jo et al., 2018). Two outlet streams are obtained from the reactor: the first one, which contains hydrogen that is used in the NH_3/H_2 fuel mixture, and the second one, which is composed mainly of nitrogen and also some small amounts of hydrogen and ammonia. This last stream can be recycled to the ammonia production and be used in the synthesis loop, reducing the production cost of renewable ammonia.

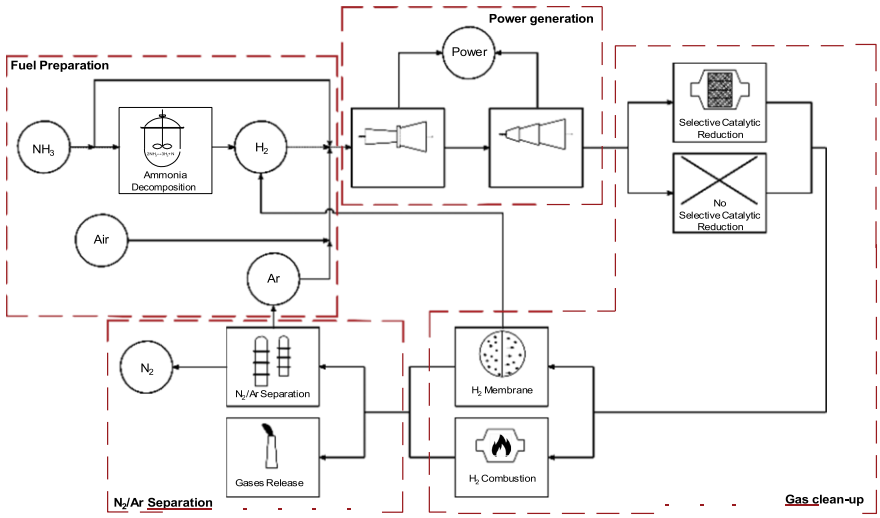

Figure 6.1: Process superstructure diagram for ammonia-to-power transformation

The blend, that is introduced into the gas turbine, is made up of hydrogen and ammonia, air and argon. Argon is fed to control the maximum temperature inside the gas turbine. If the mixture of ammonia/hydrogen is burnt as such, an outlet temperature of about 2100°C is reached (Otomo et al., 2018). However, this value is too high for the traditional gas turbine systems, mainly due to material limitations. Therefore, the maximum temperature in the combustion chamber is limited to 1600°C in this work (Gu et al., 2016). Other inerts, instead of argon, have also been evaluated as carbon dioxide or nitrogen. The first is discarded in order to generate power without any carbon component involved. The second, due to the problem of the formation of nitrogen oxides in the ammonia combustion (as explained below), that could be amplified if larger amounts of nitrogen are introduced into the combustion chamber.

The inlet gas mixture is introduced into the first step of the combined cycle: the gas turbine. Within this unit, the inlet gases are compressed, the combustion of the hydrogen/ammonia mixture takes place and the gases from the combustion chamber are expanded to produce power (Ezzat & Dincer, 2020). The outlet gases from the gas turbine are fed into the Rankine cycle. Three different sections of the steam turbine are considered in this work with various operating pressures (high, medium and low pressure).

After the Rankine cycle, some operations to clean-up the gases are required. The first one is related to the NO_x produced during the ammonia combustion. In the superstructure proposed, it is possible to remove the nitrogen oxides by selective catalytic reduction (SCR) (Resitoglu & Keskin, 2017). If the emission limit values for this pollutant (European Council, 2010) are met without the treatment, it is possible to discard this unit, and a bypass is considered. The next step in the gas clean-up section is hydrogen recovery. This stage is required because one of the products leaving ammonia combustion is hydrogen, which is a valuable component that should be recovered during gas treatment. In this study, two different options are evaluated. On the one hand, hydrogen could be separated using a membrane and recycled to the fuel mixture preparation section. On the other hand, hydrogen is burnt and the energy released during this step is used to reheat the steam within the Rankine cycle allowing for larger power generation.

Finally, the gases can be released into the atmosphere in compliance with environmental restrictions. In this case, nitrogen and argon cannot be reused in the ammonia synthesis and combustion, respectively. Another alternative is to separate the final gas stream, mainly nitrogen and argon, to be able to reuse nitrogen in the ammonia synthesis and to recycle argon for ammonia combustion. To perform this separation, cryogenic distillation is selected in this work.

6.3 modelling issues

This section presents a brief description of the different approaches to modeling the units involved in the NH_3-to-power superstructure. The modeling is based on mass and energy balances and the most relevant details are presented in this section.

6.3.1 *Ammonia Decomposition Reactor*

In the decomposition reactor (as shown in Figure 6.2), ammonia is converted into nitrogen and hydrogen according to the following reaction:

$$NH_3 \rightleftharpoons \frac{1}{2}N_2 + \frac{3}{2}H_2 \tag{6.1}$$

This stage is carried out in a fixed-bed isothermal membrane reactor (Li et al., 2013). The catalyst used is Ni/Al_2O_3, which gives a good performance in ammonia decomposition, is a cheap metal, and is widely accepted as an economical alternative to ruthenium catalysts (Chiuta et al., 2013). A H_2-selective membrane is installed to separate the H_2 in the same unit. A

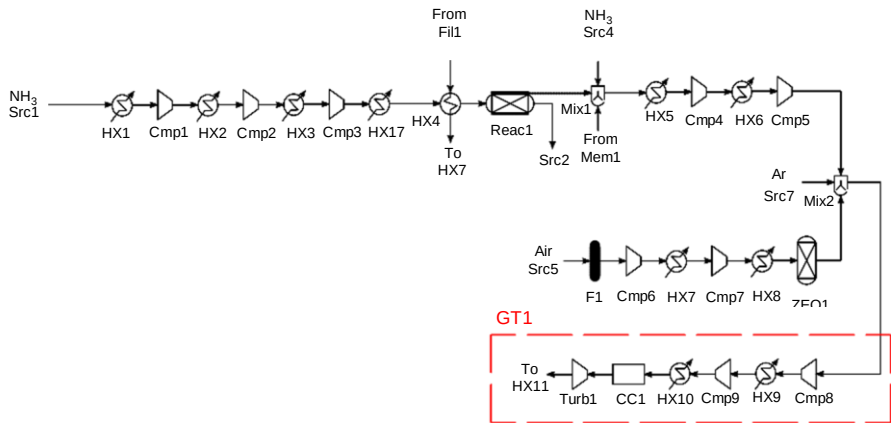

Figure 6.2: Process flow diagram for ammonia decomposition and gas turbine sections

Pd-Ag supported membrane is selected in this study (De Falco et al., 2011). The kinetic equation for the ammonia decomposition is adapted from the Temkin expression (Kim et al., 2018).

$$r = 3k_{reac}\left[K^2 a_N \left(\frac{a_{H_2}^3}{a_{NH_3}^2}\right)^{\alpha} - \left(\frac{a_{NH_3}^2}{a_{H_2}^3}\right)^{1-\alpha}\right] \Phi\Omega \qquad (6.2)$$

The permeation rate of H_2 through the membrane is expressed as a function of the gradient of partial pressure on both sides (Abashar, 2018).

$$J_{H_2} = \frac{28.84 \times 10^{-5}}{\delta} exp\left(-\frac{1888.381}{T}\right)\left(\sqrt{P_{H_2}^r} - \sqrt{P_{H_2}^p}\right) \qquad (6.3)$$

The pressure on the permeate side is fixed to 1 bar. With the kinetic expressions, the model of the membrane reactor consists of five differential equations, three for the mass balances of each of the components, the energy balance and the momentum balance computed with the Ergun equation for the catalytic side. The details of the model are presented in the Supporting Information. However, this model is too complex to be introduced in the optimization of the entire superstructure. To solve this issue and following the approach proposed by Paixão et al. (2018), metamodels or surrogate models were generated using the more rigorous model with the differential equations. Specifically, polynomial regression models have been selected for this case. The general formula to describe

this kind of surrogate models is as follows (Sánchez et al., 2020):

$$f(x) = \beta_0 + \sum_{i=1}^{n} \beta_i x_i + \sum_{i=1}^{n} \sum_{j \leq i}^{n} \beta_{ij} x_i x_j \tag{6.4}$$

Four different variables have been considered as inputs for these models: inlet pressure (P) and temperature (T), inlet gas velocity (v_{reac}) and the total conversion (X_{total}), that represents the percentage of recovered hydrogen through the membrane versus the total hydrogen contained in the inlet ammonia. The objective is to calculate the conversion in the fixed bed (X_{reac}) and the length of the reactor (L_{reac}). The p-value determines the significant coefficients in the model for each case. The surrogate models generated for each output variable are:

$$\begin{aligned} X_{reac} = {} & -2.305 - 0.0060P + 0.0051T + 0.0010v_{reac} \\ & + 2.744X_{total} - 1.424 \times 10^{-6}T^2 + 3.884 \times 10^{-6}PT \\ & + 0.0040PX_{total} - 0.0033TX_{total} \end{aligned} \tag{6.5}$$

$$\begin{aligned} L_{reac} = {} & 442.6363 + 1.1719P - 1.1936T + 12.7908v_{reac} \\ & + 31.7269X_{total} + 0.00076T^2 - 0.00077PT - 0.05051Pv_{reac} \\ & - 0.62543PX_{total} - 0.02251Tv_{reac} + 13.8569v_{reac}X_{total} \end{aligned} \tag{6.6}$$

These two surrogate models have been developed for the following ranges of the input variables: inlet temperature between 700-850 K, inlet pressure 10-50 bar, inlet gas velocity in the range of 0.85-1.5 m/s and the total conversion between 0.85-0.95.

6.3.2 *Gas turbine*

The gas turbine (as shown in Figure 6.2) is modeled using three different sections. Firstly, a multistage compression stage with intercooling, the second step is the combustion chamber and the last one, the expansion to produce power (León & Martín, 2016). Polytropic compression and expansion are assumed for the gases with a polytropic coefficient (k) equal to 1.4 and the efficiency of the process is fixed to 0.85. One of the key points in this section is to model the ammonia/hydrogen combustion. In this work, the mixture is burnt with air in the presence of argon, as an inert, to reduce the outlet temperature. The amount of air that is necessary to introduce is based on the selected equivalent ratio (ER). This parameter represents the ratio between the stoichiometric oxygen and the real one introduced into the combustion chamber. In this work, and according to previous experimental results (Valera-Medina et al., 2019; Khateeb et al.,

2020), the ER is limited within the range of 1.2-1.4. As products of the combustion, nitrogen and water are the most representative. It is assumed that ammonia is not in the outlet gases (Otomo et al., 2018). The amount of each component and the final temperature is computed using mass and energy balances. As mentioned above, the maximum temperature at the combustion chamber is limited to 1600°C. One of the main limitations in ammonia combustion is the formation of nitrogen oxides. To compute the amount of this pollutant generated in the combustion chamber, an empirical correlation is developed, based on experimental results from Valera-Medina et al. (2019), where the nitrogen oxide concentration in the outlet gases is a function of the ER (for the range used in this work).

$$NO(ppm) = 2.9951 \times 10^{19} exp(-31.9846ER) \tag{6.7}$$

6.3.3 *Rankine cycle*

After the gas turbine, the gases are introduced into the Rankine cycle in order to increase the efficiency of power production (as shown in Figure 6.3). High, medium and low pressure steam turbines (Meroueh & Chen, 2020) are introduced to represent the multistage expansion in a real steam turbine. The high-pressure unit operates between 95-125 bar in the inlet stream, the medium pressure in the range of 11-35 bar and the low pressure between 5-9.5 bar, common ranges in the operation of the Rankine cycle. The gases from the gas turbine are used to heat up and evaporate the steam. To compute the enthalpies and entropies of each of the streams involved in the Rankine cycle, the proposed correlations by León and Martín (2016) were used where the enthalpy/entropy is a function of pressure and temperature. In each of the turbines, the isoentropic efficiency is fixed to 0.9 (Sadi & Arabkoohsar, 2019).

6.3.4 *Gas cleanup*

Nitrogen oxides are produced during ammonia combustion. This is a significant pollutant and must meet strict regulation. In the proposed superstructure (as shown in Figure 6.3), there are two possible options: the first one is to use a nitrogen oxide abatement technology to remove it and the second one is not to use any as long as the flue gas complies with environmental restrictions. To remove the nitrogen oxides, different treatments have been proposed (Guerras & Martín, 2019). In this study, a selective catalytic reduction (SCR) using hydrogen is selected. Hydrogen is chosen over ammonia or other products because it is a product of ammonia combustion and is presented in the gas stream. In addition, only small

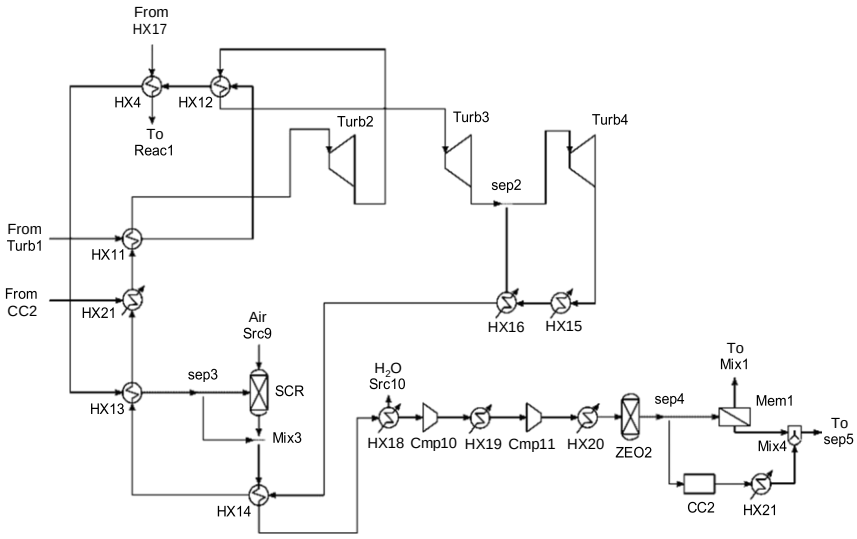

Figure 6.3: Process flow diagram for Rankine cycle and gas cleanup section

amounts of hydrogen are required for this treatment because of the reduced concentration of NO_x. The subsequent reaction takes places in the SCR reactor (Resitoglu & Keskin, 2017):

$$2NO + 4H_2 + O_2 \rightarrow N_2 + 4H_2O \tag{6.8}$$

A conversion of 100% is assumed in this work. The second stage in the gas cleanup section is related to the recovery of hydrogen. Significant amounts of this chemical leave the combustion chamber of the gas turbine, however, hydrogen is a valuable component and should be recovered. Two options have been proposed for this stage. Firstly, hydrogen can be separated using a membrane and recycled to the fuel mixture preparation section. A separation factor for H_2 equal to 68 is fixed, with an operating pressure of 6 bar (Zhu et al., 2017). The second option is to burn the hydrogen to reheat the steam within the Rankine cycle (in the heat exchanger HX21 before the high pressure steam turbine). If more heat is introduced into the cycle, higher power production is expected.

6.3.5 *N_2/Ar separation*

The final gases, after the separation of hydrogen, contain mainly nitrogen and argon. On the one hand, nitrogen has been produced out of air for the synthesis of ammonia, and, in the case of power-to-ammonia, it has been previously obtained from different air separation technologies

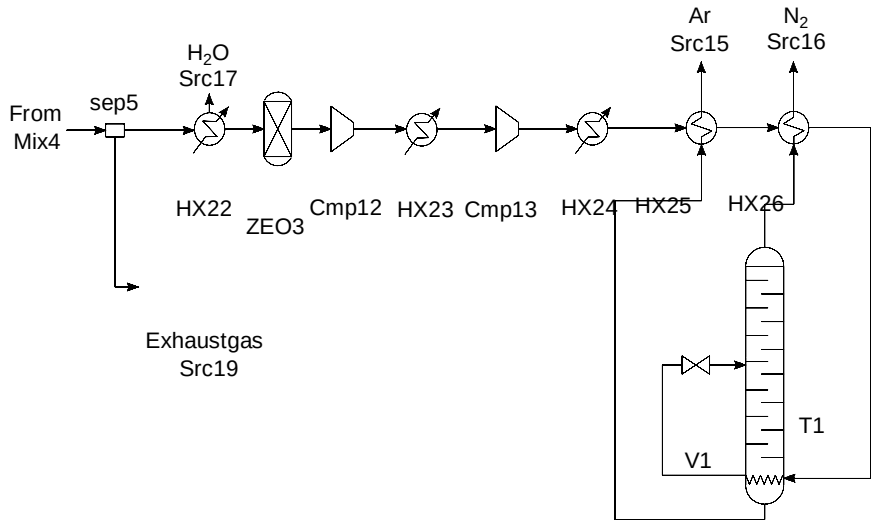

Figure 6.4: Process flow diagram for N_2/Ar separation section

(Sánchez & Martín, 2018b). On the other hand, argon is fed into the ammonia combustion to limit the maximum temperature in the gas turbine. Therefore, it is interesting to recover these two species. At this point, cryogenic distillation is proposed to separate them (as shown in Figure 6.4) following the schemes of air separation technologies. The first step is to compress the gases to a range of pressure between 40-60 bar. Then, the gases are cooled down providing the heat necessary in the reboiler of the distillation column. Finally, the gases are expanded up to ambient pressure, reducing the temperature and obtaining a biphasic stream that is introduced into the distillation column. To capture the thermodynamics of this system, difficult to model with simple equations, surrogate models have been developed to calculate the Joule-Thompson coefficient of the valve and the vapor fraction in the outlet stream. The rigorous models were developed in CHEMCAD© 7.0 using the PRSK thermodynamic model. The following two polynomial regression models have been generated:

$$JT = -0.54978 + 0.01845T_{in} - 0.01676P_{in} \tag{6.9}$$

$$f_{vapor} = -1.13843 + 0.01432T_{in} - 0.00207P_{in} \tag{6.10}$$

Finally, after the valve, the gases are introduced into the cryogenic distillation column where the separation takes place. A recovery yield equal to 99.9% for nitrogen and 0.1% for argon in the top stream is fixed according to the results of the simulation of this system in CHEMCAD© 7.0. Apart from the cryogenic distillation, it is also possible to release the

gases without separation. In this case, it is not necessary to install the separation system, but argon and nitrogen are lost.

6.4 solution procedure

The design of an ammonia-to-power facility is formulated as a mixed-integer nonlinear programming (MINLP) problem to select the technologies and operating conditions that allow to produce. Six binary variables are present in the problem to determine whether or not to remove nitrogen oxides, the technology to recover the hydrogen and, finally, whether to introduce a step for the nitrogen/argon separation. The original MINLP problem is decomposed and eight nonlinear programming (NLP) problems are solved, one per possible combination of the binary variables. As objective function, a simplified operating cost for the production of power is used as follows:

$$obj = \sum_{i \epsilon IN} f_i C_i - \sum_{j \epsilon OUT} f_j C_j \tag{6.11}$$

where f_i is the inlet flow of each of the inlet/outlet resources and C_i its cost. The optimization problem is solved to minimize this simplified operating cost for a given power demand. The ammonia cost is set to 0.5 €/kg (Pfromm, 2017), 0.037 €/kg for N_2 (Elishav et al., 2017), 0.5 €/kg for Ar (Downie, 2007) and 4 €/kg for H_2 (Matzen et al., 2015).

The problem is implemented in GAMS© and solved using a multistart optimization approach using CONOPT 3.0 as the preferred solver. The size of the problem is approximately 1500-2000 equations and variables for each of the cases. After the optimization, an economic analysis is performed based on the methodology proposed by Sinnott (2014). Further details on the economic analysis methodology are provided in Table C.1 of the Supporting Information. During the scale-up analysis, some of the units involved must be duplicated because the maximum level is reached. This behavior is included during the economic evaluation of the process.

6.5 results

6.5.1 *Main operating variables*

In this section, a brief description of the main operating variables of the ammonia-to-power facility is presented. The value of these operating variables has been determined during the optimization procedure. In Table 6.1, a summary of the main results is shown when 100 MW is fixed as

power capacity. In the ammonia decomposition section, the operating conditions of the reactor are the same regardless of the alternative: a temperature equal to 700 K, pressure to 10 bar and a gas inlet velocity of 1.5 m/s. With these conditions, a reactor conversion of more than 97% and a total recovery of hydrogen of more than 85% is reached. The temperature and pressure of the reactor are fixed to the minimum level allowed in the optimization problem. The lowest temperature is selected because the thermal energy to increase this variable is obtained from the outlet gases of the gas turbine. Therefore, if the thermal energy is used to heat up this stream, lower power generation is obtained. The minimum pressure is selected due to the cost of compression. If the inlet stream of the reactor is at a higher pressure, lower levels of power production are achieved in the facility, decreasing the energy efficiency.

Table 6.1: Main operating variables for the different alternatives: **A** - No SCR+Comb+N_2/Ar separation; **B** - No SCR+Comb+No N_2/Ar separation; **C**- No SCR+Mem+N_2/Ar separation; **D**- No SCR+Mem+No N_2/Ar separation; **E**- SCR+Comb+ N_2/Ar separation; **F**- SCR+Comb+No N_2/Ar separation; **G**- SCR+Mem+N_2/Ar separation; **H**-SCR+Mem+No N_2/Ar separation; **I** - No SCR+Mem without temperature limitation

		A	**B**	**C**	**D**	**E**	**F**	**G**	**H**	**I**
Power	Capacity (MW)	100	100	100	100	100	100	100	100	100
Inlet flows	Ammonia (kg/s)	17.79	14.74	15.83	13.31	17.86	14.74	15.97	13.30	11.07
	Air (kg/s)	88.68	64.07	92.22	75.13	88.20	64.07	92.65	75.10	64.85
	Ar (kg/s)	74.66	34.39	67.04	32.68	73.06	34.39	67.36	32.66	-
Ammonia Decomposition	Inlet T (K)	700	700	700	700	700	700	700	700	700
	Inlet P (bar)	10	10	10	10	10	10	10	10	10
	Inlet v (m/s)	1.5	1.5	1.5	1.5	1.5	1.5	1.5	1.5	0.85
Gas Turbine	Inlet P (bar)	8.41	6.00	6.80	6.90	8.49	6.00	6.30	6.93	12.26
	Combustion T (K)	1873	1873	1873	1873	1873	1873	1873	1873	2340
	Power (MW)	179.5	105.8	171.0	131.7	178.6	105.8	169.9	131.9	131.5
	ER	1.2	1.4	1.2	1.4	1.2	1.4	1.2	1.4	1.2
Steam Turbine	P high (bar)	125	125	125	125	125	125	125	125	125
	P inter (bar)	35	35	35	35	35	35	35	35	35
	P low (bar)	5	9.5	9.5	9.5	5	9.5	9.5	5	9.5
	T high (K)	782.0	991.6	785.9	785.9	782.8	991.6	785.9	782.8	785.9
	T inter (K)	564.0	745.7	567.1	567.1	564.0	745.7	567.1	564.0	567.1
	T low (K)	425.5	621.6	451.3	451.3	425.5	621.6	451.3	425.5	451.3
N_2/Ar Separation	P compr (bar)	40	-	40	-	40	-	40	-	-
	Inlet T (K)	77.13	-	77.26	-	77.42	-	77.30	-	-

For the preparation of the fuel blend, ammonia, hydrogen (produced from ammonia decomposition), argon and air are mixed. The flows of each feedstock in the facility are presented in Table 6.1. The inlet and outlet flows of the gas turbine are shown in more detail in Table C.2 of the Supplementary Information. As a general trend, when the N_2/Ar separation is introduced to recycle both chemicals, a higher flow of ammonia is required. The reason for this is that the separation requires power to compress the gases before the cryogenic distillation and, since the plant is autonomous, the power must be produced within the plant, and, therefore, more fuel is needed. The performance of the gas turbine also determines the inlet flows of the components. The equivalent ratio (ER) is set to 1.2, if the gases are released into the atmosphere, or 1.4, if the N_2 and Ar are separated. This is because, when the gases are discharged, the environmental restrictions must be met in terms of NO_x emissions. And, according to equation 6.7, following experimental results, these emissions increase when the ER decreases. Therefore, in order to comply with the maximum emission values, the ER must be reduced. The temperature of the combustion of the fuel blend is the same for all the alternatives 1873 K, limited by the upper limit for this temperature. If this constraint is relaxed, better performance in the gas turbine is expected and the introduction of argon as an inert could be avoided. In case **I** in Table 6.1, the scenario in which the temperature limitation is removed is presented. It is not necessary to introduce argon and, therefore, its separation using cryogenic distillation is also avoided, reducing considerably the capital and operating cost of the process. The maximum temperature in the gas turbine reaches 2340 K, allowing the same power generation with a small amount of inlet ammonia.

In the steam turbine, the maximum pressure value for each stage is reached, except for the value of the low-pressure turbine where the pressure range is between 5-9.5 bar. Also, as expected, higher inlet temperatures are obtained when combustion is introduced in the H_2 separation. More details about the conditions of the steam turbines are collected in Table C.3 of the Supplementary Information. Finally, in the N_2/Ar separation unit, the gases are compressed up to 40 bar (the minimum level to avoid compression work) and the inlet temperature in the column is about 77 K.

6.5.2 *Energy Efficiency*

At this point, it is also interesting to evaluate the energy performance of the ammonia-to-power process. First of all, in Figure 6.5, a Sankey diagram is presented where the different energy flows are shown. The figure presents the best case in economic terms where no SCR treatment

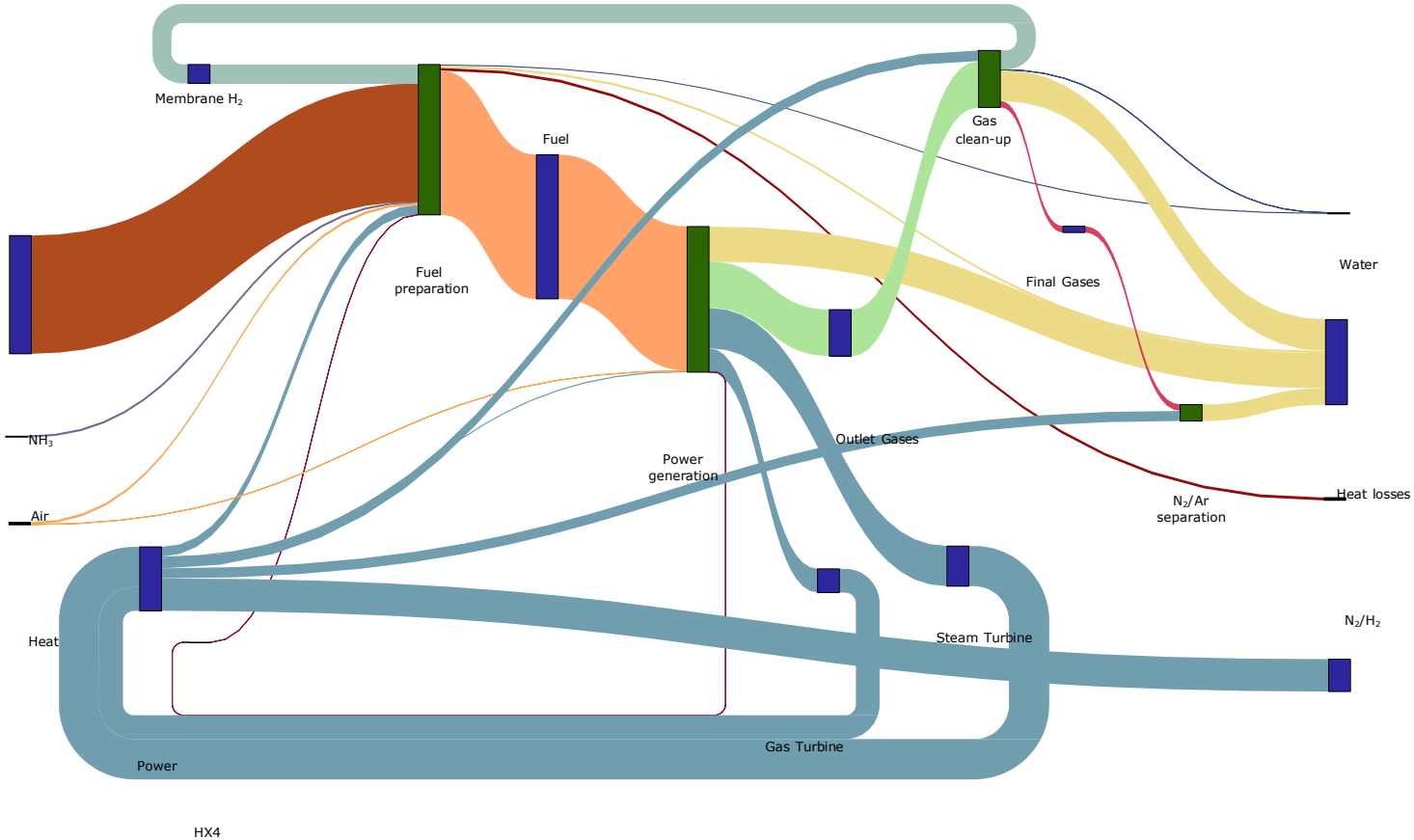
Membrane H_2
Fuel
Gas clean-up
Fuel preparation
Water
Final Gases
NH_3
Outlet Gases
Power generation
Heat losses
Air
N_2/Ar separation
Heat
N_2/H_2
Steam Turbine
Gas Turbine
Power
HX4
Output Power

Figure 6.5: Sankey diagram for the flows of energy in the ammonia-to-power facility. The blue boxes represent the main products of the process and the green ones the total energy involved in the four main sections of the facility: fuel preparation, power generation, gas clean-up and N_2/Ar separation

is included, H_2 is recovered by means of membranes and the N_2/Ar separation is included (case B in Table 6.1). The total energy involved in the main sections of the superstructure is presented in green boxes and the blue boxes represent the main products of the facility. The major input to the system is ammonia which is introduced into the fuel preparation section. This ammonia is mixed with the recycled hydrogen from the gas clean-up section to form the fuel of the combined cycle. Around 80% of the energy in the fuel blend comes from inlet ammonia. This fuel is fed to the power generation section. About 45% of the energy is transformed into power in the gas and steam turbines and approximately 30% of the total energy of the fuel remains in the flue gases. A fraction of the energy lost with the flue gases is recovered using the membranes that recycle the hydrogen to the fuel preparation section.

The energy efficiency of the process transformation is calculated as the ratio between the total power that is produced versus the heating value (LHV) of ammonia (as shown in equation 6.12):

$$\eta = \frac{W_{output}}{\dot{m}_{NH_3} LHV} 100 \tag{6.12}$$

The energy efficiencies for each of the evaluated alternatives in the ammonia-to-power superstructure are presented in Table 6.2.

Table 6.2: Energy efficiencies for the ammonia-to-power processes for a given capacity equal to 100 MW

	Process alternative	η
A	No SCR+Comb+N_2/Ar separation	30.2
B	No SCR+Comb+No N_2/Ar separation	36.5
C	No SCR+Mem+N_2/Ar separation	34.0
D	No SCR+Mem+No N_2/Ar separation	40.4
E	SCR+Comb+N_2/Ar separation	30.1
F	SCR+Comb+No N_2/Ar separation	36.5
G	SCR+Mem+N_2/Ar separation	33.7
H	SCR+Mem+No N_2/Ar separation	40.4
I	No SCR+Mem without temperature limitation	48.6

The efficiency of the process alternatives that use membranes is higher than those that burn hydrogen (2-3% higher efficiency). In addition, the introduction of N_2/Ar separation reduces the energy efficiency of the process, by around 15%. This is due to the fact that the separation involves

energy consumption that must be provided using the power produced in the facility. Therefore, the total production of power is lower. At this point, based only on energy efficiencies, the use of N_2/Ar separation is detrimental to the performance of the process. Nevertheless, the economic implications of these decisions are evaluated in the following section. If the temperature constraint is relaxed, a maximum efficiency of almost 50% is achieved in the ammonia-to-power transformation. Therefore, an enhanced design for the gas turbines can help improve the energy efficiency of the process. These results are consistent with respect to previous analysis. Božo and Valera-Medina (2020) studied the operation of a humidified gas turbine alone excluding the combined cycle, the preparation of raw materials and the gas-clean up section. The maximum efficiency of this system was 43.4%. Keller et al. (2020) carried out a thermodynamic analysis of a combined cycle, including only the gas and steam turbines. The maximum efficiency in that work increased to about 60%. Therefore, the introduction of the Rankine cycle improves the energy performance of the ammonia-to-power transformation, and the introduction of all the sections of the facility is required to obtain an accurate efficiency of the power generation from ammonia. It is also interesting to compare the values of efficiency obtained in this work (as shown Table 6.2) with those achieved from the ammonia fuel cells, the other main alternative in the use of ammonia for power production. Ezzat and Dincer (2020) computed the ammonia solid oxide fuel cell (SOFC) efficiency reaching values of about 65%. Other studies reduce this value to about 45% (Zhao et al., 2019). Therefore, the fuel cell systems may have slightly higher efficiencies than the thermo-chemical route. However, the fuel cells are developed, in general, for small-scale applications, for instance, vehicles. Thus, the thermo-chemical pathway could be appropriate for utility applications with higher power consumptions such as grid management. The value of the ammonia-to-power thermo-chemical efficiencies can also be put into perspective with the traditional power generation system. Coal-based power facilities have an efficiency of about 40%, nuclear around 45% or combined cycle using natural gas about 50% (Suppes & Storvick, 2007). These values are similar those obtained using ammonia, demonstrating the great potential of this chemical as a carbon-free fuel.

6.5.3 *Economic Analysis*

An economic analysis of the different alternatives for transforming ammonia into power is presented in this section. Figure 6.6 represents the production and capital cost for the process alternatives where SCR tech-

nology is not included. Different capacities are evaluated in the figure for analyzing the influence of the scale on the profitability of the process including the modular behavior of some units. It is clear that alternatives where N_2/Ar separation is included reduce drastically the production cost of the power from about 0.9-1 €/kWh to 0.2-0.3 €/kWh. As Figure 6.6 shows, it is necessary to increase the investment to introduce this new section, however, the possibility of recycling the obtained gases to the ammonia synthesis and to the combustion zone justifies this increase. Furthermore, the introduction of this unit decreases the global efficiency of the transformation as the previous section explained. But, the better economic performance supports the addition of the separation. If the decision regarding the gas cleanup is analyzed (membrane versus combustion for the H_2 treatment), the use of membranes reduces the capital and operating costs of the facility. An increment of about 5% is expected when combustion is selected compared to membranes. Hydrogen is a valuable component and the preferred option is to recycle it to avoid the consumption of ammonia in the membrane reactor versus the option of using it to reheat the steam in the Rankine cycle.

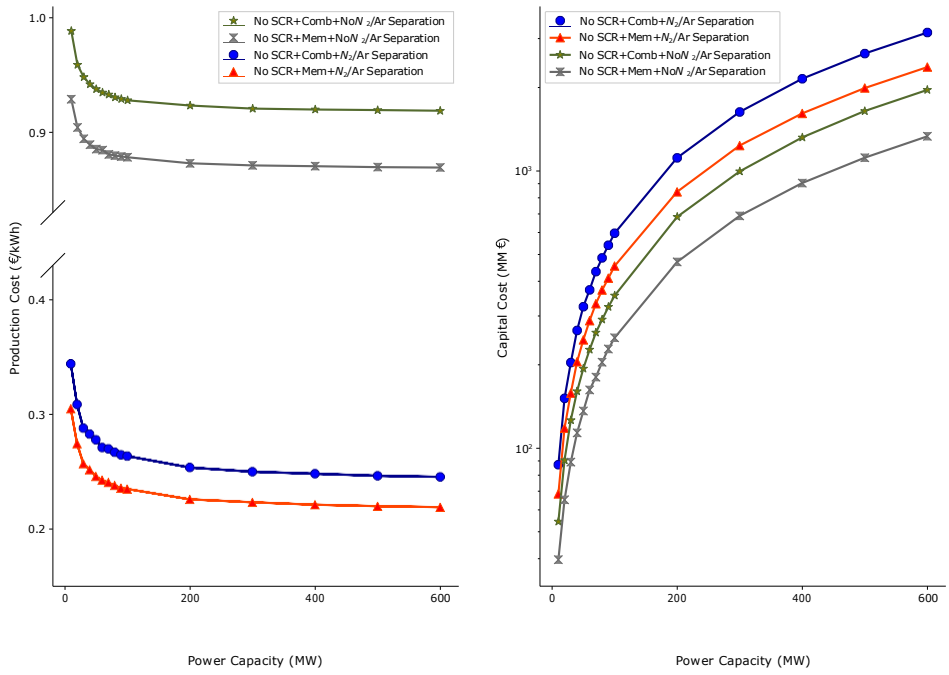

Figure 6.6: Capital and operating cost for the alternatives without SCR technology

Similarly, Figure 6.7 shows the production and capital cost when the SCR technology to remove the NO_x is introduced. As in the case where SCR is not included, the use of membranes for the recovery of hydrogen show better economic performance than the combustion of the gas

stream as clean-up stage and the N_2/Ar separation significantly reduces the production cost of power. If the introduction of SCR technology is evaluated, a logical increase in the production and capital cost takes place because the new treatment requires introducing a new unit. An increase of about 0.02-0.04 €/kWh is expected when SCR is selected. However, from a sustainable point of view, the introduction of this technology could be suitable to be able to produce CO_2-free power but also free of other pollutants such as nitrogen oxides. Consequently, this increment could be acceptable and assumed by society.

To summarize, the best alternative to carry out the ammonia-to-power transformation, from the economic standpoint, is the combination of membranes and the N_2/Ar separation excluding the SCR technology. In this case, a capital cost of about 450 MM€ and a production cost of 0.2 €/kWh is expected for a facility with a production capacity of 100 MW. If the SCR technology is included, in order to improve the sustainability of the process, the investment increase to about 550 MM€ with a production cost of 0.25 €/kWh.

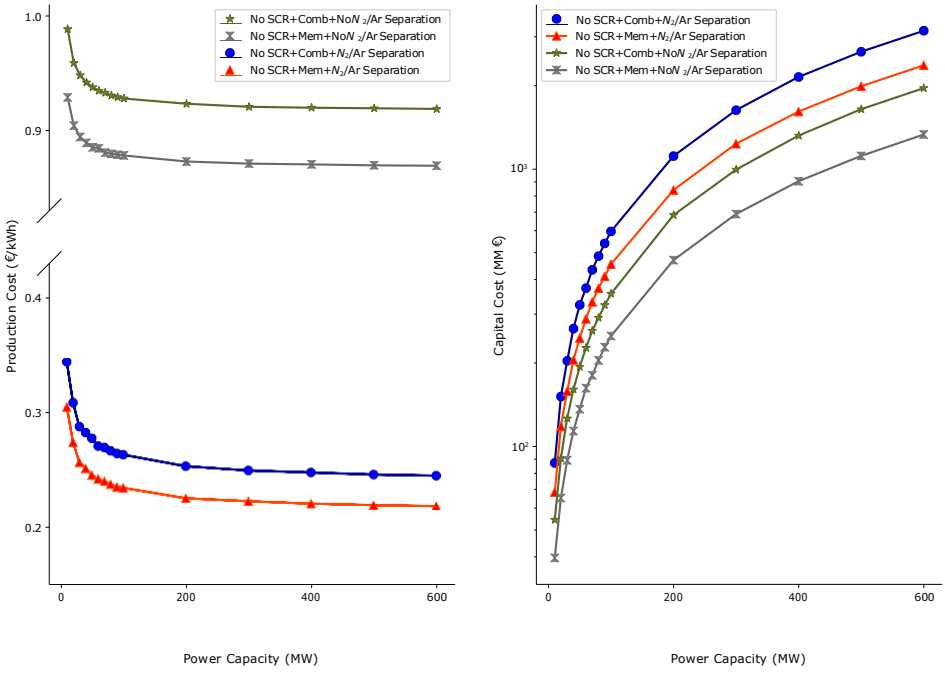

Figure 6.7: Capital and operating cost for the alternatives without SCR technology

Figure 6.8 shows the breakdown of the investment and production costs for the best alternatives, whether NO_x catalytic removal or not is implemented. This presents the two best alternatives, including or not selective catalytic removal. The heat exchangers are the main item in the distribution of the capital cost in both cases (Figure 6.8 a and 6.8 c) with

around 50% of the total inversion followed by the compressors. The NO_x treatment also represents an important percentage (≈ 20%) of the total capital cost when this technology is included in the ammonia-to-power process (Figure 6.8 a). In the case of the operating costs, the raw materials are the most important element, with about 50% of the total production cost (Figure 6.8 b and 6.8 d). The capital charges are about 20-25%, representing a higher percentage when the SCR is included due to the increment of the capital cost for these new units. These results clearly show the crucial importance of the cost of ammonia in the profitability of these power generation facilities.

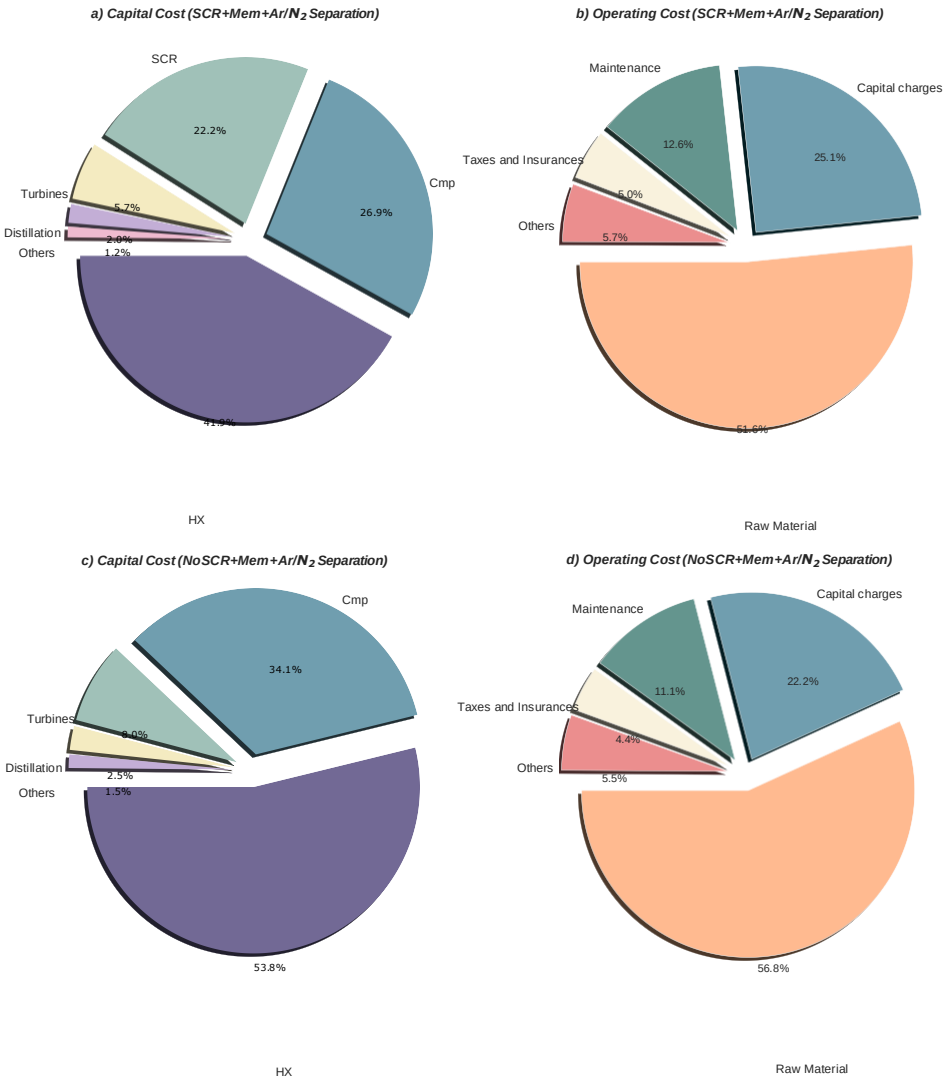

Figure 6.8: Breakdown of the capital and operating cost for the most promising technologies in the ammonia-to-power process

6.5.4 *Sensitivity Analysis*

Due to the central relevance of the price of ammonia in power generation, a sensitivity analysis is performed to assess the impact of the different ammonia prices in the power production cost. The price of green ammonia depends on the technology (power-to-ammonia (Sánchez & Martín, 2018a) or biomass gasification/digestion (Sánchez et al., 2019)) and a significant reduction is expected in the coming years, mainly, in the power-to-ammonia processes due to the reduction of the cost of PV panels and wind turbines and also in the electrolysis technologies. The influence of the ammonia price and the power production capacity in the power cost is presented in Figure 6.9.

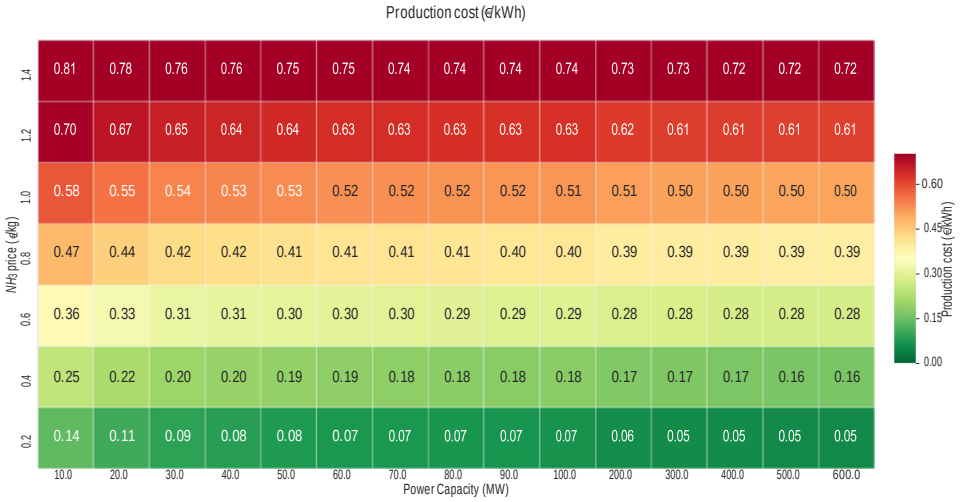

Figure 6.9: Effect of the ammonia price and the facility capacity in the power production cost

The ammonia price in the sensitivity analysis is in the range of 0.2-1.4 €/kg. Using these levels, it is possible to capture the current and expected prices of ammonia using renewable sources. The ongoing base prices levels are: ≈1.4 €/kg for power-to-ammonia using membranes for air separation, ≈ 1.3 €/kg using distillation, ≈ 1.2 €/kg for the PSA and about 0.4-0.6 €/kg for the biomass-based alternatives. The range for the power capacity is 10-600 MW.

With the current prices of ammonia, especially, power-to-ammonia alternatives, the production cost of power is about 0.5-0.8 €/kWh but a promising cost of about 0.2-0.4 €/kWh could be reached in the next years if the expected reduction in the ammonia prices comes true. For a better comparison, the cost of the ammonia-to-power is put into perspective with the production cost of different renewable energy sources. For instance, the

cost of power generation using PV panels is about 0.05-0.1 €/kWh, from wind turbines between 0.1-0.15 €/kWh or the biogas about 0.15 €/kWh (Kost et al., 2018). Note that power from PV panels or wind turbines is highly volatile while that based on ammonia can be stable over time. In other traditional sources, the cost of electricity is in the range of 0.05-0.1 €/kWh for coal facilities or up to 0.22 €/kWh in the case of gas-based power generation (Kost et al., 2018). As expected, storage alternatives are more expensive than direct power production. However, a range of 0.2-0.4 €/kWh for the ammonia-to-power process is competitive for introducing this technology into the power grid in order to increase its robustness. With these price levels, it is possible to create a competitive cost for electricity combining renewable sources and different energy storage technologies. And, by using the ammonia-to-power alternative, it is possible to provide a clean and carbon-free storage option for different time scales and capacities.

6.6 conclusions

This work presents a process scale analysis for the ammonia-to-power transformation. Ammonia could be key in the future energy system as a carbon-free technology to store energy and, also, as an energy carrier. Therefore, the evaluation of the potential transformation of ammonia into power is critical for the possible uses of ammonia in the new sustainable energy paradigm. In this work, a mixture of ammonia/hydrogen is used as fuel for the combined cycle. This hydrogen is produced through ammonia decomposition. In addition, different gas cleanup alternatives have been proposed including SCR NO_x removal, different H_2 recovery technologies and the final N_2/Ar separation. An equation-based optimization approach is developed to determine the optimal path and the conditions of ammonia-based power production. A technical and economic evaluation is presented for the different alternatives. The best alternative, in economic terms, in the ammonia-to-power transformation is the combination of membranes for hydrogen recovery and N_2/Ar separation with no treatment for nitrogen oxides removal. Energy efficiencies of around 40% are reached for the complete transformation of ammonia into power, including not only the gas turbine but also the entire process. The production cost ranges between 0.2-0.6 €/kWh, which could be competitive for the integration of this technology into a renewable energy scheme. Therefore, the potential of the use of ammonia as a fuel for energy storage is demonstrated in this work in a context where the high penetration of renewable energy sources required the implementation of the energy storage at grid scale. For the full deployment of the use of ammonia in the energy system,

further analysis is needed regarding materials for ammonia gas turbines and the potential degradation. Moreover, an analysis including all the production and storage technologies at grid-scale is necessary to determine the contribution of each of these technologies towards the goal of achieving a 100% renewable energy system.

nomenclature

a_i	Activity of component i (atm)
C_i	Cost of product i (€/kg)
ER	Equivalent ratio
f_{vapor}	vapor fraction
f_i	Total flow (kg/s)
JT	Joule-Thompson coefficient (K/bar)
L_{reac}	Length of the decomposition reactor (m)
LHV	Lower heating value (kJ/kg)
$\dot{m}_{NH_3}$	Inlet molar flow of ammonia (kg/s)
P	Pressure (atm)
P_i	Partial pressure of component i (atm)
k_{reac}	Rate constant (kmol/m^3 hr)
K_p	Equilibrium constant (1/atm)
r	Reaction rate (kmol/m^3 hr)
$r^p_{H_2}$	Permeation rate (kmol/m^2 hr)
T	Temperature (K)
v_{reac}	Inlet velocity of the gases (m/s)
W_{output}	Total power production (kJ)
X_{reac}	Conversion in the fixed bed
X_{total}	Total H_2 recovery in the membrane reactor
α	Kinetic parameter
β_i	Polynomial regression coefficient
δ	Thickness of the membrane (μm)
η	Energy efficiency
Ω	Catalytic activity
Φ	Effectiveness factor

acknowledgments

The authors acknowledge MICINN Spain grant PID2019-105434RB-C31 and the FPU, Spain grant (FPU16/06212) to A.S.

bibliography

Downie, N. A. (2007). *Industrial gases*. Springer Science & Business Media.

Suppes, G. J., & Storvick, T. (2007). *Sustainable nuclear power*. Elsevier.

European Council. (2010). Directive 2010/75/eu of the european parliament and of the council. *Off. J. Eur. Union L*, *334*, 17–119.

De Falco, M., Marrelli, L., & Iaquaniello, G. (2011). Membrane reactors for hydrogen production processes.

Chiuta, S., Everson, R. C., Neomagus, H. W., van der Gryp, P., & Bessarabov, D. G. (2013). Reactor technology options for distributed hydrogen generation via ammonia decomposition: A review. *International Journal of Hydrogen Energy*, *38*(35), 14968–14991. https://doi.org/10.1016/j.ijhydene.2013.09.067

Li, G., Kanezashi, M., Yoshioka, T., & Tsuru, T. (2013). Ammonia decomposition in catalytic membrane reactors: Simulation and experimental studies. *AIChE Journal*, *59*(1), 168–179. https://doi.org/10.1002/aic.13794

Davis, W., & Martín, M. (2014). Optimal year-round operation for methane production from co2 and water using wind and/or solar energy. *Journal of Cleaner Production*, *80*, 252–261. https://doi.org/10.1016/j.jclepro.2014.05.077

Sinnott, R. (2014). *Chemical engineering design* (Vol. 6). Elsevier.

Matzen, M., Alhajji, M., & Demirel, Y. (2015). Chemical storage of wind energy by renewable methanol production: Feasibility analysis using a multi-criteria decision matrix. *Energy*, *93*, 343–353. https://doi.org/10.1016/j.energy.2015.09.043

Pellow, M. A., Emmott, C. J. M., Barnhart, C. J., & Benson, S. M. (2015). Hydrogen or batteries for grid storage? a net energy analysis. *Energy Environ. Sci.*, *8*, 1938–1952. https://doi.org/10.1039/C4EE04041D

UN General Assembly. (2015). Transforming our world: The 2030 agenda for sustainable development. *Division for Sustainable Development Goals: New York, NY, USA*.

Götz, M., Lefebvre, J., Mörs, F., McDaniel Koch, A., Graf, F., Bajohr, S., Reimert, R., & Kolb, T. (2016). Renewable power-to-gas: A technological and economic review. *Renewable Energy*, *85*, 1371–1390. https://doi.org/10.1016/j.renene.2015.07.066

Gu, C.-w., Wang, H., Ji, X.-x., & Li, X.-s. (2016). Development and application of a thermodynamic-cycle performance analysis method of a three-shaft gas turbine. *Energy*, *112*, 307–321. https://doi.org/10.1016/j.energy.2016.06.094

León, E., & Martín, M. (2016). Optimal production of power in a combined cycle from manure based biogas. *Energy Conversion and Management*, *114*, 89–99. https://doi.org/10.1016/j.enconman.2016.02.002

Martín, M. (2016). Optimal year-round production of dme from co2 and water using renewable energy. *Journal of CO2 Utilization*, *13*, 105–113. https://doi.org/10.1016/j.jcou.2016.01.003

Sternberg, A., & Bardow, A. (2016). Life cycle assessment of power-to-gas: Syngas vs methane. *ACS Sustainable Chemistry & Engineering*, *4*(8), 4156–4165. https://doi.org/10.1021/acssuschemeng.6b00644

Di Sarli, V., Cammarota, F., Salzano, E., & Di Benedetto, A. (2017). Explosion behavior of ammonia and ammonia/methane in oxygen-enriched air. *Process Safety Progress*, *36*(4), 368–371. https://doi.org/10.1002/prs.11912

Elishav, O., Tvil, G., Mosevitzky, B., Lewin, D., Shter, G. E., & Grader, G. S. (2017). The nitrogen economy: The feasibility of using nitrogen-based alternative fuels [11th International Renewable Energy Storage Conference, IRES 2017, 14-16 March 2017, Düsseldorf, Germany]. *Energy Procedia*, *135*, 3–13. https://doi.org/10.1016/j.egypro.2017.09.482

Pfromm, P. H. (2017). Towards sustainable agriculture: Fossil-free ammonia. *Journal of Renewable and Sustainable Energy*, *9*(3), 034702. https://doi.org/10.1063/1.4985090

Resitoglu, I. A., & Keskin, A. (2017). Hydrogen applications in selective catalytic reduction of nox emissions from diesel engines. *International Journal of Hydrogen Energy*, *42*(36), 23389–23394. https://doi.org/10.1016/j.ijhydene.2017.02.011

Valera-Medina, A., Marsh, R., Runyon, J., Pugh, D., Beasley, P., Hughes, T., & Bowen, P. (2017). Ammonia–methane combustion in tangential swirl burners for gas turbine power generation [Clean, Efficient and Affordable Energy for a Sustainable Future]. *Applied Energy*, *185*, 1362–1371. https://doi.org/10.1016/j.apenergy.2016.02.073

Wang, G., Mitsos, A., & Marquardt, W. (2017). Conceptual design of ammonia-based energy storage system: System design and time-invariant performance. *AIChE Journal*, *63*(5), 1620–1637. https://doi.org/10.1002/aic.15660

Zhu, J., Meng, X., Zhao, J., Jin, Y., Yang, N., Zhang, S., Sunarso, J., & Liu, S. (2017). Facile hydrogen/nitrogen separation through graphene oxide membranes supported on ysz ceramic hollow fibers. *Journal of*

Membrane Science, *535*, 143–150. https://doi.org/10.1016/j.memsci.2017.04.032

Abashar, M. (2018). Ultra-clean hydrogen production by ammonia decomposition. *Journal of King Saud University - Engineering Sciences*, *30*(1), 2–11. https://doi.org/10.1016/j.jksues.2016.01.002

Allman, A., & Daoutidis, P. (2018). Optimal scheduling for wind-powered ammonia generation: Effects of key design parameters. *Chemical Engineering Research and Design*, *131*, 5–15. https://doi.org/10.1016/j.cherd.2017.10.010

Daggash, H. A., Patzschke, C. F., Heuberger, C. F., Zhu, L., Hellgardt, K., Fennell, P. S., Bhave, A. N., Bardow, A., & Mac Dowell, N. (2018). Closing the carbon cycle to maximise climate change mitigation: Power-to-methanol vs. power-to-direct air capture. *Sustainable Energy Fuels*, *2*, 1153–1169. https://doi.org/10.1039/C8SE00061A

Gür, T. M. (2018). Review of electrical energy storage technologies, materials and systems: Challenges and prospects for large-scale grid storage. *Energy Environ. Sci.*, *11*, 2696–2767. https://doi.org/10.1039/C8EE01419A

Jo, Y. S., Cha, J., Lee, C. H., Jeong, H., Yoon, C. W., Nam, S. W., & Han, J. (2018). A viable membrane reactor option for sustainable hydrogen production from ammonia. *Journal of Power Sources*, *400*, 518–526. https://doi.org/10.1016/j.jpowsour.2018.08.010

Kim, S., Song, J., & Lim, H. (2018). Conceptual feasibility studies of a co x-free hydrogen production from ammonia decomposition in a membrane reactor for pem fuel cells. *Korean Journal of Chemical Engineering*, *35*(7), 1509–1516.

Kost, C., Shammugam, S., Jülch, V., Nguyen, H.-T., & Schlegl, T. (2018). Levelized cost of electricity renewable energy technologies. *Fraunhofer Institute for Solar Energy Systems ISE*.

Mohammadi, A., & Mehrpooya, M. (2018). A comprehensive review on coupling different types of electrolyzer to renewable energy sources. *Energy*, *158*, 632–655. https://doi.org/10.1016/j.energy.2018.06.073

Otomo, J., Koshi, M., Mitsumori, T., Iwasaki, H., & Yamada, K. (2018). Chemical kinetic modeling of ammonia oxidation with improved reaction mechanism for ammonia/air and ammonia/hydrogen/air combustion. *International Journal of Hydrogen Energy*, *43*(5), 3004–3014. https://doi.org/10.1016/j.ijhydene.2017.12.066

Paixão, V. P., Secchi, A. R., & Melo, P. A. (2018). Preliminary design of a municipal solid waste biorefinery for environmentally friendly nh3 production. *Industrial & Engineering Chemistry Research*, *57*(45), 15437–15449. https://doi.org/10.1021/acs.iecr.8b02927

Sánchez, A., & Martín, M. (2018a). Optimal renewable production of ammonia from water and air. *Journal of Cleaner Production*, *178*, 325–342. https://doi.org/10.1016/j.jclepro.2017.12.279

Sánchez, A., & Martín, M. (2018b). Scale up and scale down issues of renewable ammonia plants: Towards modular design. *Sustainable Production and Consumption*, *16*, 176–192. https://doi.org/10.1016/j.spc.2018.08.001

Valera-Medina, A., Xiao, H., Owen-Jones, M., David, W., & Bowen, P. (2018). Ammonia for power. *Progress in Energy and Combustion Science*, *69*, 63–102. https://doi.org/10.1016/j.pecs.2018.07.001

Child, M., Kemfert, C., Bogdanov, D., & Breyer, C. (2019). Flexible electricity generation, grid exchange and storage for the transition to a 100% renewable energy system in europe. *Renewable Energy*, *139*, 80–101. https://doi.org/10.1016/j.renene.2019.02.077

Guerras, L. S., & Martín, M. (2019). Optimal gas treatment and coal blending for reduced emissions in power plants: A case study in northwest spain. *Energy*, *169*, 739–749. https://doi.org/10.1016/j.energy.2018.12.089

Kobayashi, H., Hayakawa, A., Somarathne, K. K. A., & Okafor, E. C. (2019). Science and technology of ammonia combustion. *Proceedings of the Combustion Institute*, *37*(1), 109–133. https://doi.org/10.1016/j.proci.2018.09.029

Sadi, M., & Arabkoohsar, A. (2019). Exergoeconomic analysis of a combined solar-waste driven power plant. *Renewable Energy*, *141*, 883–893. https://doi.org/10.1016/j.renene.2019.04.070

Sánchez, A., Martín, M., & Vega, P. (2019). Biomass based sustainable ammonia production: Digestion vs gasification. *ACS Sustainable Chemistry & Engineering*, *7*(11), 9995–10007. https://doi.org/10.1021/acssuschemeng.9b01158

Valera-Medina, A., Gutesa, M., Xiao, H., Pugh, D., Giles, A., Goktepe, B., Marsh, R., & Bowen, P. (2019). Premixed ammonia/hydrogen swirl combustion under rich fuel conditions for gas turbines operation. *International Journal of Hydrogen Energy*, *44*(16), 8615–8626. https://doi.org/10.1016/j.ijhydene.2019.02.041

Zhang, Y., Wang, L., Wang, N., Duan, L., Zong, Y., You, S., Maréchal, F., Van herle, J., & Yang, Y. (2019). Balancing wind-power fluctuation via onsite storage under uncertainty: Power-to-hydrogen-to-power versus lithium battery. *Renewable and Sustainable Energy Reviews*, *116*, 109465. https://doi.org/10.1016/j.rser.2019.109465

Zhao, Y., Setzler, B. P., Wang, J., Nash, J., Wang, T., Xu, B., & Yan, Y. (2019). An efficient direct ammonia fuel cell for affordable carbon-neutral

transportation. *Joule*, *3*(10), 2472–2484. https://doi.org/10.1016/j.joule.2019.07.005

Al-Qahtani, A., González-Garay, A., Bernardi, A., Galán-Martín, A., Pozo, C., Dowell, N. M., Chachuat, B., & Guillén-Gosálbez, G. (2020). Electricity grid decarbonisation or green methanol fuel? a life-cycle modelling and analysis of todays transportation-power nexus. *Applied Energy*, *265*, 114718. https://doi.org/10.1016/j.apenergy.2020.114718

BloombergNEF. (2020). New energy outlook 2020. Retrieved December 1, 2020, from https://about.bnef.com/new-energy-outlook/

Božo, M. G., & Valera-Medina, A. (2020). Prediction of novel humified gas turbine cycle parameters for ammonia/hydrogen fuels. *Energies*, *13*(21), 5749. https://doi.org/doi.org/10.3390/en13215749

Dieterich, V., Buttler, A., Hanel, A., Spliethoff, H., & Fendt, S. (2020). Power-to-liquid via synthesis of methanol, dme or fischer tropsch fuels: A review. *Energy Environ. Sci.*, *13*, 3207–3252. https://doi.org/10.1039/D0EE01187H

Ehrenstein, M., Galán-Martín, Á., Tulus, V., & Guillén-Gosálbez, G. (2020). Optimising fuel supply chains within planetary boundaries: A case study of hydrogen for road transport in the uk. *Applied Energy*, *276*, 115486. https://doi.org/10.1016/j.apenergy.2020.115486

European Commission. (2020). A hydrogen strategy for a climate-neutral europe.

Ezzat, M., & Dincer, I. (2020). Energy and exergy analyses of a novel ammonia combined power plant operating with gas turbine and solid oxide fuel cell systems. *Energy*, *194*, 116750. https://doi.org/10.1016/j.energy.2019.116750

Fúnez Guerra, C., Reyes-Bozo, L., Vyhmeister, E., Jaén Caparrós, M., Salazar, J. L., & Clemente-Jul, C. (2020). Technical-economic analysis for a green ammonia production plant in chile and its subsequent transport to japan. *Renewable Energy*, *157*, 404–414. https://doi.org/10.1016/j.renene.2020.05.041

Keller, M., Koshi, M., Otomo, J., Iwasaki, H., Mitsumori, T., & Yamada, K. (2020). Thermodynamic evaluation of an ammonia-fueled combined-cycle gas turbine process operated under fuel-rich conditions. *Energy*, *194*, 116894. https://doi.org/10.1016/j.energy.2020.116894

Khateeb, A. A., Guiberti, T. F., Zhu, X., Younes, M., Jamal, A., & Roberts, W. L. (2020). Stability limits and no emissions of technically-premixed ammonia-hydrogen-nitrogen-air swirl flames. *International Journal of Hydrogen Energy*, *45*(41), 22008–22018. https://doi.org/10.1016/j.ijhydene.2020.05.236

MacFarlane, D. R., Cherepanov, P. V., Choi, J., Suryanto, B. H., Hodgetts, R. Y., Bakker, J. M., Ferrero Vallana, F. M., & Simonov, A. N. (2020). A roadmap to the ammonia economy. *Joule*, *4*(6), 1186–1205. https://doi.org/10.1016/j.joule.2020.04.004

Meroueh, L., & Chen, G. (2020). Thermal energy storage radiatively coupled to a supercritical rankine cycle for electric grid support. *Renewable Energy*, *145*, 604–621. https://doi.org/10.1016/j.renene.2019.06.036

Mounaïm-Rousselle, C., & Brequigny, P. (2020). Ammonia as fuel for low-carbon spark-ignition engines of tomorrow's passenger cars. *Frontiers in Mechanical Engineering*, *6*, 70. https://doi.org/10.3389/fmech.2020.00070

Sánchez, A., Hernández, B., & Martín, M. (2020). Multiscale analysis for the exploitation of bioresources. *Process systems engineering for biofuels development* (pp. 49–83). John Wiley; Sons, Ltd. https://doi.org/10.1002/9781119582694.ch3

Siddiqui, O., & Dincer, I. (2020). Experimental investigation of a sustainable integrated ammonia synthesis and fuel cell system. *Fuel*, *278*, 118300. https://doi.org/10.1016/j.fuel.2020.118300

Siddiqui, O., Ishaq, H., & Dincer, I. (2020). Experimental investigation of improvement capability of ammonia fuel cell performance with addition of hydrogen. *Energy Conversion and Management*, *205*, 112372. https://doi.org/10.1016/j.enconman.2019.112372

van Renssen, S. (2020). The hydrogen solution? *Nature Climate Change*, *10*(9), 799–801. https://doi.org/10.1038/s41558-020-0891-0

Wang, L., Zhang, Y., Pérez-Fortes, M., Aubin, P., Lin, T.-E., Yang, Y., Maréchal, F., & Van herle, J. (2020). Reversible solid-oxide cell stack based power-to-x-to-power systems: Comparison of thermodynamic performance. *Applied Energy*, *275*, 115330. https://doi.org/10.1016/j.apenergy.2020.115330

Zhang, C., Greenblatt, J. B., Wei, M., Eichman, J., Saxena, S., Muratori, M., & Guerra, O. J. (2020). Flexible grid-based electrolysis hydrogen production for fuel cell vehicles reduces costs and greenhouse gas emissions. *Applied Energy*, *278*, 115651. https://doi.org/10.1016/j.apenergy.2020.115651

Cesaro, Z., Ives, M., Nayak-Luke, R., Mason, M., & Bañares-Alcántara, R. (2021). Ammonia to power: Forecasting the levelized cost of electricity from green ammonia in large-scale power plants. *Applied Energy*, *282*, 116009. https://doi.org/10.1016/j.apenergy.2020.116009

Frate, G. F., Ferrari, L., & Desideri, U. (2021). Energy storage for grid-scale applications: Technology review and economic feasibility analysis.

Renewable Energy, *163*, 1754–1772. https://doi.org/10.1016/j.renene.2020.10.070

Heras, J., & Martín, M. (2021). Multiscale analysis for power-to-gas-to-power facilities based on energy storage. *Computers & Chemical Engineering*, *144*, 107147. https://doi.org/10.1016/j.compchemeng.2020.107147

Jeerh, G., Zhang, M., & Tao, S. (2021). Recent progress in ammonia fuel cells and their potential applications. *J. Mater. Chem. A*, *9*, 727–752. https://doi.org/10.1039/D0TA08810B

Palys, M. J., Wang, H., Zhang, Q., & Daoutidis, P. (2021). Renewable ammonia for sustainable energy and agriculture: Vision and systems engineering opportunities. *Current Opinion in Chemical Engineering*, *31*, 100667. https://doi.org/10.1016/j.coche.2020.100667

Part III

BUILDING A NEW CHEMICAL INDUSTRY

7

SUSTAINABLE DMC PRODUCTION FROM CO_2 AND RENEWABLE AMMONIA AND METHANOL

abstract

One of the main goals of the green chemistry is to develop sustainable and less hazardous chemical processes and products. Dimethyl carbonate (DMC) is attracting attention due to the wide variety of applications and the possibility of producing it from carbon dioxide. In this work, the DMC production process via urea has been optimized. Two main sections can be distinguished: the synthesis of urea and the production of DMC. An equation based approach is used to model the system. The DMC production from renewable ammonia/methanol/ CO_2 presents a promising production cost, around 520 €/t. The production of urea alone has also been evaluated in this work. A sensitivity analysis is carried out showing the influence of the methanol price in the DMC cost and the ammonia price in the urea cost. A simplified sustainability index is used to evaluate the environmental performance of urea/DMC production.

Keywords: CO_2 utilization, Dimethyl carbonate, Process design, Urea

resumen

Uno de los principales objetivos de la química verde es desarrollar procesos y productos químicos sostenibles y menos peligrosos. El carbonato de dimetilo (DMC) está atrayendo la atención debido a la gran variedad de aplicaciones y a la posibilidad de producirlo a partir de dióxido de carbono. En este trabajo se ha optimizado el proceso de producción de DMC a partir de urea. Se pueden distinguir dos secciones principales: la síntesis de urea y la producción de DMC. Se utiliza un enfoque basado en ecuaciones para modelar el sistema. La producción de DMC a partir de amoníaco renovable/metanol/CO_2 presenta un coste de producción prometedor, alrededor de 520 €/t. En este trabajo también se ha evaluado la producción de urea por separado. Se realiza un análisis de sensibilidad que muestra la influencia del precio del metanol en el coste del DMC y del precio del amoníaco en el coste de la urea. Se utiliza un índice de sostenibilidad simplificado para evaluar el rendimiento medioambiental de la producción de urea/DMC.

Palabras clave: Utilización de CO_2, Carbonato de dimetilo, Diseño de procesos, Urea

7.1 introduction

One of the main goals of Green Chemistry is to design chemical products and processes with the aim of reducing the use and/or avoiding the generation of hazardous substances to human health and also to the environment (Anastas & Williamson, 1996). The essentials of Green Chemistry are summarized in the widely known "Twelve Principles of Green Chemistry"(Anastas & Eghbali, 2010). Some of these rules are the synthesis of less hazardous chemicals, the use of renewable raw materials or the degradation of the chemicals when their use is over. In this context, dimethyl carbonate (DMC) is attracting attention as one of the most interesting green chemical products nowadays. The DMC is a safe reactant with low toxicity and bioaccumulation, it shows a fast biodegradability and an excellent solubility in water (Shi et al., 2017). The current consumption of DMC is about 90,000 t/y (Pyo et al., 2017). Several applications for the DMC have been proposed. Organic carbonates have a good performance as solvents due to the low viscosity and toxicity and a good solvency power, representing a green alternative to halogenate solvents, ketones or acetate esters in several applications (Santos et al., 2014; Pyo et al., 2017). DMC is also a good substitute for methyl-tert-butyl ether (MTBE) as oxygenated fuel additive (Pacheco & Marshall, 1997) with a high octane number (Tan et al., 2018). Another growing application for DMC is as electrolyte in ion lithium batteries due to the rapid expansion of this technology (Tan et al., 2018). Finally, DMC is used as a reagent in methylation, carbonylation and methoxycarbonilation reactions (Pyo et al., 2017). One of the most important reactions in which the DMC is involved is the transesterification of phenyl acetate to generate diphenyl carbonate that is used as raw material in the polycarbonate industry (Santos et al., 2014; Contreras-Zarazúa et al., 2017). A review of the combination of DMC with different bio-substrates, as glycerol, to produce high added value products is presented by Selva et al. (2019).

Different production processes have been studied to produce DMC over time. According to the classification provided by Kongpanna et al. (2015), two main categories are identified: conventional processes and CO_2 based processes. Within the first group, one of the early process to produce DMC consists of its synthesis using phosgene and methanol. The main drawback of the process is the use of phosgene, a very toxic reagent. This route has been discarded in the last years (Tan et al., 2018). A novel route was developed to avoid the use of phosgene in the synthesis of DMC: the oxidative carbonylation of methanol. In this process, the feedstocks are methanol, carbon monoxide and oxygen and the reaction is catalysed by CuCl or KCl. This process is the most widely extended nowadays to

produce DMC (Santos et al., 2014; Pyo et al., 2017). Nevertheless, the most promising processes are those that use carbon dioxide as raw material. This alternative is attracting attention because of the possibility of providing a new usage to the CO_2 captured (Aresta et al., 2013). Lately, several bulk chemicals have been produced from renewable resources and CO_2 such as methane (Davis & Martín, 2014), methanol (Martín, 2016a) or dimethyl ether (Martín, 2016b). Different CO2 to DMC processes have been proposed: direct synthesis from CO_2 and methanol, synthesis from urea, synthesis from propylene carbonate (PC) and synthesis from ethylene carbonate (EC). The direct synthesis from CO_2 and methanol is limited by the reaction equilibrium and the activation of the CO_2 is difficult, therefore, further investigations are required (Tan et al., 2018). For instance, different materials to catalyse this reaction are being studied such as: Fe-Zr oxides (Li et al., 2017) or modified triflouroacetic acid (Xuan et al., 2018). The electrochemical route is also investigated (Lu et al., 2013; Garcia-Herrero et al., 2016). DMC from PC is based on the transesterification of propylene carbonate and methanol (Shi et al., 2017). PC, however, is obtained from propylene oxide, that for the time being is produced from crude oil. The production of DMC from ethylene carbonate is similar to the previous one. The last alternative is to synthesize DMC from urea. An alcoholysis reaction between urea and methanol takes place (Kongpanna et al., 2015). A previous step is necessary in this path: the synthesis of urea. The urea is produced from carbon dioxide and ammonia. One of the main advantages of this process is that the raw materials can also be obtained in a sustainable way. The ammonia, for instance, can be synthesized from water and air using renewable energy (Sánchez & Martín, 2018a, 2018b; Allman et al., 2019) as well as biomass (Sánchez et al., 2019). Methanol can also be produced from water and carbon dioxide (Martín, 2016a), from biomass gasification (Martín & Grossmann, 2017) or from biomass/waste digestion (Hernández & Martín, 2016). The CO_2 is obtained from carbon dioxide capture (Spigarelli & Kawatra, 2013) or biogas upgrading (Martín-Hernández et al., 2020). Therefore, the synthesis of DMC from urea and methanol is a promising alternative where further investigation at process level is necessary.

In this work, a mathematical optimization approach for an integrated facility evaluating the synthesis of DMC from ammonia, carbon dioxide and methanol is carried out. There are two main sections in the process flowsheet: the synthesis of urea and the synthesis of DMC. In the urea synthesis stage, carbon dioxide and ammonia react to synthesize urea. Then, urea and methanol react in two steps to produce DMC. The synthesis of urea alone from sustainable ammonia is also studied. The processes are evaluated in economic and environmental terms. The rest of the paper is

organized as follows: Section 7.2 describes the process devoted to producing DMC from ammonia, carbon dioxide and methanol. Section 7.3 shows the approach to model the different units involved in the process flowsheet. Section 7.4 presents the objective function, the solution procedure and the cost estimation procedure. Section 7.5 presents the results. First, a summary of the main variables involved in the optimization procedure. Second, the economic evaluation of the processes. In the third place, the sensitivity analysis of the feedstock prices (methanol and ammonia). Finally, a simplified environmental analysis of the processes. Section 7.6 draws some conclusions.

7.2 process description

In Fig.7.1, a schematic description of the entire process is shown. For the urea synthesis, a wide range of processes has been proposed. Some of them are the Stamicarbon process with its different progresses, the Snamprogetti process or the ACES process (Meessen & Petersen, 2010). In this work, a CO_2 stripping process is selected similar to the Stamicarbon process.

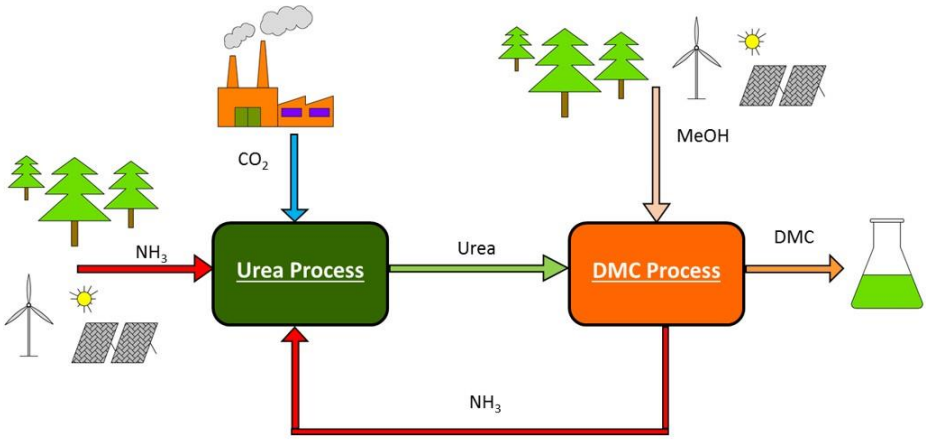

Figure 7.1: Simplified flowsheet for the entire process

Carbon dioxide is fed to the stripper at 450 K and the pressure selected in the urea reactor, see Fig.7.2. A compression step is used, followed by a heat exchanger to adjust the carbon dioxide temperature and pressure. In the stripper, the ammonium carbamate from the reactor is converted to ammonia and carbon dioxide. Heat is supplied to carry out this endothermic reaction. Besides, carbon dioxide and ammonia are transferred, mainly,

to the gas phase to be recycled to the urea reactor. The gas phase from the stripper is mixed with the recycled gases from the medium pressure flash separation. These gases are fed to the condenser where the formation of ammonium carbamate takes place removing the heat generated and producing steam. The fraction of ammonia and carbon dioxide leaving the condenser reacts in the urea reactor providing the heat necessary in this unit. The urea reactor transforms, essentially, ammonium carbamate to urea. Complete transformation is not achieved. The stream leaving the urea reactor is sent to the stripper.

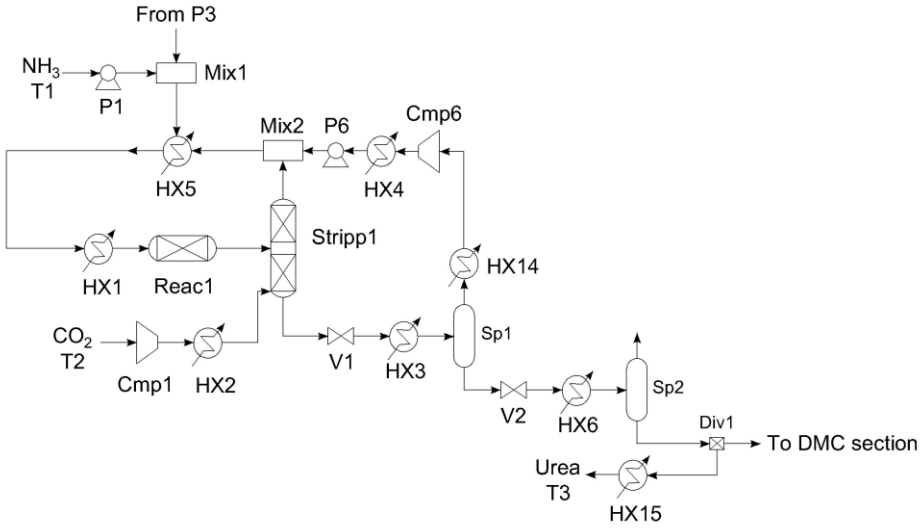

Figure 7.2: Process flow diagram for urea synthesis section

The liquid from the stripping is expanded to a medium pressure (3–20 bar). Two phases are generated. The gas phase is recompressed and recycled to the urea synthesis loop. The liquid phase, where urea and water are the most significant components, is expanded again down to atmospheric pressure. The gases are separated and sent out. The urea, with a minimum concentration of 90%w, is stored or sent to the DMC synthesis section.

The urea is mixed with the stream from the mixer 3, see Fig.7.3, mostly methanol, to form the feed to the first reactor for the synthesis of DMC. DMC is synthesized in two steps. The first one transforms urea and methanol to methylcarbamate (MC). The second one converts MC to dimethyl carbonate (DMC). After adjusting the pressure and the temperature, the stream is introduced in the first reactor. The reaction takes place without catalyst and a conversion of 100% is reached (de Groot et al., 2014). Ammonia is separated in a distillation column before introduc-

ing the stream to the second reactor due to the negative effects of this chemical in the second reaction (de Groot et al., 2014). The ammonia is recycled to the urea synthesis loop. The bottom of the distillation column is mixed with methanol from mixer 3 and a recycled stream to adjust the methanol:MC ratio for the second reactor. Before the reactor, the stream is compressed and heated up. The DMC is synthesized from methyl-carbamate and methanol, generating also ammonia. A parallel reaction takes place producing N-methyl methyl carbamate (NMMC). After this reactor, the different products are separated in a sequence of distillation columns. First, the carbon dioxide and ammonia generated are separated and recycled to the urea reaction section. The bottom product is sent to another distillation column where the DMC is separated from other heavy components such as NMMC or MC. The heavy components are recycled to the second reactor in the DMC section. A purge is allowed since the NMMC is an impurity and can build-up in the process. The DMC is separated from methanol, mainly, using a system of two columns due to the azeotrope present in the methanol-DMC system (Vázquez et al., 2018). The bottom of the last column is the final DMC that it is stored at ambient pressure and temperature. The methanol streams from both condensers are recycled and mixed with the feed of methanol.

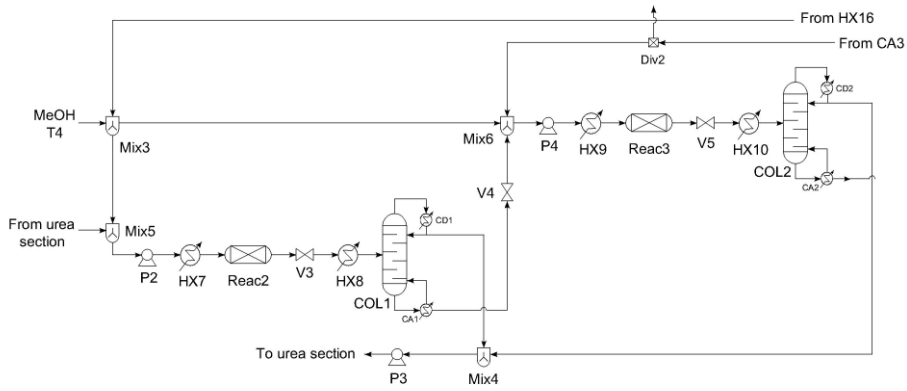

Figure 7.3: Process flow diagram for the DMC synthesis section (first zone)

7.3 modelling issues

Here, only a brief description of the modelling issues involved in the process is presented. Further details are included in the Supplementary Material.

7.3.1 *Urea section*

The following assumptions have been considered in the modelling of the urea synthesis loop. Although ammonia and carbon dioxide are supercritical under the urea synthesis conditions, the vapour-liquid equilibrium (VLE) is used to model the system with a supercritical phase and a liquid phase, containing a suitable solvent (Piotrowski et al., 1998; Zhang et al., 2005; Meessen, 2014). The VLE has been modelled assuming the ideal behaviour where the fugacity and the activity coefficient are equal to 1 (see Supplementary Material). A flowsheet of the urea section is shown in Fig.7.2.

7.3.1.1 *Urea reactor*

Urea is produced by the reaction of carbon dioxide and ammonia. Two reactions are involved in the synthesis:

$$2NH_3 + CO_2 \rightarrow NH_2COONH_4 \tag{7.1}$$

$$NH_2COONH_4 \rightleftharpoons CO(NH_2)_2 + H_2O \tag{7.2}$$

No biuret formation has been considered in the urea reactor. The first reaction is the production of ammonium carbamate from ammonia and carbon dioxide. This reaction is fast and exothermic (159 kJ/mol of carbamate). In the second one, ammonium carbamate is dehydrated to produce urea and water. This reaction is slow and endothermic (31.4 kJ/ mol of urea) (Mavrovic et al., 2010). The first reaction takes place between the carbamate condenser and the urea reactor. In the condenser, a large fraction of ammonia and carbon dioxide reacts and the heat produced is removed from the system generating steam. Only a small fraction of both reagents does not react to generate the heat necessary in the second reaction that takes place in the urea reactor itself (Meessen & Petersen, 2010). For modelling purposes, the first reaction has a conversion of 100% with the only limitation of heat removal (Meessen, 2014). For the second one, the conversion is calculated using the correlation (Eq.7.3) obtained by Inoue et al. (1972) as a function of the ammonia to carbon dioxide ratio, the water to carbon dioxide ratio and the temperature. The urea reactor is modelled as adiabatic and isobaric.

$$X = 0.2616a - 0.01945a^2 + 0.0382ab - 0.1160b - 0.02732a\left(\frac{t}{100}\right) - 0.1030b\left(\frac{t}{100}\right) + 1.640\left(\frac{t}{100}\right) - 0.1394\left(\frac{t}{100}\right)^2 - 1.869 \tag{7.3}$$

Where a is the ammonia to carbon dioxide ratio defined as in Eq.7.4 and limited to the range of 3–5 (Piotrowski et al., 1998):

$$a = \frac{fc_{NH_3} + 2fc_{Carbamate} + 2fc_{Urea}}{fc_{Carbamate} + fc_{Urea} + fc_{CO_2}} \tag{7.4}$$

The parameter b is the molar ratio between water and carbon dioxide defined as in Eq.7.5 and within the range from 0 to 1:

$$b = \frac{fc_{H_2O}}{fc_{Carbamate} + fc_{Urea} + fc_{CO_2}} \tag{7.5}$$

And, finally, t is the temperature (°C) and must be in the interval between 170–220 °C.

In this case of study, the following assumption is considered for modelling purposes: only one stream leaves the urea reactor. This assumption is supported by experimental results which show that the gas stream is 9 times smaller than the liquid stream (Zhang et al., 2005). The entire stream from the reactor is sent to the stripper where the ammonium carbamate is decomposed and the components are separated. Therefore, no gas treatment has been considered in the process.

7.3.1.2 *Stripper*

In the stripper, unreacted ammonium carbamate is decomposed (see Eq.7.1) to form ammonia and carbon dioxide providing heat. Besides, mainly, ammonia and carbon dioxide are transferred to the gas phase to be recycled to the urea synthesis reactor. To model this unit, a surrogate model has been developed. A rigorous simulation has been carried out in CHEMCAD© 7.0. A surface of response model has been developed using these data. The following variables have been considered: the stripper pressure (P), the inlet temperature from the reactor (T), the ratio between the heat supplied and the inlet molar flow of urea (Q/U), the ratio between the inlet molar flow of urea and the inlet molar flow of ammonia (U/NH_3), the ratio between the inlet molar flow of urea and the inlet molar flow

of water (U/H_2O), the ratio between the inlet molar flow of urea and the

inlet molar flow of carbon dioxide (U/CO_2) and the ratio between the inlet molar flow of urea and the inlet molar flow of carbon dioxide fed as stripping agent ($U/CO_{2,in}$). The output variables are the liquid yields (%) for each component (Urea, Ammonia, Carbon Dioxide and Water) and the temperature of the gas and liquid streams. The equations obtained through this methodology (fitted to the equation form presented in Eq.7.6) used to describe the stripper performance are shown in the supplementary material for the sake of brevity.

$$f(x) = \beta_0 + \sum_{i=1}^{n} \beta_i x_i + \sum_{j \geq i}^{n} \sum_{i=1}^{n} \beta_{ij} x_i x_j + \sum_{i=1}^{n} \omega_i x^2 \tag{7.6}$$

$$\forall i,j \in P, T, U, NH_3, H_2O, CO_2, CO_{2,in}$$

The statistical analysis (p-value) determines the coefficients selected in each model. To minimize the corrosion problems in the urea synthesis loop, a small amount of oxygen (in the form of air mainly) is typically introduced with the inlet carbon dioxide in the stripper (Meessen & Petersen, 2010). However, to model the performance of the system, this oxygen/air flow is neglected.

7.3.1.3 *Carbamate condenser*

In the carbamate condenser, ammonia and carbon dioxide are converted to ammonium carbamate following the reaction given by Eq.7.1. The conversion of the reaction is controlled by the heat withdrawn in the condenser generating steam (Hamidipour et al., 2005). The remaining carbon dioxide and ammonia react in the urea reactor delivering the heat necessary for the second urea formation reaction (transformation of ammonium carbamate to urea, Eq.7.2).

7.3.1.4 *Final urea purification*

The liquid stream leaving the stripper is expanded to a medium pressure (3–20 bar) and its temperature is adjusted (273–393 K) to remove a fraction of volatile gases such as ammonia or carbon dioxide. The valves in this work are modelled using the Joule-Thomson coefficient. The liquid fraction from the gas-liquid separator is expanded again down to ambient pressure. A final removal of the gases generated is carried out. The VLE equilibrium is used to model these stages. A minimum urea mass fraction of 0.9 is fixed on the stream leaving the urea section. Later, a prilling or a granulation unit can be set up to form a solid urea to be sold as such, but it is out of the scope of this work.

7.3.2 *DMC section*

The flowsheet for the synthesis of DMC is presented in Figs.7.3 and 7.4. In the first one, Fig.7.3, the reaction section is shown. The second one, Fig.7.4, shows the flow diagram for the sequence of distillation columns to purify the DMC.

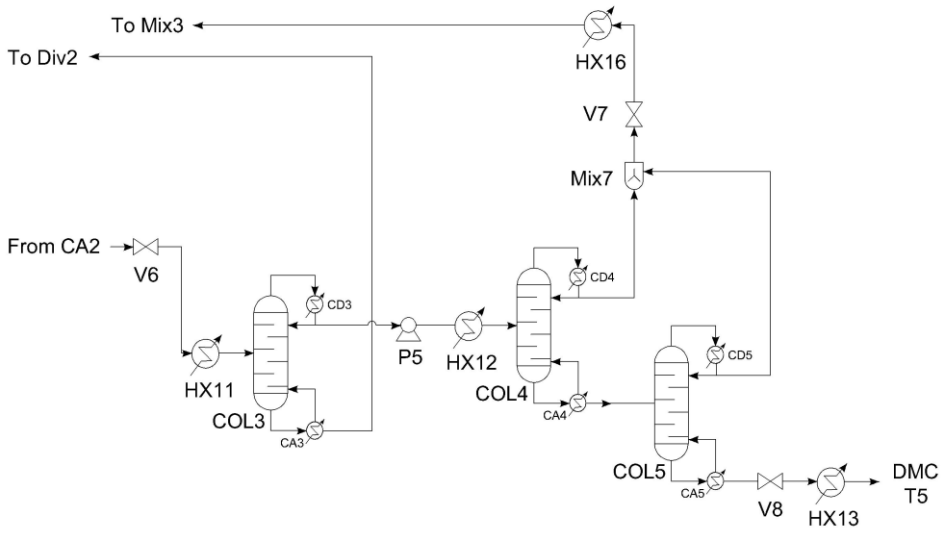

Figure 7.4: Process flow diagram for the DMC synthesis section (second zone)

7.3.2.1 *First DMC reactor*

The urea produced in the first section of the process is mixed with methanol, mainly, from mixer 3. A ratio between methanol and urea equal to 2 is fixed in the inlet stream to the reactor. The flow is pumped up to 20 bar and the temperature is adjusted to 423 K (de Groot et al., 2014). The following reaction takes place in this first reactor:

$$CO(NH_2)_2 + CH_3OH \rightarrow NH_2COOCH_3 + NH_3 \tag{7.7}$$

Urea reacts with methanol to form methyl carbamate (MC) and ammonia. The reactor is isothermal and complete conversion of urea is reached (de Groot et al., 2014). After the reactor, the stream is expanded down to 10 bar. The temperature is adjusted to feed the stream as a saturated liquid into the distillation column, Column 1. The objective in this distillation column is to separate the ammonia due to its negative effect in the next reaction (Vázquez et al., 2018). This column is modelled using the Fenske-Underwood-Gilliland (FUG) method (Geankopolis, 2005). Antoine

equations are used to compute the vapour pressure for the involved components. Ammonia is selected as light key component and methanol as heavy key component. The bottom stream from the distillation column is expanded before being mixed in mixer 6 with a stream from mixer 5 (essentially methanol) and a recycled stream from the reboiler of column 3.

7.3.2.2 *Second DMC reactor*

The second reaction to form the DMC takes places in a fixed bed reactor using ZnO over alumina as catalyst (Wang et al., 2012). A parallel reaction also occurs in the reactor producing N-methyl methyl carbamate (NMMC) from DMC and MC. The reactions are as follows:

$$NH_2COOCH_3 + CH_3OH \rightleftharpoons (CH_3O)_2CO + NH_3 \tag{7.8}$$

$$NH_2COOCH_3 + (CH_3O)_2CO \rightleftharpoons CH_3NHCOOCH_3 + CH_3OH + CO_2 \tag{7.9}$$

An empirical correlation was developed based on the experimental data provided by Wang et al. (2012) to describe the performance of this reactor. The variables are the pressure and the temperature inside the reactor and the results are the yields to DMC and to NMMC. The range of pressure is between 10–30 bar and for temperature 433–483 K. Correlations with the following form have been used to fit the data:

$$Y_i = a^i_0 + a^i_1 P + a^i_2 T + a^i_3 P^2 + a^i_4 T^2 \quad \forall i,j \in \{DMC, NMMC\} \tag{7.10}$$

Where Y_i is the yield to the specie i (DMC or NMMC) in mol/inlet mol of MC, P is the reactor pressure in MPa and T is the temperature in K. The values of the coefficients for this equation are collected in Table 7.1.

Table 7.1: Correlations to model the DMC synthesis from MC

	a_0	a_1	a_2	a_3	a_4
DMC	-1635.91493	6.14542174	18.0202336	-7.16031083	-0.04741889
NMMC	165.693701	-6.00985703	-1.95166752	0.94781939	0.00601273

The reactor is considered isothermal and isobaric. The mass ratio between MC and methanol inlet the reactor is fixed to 0.136 according to the experimental conditions (Wang et al., 2012).

7.3.2.3 *DMC purification*

After the reactor, the stream is expanded down to 12 bar. In Column 2, the ammonia and carbon dioxide, mainly, are separated and recycled to the

urea synthesis area. The FUG method is applied with ammonia as light key component and methanol as heavy key component. The bottom contains ammonia, water, methanol, MC, DMC, and NMMC. The next valve reduces the bottom pressure down to 1 bar. In Column 3 (modelled using FUG), DMC is the light key component and water the heavy key component. The heavy components, namely MC, NMMC and water principally, are recycled to mixer 6 to be fed again into the second reactor for the synthesis of DMC. A fraction is purged to avoid the building-up of the NMMC produced in the reactor or the water from the raw materials. An increase in the pressure of the light components from the column 3 is carried out up to 16 bar (Vázquez et al., 2018). A couple of columns are used to separate methanol from DMC. The first column (Column 4) is described by the FUG equations, however, the second column (Column 5) is modelled using a surrogate model due to the lack of accuracy between rigorous simulation and the FUG equations. The presence of the azeotrope determines the thermodynamics of the system. The azeotrope concentration is equal to 97%w of methanol at the operating pressure (Vázquez et al., 2018). A surrogate model (see Eq.7.11) was developed using rigorous simulation to compute the reflux ratio (R_{real}) as a function of the bottom DMC yield (R_{DMC}).

$$R_{real} = 2.49929 R_{\mathrm{DMC}} - 1.64366 \tag{7.11}$$

The yield to DMC at the bottoms is a variable while the distillate methanol yield is fixed at 99.99%. The final DMC is obtained from the bottom of the column 5. The DMC is stored at ambient pressure and temperature. The distillates from the columns 4 and 5 are recycled to be mixed with the inlet methanol.

7.4 solution procedure

The problem of producing DMC from CO_2 via the urea route is formulated as a nonlinear programming (NLP) problem according to the model equations and assumptions presented in the section above. The decision variables correspond to the operating conditions of each unit, namely, pressure, temperature and flow ratios. A simplified profit equation is chosen as objective function as follows:

$$\begin{aligned} obj = {} & F_{\mathrm{DMC}} C_{\mathrm{DMC}} + F_{\mathrm{Urea}} C_{\mathrm{Urea}} - F_{\mathrm{NH_3}} C_{\mathrm{NH_3}} - F_{\mathrm{CO_2}} C_{\mathrm{CO_2}} \\ & - F_{\mathrm{MeOH}} C_{\mathrm{MeOH}} - F_{\mathrm{steam}} C_{\mathrm{steam}} - F_{\mathrm{cooling}} C_{\mathrm{cooling}} - W_{\mathrm{total}} C_{\mathrm{elect}} \end{aligned} \tag{7.12}$$

The variables and parameters involved in the objective function are collected in Table 7.2.

Table 7.2: Variables and parameters for the objective function

Symbol	Variable	Value	Source
F_{DMC}	DMC flow production		
C_{DMC}	DMC cost	0.820 €/kg	(Vázquez et al., 2018)
F_{Urea}	Urea flow production		
C_{Urea}	Urea cost	0.322 €/kg	(Edrisi et al., 2016)
F_{NH_3}	Inlet flow of ammonia		
C_{NH_3}	Ammonia price	0.5 €/kg	(Pfromm, 2017)
F_{CO_2}	Inlet flow of carbon dioxide		
C_{CO_2}	CO_2 price	0.0509 €/kg	(Edrisi et al., 2016)
F_{MeOH}	Methanol flow demand		
C_{MeOH}	Methanol price	0.330 €/kg	(Vázquez et al., 2018)
F_{steam}	Steam flow demand		
C_{steam}	Steam price	2.20 €/GJ	(Yang & You, 2018)
$F_{cooling}$	Cooling water flow needs		
$C_{cooling}$	Cooling water price	4.58 €/kt	(Yang & You, 2018)
W_{total}	Total Power		
C_{elect}	Electricity price	7.87cent€/kWh	(Statista, 2018)

The problem proposed above consists of about 3000 variables and 2500 equations. The equation based model is implemented and solved in GAMS © using an NLP multistart optimization with CONOPT 3.0 as the preferred solver.

Using the results obtained from the optimization, an estimation of the capital and operating costs has been carried out. To estimate the capital cost, the factorial method proposed by Sinnott (2014) is employed. The major equipment capital costs are estimated using the correlations proposed by Almena and Martín (2016). The cost of the urea reactor is estimated based on the industrial size of urea reactors (Dente et al., 1992). For the methylcarbamate (MC) synthesis reactor from urea and methanol, the capital cost is estimated with the data provided by Sun et al. (2004). Finally, the reactor where the DMC is synthesized is a fixed bed reactor where the catalyst, ZnO over alumina, has a cost of 355 $\$/ft^3$ (Nexant, 2006) with a liquid hourly space velocity (LHSV) equal to 1.2 h^{-1} (Wang et al., 2012).

The operating costs include two main items: variable and fixed costs. The variable costs have been estimated with the prices used in the objective function (see Table 7.2) and the amount of raw materials and utilities

from the optimization results. Within the fixed costs, labor and capital are included among others.

7.5 results

7.5.1 *Key operating variables*

7.5.1.1 *DMC production*

In this section, a summary of the main operating variables from the optimization results is presented. The DMC production is more profitable according to the objective function than the urea synthesis alone, therefore, the total urea produced in the first section is sent to the DMC production section. However, for comparative purposes, the synthesis of urea is also evaluated. First, the results for the DMC production are presented. Then, the results when only urea is produced are also shown. In the DMC synthesis, the urea reactor works with a conversion of urea equal to 58.3% with the following parameters that determine this conversion (see equation Eq.7.3): a (NH_3/CO_2 ratio) equal to 3.111, b (H_2O/CO_2 ratio) equal to 0.439 and the outlet temperature equal to 493 K. The stripper conditions are summarized in Table 7.3.

Table 7.3: Main operating conditions in the urea stripper (DMC production)

	Stripper			
	Urea Reactor Out	CO_2 in	Stripp gas out	Stripp liquid out
T(K)	493.0	450.0	494.7	500.1
P(bar)	200.0	200.0	200.0	200.0
F (kg/s)	9.544	2.000	7.508	4.036
mass fraction				
CO_2	0.000	1.000	0.426	0.125
NH_3	0.184	0.000	0.403	0.011
Urea	0.340	0.000	0.079	0.657
H_2O	0.316	0.000	0.092	0.207
Carbamate	0.160	0.000	0.000	0.000

The flowrate fed to the stripper is fixed to 2 kg/s of CO_2 both in the synthesis of DMC and in the synthesis of urea. A trade-off exists between the operating conditions in the urea reactor and the stripper and among the yields of the different species. The yields in the stripper (to the liquid

stream) achieved for each component are as follows: 1.411% (NH_3), 13.589% (CO_2), 81.718% (Urea) and 54.726% (H_2O). The operating variables in the stripper model (see equations D.19-D.25 in the Supplementary Information) are shown in Table 7.5. The medium pressure stage to purify the urea is carried out at 11.9 bar and 393.7 K and the final purification (low pressure) takes place at 1 bar and 371.9 K. The non-reacted gases are recycled to the urea reactor via the condenser. The ammonia is also recycled from the DMC section. Due to this fact, only 1% of the inlet ammonia to the urea reactor is fresh in the DMC synthesis.

The first reactor in the DMC production section (Reac2) transforms urea and methanol to MC. The second one synthesizes DMC from MC. The main conditions for these reactors are shown in Table 7.4. In the second reactor, as it is presented in the modelling issues section, a large excess of methanol is needed that, afterwards, must be separated and recycled. The operating conditions in the second reactor are adjusted during the process optimization to minimize the amount of NMMC produced according to the equation Eq.7.10. Due to the small amount of impurities generated in the reaction, the flow of the purge that is necessary to separated is almost zero avoiding a loss in the non-reacted components.

7.5.1.2 *Renewable urea production*

Another case of study is when only urea is produced instead of DMC. In this case, the model is forced to not synthesize DMC from urea. Since the optimal facility leads to the production of DMC, the objective function for the production of urea is worse. In this case, the parameters that determine the urea reactor performance take the following values: a is equal to 3.253, b is equal to 0.569 and the final temperature equal to 493 K. In the stripper, the main variables are collected in Table 7.6. The pressure changes in comparison with the previous case (160 bar vs 200 bar). The operational model variables (see Eq.7.6) change in the stripper with respect to the production of DMC as follows, see Table 7.5.

The final urea purity changes between the two processes. In the DMC process a high purity urea is obtained because water is an impurity in the DMC process. However, when only urea synthesis is evaluated the purity is fixed to 0.9 (mass fraction) because no further processing is required and, therefore, the minimum purity value is desired to hold the specifications and reduced the objective function value. This fact determines the different operating conditions in the urea section for the two alternatives.

A graphical summary of both processes with the main yields is presented in Fig.7.5. The ammonia consumption is higher in the urea process than the DMC process. A large amount of ammonia is recycled to the urea section

Table 7.4: Main operation conditions in the reactors of the DMC synthesis section

	Reac2		Reac3	
	IN	OUT	IN	OUT
T(K)	423.0	423.0	447.3	447.3
P(bar)	20.0	20.0	19.8	19.8
F (kg/s)	5.653	5.653	60.0	60.0
mass fraction				
CO_2	0.000	0.000	0.000	0.000
NH_3	0.000	0.133	0.000	0.012
Urea	0.469	0.000	0.000	0.000
H_2O	0.000	0.000	0.001	0.001
MeOH	0.501	0.250	0.834	0.811
MC	0.000	0.587	0.113	0.058
DMC	0.030	0.030	0.051	0.117
NMMC	0.000	0.000	0.000	0.000

Table 7.5: Variables in the stripper model for the DMC/Urea process

Variable	DMC process	Urea process	Units
Temperature	493.0	493.0	K
Pressure	200.0	160.0	bar
Heat-Urea ratio (Q/U)	20.0	24.74	kJ/kmol U
Urea-NH_3 ratio (U/NH_3)	0.30	0.28	kmol U/kmol NH_3
Urea-Water ratio (U/H_2O)	0.64	0.55	kmol U/kmol H_2O
Urea-CO_2 ratio (U/CO_2)	1.4	1.4	kmol U/ kmol CO_2
Urea-inlet CO_2 ($U/CO_{2,in}$)	1.19	1.16	kmol U/ kmol CO_2

in the DMC production and only a small make up of ammonia is needed. However, the consumption of carbon dioxide is larger in the production of urea (about 0.7 kg CO_2/kg urea) compared to the process where the DMC is synthesized (0.5 kg CO_2/kg DMC). The last raw material, methanol,

is only employed when DMC is produced. The power consumption is similar in both processes. The consumption of power takes place in the compressors set up in the urea synthesis section. Therefore, the difference between the power consumption is only caused by the change in the operating conditions in the urea section in the two studied alternatives. The cooling water usage is almost zero in the urea production while for the production of DMC is it higher with a value of about 1.85 t of cooling water per kg of DMC due mainly to the condenser in the distillation columns. In the synthesis of urea the amount of steam generated and consumed is approximately the same (with a positive net consumption). However, the amount of steam needed in the DMC production is around 2-3 times the amount of steam generated in the entire process. The consumption of steam in the reboilers of the columns to separate the different components formed in the synthesis is the main cause of this increase.

7.5.2 *Economic evaluation*

The capital costs of the facility have been estimated as it was described above, see solution procedure. The total investment for the DMC production is about 91 MM€, and for the urea production only about 16 MM€ for a production capacity of 342 t/d and 253 t/d of DMC and urea respectively. A breakdown of the capital cost is shown in Fig.7.6. For the production of DMC (Fig.7.6 a), the heat exchangers (HX) represent the largest share of the investment. In this section, the reboilers and condensers from the distillation columns are included. These columns represent the second largest contribution to the investment cost. For the production of urea alone (Fig.7.6 b), the HX 's also represent the largest contribution. The stripper is another equipment with a high investment due to the complexity of the unit involving a gas-liquid contact and heat exchange.

The operating costs of the processes have also been estimated. The DMC production cost is about 520 €/t, a very promising result according to the current prices found in the literature in the range of 820–1100 $/t (de Groot et al., 2014; Vázquez et al., 2018). In Fig.7.7 a, the distribution of the production cost into the different items for the DMC synthesis is shown. The raw materials represent the largest contribution to the production cost, above all, the methanol cost due to the small amount of ammonia needed in the DMC production. The utilities include the cost of the steam, cooling water and power. The catalyst is introduced in the operating costs due to the annual replacement of it in the second DMC reactor (Nexant, 2006). In the urea synthesis, the production cost is about 340 €/t, slightly higher than the current production processes but in the same levels than other

Table 7.6: Operating Variables in the Stripper (Urea production)

	Stripper			
	Urea Reactor Out	CO_2 in	Stripp gas out	Stripp liquid out
T(K)	493.0	450.0	496.4	503.2
P(bar)	160.2	160.2	160.2	160.2
F (kg/s)	9.758	2.000	7.915	3.845
mass fraction				
CO_2	0.000	1.000	0.415	0.099
NH_3	0.198	0.000	0.406	0.001
Urea	0.325	0.000	0.068	0.685
H_2O	0.176	0.000	0.112	0.216
Carbamate	0.302	0.000	0.000	0.000

green urea production processes (Edrisi et al., 2016; Alfian & Purwanto, 2019). According to these results, an integrated plant to produce DMC and urea can provide competitive costs for both chemicals reducing the urea price with the benefits obtained from the sale of DMC. In the urea cost breakdown (see Fig.7.7 b), the raw materials item represents almost 85% of the total operating cost. The main cause is the ammonia used as feedstock since nitrogen from ammonia is fixed in the urea and no ammonia recycle is possible.

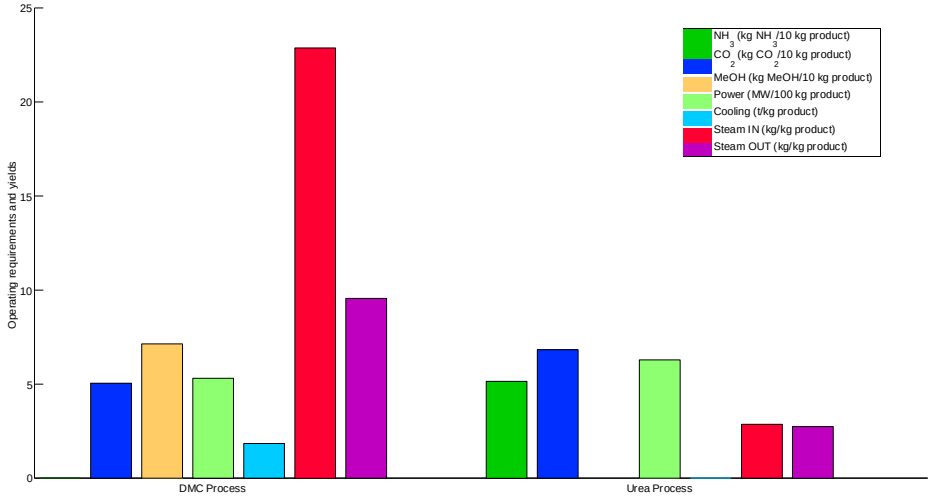

Figure 7.5: Main yields for the DMC and urea processes

7.5.3 *Sensitivity analysis*

The prices of the raw materials play a key role in the economic performance of the urea/DMC production as it is shown in Fig.7.7. The price of methanol or ammonia depends a lot of the production path used to synthesize these chemicals. If an entire green process is desired, the raw materials must also be produced following a renewable path and, in general, an increase in the production cost is expected. Therefore, a sensitivity analysis is carried out to study the influence of the different prices of the raw materials according to their different production paths.

The methanol can be produced from a wide range of green alternatives: from switchgrass via gasification and with the possibility of combining it with the hydrogenation of carbon dioxide (Martín & Grossmann, 2017), using captured CO_2 and hydrogen from electrolysis (Martín, 2016a) or from biogas via reforming (Hernández & Martín, 2016). An economic evaluation for each process was carried out in the different works resulting the following price ranges: 0.34- 0.36 €/kg for the switchgrass to methanol process (Martín & Grossmann, 2017), 0.21-0.45 €/kg for the hydrogenation of CO_2 with electrolyzed hydrogen (Martín, 2016a) and 0.46 €/kg for the biogas to methanol process (Hernández & Martín, 2016).

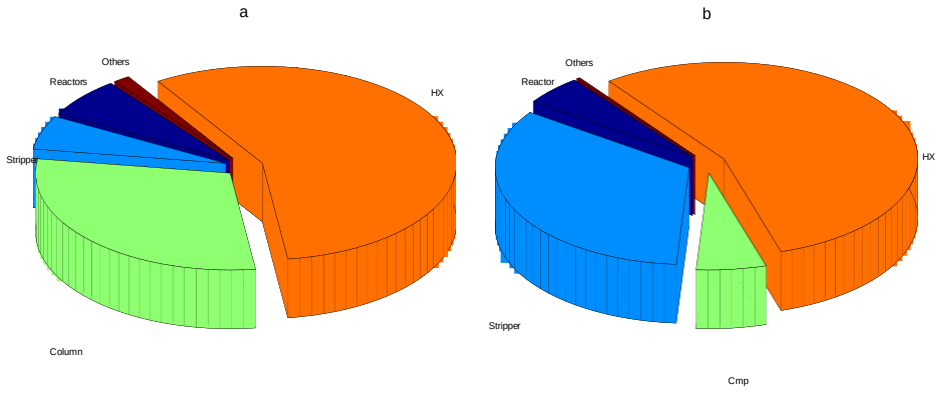

Figure 7.6: Breakdown for the equipment capital cost (a: DMC process; b: Urea process)

The sustainable ammonia production is gaining attention nowadays to develop a green path to produce ammonia and due to the possibility of using ammonia as a hydrogen carrier or as a fuel. Different processes have been proposed: using electrolysis to generate hydrogen, air separation (distillation, adsorption or membrane) to produce nitrogen and with both synthetize ammonia (Sánchez & Martín, 2018a, 2018b) or from biomass gasification or from biomass digestion (Sánchez et al., 2019). The ammonia production costs for the different alternatives are as follows: 1.37-5.6 €/kg

for the ammonia from electrolysis and separation of air using membranes (this price presents a wide range due to the different scales studied), 1.2-4.5 €/kg for electrolysis and air separation using adsorbent beds and 1.36-1.6 €/kg for electrolysis and using distillation for the separation of air (Sánchez & Martín, 2018b) , 0.38-0.69 €/kg for the ammonia production from biomass gasification and 0.87-1.24€/kg for the digestion process (Sánchez et al., 2019).

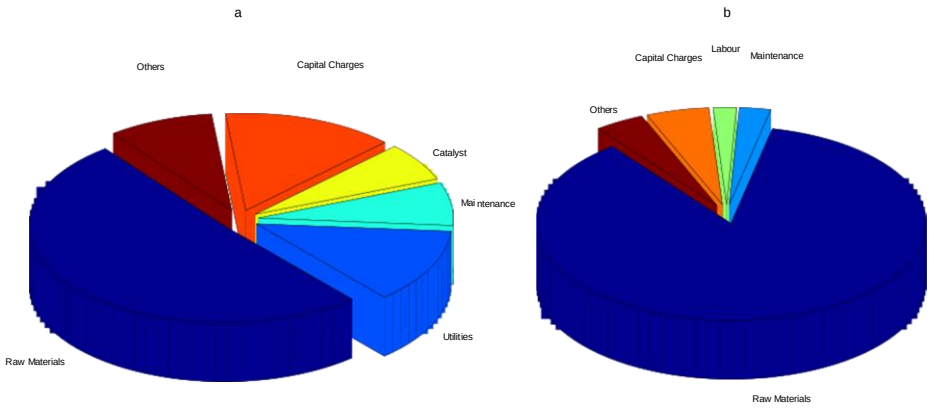

Figure 7.7: Breakdown of the operating cost (a: DMC process; b: Urea process)

Following the prices for the different species involved presented above, a sensitivity analysis is carried out to study the influence of the feedstock prices in the DMC and urea production cost. Fig.7.8 shows graphically the influence of the ammonia and methanol cost in the DMC operation cost.

The production cost of the DMC, for the ranges of prices proposed based on literature data, see Fig.7.8, is in the interval between 0.4 and 0.65 €/kg. The influence of the methanol price in the operating cost is larger than that due to the ammonia price. As it is presented previously, in the DMC production a large amount of ammonia is recycled from the DMC synthesis section to the urea section and, therefore, only a small amount of ammonia is required as raw material. Due to this small flow of ammonia, when its price is multiplied by 8 only an increase of less than 3% in the DMC production cost takes place. However, when the methanol price doubles, the DMC operating cost increases by 40%. In Table 7.7, it is presented the DMC operating cost for the lowest price of the range for each technology presented above for producing ammonia and methanol from renewable sources. The final DMC production costs are in the interval between 431.3 €/t and 614.4 €/t. The literature presents DMC price about 800 €/t, therefore, the DMC production from renewable sources can be a competitive alternative.

Table 7.7: DMC production cost sensitivity analysis for different ammonia/methanol production processes

DMC Production Cost (€/t)			Methanol Production		
			Gasification	CO_2 hydrogenation	Biogas reforming
Ammonia Production	Electrolysis	+Membrane	528.7	435.8	614.4
		+PSA	527.9	435.0	613.6
		+Distillation	5286	435.7	614.3
	Gasification	+Indirect	524.2	431.3	609.9
		+Direct O_2/Steam	524.9	432.0	610.6
		+Direct Air/Steam	524.9	432.0	610.6
	Digestion		526.4	433.5	612.1

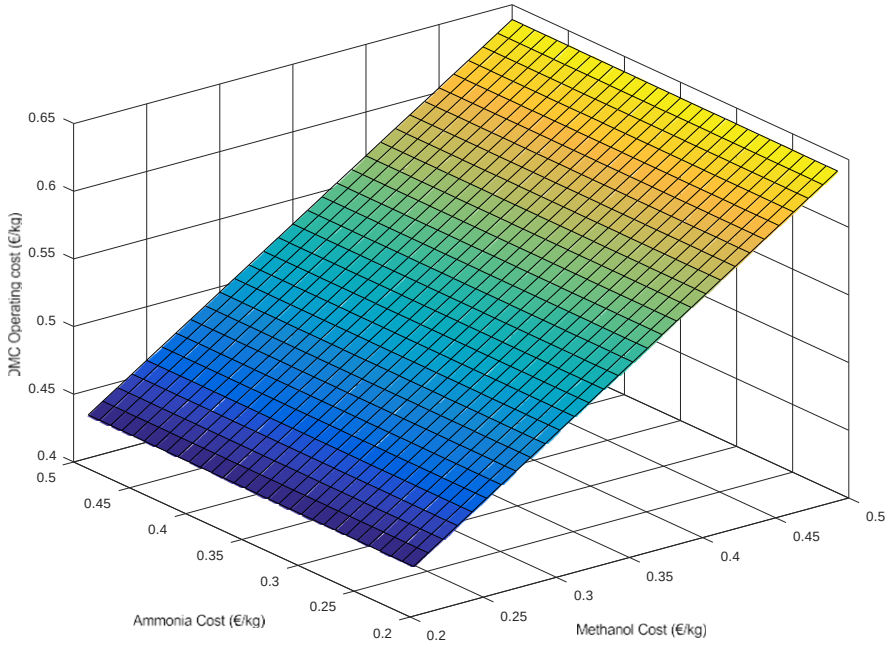

Figure 7.8: Sensitivity analysis for the DMC production cost based on the raw materials prices

For the production of urea, the results are presented in Table 7.8. In this case, only ammonia and carbon dioxide are required for the synthesis. Here, ammonia is not recycled as in the DMC production, therefore, the ammonia price has a more important influence in the urea production cost. The range of cost for urea is 277.2-787.6 €/t. The urea cost is highly related to the ammonia production technology and, within each technology, the price presents a strong link with the facility production capacity (Sánchez & Martín, 2018b).

Table 7.8: Urea production cost sensitivity analysis for different ammonia production processes

Urea Production Cost (€/t)			
Ammonia Production	Electrolysis	+Membrane	787.6
		+PSA	699.9
		+Distillation	777.2
	Gasification	+Indirect	277.5
		+Direct O_2/Steam	354.8
		+Direct Air/Steam	359.9
	Digestion		529.9

7.5.4 *Environmental analysis*

To evaluate the environmental performance of the processes, the index proposed by Martín (Martín, 2016c), RePSIM, was employed. In this simplified metric, the processes are evaluated based on the associated CO_2 emissions. For this case of study, the raw materials are: methanol, ammonia and carbon dioxide. The CO_2 associated with the production of ammonia and methanol presents a strong relationship to the production process used in its synthesis. For this environmental analysis, a level of emissions of 1.03 kg CO_2/kg NH_3 is considered associated with a production process based on water electrolysis and air distillation and -0.84 kg CO_2/kg MeOH for the methanol production by hydrogenation of CO_2 with electrolyze hydrogen (Matzen et al., 2015). The CO_2 emissions associated with the carbon capture are neglected. The CO_2 emissions associated to power are taken into account using the factor of 0.632 kg CO_2/kWh (Martín, 2016c). The CO_2 emissions related to cooling water are considered using a factor of 7775 kWh/Mgal to calculate the energy requirement and with this value and the energy to CO_2 factor the emissions related to cooling water are calculated (Hernández & Martín, 2016). The steam necessary in the process has also a CO_2 value. These CO_2 emissions are computed using the energy necessary to produce it and then with the energy to CO_2 factor as previously described.

The results for the DMC and urea production are shown in Fig.7.9. The raw materials item has a negative contribution to the emissions of CO_2 due to the use of CO_2 as raw material for the processes including the production of ammonia and methanol. The main contribution to the CO_2 emissions is the steam needed in the facility. This steam is consumed in

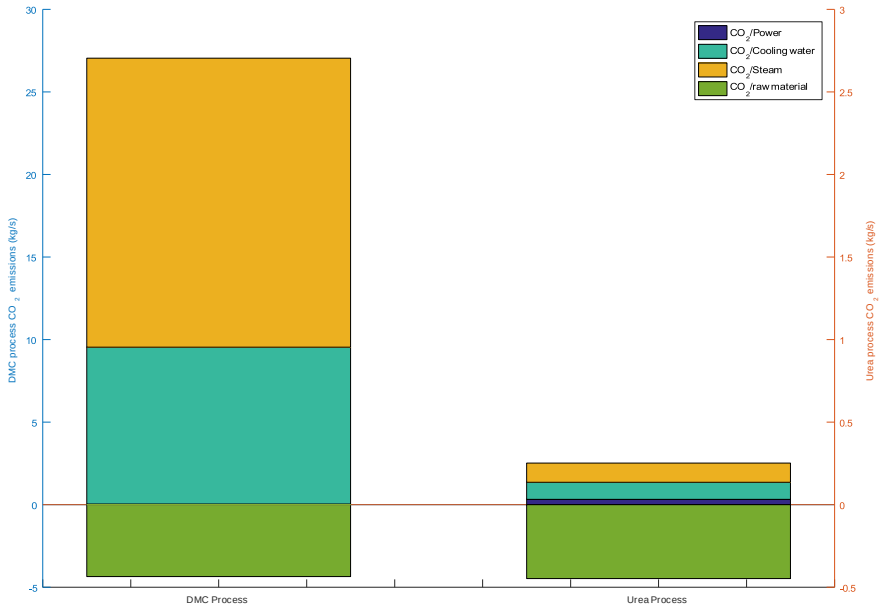

Figure 7.9: Contribution to the CO_2 emissions by process

the sequence of distillation columns to separate the different components involved in the DMC synthesis reactor. Sustainable steam can be produced from renewable sources to reduce the carbon dioxide emission related to the production of the utilities (Pérez-Uresti et al., 2019). In the process, steam is also generated in some units (for example, the urea condenser), however the net flow is positive (See Fig.7.5) and, therefore, a contribution to CO_2 emissions takes place. The DMC process presents an emission level of 5.74 kg CO_2/kg DMC and the urea one results in -0.04 kg CO_2/kg urea. The urea production is approximately carbon neutral. In this index, the CO_2 emissions related to urea hydrolysis during the application is not considered due to the fact that this index only focuses on the urea/DMC production process (Fertilizers Europe, 2008).

7.6 conclusions

In this work, a sustainable path to produce DMC via urea has been evaluated. Furthermore, for comparison the urea synthesis alone has also been studied. An equation based modelling approach has been used to analyse the two main section of the process: the urea synthesis and the DMC synthesis. Data driven models based on experimental data or rigorous simulations and first principles are used to model the processes.

The decision variables for the optimization are the operating conditions in the different units involved, for instance, pressure or temperature in the urea synthesis reactor, the urea stripper conditions, the DMC reactor outlet temperature, the inlet flows of ammonia and methanol, etc. According to the economic objective function, the DMC production is favourable with respect to the urea production. With the optimization results, an economic analysis was carried out for both alternatives. The investment for the DMC production is about 91 MM€ with a production cost of about 520 €/t. When only urea is produced, the capital cost is around 16 MM€ with a production cost of 340€/t. The sensitivity analysis shows that the methanol price plays an important role in the DMC price. The ammonia price is key in the urea cost and has only a small influence in the DMC price due to high recycle rate. Finally, a simple environmental analysis is presented showing the CO_2 emissions associated with the urea/DMC process. Urea production is near emissions neutral.

nomenclature

a	NH_3/CO_2 ratio, Eq.7.3 - 7.4
a_{0-4}	Fitting parameters, Eq.7.10
b	H_2O/CO_2 ratio, Eq.7.3 - 7.5
C_{CO_2}	Carbon dioxide price (€/kg)
C_{cooling}	Cooling water cost (€/kt)
C_{DMC}	DMC cost (€/kg)
C_{elect}	Electricity cost (cent €/kWh)
C_{MeOH}	Methanol price (€/kg)
C_{NH_3}	Ammonia price (€/kg)
C_{steam}	Steam cost (€/GJ)
C_{Urea}	Urea cost (€/kg)
fc	Molar flow (kmol/s)
F_{CO_2}	Carbon dioxide inlet flow (kg/s)
F_{cooling}	Cooling water consumption (kt/s)
F_{DMC}	DMC production (kg/s)
F_{MeOH}	Methanol inlet flow (kg/s)
F_{NH_3}	Ammonia inlet flow (kg/s)
F_{steam}	Net steam needed (GJ/s)

F_{Urea}	Urea production (kg/s)
P	Pressure (MPa), Eq.7.10
R_{DMC}	Bottom DMC yield in column 5, Eq.7.11
R_{real}	Reflux ratio in column 5, Eq.7.11
t	Temperature (^{o}C), Eq.7.3
T	Temperature (K), Eq.7.10
W_{total}	Total power (kWh)
X	Conversion, Eq.7.3
Y_i	Reaction yield, Eq.7.10
β	Linear coefficient, Eq.7.6
ω	Quadratic coefficient, Eq.7.6

acknowledgments

The authors would like to acknowledge Salamanca Research for optimization software licenses. The authors acknowledge the FPU, Spain grant (FPU16/06212) from MECD, Spain to Mr. A. Sánchez and MINECO, Spain grant DPI2015-67341-C2-1-R.

bibliography

Inoue, S., Kanai, K., & Otsuka, E. (1972). Equilibrium of urea synthesis. i. *Bulletin of the Chemical Society of Japan*, *45*(5), 1339–1345. https://doi.org/10.1246/bcsj.45.1339

Dente, M., Rovaglio, M., Bozzano, G., Sogaro, A., & Isimbaldi, A. (1992). Gas-liquid reactor in the synthesis of urea. *Chemical Engineering Science*, *47*(9), 2475–2480. https://doi.org/10.1016/0009-2509(92)87079-6

Anastas, P., & Williamson, T. C. (1996). *Green chemistry: Designing chemistry for the environment*. ACS Publications.

Pacheco, M. A., & Marshall, C. L. (1997). Review of dimethyl carbonate (dmc) manufacture and its characteristics as a fuel additive. *Energy & Fuels*, *11*(1), 2–29. https://doi.org/10.1021/ef9600974

Piotrowski, J., Kozak, R., & Kujawska, M. (1998). Thermodynamic model of chemical and phase equilibrium in the urea synthesis process. *Chemical Engineering Science*, *53*(1), 183–186. https://doi.org/10.1016/S0009-2509(97)00271-6

Sun, J., Yang, B., & Lin, H. (2004). A semi-continuous process for the synthesis of methyl carbamate from urea and methanol. *Chemical*

Engineering & Technology, *27*(4), 435–439. https://doi.org/10.1002/ceat.200401911

Geankopolis, C. J. (2005). *Transport processes and unit operations*. Prentice-Hall.

Hamidipour, M., Mostoufi, N., & Sotudeh-Gharebagh, R. (2005). Modeling the synthesis section of an industrial urea plant. *Chemical Engineering Journal*, *106*(3), 249–260. https://doi.org/10.1016/j.cej.2004.12.020

Zhang, X., Zhang, S., Yao, P., & Yuan, Y. (2005). Modeling and simulation of high-pressure urea synthesis loop. *Computers & Chemical Engineering*, *29*(5), 983–992. https://doi.org/10.1016/j.compchemeng.2004.10.004

Nexant. (2006). Equipment design and cost estimation for small modular biomass systems, synthesis gas cleanup, and oxygen separation equipment. task 2: Gas cleanup design and cost estimates –wood feedstock.

Fertilizers Europe. (2008). Energy efficiency and greenhouse gas emissions in european nitrogen fertilizer production and use.

Anastas, P., & Eghbali, N. (2010). Green chemistry: Principles and practice. *Chem. Soc. Rev.*, *39*, 301–312. https://doi.org/10.1039/B918763B

Mavrovic, I., Shirley Jr., A. R., & Coleman, G. R. " (2010). Urea. *Kirk-othmer encyclopedia of chemical technology* (pp. 1–21). American Cancer Society. https://doi.org/10.1002/0471238961.2118050113012218.a01.pub2

Meessen, J., & Petersen, H. (2010). Urea, uhlmann's encyclopedia of industrial chemistry.

Wang, D., Zhang, X., Wei, W., & Sun, Y. (2012). Synthesis of dimethyl carbonate from methyl carbamate and methanol using a fixed-bed reactor. *Chemical Engineering & Technology*, *35*(12), 2183–2188. https://doi.org/10.1002/ceat.201200217

Aresta, M., Dibenedetto, A., & Angelini, A. (2013). The changing paradigm in co2 utilization. *Journal of CO2 Utilization*, *3-4*, 65–73. https://doi.org/10.1016/j.jcou.2013.08.001

Lu, B., Wang, X., Li, Y., Sun, J., Zhao, J., & Cai, Q. (2013). Electrochemical conversion of co2 into dimethyl carbonate in a functionalized ionic liquid. *Journal of CO2 Utilization*, *3-4*, 98–101. https://doi.org/10.1016/j.jcou.2013.10.001

Spigarelli, B. P., & Kawatra, S. K. (2013). Opportunities and challenges in carbon dioxide capture. *Journal of CO2 Utilization*, *1*, 69–87. https://doi.org/10.1016/j.jcou.2013.03.002

Davis, W., & Martín, M. (2014). Optimal year-round operation for methane production from co2 and water using wind energy. *Energy*, *69*, 497–505. https://doi.org/10.1016/j.energy.2014.03.043

de Groot, F. F., Lammerink, R., Heidemann, C., van der Werff, M. P., Garcia, T. C., Van Der Ham, L., & van den Berg, H. (2014). The industrial production of dimethyl carbonate from methanol and carbon dioxide. *Chemical engineering transactions*, *39*, 1561–1566. https://doi.org/10.3303/CET1439261

Meessen, J. (2014). Urea synthesis. *Chemie Ingenieur Technik*, *86*(12), 2180–2189. https://doi.org/10.1002/cite.201400064

Santos, B. A. V., Silva, V. M. T. M., Loureiro, J. M., & Rodrigues, A. E. (2014). Review for the direct synthesis of dimethyl carbonate. *ChemBioEng Reviews*, *1*(5), 214–229. https://doi.org/10.1002/cben.201400020

Sinnott, R. (2014). *Chemical engineering design* (Vol. 6). Elsevier.

Kongpanna, P., Pavarajarn, V., Gani, R., & Assabumrungrat, S. (2015). Techno-economic evaluation of different co2-based processes for dimethyl carbonate production. *Chemical Engineering Research and Design*, *93*, 496–510. https://doi.org/10.1016/j.cherd.2014.07.013

Matzen, M. J., Alhajji, M. H., & Demirel, Y. (2015). Technoeconomics and sustainability of renewable methanol and ammonia productions using wind power-based hydrogen.

Almena, A., & Martín, M. (2016). Technoeconomic analysis of the production of epichlorohydrin from glycerol. *Industrial & Engineering Chemistry Research*, *55*(12), 3226–3238. https://doi.org/10.1021/acs.iecr.5b02555

Edrisi, A., Mansoori, Z., & Dabir, B. (2016). Urea synthesis using chemical looping process – techno-economic evaluation of a novel plant configuration for a green production. *International Journal of Greenhouse Gas Control*, *44*, 42–51. https://doi.org/10.1016/j.ijggc.2015.10.020

Garcia-Herrero, I., Cuéllar-Franca, R. M., Enríquez-Gutiérrez, V. M., Alvarez-Guerra, M., Irabien, A., & Azapagic, A. (2016). Environmental assessment of dimethyl carbonate production: Comparison of a novel electrosynthesis route utilizing co2 with a commercial oxidative carbonylation process. *ACS Sustainable Chemistry & Engineering*, *4*(4), 2088–2097. https://doi.org/10.1021/acssuschemeng.5b01515

Hernández, B., & Martín, M. (2016). Optimal process operation for biogas reforming to methanol: Effects of dry reforming and biogas composition. *Industrial & Engineering Chemistry Research*, *55*(23), 6677–6685. https://doi.org/10.1021/acs.iecr.6b01044

Martín, M. (2016a). Methodology for solar and wind energy chemical storage facilities design under uncertainty: Methanol production

from co2 and hydrogen. *Computers & Chemical Engineering*, *92*, 43–54. https://doi.org/10.1016/j.compchemeng.2016.05.001

Martín, M. (2016b). Optimal year-round production of dme from co2 and water using renewable energy. *Journal of CO2 Utilization*, *13*, 105–113. https://doi.org/10.1016/j.jcou.2016.01.003

Martín, M. (2016c). Repsim metric for design of sustainable renewable based fuel and power production processes. *Energy*, *114*, 833–845. https://doi.org/10.1016/j.energy.2016.08.031

Contreras-Zarazúa, G., Vázquez-Castillo, J. A., Ramírez-Márquez, C., Pontis, G. A., Segovia-Hernández, J. G., & Alcántara-Ávila, J. R. (2017). Comparison of intensified reactive distillation configurations for the synthesis of diphenyl carbonate. *Energy*, *135*, 637–649. https://doi.org/10.1016/j.energy.2017.06.156

Li, A., Pu, Y., Li, F., Luo, J., Zhao, N., & Xiao, F. (2017). Synthesis of dimethyl carbonate from methanol and co2 over fe–zr mixed oxides. *Journal of CO2 Utilization*, *19*, 33–39. https://doi.org/10.1016/j.jcou.2017.02.016

Martín, M., & Grossmann, I. E. (2017). Towards zero co2 emissions in the production of methanol from switchgrass. co2 to methanol. *Computers & Chemical Engineering*, *105*, 308–316. https://doi.org/10.1016/j.compchemeng.2016.11.030

Pfromm, P. H. (2017). Towards sustainable agriculture: Fossil-free ammonia. *Journal of Renewable and Sustainable Energy*, *9*(3), 034702. https://doi.org/10.1063/1.4985090

Pyo, S.-H., Park, J. H., Chang, T.-S., & Hatti-Kaul, R. (2017). Dimethyl carbonate as a green chemical. *Current Opinion in Green and Sustainable Chemistry*, *5*, 61–66. https://doi.org/10.1016/j.cogsc.2017.03.012

Shi, L., Wang, S.-J., Wong, D. S.-H., & Huang, K. (2017). Novel process design of synthesizing propylene carbonate for dimethyl carbonate production by indirect alcoholysis of urea. *Industrial & Engineering Chemistry Research*, *56*(40), 11531–11544. https://doi.org/10.1021/acs.iecr.7b02341

Sánchez, A., & Martín, M. (2018a). Optimal renewable production of ammonia from water and air. *Journal of Cleaner Production*, *178*, 325–342. https://doi.org/10.1016/j.jclepro.2017.12.279

Sánchez, A., & Martín, M. (2018b). Scale up and scale down issues of renewable ammonia plants: Towards modular design. *Sustainable Production and Consumption*, *16*, 176–192. https://doi.org/10.1016/j.spc.2018.08.001

Statista. (2018). Prices of electricity for the industry in spain from 2008 to 2017 (in euro cents per kilowatt hour). Retrieved May 7, 2020, from

https://www.statista.com/statistics/595813/electricity-industry-price-spain/

Tan, H.-Z., Wang, Z.-Q., Xu, Z.-N., Sun, J., Xu, Y.-P., Chen, Q.-S., Chen, Y., & Guo, G.-C. (2018). Review on the synthesis of dimethyl carbonate. *Catalysis Today*, *316*, 2–12. https://doi.org/10.1016/j.cattod.2018.02.021

Vázquez, D., Javaloyes-Antón, J., Medrano-García, J. D., Ruiz-Femenia, R., & Caballero, J. A. (2018). Dimethyl carbonate production process from urea and methanol. In A. Friedl, J. J. Klemeš, S. Radl, P. S. Varbanov, & T. Wallek (Eds.), *28th european symposium on computer aided process engineering* (pp. 731–736). Elsevier. https://doi.org/10.1016/B978-0-444-64235-6.50129-7

Xuan, K., Pu, Y., Li, F., Li, A., Luo, J., Li, L., Wang, F., Zhao, N., & Xiao, F. (2018). Direct synthesis of dimethyl carbonate from co2 and methanol over trifluoroacetic acid modulated uio-66. *Journal of CO2 Utilization*, *27*, 272–282. https://doi.org/10.1016/j.jcou.2018.08.002

Yang, M., & You, F. (2018). Modular methanol manufacturing from shale gas: Techno-economic and environmental analyses of conventional large-scale production versus small-scale distributed, modular processing. *AIChE Journal*, *64*(2), 495–510. https://doi.org/10.1002/aic.15958

Alfian, M., & Purwanto, W. W. (2019). Multi-objective optimization of green urea production. *Energy Science & Engineering*, *7*(2), 292–304. https://doi.org/10.1002/ese3.281

Allman, A., Palys, M. J., & Daoutidis, P. (2019). Scheduling-informed optimal design of systems with time-varying operation: A wind-powered ammonia case study. *AIChE Journal*, *65*(7), e16434. https://doi.org/10.1002/aic.16434

Pérez-Uresti, S. I., Martín, M., & Jiménez-Gutiérrez, A. (2019). Superstructure approach for the design of renewable-based utility plants. *Computers & Chemical Engineering*, *123*, 371–388. https://doi.org/10.1016/j.compchemeng.2019.01.019

Sánchez, A., Martín, M., & Vega, P. (2019). Biomass based sustainable ammonia production: Digestion vs gasification. *ACS Sustainable Chemistry & Engineering*, *7*(11), 9995–10007. https://doi.org/10.1021/acssuschemeng.9b01158

Selva, M., Perosa, A., Rodríguez-Padrón, D., & Luque, R. (2019). Applications of dimethyl carbonate for the chemical upgrading of biosourced platform chemicals. *ACS Sustainable Chemistry & Engineering*, *7*(7), 6471–6479. https://doi.org/10.1021/acssuschemeng.9b00464

Martín-Hernández, E., Guerras, L. S., & Martín, M. (2020). Optimal technology selection for the biogas upgrading to biomethane. *Journal of Cleaner Production*, *267*, 122032. https://doi.org/10.1016/j.jclepro.2020.122032

Part IV

OPERATION OF POWER-TO-*X* PROCESSES

8

OPTIMAL DESIGN OF SUSTAINABLE POWER-TO-FUELS SUPPLY CHAINS FOR SEASONAL ENERGY STORAGE

abstract

Energy storage is key in enabling high penetration of intermittent renewable sources into the energy supply mix. One attractive way of storing energy is to do so in the form of chemical fuels produced from electricity, also referred to as "power-to-fuels". Apart from its promise for large-scale seasonal energy storage, it also has advantages at the supply chain level due to the ease of transportation. Therefore, these fuels have been proposed as energy carriers for various applications. In this work, these potential benefits are assessed by optimizing the design of power-to-fuels supply chains for seasonal energy storage over large geographical regions. Distribution decisions are integrated with hourly production decisions over the time horizon of a year in order to account for seasonal changes and obtain plant capacities suitable for time-varying operation. A heuristic decomposition approach is developed to solve industrial-scale instances of the resulting optimization problem. The proposed framework is applied to a region of Spain where the energy transition is particularly significant due to the decommissioning of coal-based power generation facilities. The results show how an efficient power-to-fuels supply chain can help replace conventional with renewable energy sources.

Keywords: Power-to-fuels, Chemical energy storage, Power-to-X, Renewable energy

resumen

El almacenamiento de energía es clave para permitir una alta penetración de las fuentes renovables intermitentes en el mix de suministro eléctrico. Una forma atractiva de almacenar energía es hacerlo en forma de combustibles producidos a partir de la electricidad, también denominados "power-to-fuels". Aparte de su promesa para el almacenamiento de energía estacional a gran escala, también tiene ventajas a nivel de la cadena de suministro debido a la facilidad de transporte. Por ello, estos combustibles se han propuesto como vectores energéticos para diversas aplicaciones. En este trabajo, se evalúan estas ventajas potenciales optimizando el diseño de las cadenas de suministro de "power-to-fuels" para el almacenamiento de energía estacional en grandes regiones geográficas. Las decisiones de distribución se integran con las decisiones de producción horaria en el horizonte temporal de un año con el fin de tener en cuenta los cambios estacionales y obtener capacidades de planta adecuadas para la operación variable en el tiempo. Se desarrolla un enfoque de descomposición heurística para resolver a escala industrial el problema de optimización resultante. El marco propuesto se aplica a una región de España en la que la transición energética es particularmente significativa debido al desmantelamiento de las instalaciones de generación de energía a base de carbón. Los resultados muestran cómo una cadena eficiente de suministro de "power-to-fuels" puede ayudar a sustituir las fuentes de energía convencionales por las renovables.

Palabras clave: Power-to-fuels, Almacenamiento químico de energía, Power-to-X, Energía renovable

8.1 introduction

The power, heat, and transportation sectors combined are responsible for about 65% of the global CO_2 emissions (Nejat et al., 2015). Due to sustainability concerns, the share of renewable energy has been increasing rapidly over the last few decades (Mehigan et al., 2020). In the heating and cooling sector, decarbonization is one of the main targets to achieve climate neutrality, and, at this point, the integration of electricity and heat is crucial (Thomaßen et al., 2021). In addition, in a renewable energy scheme, a transition is required in the transportation sector. Electrification of some applications such as small vehicles combined with the use of different renewable fuels for large energy consumption such as maritime or air transport has been proposed (García-Olivares et al., 2018). In all cases, power production using renewable sources is the core activity in the new renewable energy system. According to recent predictions (BloombergNEF, 2019), in 2050, 62% of the power will be produced from renewable sources and 48% of the power generation will come from solar and wind. The main challenge in the use of these two resources is the strong weather dependence (Alves et al., 2020). The sudden and large fluctuations in wind and solar availability lead to large changes in the power output from, for example, PV panels and wind turbines, in contrast to traditional energy sources (Leonard et al., 2018). Consequently, this fact determines the operation of the energy system and its stability may be jeopardized with an increase in the penetration of renewable energy sources. To deal with this challenge, a combination of intermittent and non-intermittent renewable sources along with energy storage will be required (Heuberger et al., 2017).

In this context, a wide range of energy storage technologies are being considered (Ajanovic et al., 2020) with different environmental impacts (Sternberg & Bardow, 2015). According to Gür (2018), there are four main categories of storage: mechanical, chemical, electrochemical and electrical. The different alternatives are characterized, mainly, by their power ratings and discharge times. Only two of these options are available at commercial scale now: pumped-hydro and compressed-air energy storage (CAES). Pumped-hydro can deal with a large range of storage timescales; however, there is little room for expanding the current capacity (Larsen & Petersen, 2013). CAES is an interesting option for large-scale power storage, but has only found limited application due to its relatively low energy density and the need for suitable geological caverns (Bartela, 2020).

Producing chemical fuels from electricity and using them as energy storage has attracted much attention due to the high energy density of these chemicals, the scalable and flexible behavior of this technology and

ease of storage and transportation (Burre et al., 2020). Different fuels that have been proposed are hydrogen (Y. Zhang et al., 2019), methane (Sternberg & Bardow, 2016), methanol (Daggash et al., 2018) and ammonia (G. Wang et al., 2017). These chemicals have different properties in terms of energy density, state of aggregation, etc. (L. Wang et al., 2020). The environmental performance of the corresponding power-to-fuels processes has also been analyzed using life cycle assessment tools, for instance, for methane (Blanco et al., 2020) or methanol (Al-Qahtani et al., 2020). These fuels have also been proposed as energy carriers for heating and transportation applications (Stančin et al., 2020). Hydrogen and methane were evaluated for heating uses in the on-going project by Thema et al. (2019). Different fuels are also attracting attention for transportation such as ammonia through different conversion technologies (Giddey et al., 2017) or methanol for overseas energy transport (Al-Breiki & Bicer, 2020).

Some important considerations have to be made in order to make use of these fuels as energy carriers or in storage applications. First, the location of the production site plays a key role as wind and solar availability is highly distributed. In addition, as there are fluctuations in the power generation from solar and wind on an hourly scale, the chemical production processes have to be designed with such dynamics in mind. Q. Zhang et al. (2019) developed an integrated design framework for process networks that produce fuels and power from solar, wind and biomass. Their analysis shows that reasonable plant designs can only be obtained if detailed operational constraints are taken into account in the design optimization problem. Demirhan et al. (2020) assessed the benefit of producing fuels from electricity at one location and transporting them to another location to serve its energy demand. In their particular case study, they considered the states of Texas and New York, respectively. Other existing works focus on supply chain optimization but do not consider details in the operation of the power-to-fuels processes. Seo et al. (2020) considered hydrogen supply chain optimization in which hydrogen from different productions sites is consolidated into an integrated bulk storage to satisfy the demand of electric vehicles. Several energy sources were analyzed, including natural gas, biomass, wind and solar. Ehrenstein et al. (2020) determined the optimal hydrogen supply chain in the UK, but the intermittent nature of solar and wind is only considered through a capacity factor. Ogumerem et al. (2019) considered hydrogen, ammonia and methanol in a multi-period supply chain optimization problem for different states in the US. Here, the length of each time period was set to one year.

In this work, the synthesis of different fuels as a way to store and distribute solar/wind energy is evaluated. With sufficient fuel inventory, it is possible to ensure a stable energy supply with intermittent solar/wind

availability. This is especially important in the current context where the energy system must be adapted to achieve climate neutrality. Two levels of decision-making are considered in this work in an integrated approach: network design at the supply chain level and design and operation of the facilities at the scheduling level. At the supply chain level, the production and storage sites are determined as well as the transportation network to distribute the fuels. At the scheduling level, the detailed operation of the facilities and the impact of the intermittent resource availability is analyzed.

8.2 problem statement

The goal of this work is to determine the optimal infrastructure to transform intermittent renewable energy (wind and solar) into chemicals that can then be used as energy storage or carrier in different energy applications. A geographical region that is divided in a set of subregions is considered, with given information about solar and wind availability, CO_2 emissions and energy consumption. The objective is to meet a given energy demand in each of the locations using the chemical storage while minimizing the capital and operating costs of the network. To transport the chemicals between the different regions, there are different alternatives: rail, truck and natural gas pipeline. These transportation options are limited by the current infrastructure.

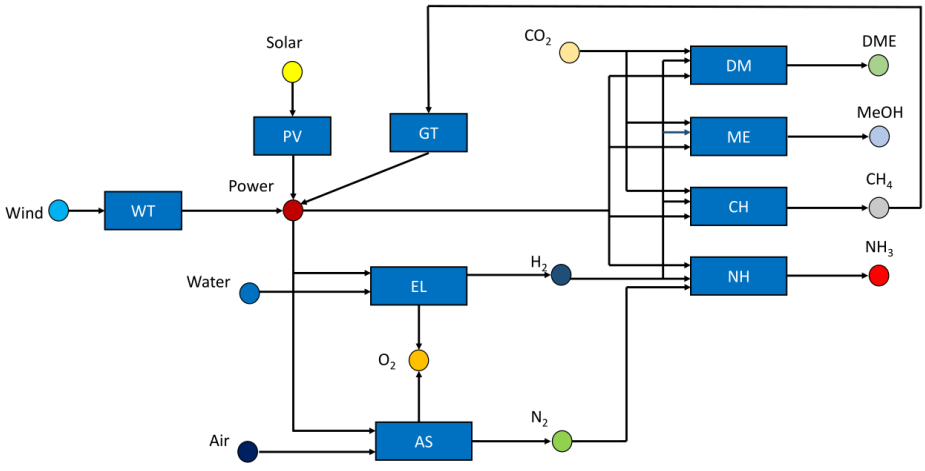

Figure 8.1: Process-resource network superstructure for the conversion of wind/solar energy to chemicals where rectangles are process nodes and circles are resources nodes.

For chemical storage of renewable energy, the superstructure proposed in Figure 8.1 is considered. It is represented as a network of processes and resources, similar to an Resource-Task Network (RTN) commonly used in production scheduling (Castro et al., 2004). The circles represent the resources involved in this power-to-fuels system and the rectangles the processes. Four chemicals are considered as energy carriers in this work: methane, methanol, dimethyl ether (DME) and ammonia. To synthesize these chemicals, power is collected from PV panels and/or wind turbines. This energy is used to split water generating hydrogen and to separate air to produce nitrogen. The three first chemicals are synthesized combining hydrogen with CO_2. This CO_2 is obtained using carbon capture. Ammonia can be produced using nitrogen and hydrogen. Power from methane can be generated using a gas turbine. As a summary, the list of the processes can be found in Table 8.1.

Intermittency is the main challenge in the operation of chemical plants using renewable energy. It requires a paradigm shift from the traditional steady-state process operation in the chemical industry. Therefore, operation over the course of a year is considered in this work, and hourly time discretization is incorporated in order to capture short-term variations in solar and wind resources. In the optimization problem, the capacities of the production processes, the storage capacities and their locations are determined, as well as the fuel distribution connections between different subregions. Additionally, for each time period, the production rate, the storage amount, the operating mode and the transportation of the different chemicals are calculated.

Table 8.1: Process description with the input/output resources

Name	Description	Input Resources	Output Resources	Reference
WT	Wind turbines	Wind	Power	de la Cruz and Martín (2016)
PV	Photovoltaic panels	Solar	Power	Sánchez and Martín (2018a)
EL	Water electrolysis	Water, Power	Hydrogen, Oxygen	Sánchez and Martín (2018a)
AS	Air separation unit (distillation, membrane, PSA)	Air, Power	Nitrogen, Oxygen	Sánchez and Martín (2018b)
DM	DME production	Hydrogen , CO_2, Power	DME	Martín (2016b)
ME	Methanol production	Hydrogen, CO_2, Power	Methanol	Martín (2016a)
CH	Methane production	Hydrogen , CO_2, Power	Methane	Davis and Martín (2014)
NH	Ammonia production	Nitrogren, Hydrogen, Power	Ammonia	Sánchez and Martín (2018a)
GT	Gas turbine	Methane	Power	León and Martín (2016)

8.3 model formulation

In this section, an integrated supply chain and scheduling model that optimizes the fuels production using wind/solar energy, the location of these plants and the distribution of the fuels to given demand points is presented. The model is based on previous works by Q. Zhang et al. (2016) and Q. Zhang et al. (2019).

8.3.1 *Process analysis*

The processes involved in the power-to-fuels network have been analyzed in previous works (see Table 8.1). The preceding analyses determined the optimal operating conditions for the different process units and provided the optimal yield for each one of them. The process design evaluation also includes the cost analysis providing the capital and operating cost of each unit of the superstructure presented in Figure 8.1. In solar PV panels and wind turbines, solar irradiance and wind velocity are used to compute the power production. An efficiency of 25% and a performance ratio of 75% are assumed for PV panels. A Nordex N100-2500 type wind turbine is selected with a nominal power of 2,500 kW. Davis and Martín (2014) studied the synthesis of methane using hydrogen from water electrolysis powered by renewable energy and CO_2. The synthesis of DME (Martín, 2016b) and methanol (Martín, 2016a) using these same resources have also been analyzed. Sánchez and Martín (2018b) optimized the synthesis of ammonia using air and water. Three different air separation units were evaluated: membrane, pressure swing adsorption and cryogenic distillation. These three alternatives to produce nitrogen were used, mainly, depending of the production scale, and are represented by the AS process in the proposed superstructure. For each of these processes, represented as a rectangle in Figure 8.1, linear yields have been calculated at the optimal conditions obtained in each of the previous works.

8.3.2 *Time representation*

In this work, a multiscale time representation is applied. The time horizon is divided into seasons, denoted by index h. The seasons do not necessarily have to match the four seasons of the year. Each season can have different lengths according to the recurring patterns presented in some of the input resources (solar, wind, etc.). Each season is described by a set of time periods with length Δt. A cyclic schedule, captured using the specified set of time periods, is applied n_h times in each season h. The time

periods of each season start at time point 0. The time periods before 0 are only used to impose constraints on the mode transitions. Although a cyclic schedule is imposed in each season, inventory can be carried over from one season to the next, allowing the seasonal storage of chemical fuels, which is an important feature of this model.

8.3.3 *Mass balance constraints for each location*

The general process mass balance for each of the locations in the selected geographical region is as follows:

$$\overline{Q}_{rjht} = \overline{Q}_{rjht-1} + B_{rjht} - S_{rjht} + \sum_i \rho_{ij} P_{riht} + \sum_{r' \in \hat{R}_{jr}} W_{jr'rht} - \sum_{r' \in \hat{R}_{jr}} W_{jrr'ht} \quad \forall r, j, h, t \in \overline{T}_h \tag{8.1}$$

with $\hat{R}_{jr}$ being the set of locations to which resource j can be distributed from location r. Five main contributions are involved in equation (8.1): storage, input and output resource at the selected location, production and transportation to other locations. The amount of resource j stored at location r at time t of season h is represented by $\overline{Q}_{rjht}$. The amounts of consumed or discharged resource at each location are denoted by B_{rjht} and S_{rjht}. The amount of reference resource produced or consumed is denoted by P_{riht}. The parameter ρ_{ij} denotes the conversion factor between resource j and the reference resource of process i. Finally, $W_{jrr'ht}$ is the amount of resource j transported from location r to location r'.

The production of the reference resource in each process i is limited by the plant capacity:

$$P_{riht} = \eta_{riht} C_{ri} \quad \forall r, i \in \{PV, WT\}, h, t \in T_h \tag{8.2}$$

$$P_{riht} \leq \eta_{riht} C_{ri} \quad \forall r, i \in I \setminus \{PV, WT\}, h, t \in T_h \tag{8.3}$$

The plant capacity is denoted by C_{ri}. The parameter η_{rikt} is used to represent the time-varying process capacity, for instance, wind or solar generation, where the capacity is not only a function of the plant size but also of the wind/solar availability. This parameter is calculated using the solar irradiance or the wind velocity for each time period and location.

The storage capacity $\overline{C}_{rj}$ is an upper bound for the inventory level.

$$\overline{Q}_{rjht} \leq \overline{C}_{rj} \quad \forall r, j \in \hat{S}, h, t \in \overline{T}_h \tag{8.4}$$

$$\overline{Q}_{rjht} = 0 \quad \forall r, j \notin \hat{S}, h, t \in \overline{T}_h \tag{8.5}$$

The set $\hat{S}$ consists of all resources that can be stored (hydrogen, DME, methane, methanol and ammonia).

There is a maximum value for the capacity for each process involved in the network. The binary variable x_{ri} indicates whether process i is selected in the process network at location r. The maximum allowed process capacity is denoted by $C_i^{\max}$.

$$C_{ri} \leq C_i^{\max} x_{ri} \quad \forall r, i \tag{8.6}$$

Similarly, there is also a maximum value for the storage capacity denoted by $\overline{C}_j^{\max}$. The binary variable $\bar{x}_{rj}$ is equal to 1 if a storage facility for product j is built at location r.

$$\overline{C}_{rj} \leq \overline{C}_j^{\max} \bar{x}_{rj} \quad \forall r, j \tag{8.7}$$

The resource availability is also limited for those resources used as raw materials in the system (indicated by the set $\hat{B}$).

$$B_{rjht} \leq B_{rjht}^{\max} \quad \forall r, j \in \hat{B}, h, t \in \overline{T}_h \tag{8.8}$$

$$B_{rjht} = 0 \quad \forall r, j \notin \hat{B}, h, t \in \overline{T}_h \tag{8.9}$$

Some resources do not have an associated demand (i.e., they are not in the set $\hat{J}$). Therefore, the outlet flowrate of these species is fixed to 0:

$$S_{rjht} = 0 \quad \forall r, j \notin \hat{J}, h, t \in \overline{T}_h \tag{8.10}$$

8.3.4 *Transportation constraints*

To reduce the size of the problem, only transportation connections between neighboring subregions are considered. Three different modes of transportation are contemplated in this study: truck, rail and pipeline. Truck connections are available for all the subregions but rail and pipeline are limited according to the current infrastructure in the region.

The amount of resource j transported from location r to location r' is the summation of the amounts transported using the different transportation modes:

$$W_{jrr'ht} = \sum_{d \in \hat{N}_{jrr'}} T_{jrr'dht} \quad \forall j, r, r', h, t \in \overline{T}_h \tag{8.11}$$

The variable $T_{jrr'dht}$ represents the amount of resource j transported from location r to r' using the mode of transportation d. The set of transportation options that can be selected for shipping resource j from location r to r' according to the limitation in the current infrastructure is denoted by $\hat{N}_{jrr'}$.

8.3.5 *Mode-based operation*

Each of the processes can operate in four different operating modes: off, startup, on and shutdown. The binary variable y_{rimht} indicates if a process i is operating in a certain mode m. If a process is selected, one of the operating modes must be assigned:

$$\sum_{m \in M_{ri}} y_{rimht} = x_{ri} \quad \forall r, i, h, t \in \overline{T_h} \tag{8.12}$$

The set M_{ri} denotes the set of allowed operating modes for process i at location r.

The amount of reference resource consumed or produced by process i, P_{riht}, must be produced or consumed in one of the different operating modes. The variable P_{rimht} denotes the quantity of reference resource consumed or produced in mode m:

$$P_{riht} = \sum_{m \in M_{ri}} \overline{P}_{rimht} \quad \forall r, i, h, t \in \overline{T_h} \tag{8.13}$$

A maximum ($\overset{\max}{\bigcirc}_{rim}$) and minimum ($\overset{\min}{\bigcirc}_{rim}$) value for the amount of reference resource produced or consumed for each mode is introduced:

$$\overset{\min}{\bigcirc}_{rim} y_{rimht} \le \overline{P}_{rimht} \le \overset{\max}{\bigcirc}_{rim} y_{rimht} \quad \forall r, i, m \in M_{ri}, h, t \in \overline{T_h} \tag{8.14}$$

The following constraints are related to the transition between operating modes for the same process unit. The maximum rate of change within a mode is limited by an upper bound ($\overline{\Delta}^{\max}_{rim}$):

$$\begin{aligned} &-\overline{\Delta}^{\max}_{rim} - \overline{M}(2 - y_{rimht} - y_{rimh,t-1}) \le \overline{P}_{rimht} - \overline{P}_{rimh,t-1} \\ &\le \overline{\Delta}^{\max}_{rim} + \overline{M}(2 - y_{rimht} - y_{rimh,t-1}) \quad \forall r, i, m \in M_{ri}, h, t \in \overline{T_h} \end{aligned} \tag{8.15}$$

The binary variable $z_{rim'mht}$ is introduced to indicate that process i switches from mode m to mode m' at time t. The possible transitions are defined by the following equation:

$$\sum_{m' \in TR_{rim}} z_{rim'mh,t-1} - \sum_{m' \in TR_{rim}} z_{rimm'h,t-1} = y_{rimht} - y_{rimh,t-1} \tag{8.16}$$

$$\forall r, i, m \in M_{ri}, h, t \in \overline{T_h}$$

where the set TR_{ri} includes all the possible mode-to-mode transitions for the process i at location r, and $\overline{TR}_{rim} = \{m' : (m', m) \in TR_{ri}\}$ and $TR_{rim} = \{m' : (m, m') \in TR_{ri}\}$.

A process i must remain for a certain minimum number of time periods ($\theta_{imm'}$) in an operating mode m before switching to another mode m':

$$y_{rim'ht} \geq \sum_{k=1}^{\theta_{im}^{m'}} z_{rimm'h,t-k} \qquad \forall r, i, (m,m') \in TR_i, h, t \in \overline{T_h} \tag{8.17}$$

Finally, predefined sequences of modes (from mode m to mode m' to mode m'') for a process i can be defined, establishing a fixed stay time for each of the modes involved in the sequence.

$$z_{rimm'h,t-\bar{\theta}_{imm'm''}} = z_{rim'm''ht} \qquad \forall r, i, (m,m',m'') \in SQ_i, h, t \in \overline{T_h} \tag{8.18}$$

The set SQ_i denotes the set of predefined sequences for process i and $\theta_{imm'm''}$ is the fixed stay time in mode m in the predefined sequence.

8.3.6 *Continuity constraints*

Continuity constraints ensure the feasible transition between seasons. A cyclic schedule is imposed; therefore, the initial mode of a season must be the same as the final one.

$$y_{rimh,0} = y_{rimh,|\overline{T}_h|} \qquad \forall r, i, m \in M_{ri}, h \tag{8.19}$$

$$z_{rimm'ht} = z_{rimm'h,t+|\overline{T}_h|} \qquad \forall r, i, (m,m') \in TR_i, h, -\theta_i^{\max}+1 \leq t \leq -1 \tag{8.20}$$

For the transitions between seasons, the state at the final time of one season and at the initial time of the next season must be the same.

$$y_{rimh,|\overline{T}_h|} = y_{rim,h+1,0} \qquad \forall r, i, m \in M_{ri}, h \in H \setminus |H| \tag{8.21}$$

$$z_{rimm'h,t+|\overline{T}_h|} = z_{rimm',h+1,t} \qquad \forall r, i, (m,m') \in TR_i, h \in H \setminus |H|, -\theta_i^{\max}+1 \leq t \leq -1. \tag{8.22}$$

The storage of chemicals is allowed between seasons since that is the key of using fuels for seasonal storage. The following equations determine the change in inventory levels from one season to the next.

$$\hat{Q}_{rjh} = \overline{Q}_{rjh,|\overline{T}_h|} - \overline{Q}_{rjh,0} \qquad \forall r, j \in \hat{S}, h \tag{8.23}$$

$$\overline{Q}_{rjh,0} + n_h \hat{Q}_{rjh} = \overline{Q}_{j,h+1,0} \qquad \forall j, h \in H \setminus |H| \tag{8.24}$$

$$\overline{Q}_{rj,|H|,0} + n_{|H|} \hat{Q}_{rj,|H|} = \overline{Q}_{rj,1,0} \qquad \forall j \tag{8.25}$$

8.3.7 *Objective function*

The objective of this work is to meet a given energy demand $D_{r,power,h,t}$ using chemical fuels. The fuels' heating values (H_j) and their average efficiencies (ν_j) are used to compute the amount of energy that can be produced from them.

$$\sum_{j \in \hat{J}} S_{rjht} H_j \nu_j \geq D_{r,power,h,t} \quad \forall r, h, t \in \overline{T_h} \tag{8.26}$$

The goal is to minimize the following objective function:

$$OP = \sum_i \sum_{m \in M_{ri}} \sum_r \sum_h \sum_t J_{rimht} + \sum_i \sum_m \sum_r \left(\alpha_j \bar{x}_{rj} + \beta_j C_{rj} \right) + \sum_{r,r'} \left(\sum_{j \in \hat{S}^r} \sum_j \sum_r \sum_{r'} \sum_m \sum_h \sum_t T_{jrr'dht} \Gamma_{jd} \right) \gamma_{rr'} + \sum_r \sum_h \sum_t \phi_{CO_2} B_{r,CO_2,ht} \tag{8.27}$$

which comprises the costs of production, storage and transportation. To estimate the production costs associated with the different processes, the methodology proposed by Sinnott (2014) is used. Two terms contribute to this cost for each process. The variable J_{rimht} is the operating cost of process i in mode m in time period t at location r. This term is calculated through a piece-wise linear approximation. The second term represents the part of the production cost related to the capital investment. A linear capital cost for each of the processes is assumed in this work. The linearization of the different capital costs of each of the procceses has been obtained from previous works (see Table 8.1). The cost associated with storage is represented by the third term of equation (8.27). It is assumed that the main contributor to this cost is the amortization of the capital cost for the storage facilities. A linear investment cost for the storage sites is assumed. The operating cost for storage is neglected as it is only a very small fraction of the total storage cost in the case of the considered chemical fuels (Connolly et al., 2016). The next term includes the transportation cost. The parameter Γ_{jd} denotes the shipment cost for resource j in the transportation mode d and $\gamma_{rr'}$ the distance between locations r and r'. Finally, to include the cost of CO_2 capture, a CO_2 price is included (ϕ_{CO_2}) in the objective function.

The piece-wise linear approximation used to compute the first term of equation (8.27), J_{rimht}, is as follows:

$$P_{rimht} = \sum_{l \in L_i} \left(\lambda_{rimhtl} \left(\hat{P}_{im,l-1} - \hat{P}_{im,l} \right) + \hat{P}_{iml}\, \omega_{rimhtl} \right) \quad \forall r, i, m \in M_{ri}, h, t \tag{8.28}$$

$$J_{rimht} = \sum_{l \in L_i} \left(\lambda_{rimhtl} \left(\hat{J}_{im,l-1} - \hat{J}_{im,l} \right) + \hat{J}_{iml}\, \omega_{rimhtl} \right) \quad \forall r, i, m \in M_{ri}, h, t \tag{8.29}$$

$$\lambda_{rimhtl} \leq \omega_{rimhtl} \quad \forall r, i, m \in M_{ri}, h, t, l \in L_i \tag{8.30}$$

$$\sum_{l \in L_i} \omega_{iktl} = y_{ikt} \quad \forall r, i, m \in M_{ri}, h, t \tag{8.31}$$

The optimization problem resulting from equations (8.1)-(8.31) is a mixed-integer linear program (MILP). All models used in this work were implemented in Julia using the JuMP package (Lubin & Dunning, 2015). The MILP problems were solved using CPLEX 12.8 with an optimality gap of 1%.

8.4 heuristic decomposition

If the proposed integrated model from Section 8.3 is solved as such, a large computational time is required, if tractable at all. Hence, a heuristic decomposition approach was considered to address the integrated supply chain and scheduling problem. The first step is to solve the supply chain problem using an aggregated production model. This multiperiod supply chain problem only includes a monthly time discretization; therefore, only average values of wind velocity or solar irradiance can be considered for each month. After solving this problem, the following results are extracted: the locations of the different production and storage facilities, the types of fuels to be produced and the transportation network including the mode of transportation used to meet the energy demand in each of the subregions.

In the second step, a detailed scheduling problem is solved for each of the production facilities to be built. The processes and storage alternatives (but not their capacities) selected in the supply chain optimization step are fixed in the scheduling problem. The demand of the different fuels is also fixed according to the supply chain results. Gas turbine and methane production can further be selected in the scheduling step in order to guarantee a minimum level of production in the chemical process units if no wind and solar sources are available. At the scheduling level, the production and storage capacities for the different production plants are optimized and the operating schedules for the installed facilities are determined.

Note that the supply chain problem in the first step is formulated such that all the energy storage required for each month is delivered at the beginning of the month. Since the energy storage can then be dispatched to generate energy on demand, it can be used to meet any hourly energy demand profile. As a result, the proposed heuristic approach is guaranteed to provide a feasible solution. This insight further highlights the advantage of long-term chemical energy storage, which allows us to decouple the production and distribution problem from the problem of operating the energy storage to meet the demand in different energy applications.

To get a sense of the effectiveness of this heuristic decomposition approach, a small problem is solved which allows a comparison between the results from solving the full size model and those obtained from the heuristic decomposition. Three locations and a time horizon of one month are selected (more details of this case study can be found in the Supplementary Information). The transport of chemicals is allowed only one time per month in the case of using train or truck, but continuous distribution is possible if a pipeline is used to transport the methane. First, the full integrated supply chain and scheduling problem is evaluated. This integrated model has approximately 1,065,000 variables and 621,000 constraints and was solved in about 150,000 s. Only one production facility is set up at location 1. In terms of the chemicals produced to meet the energy demand, only methane is selected. From location 1, methane is distributed to the other two locations. A combination of solar and wind is selected to capture the power required for the chemical production (see Table 8.2). A gas turbine is also selected to maintain a minimum rate of methane production when no wind or solar are available. Methane and hydrogen storages at the production facility (location 1) are used and methane is stored at locations 2 and 3 since no pipeline connection is available for these three places.

This problem is also solved using the proposed heuristic decomposition. Firstly, the supply chain problem is solved. The problem has around 950 variables and 720 equalities/inequalities and the solution time is less than 1 second. At this level, the location of the production facilities is determined with only one plant located at location 1 (as in the integrated problem). Only methane is produced and distributed among the locations. The amount of methane that must be transported is also determined at this step. In Table 8.2, the production capacities obtained solving the supply chain problem are included. These are only internal results of the heuristic decomposition because the actual values of these capacities are those obtained from the scheduling problem as explained next. For the production facility, located at location 1, the scheduling level is computed. From the supply chain solution, the process is fixed to use an eletrolyser and produce methane. PV panels and wind turbines are included to

Table 8.2: Comparison between the integrated model and the heuristic decomposition for the production capacities

	Integrated Model	Heuristic Decomposition	
		Supply Chain Problem (intermediate results)	Scheduling Problem (final results)
Solar	14,374 m^2 ($2 MM)	0 m^2 ($0 MM)	14,377 m^2 ($2 MM)
Wind	17,789 m^2 ($9 MM)	4,998 m^2 ($3 MM)	17,793 m^2 ($10 MM)
Eletrolyser	8,504 kW ($36 MM)	1,897 kW ($23 MM)	8,506 kW ($36 MM)
Methane	24 kW ($0.8 MM)	8 kW ($0.5 MM)	24 kW ($0.8 MM)
Gas Turbine	12 kW ($0.1 MM)	0 kW ($0 MM)	13 kW ($0.1 MM)

determine the optimal combination in the scheduling model. Finally, a gas turbine is also selected to maintain a certain level of production if no wind or solar based power is generated. This problem is around 295,000 variables and 194,000 constraints and was solved in approximately 3,001 s. The final production and storage capacities for the facility are obtained from this scheduling problem, see Table 8.2 for the details. One can observe a significant increase in the production capacities compared to those obtained in the supply chain problem. The total investment for the facility increases from $26.5 MM to $48.9 MM, about 80%. Solar PV panels and the gas turbine are included in the scheduling level regarding the supply chain results. This reflects the paramount importance of including the hourly time discretization in order to calculate the capacities required to handle the fast fluctuations in solar and wind availability.

From these results, one can see that by solving the supply chain problem, appropriate (i.e. optimal or near-optimal for the full problem) discrete decisions related to process selection and location are determined. Then, the scheduling problem determines the required capacities and the optimal operational decisions. Consequently, this heuristic decomposition provides a simple but effective means of obtaining a high-quality solution of the integrated supply chain and scheduling problem. In this particular case, it yields the same results as the original full model while reducing the computational time by more than 99%.

8.5 results and discussion

In the presented computational case study, a region of Spain, the province of Leon, is considered where coal-based power generation is especially significant, and, therefore, energy transition is particularly urgent. Currently, there are three coal-fired power plants with an installed capacity of about 2,300 MW. These facilities are being decommissioned in 2020 due to the new environmental restrictions imposed by the European Commission. This will have significant economic, environmental, and social impacts on the region. Therefore, an effective transition towards a more sustainable energy system is of utmost and urgent importance.

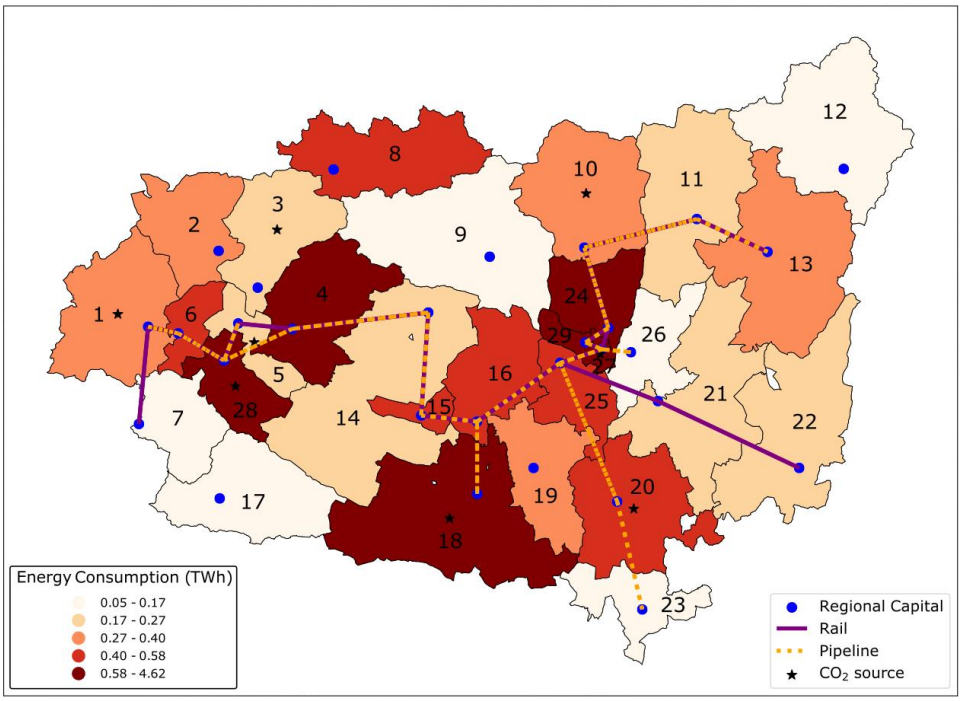

Figure 8.2: Province of Leon. Energy demand, installed infrastructure and CO_2 sources

The objective is to design a supply chain that is able to meet a given fraction of the local energy demand using the chemical fuels presented in Section 8.2. The total energy consumption in this region is about 17.2 TWh per year and it is distributed among four main items: power (11%), natural gas (13%), LPG (1%), and liquid fuels (75%) (Junta de Castilla y Leon, 2020). The province is divided into 29 subregions (see Figure 8.2) according to the administrative distribution (Junta de Castilla y Leon, 2017). The solar (ADRASE, 2020; ITACYL, 2020) and wind (DatosClima, 2020; ITACYL, 2020) availability are obtained for each of the locations from

public databases. It is assumed that CO_2 is obtained from the different plants with CO_2 emissions, such as sugar factories, co-generation facilities, paper industry, etc. through a carbon capture process. The cost of CO_2 is set to 50 \$/t (Rubin et al., 2015). Transportation by truck is available from one subregion to all its neighboring subregions. The connection by rail and pipeline are limited according to the installed infrastructure. In Figure 8.2, all the data about the current infrastructure and CO_2 sources are included with the energy consumption associated with each subregion with different color intensities (Secretaría de Estado de Energía, 2020). The cost of transportation is obtained from different sources for truck (Ministerio de Fomento, 2018), rail (Comisión Nacional de los Mercados y la Competencia, 2017) or pipeline (Saadi et al., 2018).

The maximum area to install PV panels and wind turbines is limited up to 0.5% of the total area of the subregion for each technology, and a maximum utilization of 30% of the total CO_2 emissions is also imposed. A time representation in which the year is divided into 24 seasons, two for each month, with each season represented by a time horizon of a week is applied. For each month, the first corresponding season is the first week of that month in which transportation of chemical fuels using truck or rail is allowed. The second season represents the remaining three weeks of the month in which no distribution via truck and rail is considered.

The heuristic decomposition of Section 8.4 is applied to solve this problem. The first step is the supply chain level. The size of supply chain problem of this region is about 73,000 variables (18,000 binary variables) and about 110,000 constraints. Considering the total energy consumption of the region, 17.2 TWh, a total energy demand of 1 TWh has been considered as the maximum level for the fuels. Then, the problem is solved for different levels of this maximum energy demand (25%, 50%, 75% and 100%). Figure 8.3 shows the locations of the production facilities for the four different energy demand rates and the fuels that are produced in each of the facilities.

When the target is to produce 25% of the total energy demand, only three production plants are built and only carbon-based fuels are used (methane and methanol). However, when the energy demand increases, more fuel production is required and the use of ammonia is introduced in the network. As ammonia is a carbon-free chemical, it can be produced in every subregion. According to the results, ammonia is more expensive to produce than some of the carbon-based fuels, however, it is needed when the availibility of CO_2 is limited, which may become an important factor as CO_2 emissions will decrease in the future. As one can see in Figure 8.3, ammonia represents a high percentage of the chemicals to be synthesized when the energy demand rate increases to 75% or 100%. The areas where

carbon-based fuels are synthesized remain almost constant for the high rates of energy demand (75% or 100%).

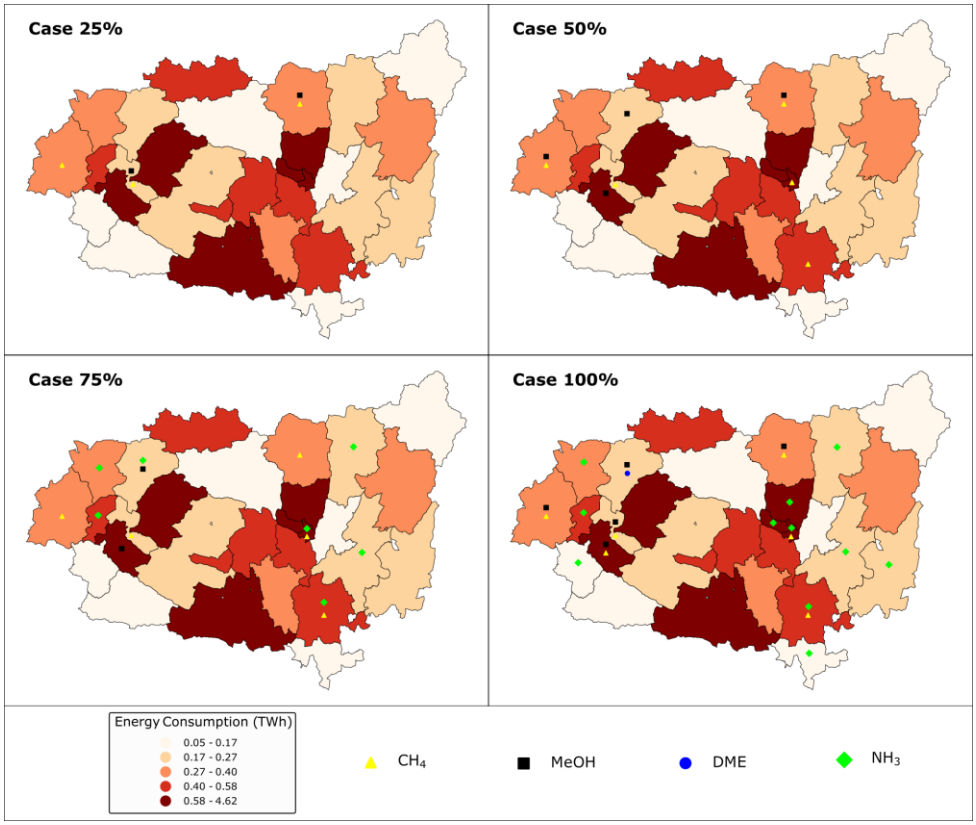

Figure 8.3: Supply chain results for different rates of the energy demand

For further analysis, this work focuses on the case of 50% energy demand. The transportation network for this particular case is shown in Figure 8.4. The preferred way of transporting methane is via the existing pipeline. This alternative allows a continuous transfer of the product, reducing the storage capital and operating cost, and it is competitive in economic terms. Between the truck and rail connections, the latter is preferred due to the lower operating cost. Therefore, if rail infrastructure is available, this way is selected to distribute the fuels.

The amount of fuels transported is higher during the spring/summer months (for instance, April or July in Figure 8.4). This is due to the higher production of power during spring/summer months (as it is shown later), therefore the fuel production increases and the amount of products to ship is larger.

The next step is to solve the scheduling problem for the seven selected production facilities. Some of the results are presented here to illustrate the

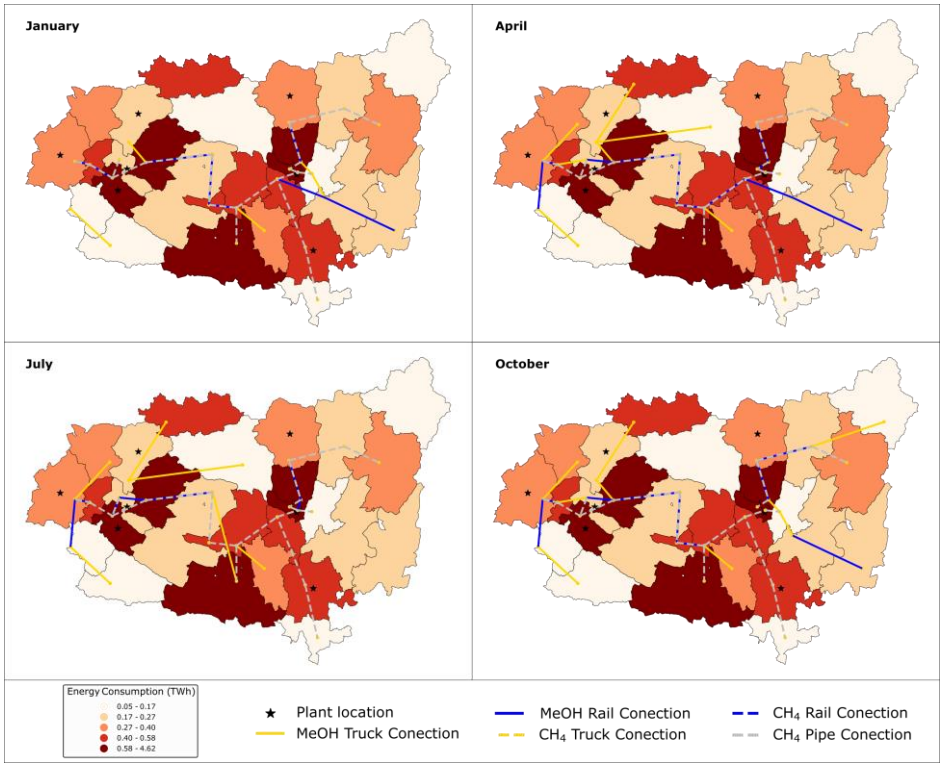

Figure 8.4: Transportation network for different months of the year

behavior of the production plants. For each plant, the scheduling model has about 3.1 million variables (including 1.9 million binary variables) and 2.1 million constraints. For the sake of brevity, the results for only two of the plants are shown. The first one (located in subregion 27) produces only methane and is located at the center of the province. The second is in the most western subregion (subregion 1) where two fuels are produced, methanol and methane.

First, the facility with only methane production is analyzed. Figure 8.5 shows the scheduling results of two representative weeks for two different months: July and November. There are three sources of power for the different processes: PV panels, wind turbines or gas turbine. The storage level of hydrogen for the different hours is represented by the black line. In July, the power production is higher than in November. During July, more solar-based power generation is produced because the solar irradiance received is larger. In November, solar energy is much lower and wind represents the main power source during this period. The gas turbine only represents a minor fraction of the total power production, reaching zero in some hours. The hydrogen storage is used to mitigate the fluctuations in

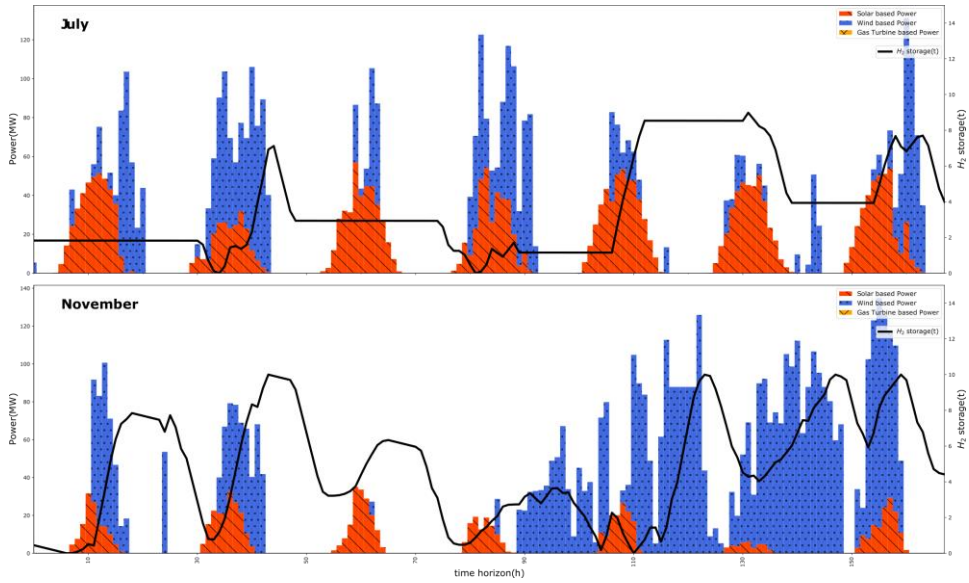

Figure 8.5: Scheduling results for facility at location one for two different months

the renewable based power generation to keep a certain level of production in the chemical manufacturing. In July, hydrogen is stored mainly during the daytime and used at night. The more time-sensitive profile of wind velocity in November results in a different storage schedule for this month.

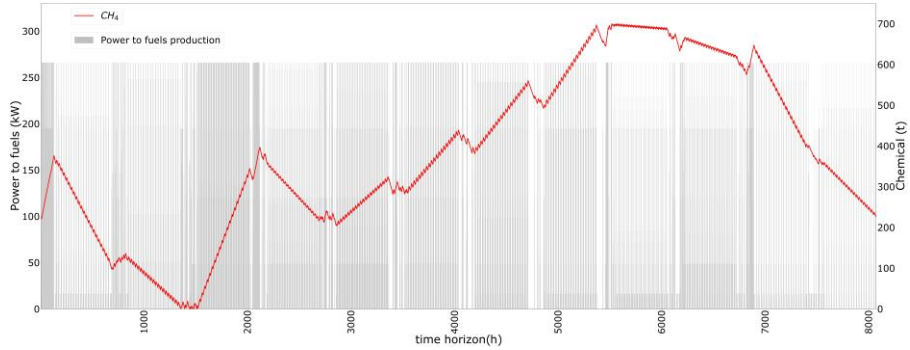

Figure 8.6: Methane storage/production along the year for facility in subregion 27

Figure 8.6 presents the methane storage level for this facility over the course of the year (red line) and, in gray columns, the power used for the production of methane in each time period. Methane synthesis is more intense during the spring/summer time due to the higher power generation from wind and solar. It is stored during spring/summer reaching the maximum storage level in September/October. Methane is consumed, mainly, during autumn/winter, with the minimum storage in February.

It is clear that a significant seasonal storage of the chemical is shown, revealing one of the most important advantages of the use of chemical fuels for energy storage.

The next facility analyzed produces methanol and methane. The scheduling results for a facility where two fuels are synthesized are shown in this section. Firstly, as in the previous case, the power production of two different representative weeks in two particular months is presented (see Figure 8.7). The results are similar to those obtained in the previous case. Power production is more intense in July than in November. About 250 MW can be produced during some hours of July; however, in November the maximum power production is around 175 MW. Solar is the main source in July, where the longer days translate into higher energy production. Wind has a larger share in November. Different hydrogen storage level profiles are obtained following the availability of solar and wind trying to mitigate their fluctuations.

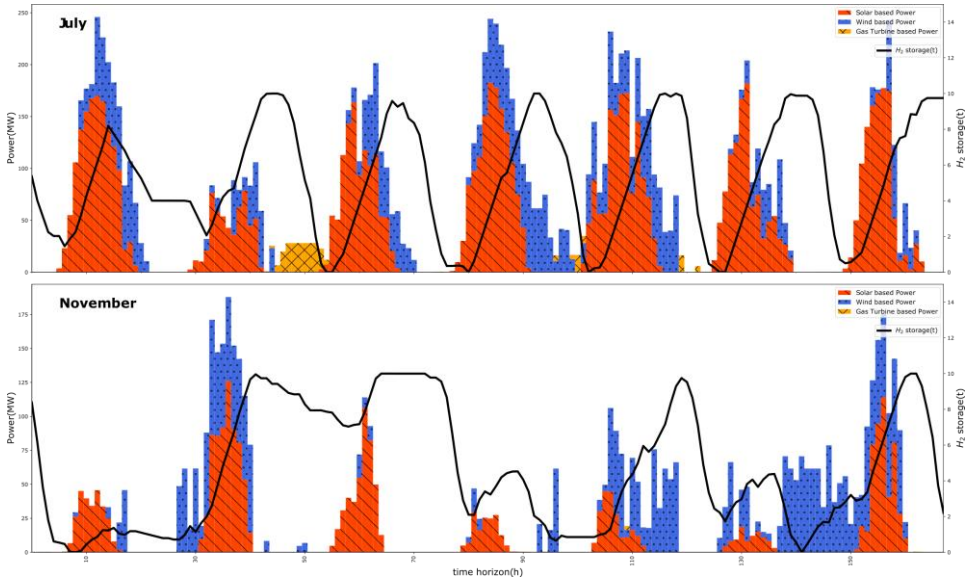

Figure 8.7: Scheduling results for facility at location three for two different months

Figure 8.8 presents the storage levels for methanol and methane over the course of the year. Power devoted to the production of chemicals is depicted as gray columns. As methanol is a liquid fuel, only rail and truck are available to transport it. Therefore, only one load each month is allowed (at the beginning of the month). During spring/summer time, methanol (blue line) is stored reaching the maximum storage in October/November with about 2,500 t of methanol. The stored methanol is mainly used to meet the demand during winter, and the minimum storage level is achieved

in February/March. In the case of methane, since can be distributed continuously through pipelines, the storage levels are lower. Storage of a gas such as methane is difficult, therefore, the preferred option for seasonal storage is liquid fuels such as methanol at this location.

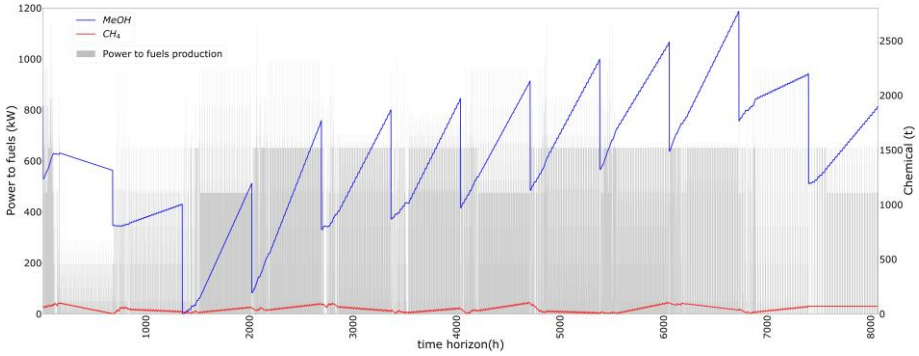

Figure 8.8: Methanol/Methane storage/production along the year for facility in subregion 1

The design decisions for all facilities built in the network are presented in Table 8.3. In total, the network requires an investment of $2,341 MM, including the production facilities and the storage sites, and the total production cost of the network is up to $198 MM per year.

Table 8.3: Production capacities for the facilities in the region of Leon (Spain)

	Plant 1	Plant 3	Plant 5	Plant 10	Plant 20	Plant 27	Plant 28
PV panels (km^2)	0.882	0.365	0.069	1.230	0.115	0.264	1.077
Wind Turbine (number of turbines)	25	11	2	32	5	36	0
Electrolyser (kW)	84,741	35,263	5,424	89,233	11,432	86,779	64,816
DME (kW)	0	0	0	0	0	0	0
CH_4 (kW)	487	5	17	487	25	266	5
MeOH (kW)	651	494	0	1,423	0	0	996
NH_3 (kW)	0	0	0	0	0	0	0
Gas turbine (kW)	28,046	485	6	442	0	0	485

8.6 conclusions

In this work, an integrated supply chain and scheduling model has been proposed to determine the optimal power-to-fuels supply network for a given geographical region. A heuristic decomposition method has been developed that achieves high-quality solutions in a reasonable computa-

tional time. The proposed decomposition has been validated for a small case study achieving the same results as using the full formulation. The proposed framework has been applied to a region of Spain, where the energy transition is especially significant. The results show that carbon-based fuels such as methane or methanol are preferred when energy demand is low but ammonia is introduced when this demand increases because its production is not limited by the availability of CO_2. Liquid fuels such as methanol or ammonia are used for seasonal storage of energy due to the ease and low cost storage. During spring/summer time more energy is produced and devoted to the manufacturing of fuels that are stored for use during autumn/winter seasons. This work shows the potential of power-to-fuels technologies to provide seasonal energy storage, ultimately enabling higher penetration of renewable energy sources. In particular, these results indicate the significant advantages of power-to-fuels supply chains in addressing changes at multiple temporal scales and serving demands at distributed locations.

nomenclature

Indices / sets/ subsets

$\hat{B}$	resources use as raw material of the network
$h \in H$	seasons in the multiscale time representation
$i \in I$	processes evaluated in the power to fuel network
$j \in J$	resources involved in the network
$\hat{J}$	product with associated demand
$l \in L$	segments in operating cost
	piecewise-linear approximations
L_i	segments in piecewise-linear approximation
$m \in M$	operating modes for each of the process
M_{ri}	operating modes for a process
$\hat{N}_{jrr'}$	transportation modes available between two locations
$\hat{R}_{jr}$	location to distribute a product from one site
$\hat{S}$	resources that could be stored
$t \in T$	time periods in the multiscale time representation
$\overline{T}_h$	time periods in season h
$\overline{TR}_{im}$	mode transitions to reach mode m

TR_{im} mode transtions to progress from mode m

TR_i predefined sequences of mode transitions

Parameters

$R_{rjmt}^{\max}$ maximum resource that can be consumed

$C_i^{\max}$ maximum production capacity

$\overline{C}_i^{\max}$ maximum storage capacity

$\overline{\mathbf{v}}_{im}^{\max}$ maximum production in a given mode

$\underline{\mathbf{v}}_{im}^{\min}$ minimum production in a given mode

$D_{r,power,h,t}$ power demand

$\hat{J}_{iml}$ operating cost for piecewise-linear approximation

$\overline{M}$ big-M parameter

n_h number of repetition of the horizon scheduling for a season

$\hat{P}_{iml}$ production level for piecewise-linear approximation

ρ_{ij} conversion factor of the different products with respect to the reference resource

η_{riht} availability of production capacity for wind/solar

$\overline{\Lambda}_{im}^{\max}$ maximum rate of change

$\theta_{imm'}$ minimum stay time in a certain mode

$\theta_{imm'm''}$ fixed stay time for a predefined sequence

$\theta^{\max}$ stay time in a mode

σ_i conversion factor between capital and operating cost for a process

δ_i fixed capital cost coefficient

γ_i unit capital cost coefficient

α_j annualized fixed capital cost for storing

β_j annualized unit capital cost for storing

$\Gamma_{j,d}$ unit cost of transportation

$\Upsilon_{r,r'}$ distance between two locations

Δt length of one time period

λ_{rimhtl} coefficient for piecewise-linear approximation

ν_j average efficiency in the fuel

	to power transformation
ϕ_{CO_2}	Cost of captured carbon dioxide

Variables

B_{rjht}	amount of resource consumed
C_{ri}	production capacity for different processes
$\overline{C}_{rj}$	storage capacity for different resources
J_{rimht}	process operating cost not related to capital cost
OP	Operating cost
P_{riht}	amount of reference resource produced
$\overline{P}_{imht}$	reference resource produced in certain mode
$\overline{Q}_{rjht}$	inventory level
$\hat{Q}_{rjh}$	net inventory in a season
S_{rjht}	amount of resource release
$T_{jrr'dht}$	amount of transported resource in the different transportation alternatives
$W_{jrr'ht}$	amount of transported resource
x_{ri}	binary variable to select process units
$\overline{x}_{ri}$	binary variable to select storage units
y_{imht}	binary variable to select a mode for a specific process
$z_{imm'ht}$	binary variable for mode transitions
w_{rimhtl}	binary variable for piecewise-linear aproximation

acknowledgments

The authors acknowledge the FPU, Spain grant (FPU16/06212) and the mobility grant (EST18/0052) from Government of Spain to A.S., and MINECO, Spain grant DPI2015-67341-C2-1-R.

bibliography

Castro, P. M., Barbosa-Póvoa, A. P., Matos, H. A., & Novais, A. Q. (2004). Simple continuous-time formulation for short-term scheduling of batch and continuous processes. *Industrial & Engineering Chemistry Research*, *43*(1), 105–118. https://doi.org/10.1021/ie0302995

Larsen, H. H., & Petersen, L. S. (2013). *Dtu international energy report 2013: Energy storage options for future sustainable energy systems*. Technical University of Denmark.

Davis, W., & Martín, M. (2014). Optimal year-round operation for methane production from co2 and water using wind and/or solar energy. *Journal of Cleaner Production*, *80*, 252–261. https://doi.org/10.1016/j.jclepro.2014.05.077

Sinnott, R. (2014). *Chemical engineering design* (Vol. 6). Elsevier.

Lubin, M., & Dunning, I. (2015). Computing in operations research using julia. *INFORMS Journal on Computing*, *27*(2), 238–248. https://doi.org/10.1287/ijoc.2014.0623

Nejat, P., Jomehzadeh, F., Taheri, M. M., Gohari, M., & Abd. Majid, M. Z. (2015). A global review of energy consumption, co2 emissions and policy in the residential sector (with an overview of the top ten co2 emitting countries). *Renewable and Sustainable Energy Reviews*, *43*, 843–862. https://doi.org/10.1016/j.rser.2014.11.066

Rubin, E. S., Davison, J. E., & Herzog, H. J. (2015). The cost of co2 capture and storage. *International Journal of Greenhouse Gas Control*, *40*, 378–400. https://doi.org/10.1016/j.ijggc.2015.05.018

Sternberg, A., & Bardow, A. (2015). Power-to-what? – environmental assessment of energy storage systems. *Energy Environ. Sci.*, *8*, 389–400. https://doi.org/10.1039/C4EE03051F

Connolly, D., Lund, H., & Mathiesen, B. (2016). Smart energy europe: The technical and economic impact of one potential 100% renewable energy scenario for the european union. *Renewable and Sustainable Energy Reviews*, *60*, 1634–1653. https://doi.org/10.1016/j.rser.2016.02.025

de la Cruz, V., & Martín, M. (2016). Characterization and optimal site matching of wind turbines: Effects on the economics of synthetic methane production. *Journal of Cleaner Production*, *133*, 1302–1311. https://doi.org/10.1016/j.jclepro.2016.06.019

León, E., & Martín, M. (2016). Optimal production of power in a combined cycle from manure based biogas. *Energy Conversion and Management*, *114*, 89–99. https://doi.org/10.1016/j.enconman.2016.02.002

Martín, M. (2016a). Methodology for solar and wind energy chemical storage facilities design under uncertainty: Methanol production from co2 and hydrogen. *Computers & Chemical Engineering*, *92*, 43–54. https://doi.org/10.1016/j.compchemeng.2016.05.001

Martín, M. (2016b). Optimal year-round production of dme from co2 and water using renewable energy. *Journal of CO2 Utilization*, *13*, 105–113. https://doi.org/10.1016/j.jcou.2016.01.003

Sternberg, A., & Bardow, A. (2016). Life cycle assessment of power-to-gas: Syngas vs methane. *ACS Sustainable Chemistry & Engineering*, *4*(8), 4156–4165. https://doi.org/10.1021/acssuschemeng.6b00644

Zhang, Q., Sundaramoorthy, A., Grossmann, I. E., & Pinto, J. M. (2016). A discrete-time scheduling model for continuous power-intensive process networks with various power contracts. *Computers & Chemical Engineering*, *84*, 382–393. https://doi.org/10.1016/j.compchemeng.2015.09.019

Comisión Nacional de los Mercados y la Competencia. (2017). Informe sobre los servicios de transprote de mercancías por ferrocarril 2017. Retrieved May 8, 2020, from https://www.cnmc.es/sites/default/files/2264652_5.pdf

Giddey, S., Badwal, S. P. S., Munnings, C., & Dolan, M. (2017). Ammonia as a renewable energy transportation media. *ACS Sustainable Chemistry & Engineering*, *5*(11), 10231–10239. https://doi.org/10.1021/acssuschemeng.7b02219

Heuberger, C. F., Staffell, I., Shah, N., & Dowell, N. M. (2017). A systems approach to quantifying the value of power generation and energy storage technologies in future electricity networks. *Computers & Chemical Engineering*, *107*, 247–256. https://doi.org/10.1016/j.compchemeng.2017.05.012

Junta de Castilla y Leon. (2017). La junta aprueba el mapa de unidades básicas de ordenación y servicios del territorio de castilla y león. Retrieved July 2, 2020, from http://comunicacion.jcyl.es/web/jcyl/Comunicacion/es/Plantilla100Detalle/1281372057192/_/1284703452143/Comunicacion?platform=hootsuite

Wang, G., Mitsos, A., & Marquardt, W. (2017). Conceptual design of ammonia-based energy storage system: System design and time-invariant performance. *AIChE Journal*, *63*(5), 1620–1637. https://doi.org/10.1002/aic.15660

Daggash, H. A., Patzschke, C. F., Heuberger, C. F., Zhu, L., Hellgardt, K., Fennell, P. S., Bhave, A. N., Bardow, A., & Mac Dowell, N. (2018). Closing the carbon cycle to maximise climate change mitigation: Power-to-methanol vs. power-to-direct air capture. *Sustainable Energy Fuels*, *2*, 1153–1169. https://doi.org/10.1039/C8SE00061A

García-Olivares, A., Solé, J., & Osychenko, O. (2018). Transportation in a 100% renewable energy system. *Energy Conversion and Management*, *158*, 266–285. https://doi.org/10.1016/j.enconman.2017.12.053

Gür, T. M. (2018). Review of electrical energy storage technologies, materials and systems: Challenges and prospects for large-scale grid storage. *Energy Environ. Sci.*, *11*, 2696–2767. https://doi.org/10.1039/C8EE01419A

Leonard, M. D., Michaelides, E. E., & Michaelides, D. N. (2018). Substitution of coal power plants with renewable energy sources – shift of the power demand and energy storage. *Energy Conversion and Management*, *164*, 27–35. https://doi.org/10.1016/j.enconman.2018.02.083

Ministerio de Fomento. (2018). Obsrvatorio de costes del transporte de mercancías por carretera. Retrieved May 7, 2020, from http://www.fomento.es/MFOM.CP.Web/handlers/pdfhandler.ashx?idpub=TTW128

Saadi, F. H., Lewis, N. S., & McFarland, E. W. (2018). Relative costs of transporting electrical and chemical energy. *Energy Environ. Sci.*, *11*, 469–475. https://doi.org/10.1039/C7EE01987D

Sánchez, A., & Martín, M. (2018a). Optimal renewable production of ammonia from water and air. *Journal of Cleaner Production*, *178*, 325–342. https://doi.org/10.1016/j.jclepro.2017.12.279

Sánchez, A., & Martín, M. (2018b). Scale up and scale down issues of renewable ammonia plants: Towards modular design. *Sustainable Production and Consumption*, *16*, 176–192. https://doi.org/10.1016/j.spc.2018.08.001

BloombergNEF. (2019). New energy outlook 2019. Retrieved July 7, 2020, from https://about.bnef.com/new-energy-outlook/

Ogumerem, G. S., Tso, W. W., Demirhan, C. D., Lee, S. Y., Song, H. E., & Pistikopoulos, E. N. (2019). Toward the optimization of hydrogen, ammonia, and methanol supply chains. *IFAC-PapersOnLine*, *52*(1), 844–849. https://doi.org/10.1016/j.ifacol.2019.06.167

Thema, M., Bauer, F., & Sterner, M. (2019). Power-to-gas: Electrolysis and methanation status review. *Renewable and Sustainable Energy Reviews*, *112*, 775–787. https://doi.org/10.1016/j.rser.2019.06.030

Zhang, Q., Martín, M., & Grossmann, I. E. (2019). Integrated design and operation of renewables-based fuels and power production networks. *Computers & Chemical Engineering*, *122*, 80–92. https://doi.org/10.1016/j.compchemeng.2018.06.018

Zhang, Y., Wang, L., Wang, N., Duan, L., Zong, Y., You, S., Maréchal, F., Van herle, J., & Yang, Y. (2019). Balancing wind-power fluctuation via onsite storage under uncertainty: Power-to-hydrogen-to-power versus lithium battery. *Renewable and Sustainable Energy Reviews*, *116*, 109465. https://doi.org/10.1016/j.rser.2019.109465

ADRASE. (2020). Acceso a datos de radiación solar de españa, mapa zona península. Retrieved May 7, 2020, from http://www.adrase.com/

Ajanovic, A., Hiesl, A., & Haas, R. (2020). On the role of storage for electricity in smart energy systems. *Energy*, *200*, 117473. https://doi.org/10.1016/j.energy.2020.117473

Al-Breiki, M., & Bicer, Y. (2020). Technical assessment of liquefied natural gas, ammonia and methanol for overseas energy transport based on energy and exergy analyses. *International Journal of Hydrogen Energy*, *45*(60), 34927–34937. https://doi.org/10.1016/j.ijhydene.2020.04.181

Al-Qahtani, A., González-Garay, A., Bernardi, A., Galán-Martín, Á., Pozo, C., Dowell, N. M., Chachuat, B., & Guillén-Gosálbez, G. (2020). Electricity grid decarbonisation or green methanol fuel? a life-cycle modelling and analysis of todays transportation-power nexus. *Applied Energy*, *265*, 114718. https://doi.org/10.1016/j.apenergy.2020.114718

Alves, M., Segurado, R., & Costa, M. (2020). On the road to 100% renewable energy systems in isolated islands. *Energy*, *198*, 117321. https://doi.org/10.1016/j.energy.2020.117321

Bartela, L. (2020). A hybrid energy storage system using compressed air and hydrogen as the energy carrier. *Energy*, *196*, 117088. https://doi.org/10.1016/j.energy.2020.117088

Blanco, H., Codina, V., Laurent, A., Nijs, W., Maréchal, F., & Faaij, A. (2020). Life cycle assessment integration into energy system models: An application for power-to-methane in the eu. *Applied Energy*, *259*, 114160. https://doi.org/10.1016/j.apenergy.2019.114160

Burre, J., Bongartz, D., Brée, L., Roh, K., & Mitsos, A. (2020). Power-to-x: Between electricity storage, e-production, and demand side management. *Chemie Ingenieur Technik*, *92*(1-2), 74–84. https://doi.org/10.1002/cite.201900102

DatosClima. (2020). Datos de viento para una estación meteorológica. Retrieved May 7, 2020, from https://datosclima.es/Aemethistorico/Viento.php

Demirhan, C. D., Tso, W. W., Powell, J. B., Heuberger, C. F., & Pistikopoulos, E. N. (2020). A multiscale energy systems engineering approach for renewable power generation and storage optimization. *Industrial & Engineering Chemistry Research*, *59*(16), 7706–7721. https://doi.org/10.1021/acs.iecr.0c00436

Ehrenstein, M., Galán-Martín, Á., Tulus, V., & Guillén-Gosálbez, G. (2020). Optimising fuel supply chains within planetary boundaries: A case study of hydrogen for road transport in the uk. *Applied Energy*, *276*, 115486. https://doi.org/10.1016/j.apenergy.2020.115486

ITACYL. (2020). Datos meteorógicos. Retrieved May 7, 2020, from http://www.itacyl.es/agro- y- geo- tecnologia/agrometeorologia- y-suelos/datos-meteorologicos

Junta de Castilla y Leon. (2020). Estadisticas energéticas de castilla y león. Retrieved February 2, 2021, from https://energia.jcyl.es/web/es/biblioteca/boletin-estadisticas-energeticas.html

Mehigan, L., Al Kez, D., Collins, S., Foley, A., Ó'Gallachóir, B., & Deane, P. (2020). Renewables in the european power system and the impact on system rotational inertia. *Energy*, *203*, 117776. https://doi.org/10.1016/j.energy.2020.117776

Secretaría de Estado de Energía. (2020). Estadísticas y balances energéticos: Eléctricas 2016-2018. Retrieved May 7, 2020, from https://energia.gob . es / balances / Publicaciones / ElectricasAnuales / Paginas / Electricas-Anuales2016-2018.aspx

Seo, S.-K., Yun, D.-Y., & Lee, C.-J. (2020). Design and optimization of a hydrogen supply chain using a centralized storage model. *Applied Energy*, *262*, 114452. https://doi.org/10.1016/j.apenergy.2019.114452

Stančin, H., Mikulčić, H., Wang, X., & Duić, N. (2020). A review on alternative fuels in future energy system. *Renewable and Sustainable Energy Reviews*, *128*, 109927. https://doi.org/10.1016/j.rser.2020.109927

Wang, L., Zhang, Y., Pérez-Fortes, M., Aubin, P., Lin, T.-E., Yang, Y., Maréchal, F., & Van herle, J. (2020). Reversible solid-oxide cell stack based power-to-x-to-power systems: Comparison of thermodynamic performance. *Applied Energy*, *275*, 115330. https://doi.org/10.1016/j.apenergy.2020.115330

Thomaßen, G., Kavvadias, K., & Jiménez Navarro, J. P. (2021). The decarbonisation of the eu heating sector through electrification: A parametric analysis. *Energy Policy*, *148*, 111929. https://doi.org/10.1016/j.enpol.2020.111929

9

TOWARDS A NEW RENEWABLE POWER SYSTEM USING ENERGY STORAGE: AN ECONOMIC AND SOCIAL ANALYSIS

abstract

The energy transition is one of the main challenges in mitigating the CO_2 emissions from the power sector. Solar and wind resources are presented as the two most promising alternatives in the future energy mix. However, the inherent fluctuations of these two resources jeopardize the stability of the grid. To overcome this issue, the combination of intermittent and non-intermittent renewable energies along with different storage technologies is proposed. In this work, the integration of these technologies is evaluated using different future scenarios. Three renewable resources have been analyzed (solar, wind, and biomass) in combination with four different storage systems (battery, hydrogen, methane, and ammonia). This problem has been evaluated from two different perspectives, economic and social (for which a new indicator is developed), for several regions of Spain. The results show the paramount importance of using storage alternatives to satisfy the demand and to store energy seasonally. In economic terms, an average cost of electricity of about 100-200 €/MWh is expected with a high influence of the ratios of wind and solar in the different locations and the selected storage alternatives. Additionally, the proposed social index indicates the regions where these facilities could be installed to mitigate social inequalities. With this two-pronged approach, an orderly, fair, and efficient planning of the energy transition can be realized to achieve climate sustainability goals.

Keywords: Energy storage, Energy transition, Power-to-X, Renewable energy, Social index

resumen

La transición energética es uno de los principales retos para mitigar las emisiones de CO_2 del sector eléctrico. Los recursos solar y eólico se presentan como las dos alternativas más prometedoras en el futuro mix energético. Sin embargo, las fluctuaciones inherentes a estos dos recursos ponen en peligro la estabilidad de la red. Para superar este problema, se propone la combinación de energías renovables intermitentes y no intermitentes junto con diferentes tecnologías de almacenamiento. En este trabajo se evalúa la integración de estas tecnologías utilizando diferentes futuros escenarios. Se han analizado tres recursos renovables (solar, eólica y biomasa) en combinación con cuatro sistemas de almacenamiento diferentes (batería, hidrógeno, metano y amoníaco). Este problema se ha evaluado desde dos perspectivas diferentes, la económica y la social (para la que se desarrolla un nuevo indicador), para varias regiones de España. Los resultados muestran la gran importancia de utilizar alternativas de almacenamiento para satisfacer la demanda y almacenar energía estacionalmente. En términos económicos, se espera un coste medio de la electricidad de unos 100-200 €/MWh, con una gran influencia de los ratios de eólica y solar en las diferentes localizaciones y de las alternativas de almacenamiento seleccionadas. Además, el índice social propuesto indica las regiones donde podrían instalarse estas instalaciones para mitigar las desigualdades sociales. Con este doble enfoque, se puede realizar una planificación ordenada, justa y eficiente de la transición energética para alcanzar los objetivos de sostenibilidad climática.

Palabras clave: Almacenamiento energético, Transición energetica, Power-to-X, Energía renovable, Índice social

9.1 introduction

The energy transition is an especially urgent issue today to meet global environmental agreements. The Sustainable Development Goals (SDGs) by the United Nations state, in SDG 7, that access to affordable, reliable, sustainable, and modern energy must be ensured for all (UN General Assembly, 2015). In line with this goal, the Paris Agreement emphasizes sustainable energy production as a major means to reduce global temperature rise to below 2°C above pre-industrial levels (Roelfsema et al., 2020). To meet the proposed targets, the entire energy system needs to be decarbonized. In this objective, the decarbonization of the power system is crucial since this sector accounts for around 25% of the total CO_2 emissions (EPA, 2021). Increasing the share of renewable energy sources (RES) will be the main strategy for sustainable electricity generation. Wind and solar will represent the two main RES with 56% of the total electricity generation by 2050 (BloombergNEF, 2020). However, these resources are inherently intermittent, and coping with this nature constitutes the main challenge for the new electricity system. To ensure the robustness and stability of the grid as well as the balance between electricity production and demand, a new integrated system based on intermittent and non-intermittent renewable sources and energy storage is needed (Bagherian & Mehranzamir, 2020).

Numerous energy storage technologies have been proposed for various time scales and power capacities (Gür, 2018), and with different environmental impacts (Sternberg & Bardow, 2015). While compressed-air energy storage (CAES) and pumped-hydro are the two options for commercial-scale at present (Alirahmi et al., 2021), batteries and H_2-based alternatives has risen as the two most promising choices for minimizing the cost of storage (Schmidt et al., 2019). On the one hand, batteries have been proposed for different applications in residential and grid-scale uses. Corengia and Torres (2018) optimize the operation of a consumer Li-ion battery considering tariff policy and battery degradation. The main trade-off lies between energy saving due to the possibility of storing low-price electricity and the cost of battery replacement. Different types of batteries have also been analyzed for this storage purpose such as lead-acid, NaS, or Li-ion (Jiang et al., 2020). On the other hand, H_2 and different H_2-derived fuels (such as methanol (Chen & Yang, 2021) or ammonia (H. Zhang et al., 2020)) have been considered for seasonal and long-term storage (Stančin et al., 2020). Wulf et al. (2020) summarized the main Power-to-X projects in Europe showing the rapid rate of increase in the current years with more than 220 project by June 2020. At this point, different works have addressed the problem of integrating renewable power generation with

energy storage. Leonard et al. (2018) integrated power generation using wind turbines or solar PV panels with H_2 production as a pathway for energy storage. They proposed this alternative as an option to replace traditional base load coal power production. No restrictions have been imposed on H_2 storage, resulting in large storage capacities that are a challenge today. Palys and Daoutidis (2020) proposed a system with H_2 and NH_3 as energy storage alternatives. The cost of electricity for different locations in the U.S. has been assessed using the proposed system. The integrated ammonia energy storage framework is especially suitable for areas with high wind potential and strong demand variability. Demirhan et al. (2020) proposed the synthesis of dense energy carriers (DEC) to reduce the cost of renewable energy in areas with lower potential, in particular, they studied the connection between Texas and New York in the U.S. Other authors have evaluated the impact of integrating intermittent and non-intermittent renewables. Bagheri et al. (2019) proposed a 100% renewable system based on a combination of wind, solar, and biomass together with batteries. According to their results, biomass can mitigate the high cost of electricity in an integrated renewable system. The integration of concentrated solar power (CSP) and different biomass (Vidal & Martín, 2015) or waste (de la Fuente & Martín, 2020) has also been evaluated. The location plays a key role due to the different solar irradiance profiles and the contrasting biomass/waste availability of rural and urban areas.

But, the energy transition is not only a technical or economic challenge. The social impact of the energy transition must also be taken into account (Carley & Konisky, 2020). One of the main consequences of the energy transition is the decline in the use of coal as an energy resource. Therefore, employment opportunities decrease in this sector including mining and power facilities. In particular, job losses are concentrated in rural areas with low population density, aging problems, etc. This is the case of Spain, which this work focuses on, with the main traditional power plants located in rural areas. The Spanish government has introduced a new strategy to try to mitigate the effects of the energy transition in areas where coal and nuclear sources are in decline. The public policies are focused on creating new job opportunities, increasing the population in rural areas, or promoting new economic activities. All these measures are included under the umbrella of the so-called "fair transition strategy" (Ministerio para la Transicion Ecologica y el Reto Demografico, 2021). The introduction of renewable energies and also the storage technologies at grid-scale can mitigate the social effects of the transition if these facilities are installed in these particularly affected areas (Fragkos & Paroussos, 2018). Different job opportunities can be generated depending on the stage of the facilities: construction, manufacturing, etc. (Cartelle Barros et al., 2017). But, clearly,

this social factor should be considered in the implementation of a new renewable energy system.

Therefore, a holistic approach is necessary to tackle this energy production/storage problem in the context of the energy transition considering economic and social aspects. First, an integrated facility for power production and storage is evaluated considering a combination of intermittent (wind/solar) and non-intermittent (biomass) resources together with energy storage. Four different storage alternatives have been evaluated: batteries, hydrogen, and ammonia/methane to capture the different storage timescales. In previous literature, only a partial approach is considered either using only batteries or Power-to-X storage in combination with wind or solar production or considering intermittent and non-intermittent sources but without energy storage. However, an integrated approach is necessary to develop a new power system considering all the available technologies to guarantee demand satisfaction. And this approach has been followed in this work. But, it is not only the economic and technical aspects that have been previously and traditionally mentioned. The social impact of the energy transition to locate these integrated facilities have also been assessed. To evaluate this impact, this work has proposed a new social index based on two main factors: the impact of the energy transition and the general social environment of the region. Only very few previous works have addressed this issue by quantifying the social impact (Heras & Martín, 2020). Consequently, the integration of all sources and technologies to ensure power production is required in addressing this challenge from a social and economic perspective, and, to the best of our knowledge, no research in this area is performed.

The remainder of this work is organized as follows. In Section 9.2, an overview of the proposed superstructure for an integrated facility including power production and storage is included together with the modeling approach follows in this work. In Section 9.3, to evaluate the social impact of these facilities, a new social index is proposed. Section 9.4 presents the main results of the work grouped in three blocks: operating, economic and social results. Finally, some conclusions are drawn in Section 9.5.

9.2 process description and model formulation

The first goal of this work is to determine the optimal design and scheduling of power facilities integrating different intermittent and non-intermittent renewable resources and various energy storage alternatives to minimize the operating cost of satisfying a given power demand regardless of the availability of renewable resources. For this purpose, the

superstructure presented in Figure 9.1 is considered with all the processes listed in Table 9.1. Two different intermittent RES have been introduced in the framework: solar (photovoltaic panels) and wind (wind turbines). In addition, biomass is also incorporated as a non-intermittent RES. For energy storage, four different pathways have been evaluated: Li-ion batteries, hydrogen, and methane/ammonia. Methane has been selected due to the possibility of using the existing natural gas infrastructure for energy storage. Furthermore, ammonia has also been evaluated because it is a carbon-free chemical that can be used for energy storage in the future scenario aiming for complete decarbonization. Using this general framework, three different scenarios have been studied:

- **Scenario 1**: Wind and solar have been considered as input resources. Biomass is not introduced at this level. Three different storage alternatives have been evaluated: Li-ion battery, hydrogen, and methane. This scenario is considered as the base case.
- **Scenario 2**: Wind and solar are introduced as intermittent renewable sources and, additionally, biomass is also included. The same three storage alternatives have been considered as in scenario 1. With this option, the integration of intermittent and non-intermittent resources together with energy storage is assessed.
- **Scenario 3**: Only wind and solar have been considered as input resources. In order to envision a future electricity system without associated CO_2, biomass has not been introduced and, as forms of storage, battery, hydrogen, and ammonia (a carbon-free energy carrier) are used.

The detailed models, technical and economic parameters, etc. for the different processes have been obtained from previous works (as shown in Table 9.1). For solar PV panels, the efficiency is fixed to 25% and the performance ratio is calculated as a function of the ambient temperature and incident radiation (Hlal et al., 2019). Each module has a nominal power of 0.3 kWp with an area of 1.96 m^2. As a wind turbine, a Nordex N100 (de la Cruz & Martín, 2016) with a nominal power of 2,500 kW is employed with direct land requirement of 7,500 m^2 per turbine (Denholm et al., 2009). A Li-ion battery is selected due to its paramount properties for energy storage (Schmidt et al., 2019). A maximum capacity of 30,000 kWh is set with a limiting charge or discharge ratio in a given hour of 10% of the total capacity (Allman et al., 2019). H_2 is produced by electrolysis of water. This hydrogen can be stored as such and, subsequently, converted into power using a fuel cell yielding 50 kWh/kg H_2. Alternatively, hydrogen can be used for the synthesis of methane, with simple conditions for a long-term

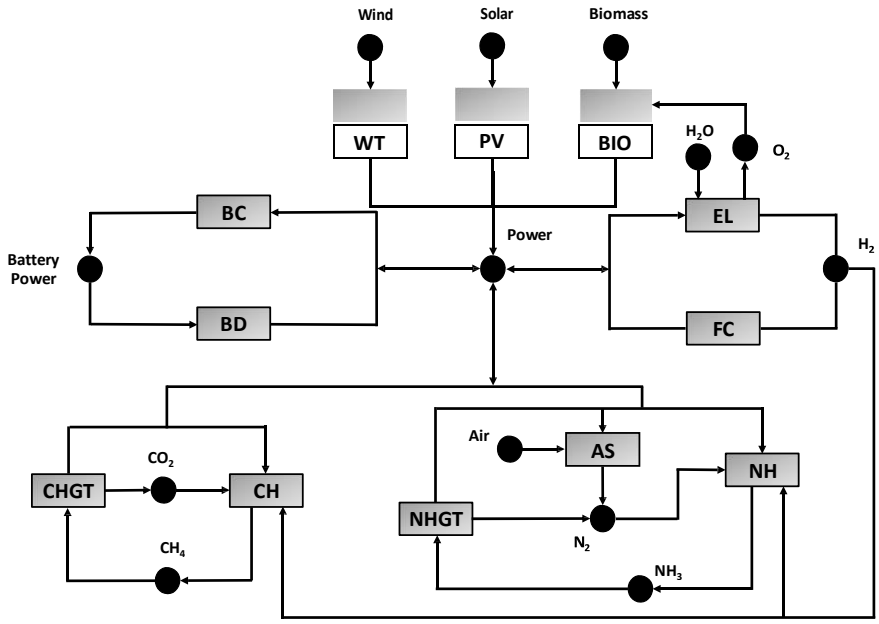

Figure 9.1: Process-resource network superstructure for power production. WT: Wind turbines; PV: Photovoltaic panels; BIO: Biomass; BC: Battery charge; BD: Battery discharge; EL: Water electrolysis; FC: Fuel cell; CH: Methane production; CHGT: Methane gas turbine; AS: Air separation unit; NH: Ammonia synthesis; NHGT: Ammonia-to-power.

storage horizon (Davis & Martín, 2014). This methane can be transformed into power via a gas turbine. From a carbon-free perspective, ammonia can be synthesized from H_2 and N_2, which can be produced by different air separation technologies (Sánchez & Martín, 2018b). Finally, power can be obtained from ammonia by two different routes: electrochemical (fuel cell) or thermochemical (combustion). For large production capacities, the most suitable is thermo-chemical using a combined cycle with an ammonia/hydrogen blend as the feed stream (Sánchez, Castellano, et al., 2021). The use of biomass for power production is based on the scheme of gasification plus gas turbine (Lan et al., 2018). Direct gasification as proposed by Sánchez et al. (2019) has been used to treat the inlet biomass. The data required in the model for the different processes have been included in the Supporting Information.

To model the operation of these integrated storage facilities, a scheduling model is proposed based on the previous models of Q. Zhang et al. (2016) and Sánchez, Martín, and Zhang (2021). Only a brief description of the model is included here and the full formulation is presented in the Supporting Information. The model is based on a multiscale time representation

Table 9.1: Process description with the input/output resources

Name	Description	Input Resources	Output Resources	Reference
WT	Wind turbines	Wind	Power	de la Cruz and Martín (2016)
PV	Photovoltaic panels	Solar	Power	Sánchez and Martín (2018a) ; Hlal et al. (2019)
BIO	Biomass integrated gasifier/gas turbine	Biomass, O_2	Power	Sánchez et al. (2019) ; León and Martín (2016)
BC	Battery charge	Power	Battery power	Gonzalez-Castellanos et al. (2020)
BD	Battery discharge	Battery power	Power	Gonzalez-Castellanos et al. (2020)
EL	Water electrolysis	Power,Water	O_2, H_2	Sánchez and Martín (2018a)
FC	Hydrogen fuel cell	Hydrogen	Power	Kashefi Kaviani et al. (2009); Palys and Daoutidis (2020)
CH	Methane production	CO_2, Hydrogen, Power	Methane	Davis and Martín (2014)
CHGT	Methane gas turbine	Methane	Power	León and Martín (2016)
AS	Air Separation Unit (PSA)	Air, Power	N_2	Sánchez and Martín (2018b)
NH	Ammonia synthesis	N_2, H_2, Power	NH_3	Sánchez and Martín (2018a)
NHGT	Power production from ammonia	NH_3	Power	Sánchez, Castellano, et al. (2021)

where the time horizon of one year is divided into a set of arbitrary seasons. Each season can have diverse lengths to capture the different patterns of input resources. Cyclic scheduling is applied to each season, although inventory can be carried over from one season to the next to allow for seasonal storage, which is key for the long-term horizon. From a process perspective, each unit can operate in four different operating modes (off, startup, on, and shutdown) with a minimum time period at each stage. A given power demand must be satisfied by using the available power production technologies. As the objective function of the optimization problem, the operating cost (OC) of the framework is used:

$$OC = \sum_{i} \sum_{m \in M_i} \sum_{h} \sum_{t} J_{imht} + \sum_{i} \sigma_i \left(\delta_i x_i + \gamma_i C_i \right) + \sum_{j \in \hat{S}} \left(\alpha_j \bar{x}_j + \beta_j C_j \right) + \sum_{i} \sum_{j} \sum_{h} \sum_{t} \xi_j \rho_{ij} P_{iht} + \sum_{h} \sum_{t} \phi_{CO_2} B_{CO_2,ht} \tag{9.1}$$

which includes the operating cost of the production processes and storage. The cost of the processes is divided into two terms. The first one, J_{imht}, includes all the terms non-related to the capital cost of the facility as raw materials or utilities. The second one, last term in the first line of the equation, includes all the operating costs associated with the initial investment as capital charges or maintenance (Sinnott, 2014). A linear approximation of the capital cost of the processes is considered. For the storage cost, as in the previous case, two terms are included. One is related

to the amortization of the capital cost (also assuming a linear behavior, first term of the second line of the equation) and the other to the operating and

maintenance cost of storage (last term of the second line). Finally, the cost of captured carbon dioxide (ϕ_{CO_2}), the raw material of methane production and captured in different industrial plants, is added with a price of 50 \$/t (third line of the equation 9.1) (Rubin et al., 2015).

The optimization problem proposed is a mixed-integer linear program (MILP) that has been implemented in Julia using the JuMP package and solved with Gurobi with an optimality gap of 1%.

9.3 social index

To be able to quantify the social impact of the energy transition and to provide tools to determine the best location of the energy facilities involving the social impact, a new social index has been developed. In this particular case, the social index has been used to determine the social effects of the installation of one integrated power production/storage facility in the different study regions. The social index proposed in this work is organized into ten different items. The first three involve the social impact of the energy transition in the studied area, and the rest quantify the global social situation of the region. All the items are normalized (as shown in equation 9.2) on a minimum score of 0 and a maximum of 10, with this value corresponding to the worst social situation of the indicator. Therefore, the maximum score of the index is equal to 100, corresponding to regions very affected by social issues and where the installation of different facilities is highly beneficial from a social perspective. This index is calculated in parallel to the economic evaluation of the system. This proposed indicator assesses the social situation of the region prior to the implementation of the integrated power facilities. The objective is to determine the best location in social terms, based on the assumption that if one of these plants is installed in a region, new investments, employment opportunities, local taxes, etc. could be generated. Throughout this section, each of the items of the social index has been explained and further details can be found in the Supporting Information.

$$SocialScore = 10 \quad \frac{Value - Value_{Min}}{Value_{Max} - Value_{Min}} \tag{9.2}$$

1. **Loss of installed capacity in the region vs. total capacity lost**: in the energy transition, some facilities will be decommissioned, mainly coal and nuclear power plants. The regions where these units are installed are particularly affected by the loss of job opportunities, economic activities, local taxes, etc. Therefore, regions with a higher rate of decommissioning will have a higher social impact. The lost

installed capacity is calculated by multiplying the total capacity by a factor that is the inverse of the remaining useful life years. This factor takes into account facilities with an established closing date in the near future.

2. **Loss of jobs related to energy transition vs. total employment in the region**: The decommissioning of the traditional power facilities involves a loss of direct and indirect jobs in the region. And, this loss is especially significant in those regions where the total active population is reduced. Therefore, regions with a high percentage of loss of jobs versus the total active population will have a higher social impact on the energy transition. To compute the loss of jobs, as in the previous item, the factor to take into account the active life years is applied. The number of employments in the sectors concerned has been obtained from different reports from trade unions, employers' organizations, or public authorities.

3. **Loss of installed capacity vs. total GDP of the region**: The aim of this item is to reflect the relative importance of the power industry in the productive sector of the region. If the power sector represents an important share of the total GDP of the province, the social importance of the energy transition increases. Due to the problems in obtaining the contribution to GDP of the power sector in specific regions, the ratio of the total loss of installed capacity to the GDP of the region is employed as an indicator.

4. **GDP of the region vs. total GDP of the country**: This component is the first item related to the total social environment of the region. In regions with a lower share of the total GDP of the country, the social impact of introducing new facilities such as the one proposed in this work is higher.

5. **Unemployment rate**: Some regions are especially affected by higher unemployment rates, therefore, the power production/storage facilities could be an attractive measure to alleviate this to some extent. Thus, regions with higher unemployment rates required more social actions and higher scores on the social index.

6. **Population decline over the last 20 years**: The population decline, expressed as percentage of decrease, is particularly significant in some rural areas where the migration from small/medium villages to towns has reduced the population at alarming levels. The introduction of the facilities studied in this work could help to fix the population and to fight against this demographic problem. Therefore,

a higher social impact is expected in those regions where a deep population decline has taken place.

7. **Aging index**: the aging of the population is one of the emerging problems in some areas due to the migration of young people to other areas with larger economic perspectives and the low birth rate. This is a challenge for the authorities in terms of public services, the sustainability of the pension system, etc. To take into account this aspect in the proposed metric, the aging index is used. This index is determined as the ratio between the number of elderly people and the number of children and young people and is reported by national statistical offices. The higher the rate of aging, the greater the social impact.

8. **Population density**: Some areas are severely affected by the problem of the low population over a very large territory. This problem is a major challenge for the different governments because of the cost of public services, maintenance of infrastructures, etc. In the proposed metric, population density is introduced considering the high social impact of new facilities in those areas with lower levels of this parameter.

9. **Youth migration in the last 10 years**: A migratory movement of youth from, mainly, rural to urban areas is taking place. This leads to a loss of productive labor in villages, a lack of generational replacement in certain economic activities, or a major demographic problem. Therefore, the installation of new infrastructures associated with the energy transition could help to mitigate this problem. Data on youth migration, measured as number of migrations, has been collected from the national statistical office and the time period is set between 2010 and 2020.

10. **GDP per capita**: GDP per capita is often linked to a better economic situation, better public services, etc. Thus, the new energy infrastructure in areas with low GDP per capita can contribute to mitigating inequalities in income distribution, reducing the social gap between territories.

9.4 results and discussion

In the presented case study, the implementation of the proposed integrated power production/storage facilities in different regions (provinces) of Spain has been evaluated from a technical/economic perspective fol-

Figure 9.2: Selected regions in Spain for the analysis including the current nuclear or coal power plants

lowing the methodology of section 9.2 and from a social angle using the new social index proposed in section 9.3. The energy transition is a major challenge in Spain due to the new European aims to be climate-neutral by 2050 and, therefore, the necessary high penetration of renewables in the energy system. Fourteen locations have been evaluated (as shown in Figure 9.2). Six are areas particularly affected by the energy transition due to the decommissioning of coal and nuclear power plants and with special measures by the Spanish government (Ministerio para la Transicion Ecologica y el Reto Demografico, 2021): Asturias, Teruel, Leon, Coruña, Almeria, and Cordoba. Three others are included for their high solar potential: Badajoz, Ciudad Real, and Sevilla. Zaragoza, Burgos, and Navarra are areas with high availability of wind resources. Finally, two areas with significant social problems have been included: Salamanca and Soria. Solar irradiation and wind speed data have been obtained from public databases (JRC European Commission, 2019; Energy Data, 2021). Additionally, the power demand of Spain has been collected from the grid operator's website (Red Electrica de España, 2021). For the different installations analyzed in this work, the demand for electricity to be satisfied is set at 0.5% of the total demand in Spain in each time period, which corresponds with an energy demand of 1275 GWh per year with a maximum hourly peak demand of about 205 MW. For the scenario in which biomass is introduced (scenario 2), the total availability of biomass in the specific region is calculated (Cabrera et al., 2011). For each region, it is determined which is the largest contributor

to the total biomass production: forest, herbaceous agricultural, or woody agricultural biomass. For this value, the maximum biomass availability is taken, and only 10% of this biomass can be processed in the proposed power plant to make a conservative estimation.

9.4.1 *Operating results*

In this section, the operation of integrated energy production and storage facilities is analyzed in depth. Only two different locations, for the sake of brevity, are shown in this section, Asturias and Almeria, in order to capture two different regions with contrasting weather conditions (additional operating results can be found in Figures F.1-F.3 and Tables F.1-F.3 of the Supporting Information). First, for scenario 1, Figure 9.3 shows the profile for two different weeks in July (summer) and December (winter) in Asturias. The columns, in different colors, indicate the power generation for each of the production technologies (including indirect production from storage). The black line shows the power demand to be satisfied, and the maroon line, the total power dispatched at the facility.

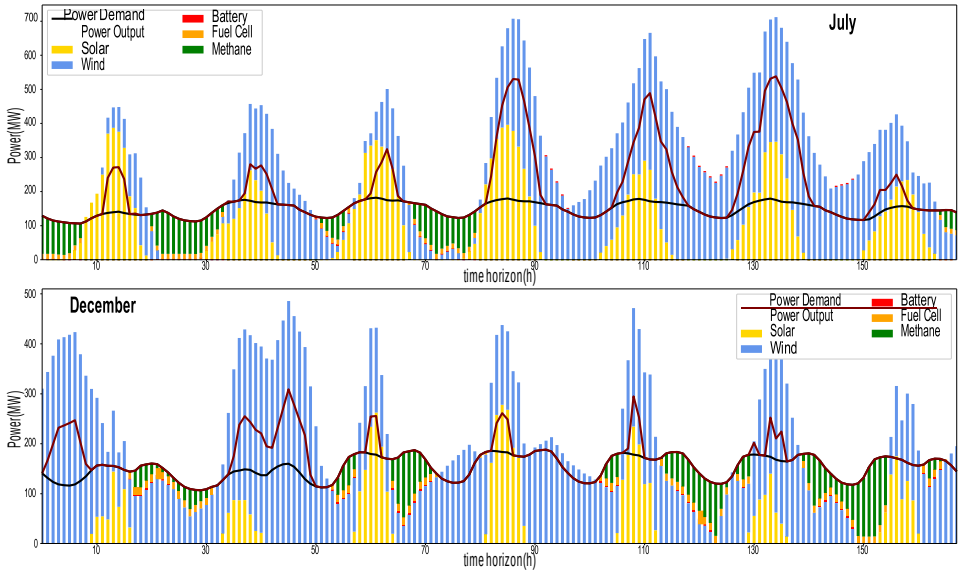

Figure 9.3: Scheduling results for the Scenario 1 in Asturias

In Asturias, wind is the preferred resource with about 71% of the total power generation. This is reflected in the weekly profiles of Figure 9.3. In December, wind production is the major contributor to meet the given demand. In the summertime, solar production is higher than in winter due to higher solar radiation and longer sunshine hours. However, the

wind resource is also significant in this season. Solar production follows a more recurrent pattern with a range of sunshine hours (higher in summer) and with different intensities (higher in summer). In contrast, wind availability is more stochastic and does not follow an expected pattern which is a major challenge in terms of the operability of these facilities. Storage technologies are used when solar/wind production is not enough to meet the demand. If only wind/solar technologies are introduced, it is not possible to guarantee demand satisfaction in this context of variable renewable energy sources. Therefore, these technologies emerge as essential in the future energy system to ensure the robustness and stability of the grid. Storage technologies are mainly operated at night due to the lack of solar resource and the fluctuating availability of wind. Within the different storage technologies, battery and fuel cell are first used to bridge the gap between production and demand. If these alternatives are not sufficient due to the limited capacity, methane is introduced, which allows for higher storage and production capacities. Due to the use of energy storage, power demand is satisfied in each time period regardless of the weather conditions. However, power production is higher than the power demand at different times throughout the year, in which wind/solar production exceeds energy demand (as can be seen in the black and maroon lines in Figure 9.3). This excess power could be used to store energy using the different technologies proposed but energy storage is expensive and minimum required levels are used to meet the demand. Therefore, even using these storage alternatives, some of the excess energy must be discharged. This is particularly important in the summer hours when high solar and wind generation converge. At this time, where, for example, in the Spanish national grid about 40% of power is produced from renewables, this excess could be also introduced in the grid by avoiding the introduction of natural gas combined cycle or other non-renewable technologies in the power mix. However, in a context where 97% of national electricity is expected to be produced from renewable energies by 2050 (Ministerio para la Transicion Ecologica y el Reto Demografico, 2020), this excess can hardly be integrated into the electricity grid. This raises the possibility of integrating this excess energy with other electricity-consuming industries that do not have such a restrictive hourly demand or where the storage of the products is possible. A promising alternative is the integration of power and chemical industry due to the future expected electrification of the latter sector. An interesting example is ammonia synthesis where an increasing number of projects to electrify the current production devoted to fertilizer require new renewable electricity. Therefore, excess of energy could be used in ammonia production and the chemical could be stored for use on demand. This perspective can also be extended to other chemicals

although further research in the operation of these new non steady-state chemical plants is required. Possible synergies between the use of these chemicals as a storage pathway and the production as such for the chemical industry should be also explored.

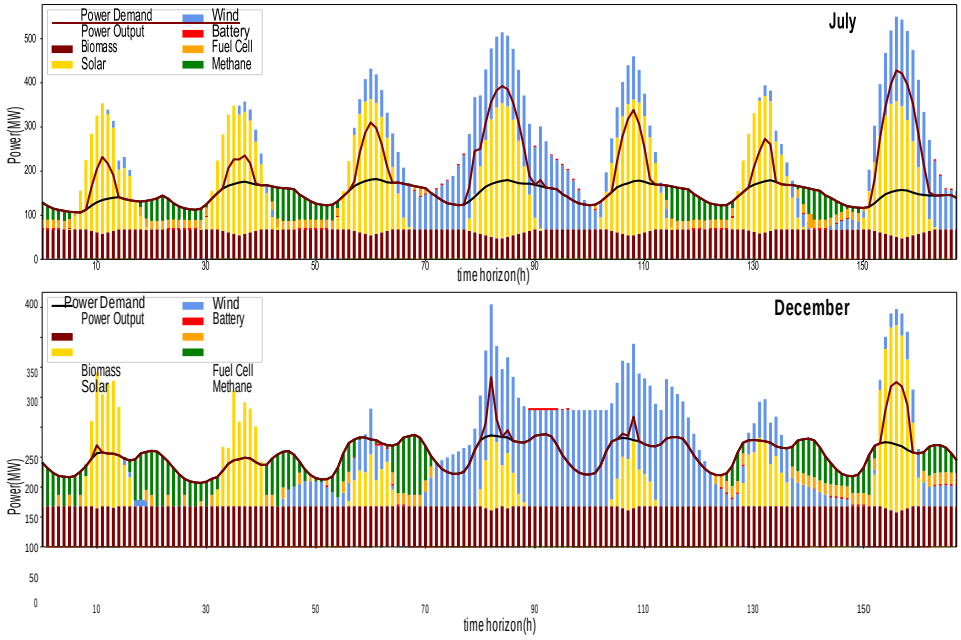

Figure 9.4: Scheduling results for the Scenario 2 in Almeria

In Figure 9.4, the results for scenario 2 for the province of Almeria are presented. In this scenario, biomass is introduced into the power generation pool to evaluate the optimal scenario in which a non-intermittent renewable source is available. The optimization results show that the biomass is used as a base-load generation source. The biomass-based power production is almost constant over time with only small fluctuations in time periods when solar and wind generation is particularly high (mainly during the central hours of the day). The fluctuations in the biomass units are limited in the model (using the minimum time period in each mode) due to this technology normally operating at or near steady-state. The introduction of biomass power production reduces the installed capacity of wind and solar, thus, reducing the difference between the total electricity discharged and the power demand. In terms of process capacities, in Almeria, a reduction of more than 40% in solar PV panels and 50% in wind turbines is expected compared to scenario 1 (as shown in Table 9.2). This reduction also affects electrolysis/fuel cell and methane production/gas turbine due to lower storage requirements. For example, the methane storage capacity decreases from about 5,700 t of methane to around 3,100 t. As it is explained in the next section, the use of biomass is economically beneficial compared to the

Table 9.2: Process capacities for the different scenarios in Asturias and Almeria

	Scenario 1		Scenario 2		Scenario 3	
	Asturias	Almeria	Asturias	Almeria	Asturias	Almeria
Solar (ha)	193.18	282.87	103.59	158.03	317.52	438.76
Wind (ha)	107.55	98.22	59.09	48.17	127.51	134.02
Battery (MW)	3.00	3.00	3.00	3.00	3.00	3.00
Electrolysis (MW)	173.76	223.08	85.16	118.81	195.07	321.43
Fuel Cell (MW)	14.16	40.65	3.14	18.81	78.29	85.17
CH_4 production (kW)	6.64	7.90	3.10	3.69	0	0
CH_4 Turbine (MW)	174.55	148.06	117.52	101.85	0	0
Biomass (MW)	0	0	68.05	68.05	0	0
ASU (MW)	0	0	0	0	9.18	13.18
NH_3 (MW)	0	0	0	0	10.94	17.13
NH_3 power production (MW)	0	0	0	0	111.27	104.39

use of storage technologies in order to ensure demand satisfaction, which justifies the use of biomass in electricity production. Figure 9.4 shows the results for a province dominated by solar generation contrasting with the case of Asturias. In scenario 2, almost 40% of the power is produced from solar PV panels in Almeria, and, this percentage increases to 55% in scenario 1. Due to this fact, the excess of energy during the central hours of summertime is particularly significant in locations such as Almeria.

Finally, Figure 9.5 shows the scheduling results in scenario 3 where ammonia is introduced and there are no direct CO_2 emissions associated with power production. In particular, the results are presented for the province of Asturias. A significant increase in the installed capacity takes place, mainly in the solar PV panels (as shown in Table 9.2), which is associated with an increase in the excess of produced power. For example, in scenario 1 in Asturias, there is a 30% energy excess but, when scenario 3 is evaluated, this value rises to about 60%. The use of H_2 also grows compared to the previous scenarios. The reason for these increases is the high cost of ammonia production and its respective conversion into power. Hence, the use of ammonia is reduced to the minimum necessary to meet the given demand prioritizing other forms of storage. Therefore, the results in scenario 3 show an increase in the installed capacity of the renewable sources, which implies a larger excess of energy when solar and wind availabilities are higher.

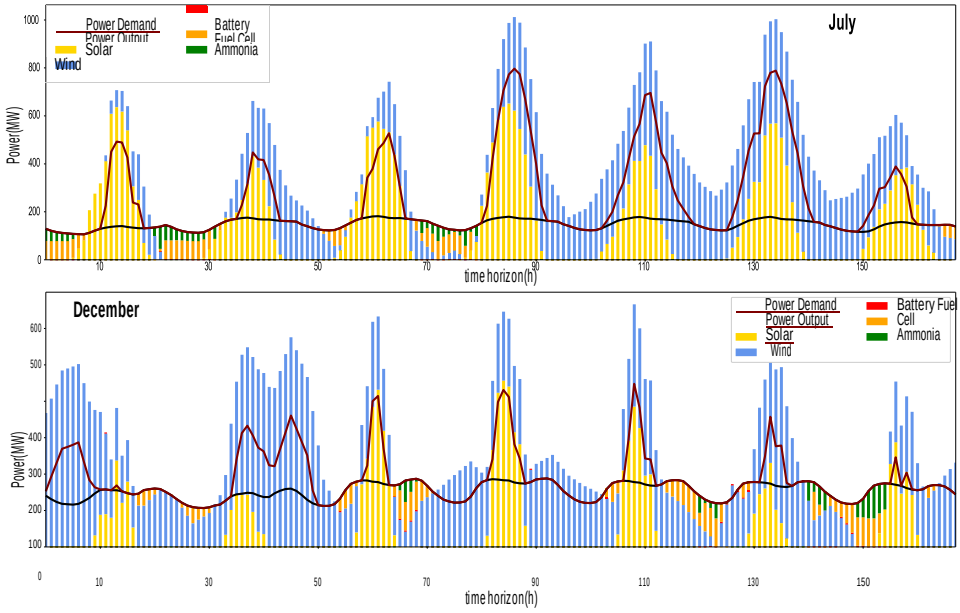

Figure 9.5: Scheduling results for the Scenario 3 in Asturias

It is also interesting to highlight that in all the locations, a combination of wind and solar energies is selected. In none of the locations studied has a single renewable source been chosen. The advantages in terms of operation of the facility justify the introduction of both technologies. Therefore, the use of scheduling models for this kind of problem is essential in order to determine the correct combination of renewable resources and the appropriate production capacities in each case.

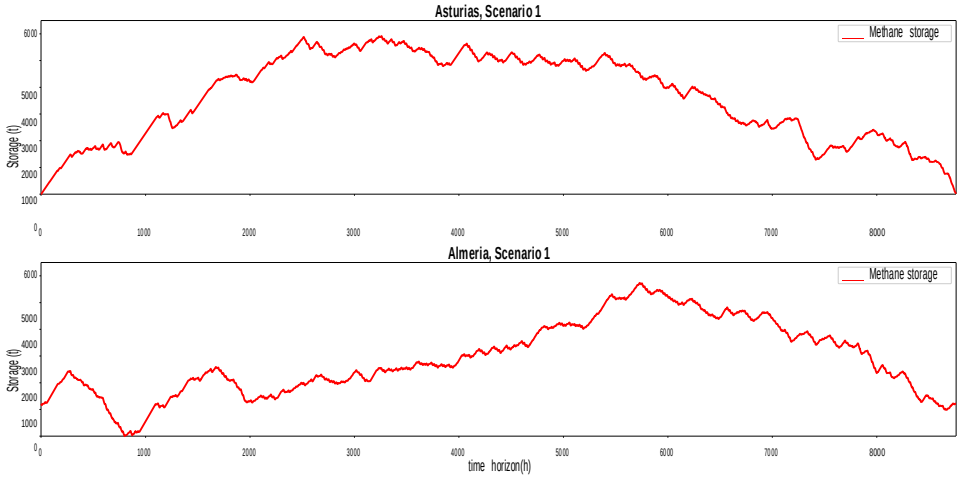

Figure 9.6: Storage results for methane in scenario 1

The seasonal storage of chemicals as methane or ammonia in the different scenarios is one of the main advantages of the Power-to-X alternatives. In

Figure 9.6, the storage results for methane in scenario 1 are presented for two different locations: Asturias and Almeria. Similar results are obtained for the other two scenarios. In both cases, there is a seasonal storage with different profiles depending on the weather conditions in the region. As a general trend, during spring/summer time higher solar power production is expected, which leads to an increase in the production of chemicals as storage systems. Within the two locations shown, this is especially visible in Almeria, where solar radiation is predominant. Seasonal storage is a technology to ensure demand satisfaction but also to reduce the installed capacity of the different power generation technologies, because it is not necessary to increase it to meet the demand in all the time periods of the year.

9.4.2 *Economic Results*

Based on the optimization results, the cost of electricity in the analyzed integrated facilities is calculated for each of the locations in the different scenarios proposed. Table 9.3 shows the results for scenario 1. Two different prices (annual average) are presented in the table. The "Demand cost" assumes that only power that satisfies the demand can be sold. Therefore, the excess of energy in periods with a high generation rate cannot be computed in the cost of electricity. On the contrary, the "Total cost" assumes that all the power can be discharged at the same price including the excess of energy.

The demand costs for scenario 1 are in the range of 100-200 €/MWh which is higher than the direct generation using solar/wind energy as expected. IRENA (2020) determines an average electricity price of 53 €/MWh for wind energy and 68 €/MWh for solar energy, therefore, the cost of electricity in an integrated facility is significantly higher than the cost when only power caption units are included. The results are expected because the investment and maintenance cost required when storage technologies are included. If the total power that can be produced is computed, the range of prices decreases to 70-90 €/MWh, closer to the renewable technologies themselves. The main advantage of using these integrated facilities is that power demand can be guaranteed regardless of the weather condition (security of the energy supply). If storage technologies are not included, in different periods of time, power production does not meet power demand, which cannot be assumed in a modern electricity system. This is particularly important in the context of a power generation mix where a 97-98% share of renewable resources is expected by 2050.

Table 9.3: Economic results for scenario 1

	Excess (%)	% Solar	% Wind	Demand cost (€/MWh)	Total cost (€/MWh)
Asturias	31.0	28.5	71.5	108.7	83.1
Almeria	42.7	54.7	45.3	127.8	89.8
Badajoz	113.9	67.7	32.3	168.7	79.0
Teruel	39.7	51.2	48.8	128.1	91.8
Leon	53.7	55.4	44.6	146.2	95.3
Coruña	29.0	29.8	70.2	100.8	78.3
Cordoba	165.1	70.8	29.2	196.2	74.2
Ciudad Real	107.6	66.1	33.9	167.8	81.0
Sevilla	59.8	58.2	41.8	142.9	89.6
Zaragoza	37.0	40.2	59.8	118.8	86.9
Burgos	38.2	48.6	51.4	131.5	95.4
Navarra	37.8	33.8	66.2	112.9	82.1
Soria	39.2	50.5	49.5	132.3	95.2
Salamanca	68.0	57.1	42.9	149.1	88.9

Looking at the cost behavior, when the excess of energy is higher, the demand cost increases, and the total cost decreases. More excess of energy is due to a large number of collection units, therefore more investment is required and, if the excess of energy cannot be sold, the demand cost significantly increases. As a general trend, locations where solar energy is predominant, have more excess of power production compared to those where the wind is the principal source where the excess is considerably less. To illustrate this point, the largest excess takes place in Cordoba where solar generation rises to about 71%. On the contrary, Coruña is the location with the lowest excess and, in this area, 70% of the power is produced from wind turbines. In general, when the solar share increases, the total demand cost is higher. The reason for this lies in the strong seasonal nature of solar energy. Solar availability follows a recurring pattern during the day and night hours but the differences between seasons are very significant. In summer, solar production is clearly higher than in winter. Therefore, satisfying the power demand in the most restrictive time periods, implies a certain installed capacity leading to an excess of energy during the time when the resource is more available. In contrast, wind production is more stochastic but does not show such strong seasonal differences.

Table 9.4: Economic results for scenario 2

	Excess (%)	% Solar	% Wind	% Biomass	Demand Cost (€/MWh)	Total Cost (€/MWh)
Asturias	14.2	19.2	49.3	31.5	87.8	76.8
Almeria	19.7	39.3	28.6	32.1	96.2	80.3
Badajoz	28.3	56.7	15.7	27.6	113.2	88.3
Teruel	19.0	36.6	30.8	32.6	96.1	80.9
Leon	23.4	46.8	29.3	23.9	112.3	91.2
Coruña	12.8	20.5	48.1	31.4	83.6	74.2
Cordoba	27.5	58.1	10.7	31.2	110.4	86.7
Ciudad Real	31.5	58.3	19.1	22.6	117.9	89.4
Sevilla	21.5	46.7	20.4	32.9	101.2	83.5
Zaragoza	18.6	28.3	40.2	31.5	91.6	77.3
Burgos	22.3	39.2	36.8	24.0	105.1	86.1
Navarra	19.3	24.6	48.0	27.4	92.9	78.1
Soria	20.5	40.9	34.8	24.3	105.1	87.3
Salamanca	39.5	53.6	27.5	18.9	116.4	83.6

Table 9.4 includes all the economic information about scenario 2 where biomass is introduced in order to assess the combination of intermittent and non-intermittent sources, and storage alternatives. As a general comment, the introduction of biomass is beneficial in economic terms with a significant reduction in the demand cost of more than 20% in most cases. One of the main reasons for the decrease in the cost of electricity when biomass is introduced is the level of utilization of the different production technologies. One of the most extended indexes to measure this utilization ratio is the capacity factor (George, 2015). For scenario 2, the average capacity factors are around 29% for solar PV panels, 37% for wind turbines, and 94% for biomass (as mentioned in the previous section, biomass operates almost as a base load generation). This large difference makes investment in biomass much more profitable (due to longer hours of operation) comparatively than in the case of solar or wind energy and can reduce the overall price of electricity. In the results of scenario 2, the excess of energy is significantly lower than in the case of scenario 1. The average value for the excess in scenario 1 is approximately 62% which decreases to about 23% when biomass is introduced. The inclusion of biomass in the generation pool reduces the variability in power production because it is a non-intermittent renewable source. The reduction in the excess of energy also implies a depletion in the gap between the demand and the total cost. These results show the great potential of the combination of

Table 9.5: Economic results for scenario 3

	Excess (%)	% Solar	% Wind	Demand Cost (€/MWh)	Total Cost (€/MWh)
Asturias	60.6	35.7	64.3	223.0	139.3
Almeria	78.0	57.6	42.4	259.8	146.6
Badajoz	135.9	64.9	35.1	344.9	146.5
Teruel	76.5	55.4	44.6	263.9	149.8
Leon	71.4	54.7	45.3	291.4	170.4
Coruña	64.7	37.8	62.2	213.5	129.9
Cordoba	188.9	64.5	35.5	389.3	135.0
Ciudad Real	122.3	62.7	37.3	340.5	153.5
Sevilla	80.7	57.1	42.9	277.6	153.9
Zaragoza	87.3	48.1	51.9	246.1	131.7
Burgos	80.4	55.4	44.6	266.6	148.1
Navarra	73.4	40.1	59.9	222.9	128.9
Soria	70.0	48.1	51.9	266.8	157.2
Salamanca	122.0	63.3	36.7	310.3	140.0

intermittent and non-intermittent production technologies together with storage alternatives to meet a given demand independently of the weather conditions at competitive costs. The use of biomass could be an interesting option due to the reduction of the production cost using only a small fraction of the total biomass in the region.

Finally, Table 9.5 contains the main results of scenario 3, where the use of ammonia is introduced as a storage alternative to develop a power facility without direct CO_2 emissions. This scenario could be feasible in a horizon in which a complete decarbonization is achieved. Ammonia as a long-term storage pathway significantly increases the cost of electricity. For the demand cost, the average value is around 280 €/MWh, and for the total cost around 145 €/MWh. Ammonia technology is a more complex process that requires higher power consumption to synthesize this chemical. All these factors translate into higher capital and operating costs which determine the final cost of electricity. Further improvements in the Haber-Bosch ammonia process could lead to a substantial reduction of the operating cost, for example, by reducing the pressure of the synthesis loop (Smith et al., 2020). The high cost of storage leads to high excess of electricity. While the average excess in scenario 1 was about 60%, in this case, the average rises to about 90%. The results minimize the storage increasing

the installed capacity of wind/solar resources, which on high production days leads to large energy excesses.

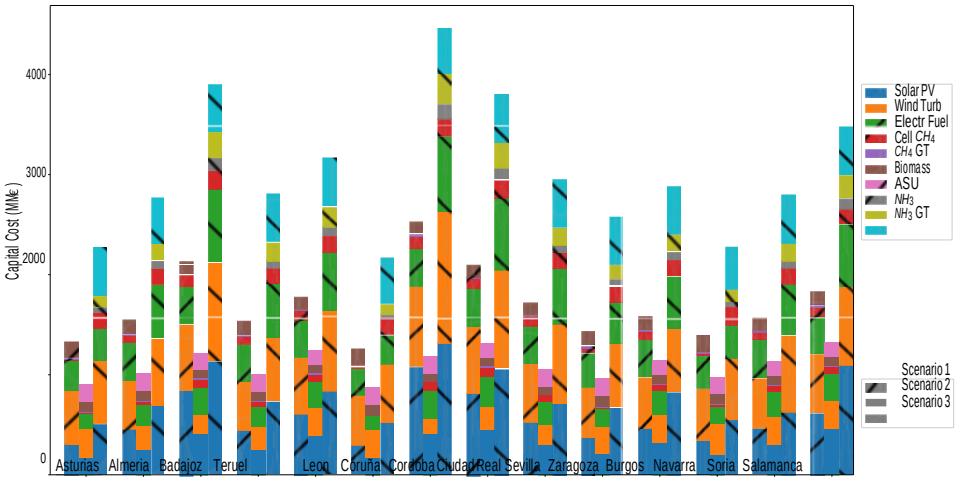

Figure 9.7: Capital cost for the different locations and scenarios

Regarding the total investment required, Figure 9.7 shows the capital costs for the different scenarios and for the different regions with an associated satisfied demand of about 1275 GWh per year. For scenario 1, capital costs range between 1,000-2,000 MM€. The main source of this investment is the power production technologies. In all cases, wind and solar accounts for about 60-70% of the total capital cost. Investment in wind/solar falls sharply in scenario 2 to levels close to 50%. The share of storage technologies also decreases due to the non-intermittent nature of the biomass source. The introduction of this renewable source also reduces the total capital cost in all regions, as expected based on the capacity factor calculated above. To satisfy a given level of demand, the lower the capacity factor of a technology, the higher the installed capacity required and, hence, the higher the investment. Finally, when scenario 3 is analyzed, there is a very substantial increase in the total capital cost. Investment in solar/wind technology and in electrolysis rises to avoid the use of ammonia that presents a higher cost. Large differences can be found between investments in the different regions. In general, in locations with a high proportion of solar-based power production, the total capital cost of the integrated facility increases. For example, Cordoba is one of the provinces with the highest share of solar energy, and the investment in this region, for example in scenario 3, exceeds 4,000 MM€ while in Coruña, with high wind penetration, the total capital cost is around 2,000 MM€.

As expected, the introduction of storage technologies into power generation in order to ensure demand satisfaction in the context of a new energy

Table 9.6: Results of the social index for the studied locations

	1 - MW	2- Loss of jobs	3- MW/GDP	4 - % GDP	5 - Unemployment	6 - Loss of pop.	7- Ageing	8 - Pop. density	9 - Youth mig.	10 - GDP per cap.	Total
Asturias	7,47	6,53	2,84	4,38	3,10	9,25	8,95	3,40	4,38	8,95	59,24
Teruel	3,80	10,00	10,00	9,73	0,62	8,50	5,84	9,97	7,94	5,84	72,24
Leon	6,99	6,06	6,19	7,95	3,12	10,00	10,00	8,44	7,36	10,00	76,11
Coruña	10,00	1,05	3,32	3,46	2,11	7,92	6,97	0,00	1,99	6,97	43,78
Almeria	4,00	0,92	2,54	6,88	5,26	0,00	0,00	4,39	3,41	0,00	27,40
Cordoba	1,12	0,42	0,68	6,73	7,34	7,84	2,58	6,37	7,68	2,58	43,35
Badajoz	0,00	0,00	0,00	7,30	8,34	7,85	2,86	8,32	7,01	2,86	44,54
Ciudad Real	0,00	0,00	0,00	7,76	7,29	7,38	3,19	8,77	10,00	3,19	47,57
Sevilla	0,00	0,00	0,00	0,00	10,00	5,66	0,69	0,16	3,38	0,69	20,59
Zaragoza	0,00	0,00	0,00	3,28	2,30	5,20	3,51	6,40	1,67	3,51	25,86
Burgos	1,61	3,14	1,36	7,81	0,11	7,56	5,82	8,73	6,28	5,82	48,22
Navarra	0,00	0,00	0,00	5,25	1,22	3,81	2,37	5,56	0,00	2,37	20,56
Soria	0,00	0,00	0,00	10,00	0,00	8,61	7,05	10,00	6,95	7,05	49,66
Salamanca	0,00	0,00	0,00	8,74	4,62	9,35	8,39	8,64	9,88	8,39	58,01

system based on variable renewable energies is a challenge in economic terms. The use of storage technologies increases the cost of electricity, but is necessary for a robust power system. To incentivize the introduction of storage technologies in the power grid, an interesting option could be to use the existing capacity payments. These, in the current system, guarantee a sufficient generation capacity to meet the demand for electricity at all times (including the peak demand). In the case study assessed in this work, the capacity payment budget amounts to around 658 MM€ per year distributed, mainly, between natural gas power plants and, during the last years, also coal-based facilities (now decommissioned) (Fundacion Naturgy, 2020). Therefore, if this budget is used in terms of energy storage technologies, the cost of electricity in these integrated facilities could be reduced targeting a competitive cost. All these measurements to introduce energy storage at grid scale will be included in the future regulations of the capacity market, the tool to face the new power system with high penetration of renewable generation (Huhta, 2019).

9.4.3 *Social results*

In addition to the economic results, the social impact of the energy transition must also be assessed. The results for the proposed social index are presented in Table 9.6. As indicated, the higher the social index, the worse the social situation of the region under study. The original data to calculate this index for each location is presented in the Supplementary Information.

As mentioned above, the first three items of the index are related to the energy transition and its social impact, and the last seven are to the general social situation of the region. In terms of the social impact of the

energy transition, Teruel emerges as one of the regions with the highest impact. The small size in economic and employment terms of this province means that the relative importance of the traditional electricity sector is high. In general, the regions located in the northwest of Spain (Leon, Asturias, Coruña) are the most affected group by the energy transition due to the high importance of the coal sector (including mining and power generation). If the entire social environment is analyzed, the results are different. Various regions of the center of Spain are the most affected by social issues, for example, Leon, Soria, Salamanca, or Ciudad Real. Therefore, the investment in the new energy system can help to mitigate the social distance to other parts of the country. Several job opportunities could be created in the different phases of the plant. During operating and maintenance of the solar PV panels and wind turbines, around 0.4 jobs/MW and 0.3 jobs/MW respectively could be generated (Cartelle Barros et al., 2017). For the Power-to-X storage processes, the correlation for job creation in chemical plants developed by Heras and Martín (2020) could quantify the new jobs opportunities. Additionally, in the areas where these facilities are installed, different local and regional taxes on these facilities could improve public services in the selected areas. Furthermore, the region's economic activity is boosted by new capital investments, land rental fees, etc. (Springer & Daue, 2020).

If all factors of the index are included, Leon is selected as the region with the most social disturbances (the highest social index) and, therefore, where the new investment and the public policies should be targeted to ensure equal opportunities for citizens regardless of territory. This region is affected by the energy transition, with important mines and about 2,000 MW of the coal-based power capacity decommissioned, and, also, by social problems such as aging or low population density. On the other end, regions such as Sevilla or Navarra have the lowest social impact. Although these regions have been selected to be included in this work due to the high potential in wind or solar energy, the social impact of the investment in these locations is significantly lower. Therefore, the trade-off between economic and social impact arises. For scenario 1, Figure 9.8 shows the comparison between the social index and the cost of electricity (demand cost) for all the studied regions. Similar results are obtained for the other two proposed scenarios (as shown in the Supporting Information).

In this Figure, it is possible to divide the space into four different sections: high social impact and low cost of electricity (1), high social impact and high cost of electricity (2), low social impact and low cost of electricity (3) and low social impact and high cost of electricity (4). The most promising regions are those in the first sector (1) where the social impact of the new facilities is high and it is possible to produce renewable electricity at a low

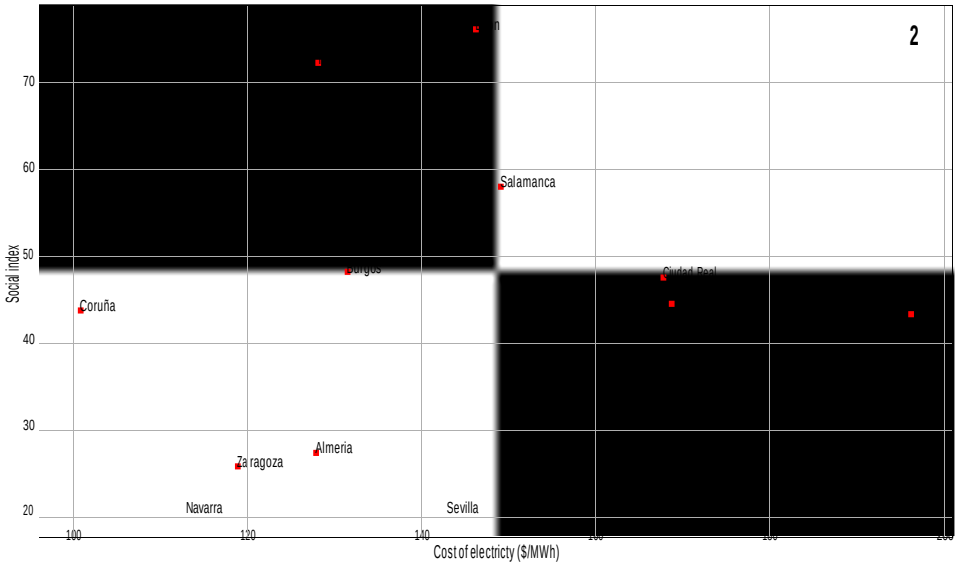

Figure 9.8: Social and economic results for scenario 1

cost. Particularly, Asturias and Teruel could be the two best performing locations in both indexes. In these two locations, the energy transition is significant and the weather conditions make it possible to reduce the electricity cost. In other places, the cost of electricity may be reduced or be similar, however, the social impact is lower. For example, Navarra and Asturias have similar costs of electricity, but, if the facility is located in Asturias, the social impact increases drastically, helping to mitigate the effects of energy transition and social problems in these areas.

Therefore, these results show the paramount importance of using these two indicators, economic and social, to plan the energy transition in a scenario targeting a 100% renewable power system. Using this dual perspective, stakeholders could take the fairness decisions in this uncertain horizon of a new energy system.

9.5 conclusions

This work presents an optimization analysis of integrated facilities combining intermittent and non-intermittent renewable sources together with different storage technologies. The objective is to ensure demand satisfaction regardless of the weather conditions. Three different scenarios are evaluated for various power sources and energy storage alternatives. For all regions and scenarios, it is demonstrated that the use of storage alternatives is required to guarantee the demand at all times of the year.

These storage technologies also allow for seasonal storage of energy since solar energy is more intense during summertime. In all cases, there is an excess of power production, mainly, when high availability of solar and wind is expected. In a context with high penetration of renewables in the power system, the grid cannot absorb this energy surplus. Therefore, different alternatives should be evaluated, for example, the integration of a new chemical industry based on electrochemical processes.

If biomass is introduced in the power generation pool, the optimization results show that a base-load behavior is expected with only small fluctuations when the solar/wind based power production is high. The use of this non-intermittent renewable source is beneficial from an operational and economic point of view. In this work, the use of biomass has been assessed due to the more mature state of the art. Other non-intermittent sources as geothermal, with a more limited expansion at present, could be analyzed in future works. Finally, in a forthcoming economic system free of CO_2 emissions, the use of ammonia as an energy storage alternative could be an interesting and feasible solution. According to the presented results, ammonia-based storage is expensive compared to the methane alternatives evaluated in scenarios 1 and 2. Further improvements in the Haber-Bosch process, especially aimed at reducing the operating pressure, could reduce the cost of this alternative. On a long-term horizon, the use of electrochemical methods to produce ammonia could turn this option into a technically and economically feasible solution.

In the planning of the new energy system based on sustainable criteria, the economic factor should not be the only one evaluated, directing the actions of all actors involved. The social aspect is very significant, in order to mitigate the social effects of the energy transition and the social inequalities of the societies. In this work, a new social indicator has been developed to determine the regions that require special social support to mitigate the social impact and, therefore, where investment in the new energy system could have the strongest impact. The results show that in certain regions (as Teruel or Asturias), it is possible to ensure a good economic performance of the integrated facilities in locations with a high social impact of the new projects. The complete planning of the new energy system using this methodology (social and economic perspectives) at country/continent level is a challenging future work in this area. To conclude, the importance of introducing non-intermittent renewable sources and energy storage at the grid level is demonstrated in order to guarantee demand satisfaction in a new energy paradigm based on, mainly, solar and wind renewable sources. To deploy these new technical requirements, this work provides an economic and social evaluation for different regions with the objective

of providing the tools to make the best decisions to achieve a fairer and more sustainable society.

nomenclature

Indices / sets/ subsets

$h \in H$	Seasons in the multiscale time representation
$i \in I$	Processes evaluated in network
$j \in J$	Resources involved in the network
$m \in M$	Operating modes for each of the process
M_i	Operating modes for a process
$\hat{S}$	Resources that could be stored
$t \in T$	Time periods in the multiscale time representation

Variables/ parameters

$B_{CO_2,iht}$	Amount of CO_2 introduced
C_i	Production capacity for different processes
$\bar{C}_j$	Storage capacity for different resources
J_{imht}	Process operating cost not related to capital cost
OC	Operating cost
P_{iht}	Amount of reference resource produced
x_i	Binary variable to select process units
$\bar{x}_j$	Binary variable to select storage units
α_j	Annualized fixed capital cost for storing
β_j	Annualized unit capital cost for storing
γ_i	Unit capital cost coefficient
δ_i	Fixed capital cost coefficient
ρ_{ij}	Conversion factor of the different products with respect to the reference resource
σ_i	Conversion factor between capital and operating cost for a process
ξ_j	O&M cost for storing
ϕ_{CO_2}	Cost of carbon dioxide

acknowledgments

The authors acknowledge MICINN Spain grant PID2019-105434RB-C31 and the FPU, Spain grant (FPU16/06212) to A.S.

bibliography

Denholm, P., Hand, M., Jackson, M., & Ong, S. (2009). *Land use requirements of modern wind power plants in the united states* (tech. rep.). National Renewable Energy Lab.(NREL), Golden, CO (United States).

Kashefi Kaviani, A., Riahy, G., & Kouhsari, S. (2009). Optimal design of a reliable hydrogen-based stand-alone wind/pv generating system, considering component outages. *Renewable Energy*, *34*(11), 2380–2390. https://doi.org/10.1016/j.renene.2009.03.020

Cabrera, M., Vera, A., Cornejo, J., Ordás, I., Tolosana, E., Ambrosio, Y., Martínez, I., Vignote, S., Hotait, N., Lafarga, A., et al. (2011). Evaluación del potencial de energía de la biomasa. *Estudio Técnico PER*, *2020*.

Davis, W., & Martín, M. (2014). Optimal year-round operation for methane production from co2 and water using wind and/or solar energy. *Journal of Cleaner Production*, *80*, 252–261. https://doi.org/10.1016/j.jclepro.2014.05.077

Sinnott, R. (2014). *Chemical engineering design* (Vol. 6). Elsevier.

George, A. (2015). Utility-scale solar photovoltaic power plants. *International Finance Corporation*.

Rubin, E. S., Davison, J. E., & Herzog, H. J. (2015). The cost of co2 capture and storage. *International Journal of Greenhouse Gas Control*, *40*, 378–400. https://doi.org/10.1016/j.ijggc.2015.05.018

Sternberg, A., & Bardow, A. (2015). Power-to-what? – environmental assessment of energy storage systems. *Energy Environ. Sci.*, *8*, 389–400. https://doi.org/10.1039/C4EE03051F

UN General Assembly. (2015). Transforming our world: The 2030 agenda for sustainable development. *Division for Sustainable Development Goals: New York, NY, USA*.

Vidal, M., & Martín, M. (2015). Optimal coupling of a biomass based polygeneration system with a concentrated solar power facility for the constant production of electricity over a year. *Computers & Chemical Engineering*, *72*, 273–283. https://doi.org/10.1016/j.compchemeng.2013.11.006

de la Cruz, V., & Martín, M. (2016). Characterization and optimal site matching of wind turbines: Effects on the economics of synthetic

methane production. *Journal of Cleaner Production*, *133*, 1302–1311. https://doi.org/10.1016/j.jclepro.2016.06.019

León, E., & Martín, M. (2016). Optimal production of power in a combined cycle from manure based biogas. *Energy Conversion and Management*, *114*, 89–99. https://doi.org/10.1016/j.enconman.2016.02.002

Zhang, Q., Sundaramoorthy, A., Grossmann, I. E., & Pinto, J. M. (2016). A discrete-time scheduling model for continuous power-intensive process networks with various power contracts. *Computers & Chemical Engineering*, *84*, 382–393. https://doi.org/10.1016/j.compchemeng.2015.09.019

Cartelle Barros, J. J., Lara Coira, M., de la Cruz López, M. P., & del Caño Gochi, A. (2017). Comparative analysis of direct employment generated by renewable and non-renewable power plants. *Energy*, *139*, 542–554. https://doi.org/10.1016/j.energy.2017.08.025

Corengia, M., & Torres, A. I. (2018). Effect of tariff policy and battery degradation on optimal energy storage. *Processes*, *6*(10), 204. https://doi.org/10.3390/pr6100204

Fragkos, P., & Paroussos, L. (2018). Employment creation in eu related to renewables expansion. *Applied Energy*, *230*, 935–945. https://doi.org/10.1016/j.apenergy.2018.09.032

Gür, T. M. (2018). Review of electrical energy storage technologies, materials and systems: Challenges and prospects for large-scale grid storage. *Energy Environ. Sci.*, *11*, 2696–2767. https://doi.org/10.1039/C8EE01419A

Lan, W., Chen, G., Zhu, X., Wang, X., Liu, C., & Xu, B. (2018). Biomass gasification-gas turbine combustion for power generation system model based on aspen plus. *Science of The Total Environment*, *628-629*, 1278–1286. https://doi.org/10.1016/j.scitotenv.2018.02.159

Leonard, M. D., Michaelides, E. E., & Michaelides, D. N. (2018). Substitution of coal power plants with renewable energy sources – shift of the power demand and energy storage. *Energy Conversion and Management*, *164*, 27–35. https://doi.org/10.1016/j.enconman.2018.02.083

Sánchez, A., & Martín, M. (2018a). Optimal renewable production of ammonia from water and air. *Journal of Cleaner Production*, *178*, 325–342. https://doi.org/10.1016/j.jclepro.2017.12.279

Sánchez, A., & Martín, M. (2018b). Scale up and scale down issues of renewable ammonia plants: Towards modular design. *Sustainable Production and Consumption*, *16*, 176–192. https://doi.org/10.1016/j.spc.2018.08.001

Allman, A., Palys, M. J., & Daoutidis, P. (2019). Scheduling-informed optimal design of systems with time-varying operation: A wind-

powered ammonia case study. *AIChE Journal*, *65*(7), e16434. https://doi.org/10.1002/aic.16434

Bagheri, M., Delbari, S. H., Pakzadmanesh, M., & Kennedy, C. A. (2019). City-integrated renewable energy design for low-carbon and climate-resilient communities. *Applied Energy*, *239*, 1212–1225. https://doi.org/10.1016/j.apenergy.2019.02.031

Hlal, M. I., Ramachandaramurthy, V. K., Sarhan, A., Pouryekta, A., & Subramaniam, U. (2019). Optimum battery depth of discharge for off-grid solar pv/battery system. *Journal of Energy Storage*, *26*, 100999. https://doi.org/10.1016/j.est.2019.100999

Huhta, K. (2019). *Capacity mechanisms in eu energy law: Ensuring security of supply in the energy transition*. Kluwer Law International BV.

JRC European Commission. (2019). Photovoltaic geographical information system-interactive maps. https://re.jrc.ec.europa.eu/pvg_tools/en/#MR

Sánchez, A., Martín, M., & Vega, P. (2019). Biomass based sustainable ammonia production: Digestion vs gasification. *ACS Sustainable Chemistry & Engineering*, *7*(11), 9995–10007. https://doi.org/10.1021/acssuschemeng.9b01158

Schmidt, O., Melchior, S., Hawkes, A., & Staffell, I. (2019). Projecting the future levelized cost of electricity storage technologies. *Joule*, *3*(1), 81–100. https://doi.org/10.1016/j.joule.2018.12.008

Bagherian, M. A., & Mehranzamir, K. (2020). A comprehensive review on renewable energy integration for combined heat and power production. *Energy Conversion and Management*, *224*, 113454. https://doi.org/10.1016/j.enconman.2020.113454

BloombergNEF. (2020). New energy outlook 2020. Retrieved December 1, 2020, from https://about.bnef.com/new-energy-outlook/

Carley, S., & Konisky, D. M. (2020). The justice and equity implications of the clean energy transition. *Nature Energy*, *5*(8), 569–577. https://doi.org/10.1038/s41560-020-0641-6

de la Fuente, E., & Martín, M. (2020). Site specific process design for hybrid csp-waste plants. *Computers & Chemical Engineering*, *135*, 106770. https://doi.org/10.1016/j.compchemeng.2020.106770

Demirhan, C. D., Tso, W. W., Powell, J. B., Heuberger, C. F., & Pistikopoulos, E. N. (2020). A multiscale energy systems engineering approach for renewable power generation and storage optimization. *Industrial & Engineering Chemistry Research*, *59*(16), 7706–7721. https://doi.org/10.1021/acs.iecr.0c00436

Fundacion Naturgy. (2020). El sector electrico español en numeros. informe 2019.

Gonzalez-Castellanos, A., Pozo, D., & Bischi, A. (2020). Detailed li-ion battery characterization model for economic operation. *International Journal of Electrical Power & Energy Systems*, *116*, 105561. https://doi.org/10.1016/j.ijepes.2019.105561

Heras, J., & Martín, M. (2020). Social issues in the energy transition: Effect on the design of the new power system. *Applied Energy*, *278*, 115654. https://doi.org/10.1016/j.apenergy.2020.115654

IRENA. (2020). Renewable power generation costs in 2019. report.

Jiang, Y., Kang, L., & Liu, Y. (2020). Optimal configuration of battery energy storage system with multiple types of batteries based on supply-demand characteristics. *Energy*, *206*, 118093. https://doi.org/10.1016/j.energy.2020.118093

Ministerio para la Transicion Ecologica y el Reto Demografico. (2020). Estrategia de descarbonizacion a largo plazo 2050. Retrieved June 7, 2020, from https://www.miteco.gob.es/es/prensa/documentoelp_tcm30-516109.pdf

Palys, M. J., & Daoutidis, P. (2020). Using hydrogen and ammonia for renewable energy storage: A geographically comprehensive techno-economic study. *Computers & Chemical Engineering*, *136*, 106785. https://doi.org/10.1016/j.compchemeng.2020.106785

Roelfsema, M., van Soest, H. L., Harmsen, M., van Vuuren, D. P., Bertram, C., den Elzen, M., Höhne, N., Iacobuta, G., Krey, V., Kriegler, E., et al. (2020). Taking stock of national climate policies to evaluate implementation of the paris agreement. *Nature communications*, *11*(1), 1–12. https://doi.org/10.1038/s41467-020-15414-6

Smith, C., Hill, A. K., & Torrente-Murciano, L. (2020). Current and future role of haber–bosch ammonia in a carbon-free energy landscape. *Energy Environ. Sci.*, *13*, 331–344. https://doi.org/10.1039/C9EE02873K

Springer, N., & Daue, A. (2020). *Key economic benefits of renewable energy on public lands* (tech. rep.). Yale Center for Business and the Environment.

Stančin, H., Mikulčić, H., Wang, X., & Duić, N. (2020). A review on alternative fuels in future energy system. *Renewable and Sustainable Energy Reviews*, *128*, 109927. https://doi.org/10.1016/j.rser.2020.109927

Wulf, C., Zapp, P., & Schreiber, A. (2020). Review of power-to-x demonstration projects in europe. *Frontiers in Energy Research*, *8*, 191. https://doi.org/10.3389/fenrg.2020.00191

Zhang, H., Wang, L., Van herle, J., Maréchal, F., & Desideri, U. (2020). Techno-economic comparison of green ammonia production processes. *Applied Energy*, *259*, 114135. https://doi.org/10.1016/j.apenergy.2019.114135

Alirahmi, S. M., Bashiri Mousavi, S., Razmi, A. R., & Ahmadi, P. (2021). A comprehensive techno-economic analysis and multi-criteria optimization of a compressed air energy storage (caes) hybridized with solar and desalination units. *Energy Conversion and Management*, *236*, 114053. https://doi.org/10.1016/j.enconman.2021.114053

Chen, C., & Yang, A. (2021). Power-to-methanol: The role of process flexibility in the integration of variable renewable energy into chemical production. *Energy Conversion and Management*, *228*, 113673. https://doi.org/10.1016/j.enconman.2020.113673

Energy Data. (2021). Global wind atlas. https://globalwindatlas.info/

EPA. (2021). Sources of greenhouse gas emissions. Retrieved May 8, 2020, from https://www.epa.gov/energy/distributed-generation-electricity-and-its-environmental-impacts

Ministerio para la Transicion Ecologica y el Reto Demografico. (2021). Transicion justa. Retrieved May 8, 2021, from https://www.miteco.gob.es/es/transicion-justa/default.aspx

Red Electrica de España. (2021). Demanda de energia electrica en tiempo real. https://demanda.ree.es/visiona/peninsula/demanda/total

Sánchez, A., Castellano, E., Martín, M., & Vega, P. (2021). Evaluating ammonia as green fuel for power generation: A thermo-chemical perspective. *Applied Energy*, *293*, 116956. https://doi.org/10.1016/j.apenergy.2021.116956

Sánchez, A., Martín, M., & Zhang, Q. (2021). Optimal design of sustainable power-to-fuels supply chains for seasonal energy storage. *Energy*, *234*, 121300. https://doi.org/10.1016/j.energy.2021.121300

10

CONCLUSIONS AND FUTURE WORK

To summarize the conclusions of the different chapters presented in this thesis, the following general conclusions can be drawn:

- The sustainable ammonia production using water electrolysis, air separation, and the Haber-Bosch process is optimized determining the optimal operating conditions of the units. For an industrial scale, air separation is produced from cryogenic distillation. However, for a distributed perspective, other air separation technologies have been analyzed such as membranes or pressure swing adsorption.

- From an economic perspective, pressure swing adsorption emerges as one of the most interesting technologies to produce ammonia in a sustainable way at smaller scale. The reduced energy consumption is the major advantage of this process in contrast to cryogenic distillation, traditionally proposed for high capacities ranges. As the power comes from renewables, and this power is expensive, the less energy-intensive alternatives are the most promising in economic terms.

- Distributed production using modular units is an emerging trend in the chemical industry. Different advantages of this configuration have been pointed out such as higher worker safety or fewer capital risks with novel technologies. The modular performance of ammonia facilities is demonstrated in this thesis, but, with the available data, the economic savings of modular behavior are difficult to quantify.

- The use of biomass as feedstock for the chemical industry is broadly proposed. Biomass-based ammonia production is assessed in this thesis using two different routes, thermochemical (gasification) and biochemical (anaerobic digestion). The technical and economic performance is shown with lower production costs than the Power-to-X alternatives. The best synthesis pathway is the combination of indirect gasifier, steam reforming, and direct cooling ammonia reactor. The use of anaerobic digestion is limited by the economic results, however, this route can be useful for the valorization of different wastes.

- The transformation of ammonia into power is still a challenge and further research is required. A techno economic analysis of the ammonia-to-power conversion process is performed in this thesis using the combustion route. The use of a mixture of hydrogen and ammonia in the combustion chamber is required to improve the flammability properties of ammonia. Different gas clean-up operations are required in order to purify the outlet gases from the power production section such as membrane for hydrogen recovery or selective catalytic removal from nitrogen oxide abatement. The cost of electricity is highly influenced by the cost of ammonia, therefore, so the lowest the production cost of ammonia, the greater the potential to introduce this alternative as a feasible option for grid-scale storage.

- A new green chemical industry requires new alternative chemicals with lower toxicity, better biodegradability, etc., and also new chemical processes with renewable raw materials and less waste generation. In this thesis, dimethyl carbonate is analyzed due to the paramount importance of this component. A two-step synthesis is studied: the first step is the urea production using renewable ammonia and carbon dioxide and the second step is the DMC production using the urea and renewable methanol. A competitive price of DMC can be obtained but it is highly influenced by the cost of raw materials. DMC can be used as a chemical platform in the new paradigm of green chemistry in order to develop a chemical industry 100% sustainable.

- The use of chemical processes in which solar and wind are the raw materials arises two particular challenges: the operation of the facilities and the location of this plant due to the highly distributed resources. In this thesis, an integrated supply chain and scheduling approach is proposed, particularly, for the synthesis of chemical products as carries for different local energy applications. At this point, a heuristic decomposition technique is proposed to solve this large scale optimization problem. The results show the paramount importance of seasonal storage, one of the main advantages of Power-to-X processes. Additionally, the use of hourly scheduling is necessary in order to determine the capacities of the different process units involved.

- The integration of different intermittent and non-intermittent renewable sources together with several storage technologies is required to ensure the robustness and stability of the power grid in the new context of a system dominated by wind and solar. A design and scheduling problem is proposed in this thesis to determine the con-

tribution of each technology to meet a given demand. The results highlight the importance of energy storage technologies to guarantee the demand. Batteries are included for short-term storage and Power-to-X alternatives are used due to the higher rates of storage and the possibility of seasonal storage. The use of biomass as a non-intermittent source reduces the cost of electricity of the integrated facility.

- The social aspects of the energy transition and the overall social situation must be considered in decision-making by all stakeholders. In this thesis, a new social index is proposed providing a tool to ensure a fair energy transition. With this index, the locations where the energy transition is particularly intense (due to the decommissioning of the coal and nuclear plant) and with high social disturbances are identified and proposed as areas where new facilities of the new energy system can be installed. It is demonstrated that some areas of Spain can be competitive in economic and social terms.

Finally, some possible future lines of work are introduced:

- The use of electrochemical synthesis in ammonia production is one of the most promising alternatives for producing green ammonia that combines renewable electricity with the synthesis of chemicals. Further investigation at laboratory scale is required, and, subsequently, a process design and scheduling approach for this new route.

- The chemical industry traditionally operates at or near steady-state. The integration of solar and wind with the chemical process makes it difficult to continue with this paradigm. Therefore, further scheduling and also control analyses are required to use Power-to-X processes as source of chemicals or as energy storage alternatives.

- The synthesis of DMC is analyzed in this thesis. However, further analysis to build a completely new chemical industry based on sustainability is required to replace the traditional production of polymers, fertilizers, etc.

- The transformation of H_2 derived fuels into power must be analyzed to integrated these technologies into real applications. The combustion of ammonia is analyzed in this thesis, however, the electrochemical synthesis must be also evaluated. This process design approach must also be extended to other chemicals, for example, methanol.

- The integration of different renewable energy sources together with energy storage is analyzed for different locations in Spain. A future and challenging work is to extend this useful approach to the entire country in order to determine the contribution of each technology to ensure the total demand for electricity.

Part V

APPENDIX

A

APPENDIX A: SUPPLEMENTARY INFORMATION OF CHAPTER 3

a.1 direct cooling reactor

Below in Figures A.1 shows the profiles of the pressure drop. Next, Figures A.2-A.4 show different temperature profiles corresponding to reacting gas temperature, the temperature in the external annulus, Fig. A.3, and the temperature of the gas ascending through the inner pipe, Figure A.4.

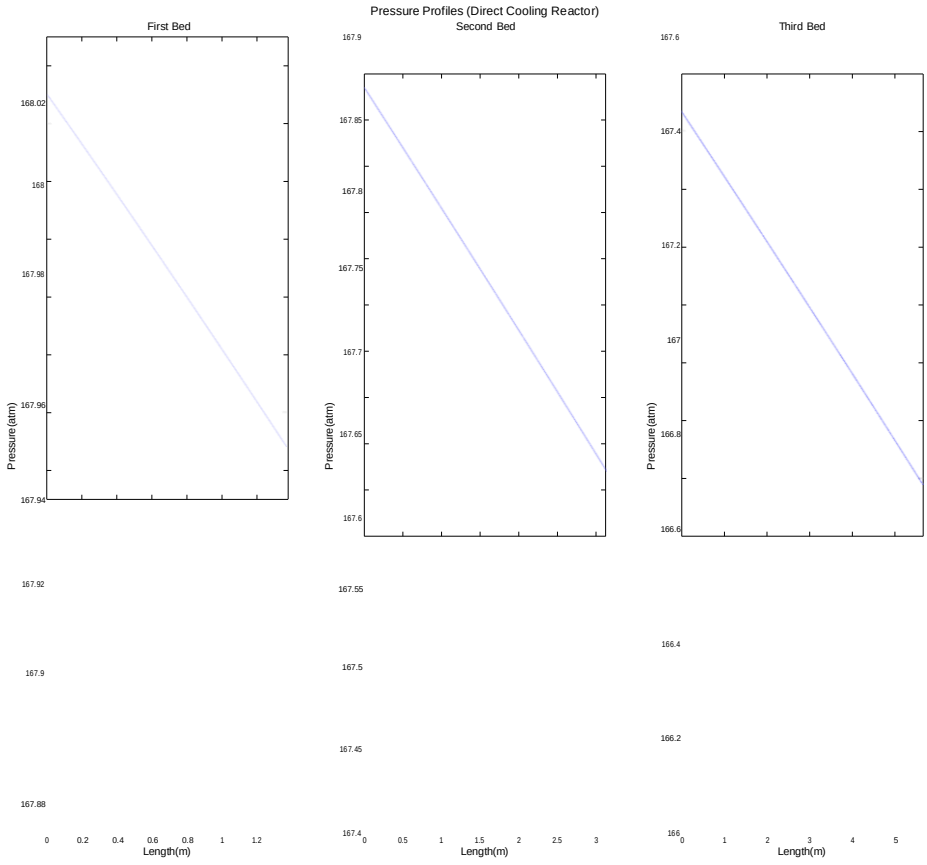

Figure A.1: Pressure drop across the three beds: Direct cooling

a.2 indirect cooling reactor

Figure A.5 shows the pressure drop profile across the three beds in case of the indirect cooled reactor solved in section 3.4 of the main manuscript. Furthermore, Figures A.6 and A.7 show the temperature profiles of the reacting gas and the external annulus flow rate.

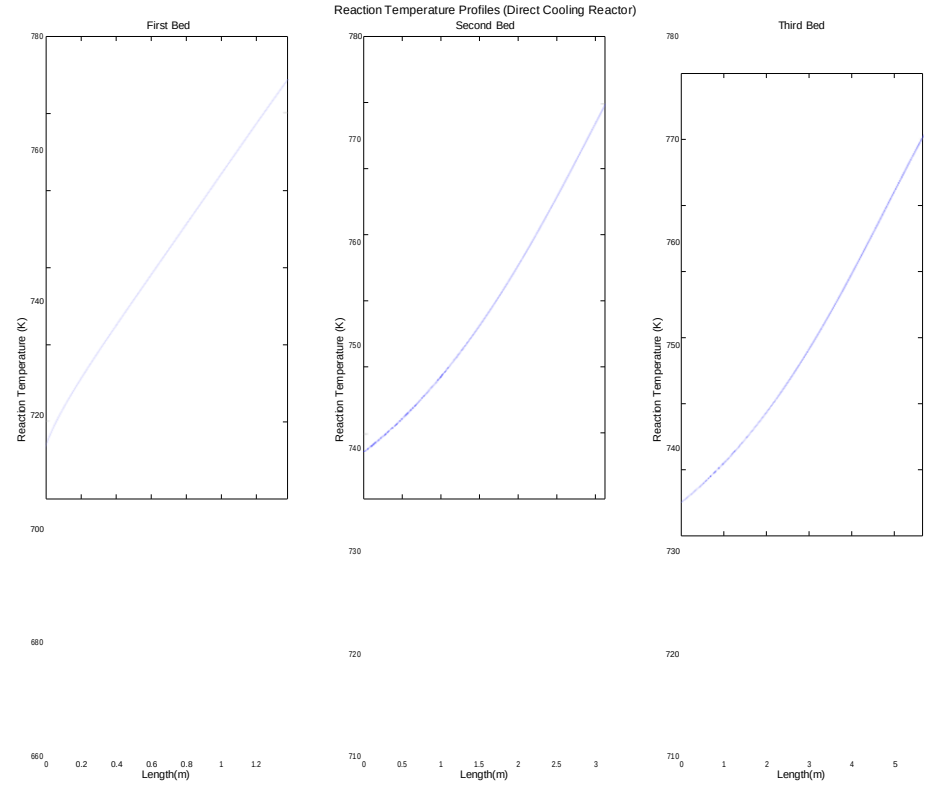

Figure A.2: Reacting Temperature across the three beds: Direct cooling

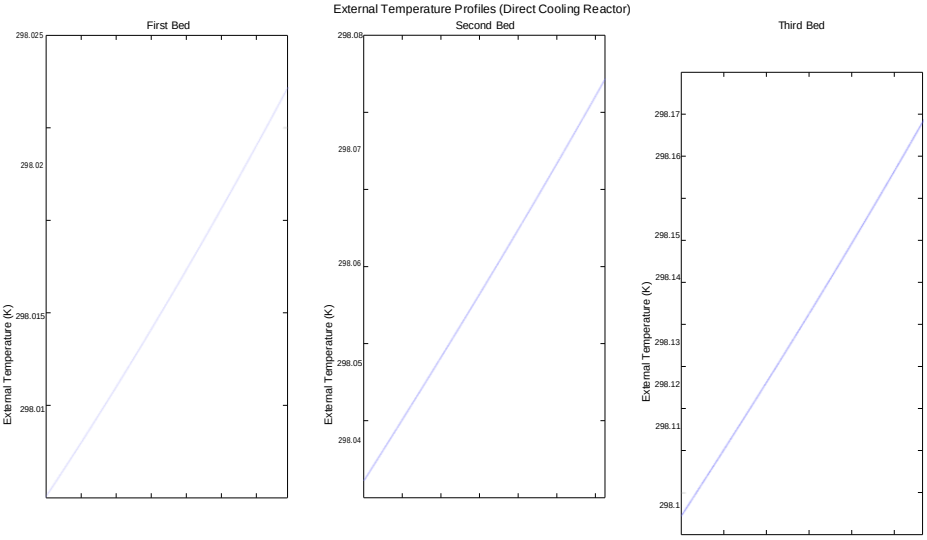

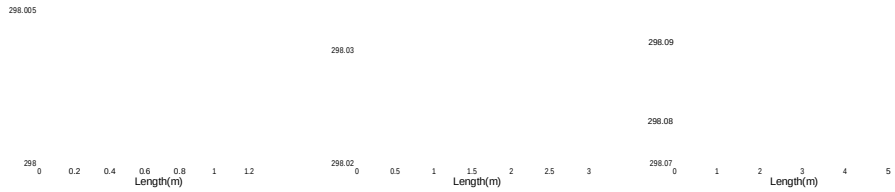

Figure A.3: Annulus Temperature across the three beds: Direct cooling

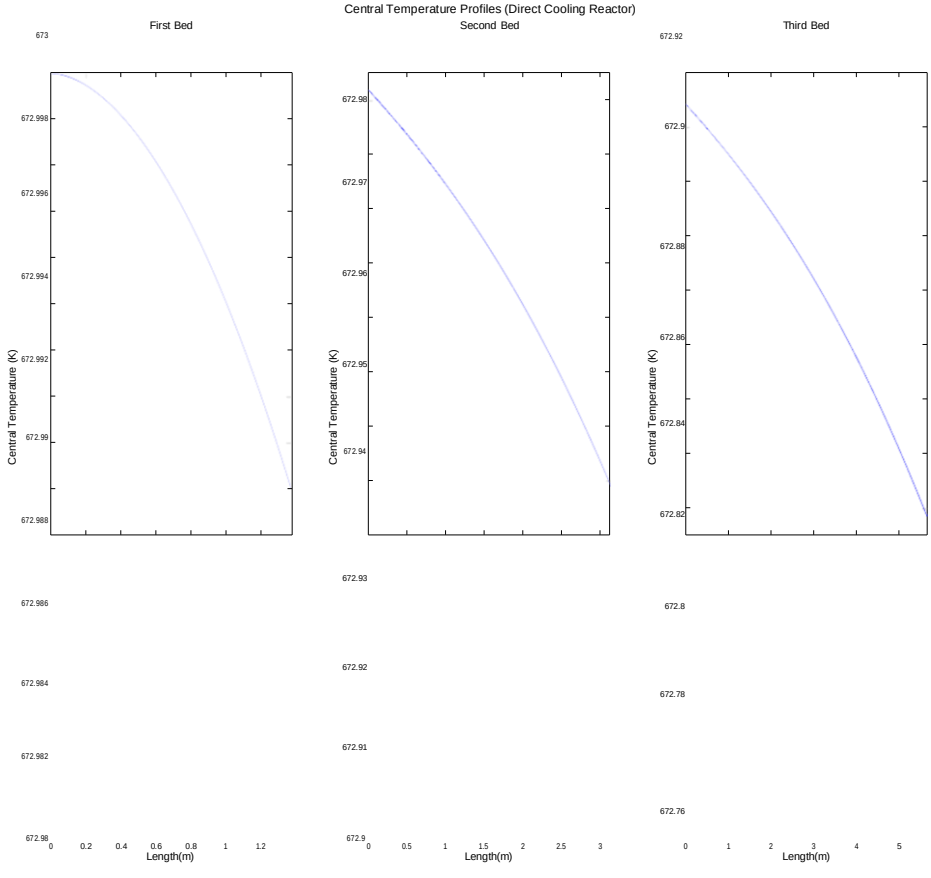

Figure A.4: Inner gas temperature across the three beds: Direct cooling

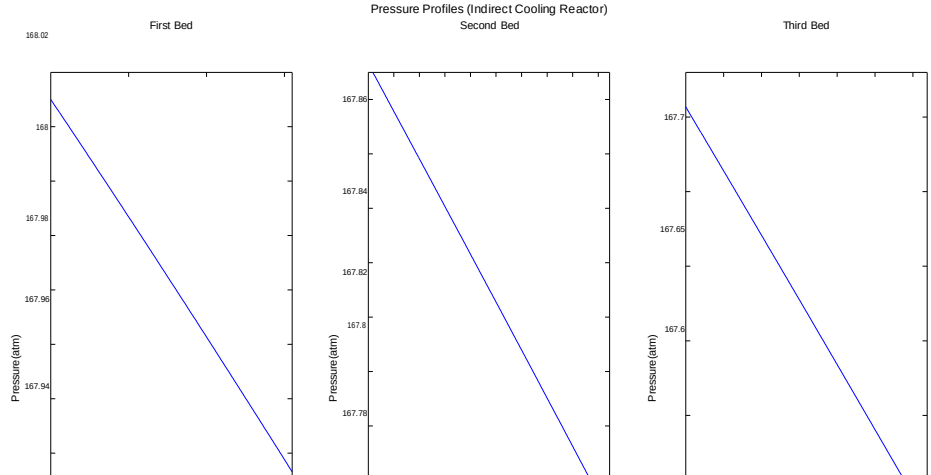

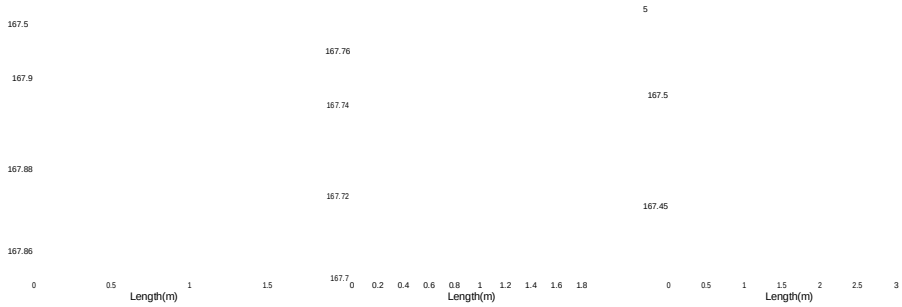

Figure A.5: Pressure drop across the three beds: Indirect cooling

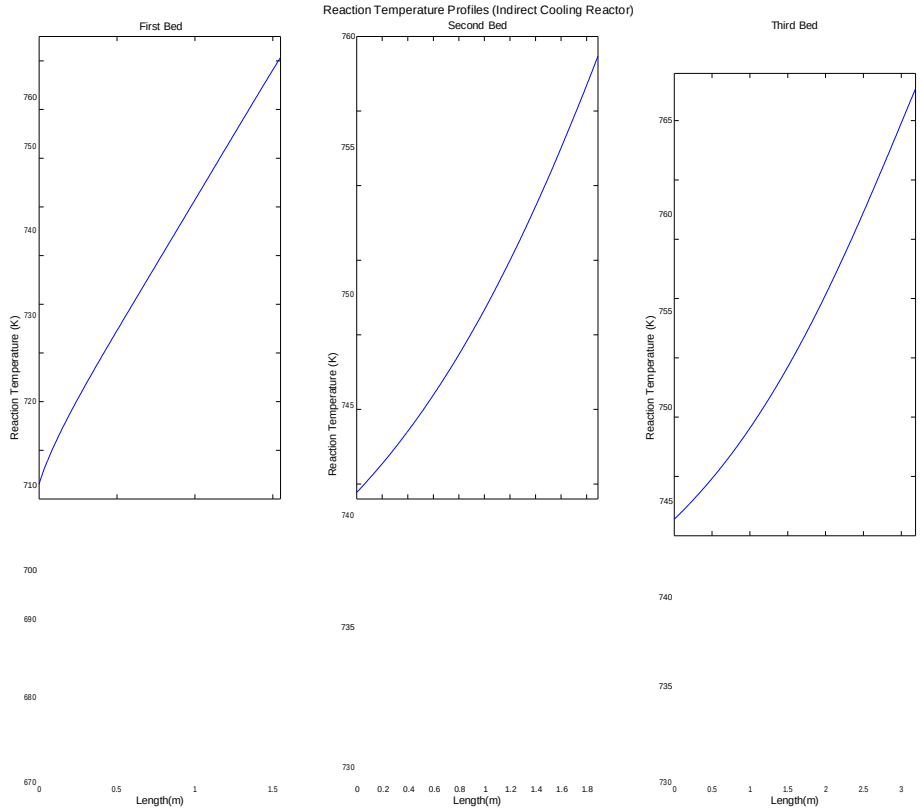

Figure A.6: Reacting Temperature across the three beds: Indirect cooling

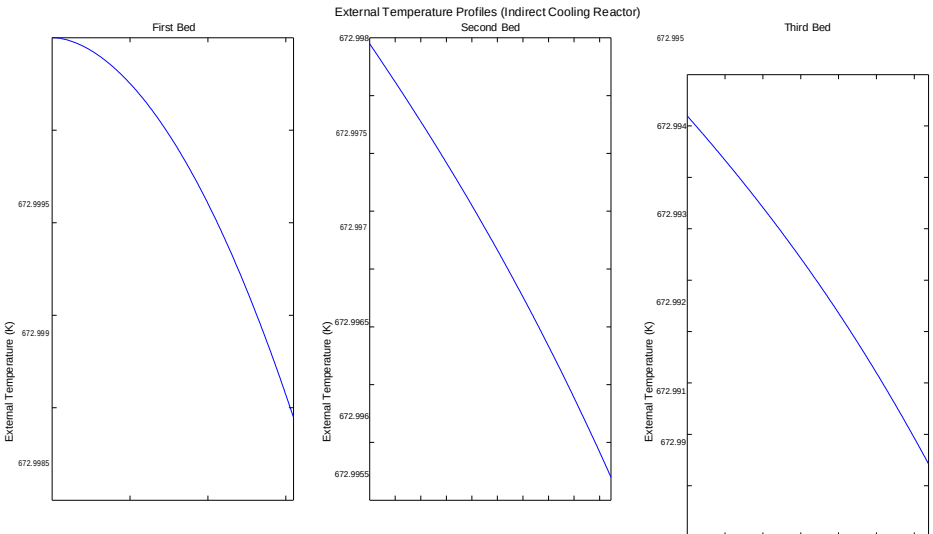

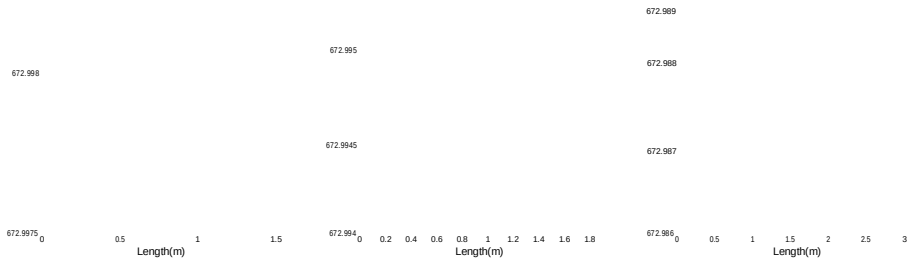

Figure A.7: Annulys gas temperature across the three beds: Indirect cooling

B

APPENDIX B: SUPPLEMENTARY INFORMATION OF CHAPTER 5

b.1 process model

The modelling issues of the different unit involved in the process have been described in this section.

b.1.1 *Gasification*

Three gasification alternatives have been considered: indirect gasification, direct gasification with oxygen/steam and direct gasification with air/steam (see Figure 5.2).

b.1.1.1 *Indirect gasification*

Indirect gasification (Figure 5.2-A) consists of two chambers: one to gasify the biomass using steam as gasifying agent and the other one to burn the char produced during the biomass gasification to generate the heat necessary for the gasification of the biomass. Olivine is the solid used as heat transfer agent between the two chambers. The pressure in the gasifier is fixed to 1.6 bar (Zhu et al., 2008). The ratios between steam and dry biomass and olivine and dry biomass are taken from Phillips et al. (2007) and are equal to 0.4 kg steam/kg dry biomass and 27 kg olivine /kg dry biomass, respectively.

To determine the outlet gas flow and its composition, the experimental correlations and methodology proposed by Phillips et al. (2007) have been considered. The temperature range for the correlation is 966-1287 K. The equation for each variable (X) collected in Table B.1 is as follow:

$$X = a + bT + cT^2 \tag{B.1}$$

where T is the temperature in ºF.

The amount of oxygen, sulphur and nitrogen in the char is fixed to 4%, 8.3% and 6.6% with respect to the original component in the inlet biomass. The mass balances complete the equations to describe the gasifier operation.

The stream exiting the gasifier contains the gases generated, char, ash from biomass and olivine. In the cyclone, solid components are separated

Table B.1: Correlations for modelling the indirect gasification (Phillips et al., 2007)

X	a	b	c	Units
Dry Syngas	28.993	-0.043325	0.000020966	scf gas/ lb maf wood
CO	133.46	-0.1029	0.000028792	% mol dry gas
CO_2	-9.5251	0.037889	-0.000014927	% mol dry gas
CH_4	-13.82	0.044179	-0.000046467	% mol dry gas
C_2H_4	-38.258	0.058435	-0.000019868	% mol dry gas
C_2H_6	11.114	-0.011667	0.000003064	% mol dry gas
H_2	17.996	-0.026448	0.00001893	% mol dry gas
C_2H_2	-4.3114	0.0054499	-0.000001561	% mol dry gas
Tar	0.045494	-0.000019759	0	lb/lb dry wood

with an efficiency of 99.99%. These are sent to the combustor while the gas continues to the cleaning stages.

In the combustor, the char is burnt with air. An excess of air of 20% is assumed and this air is preheat before being introduced in the combustor up to 473 K (Martín & Grossmann, 2011). Mass and energy balances are used to compute the composition of the leaving gases and their final temperature. Total combustion of the char is assumed. A specific heat of combustion for char of 25000 kJ/kg is taken (Di Blasi, 2004). Olivine is added to the combustor to replace the small solid amount dragged by the gases. The particles leaving with the outlet gases from the combustor are removed and cooled down to ambient temperature before they are released.

b.1.1.2 *Direct gasification with O_2/Steam*

Direct gasification (Figure 5.2-B) uses only one chamber to carry out the gasification process. To model the gasifier performance, the correlation from Dutta and Phillips (2009) are used. The correlation is of the form:

$$f_i = A + BP + CT + D\ \frac{O_2}{FeedC} + E\ \frac{H_2O}{FeedC} \tag{B.2}$$

where f_i is the molar ratio for each component according to Table B.2, P is the gasifier pressure in psi, T is the temperature in ^{o}F, (O2/Feed C) is the molar ratio between fed oxygen and the inlet carbon in the biomass and (H2O/Feed C) is the molar ratio between inlet steam and the inlet carbon in the biomass. The coefficients for the equation are collected in Table B.2.

Table B.2: Correlations to describe the behaviour of O_2/Steam direct gasification (Dutta & Phillips, 2009)

Molar ratio (f_i)	A	B	C	D	E
H_2/Feed H	-3.830761E-1	1.894350E-4	2.666675E-4	1.060088E-1	7.880955E-2
CO/Feed C	-8.310017E-2	-3.340050E-4	2.614482E-4	1.495730E-1	-5.268367E-2
CO_2/Feed C	7.157172E-2	3.843454E-4	1.286060E-5	6.124545E-1	9.980868E-2
CH_4/Feed C	1.093589E-2	1.388446E-4	8.812765E-5	-2.274854E-1	3.427825E-2
C_2H_4/Feed C	5.301812E-2	-6.740399E-5	-1.372749E-5	-9.076286E-3	-4.854082E-3
C_2H_6/Feed C	1.029750E-1	-5.440777E-6	-5.350103E-5	-3.377091E-2	-1.915339E-3
C_6H_6/Feed C	4.676833E-2	-1.937444E-5	-1.270868E-5	-1.046762E-2	-8.459647E-3
C_10H_8/Feed C	1.827359E-2	-2.328921E-6	-5.951746E-6	-1.936385E-2	-7.678310E-4
Char					
%Feed N in Char	3.36	0.00	0.00	0.00	0.00
%Feed S in Char	8.45	0.00	0.00	0.00	0.00
%Feed O in Char	1.512040	1.582010E-4	-6.972612E-4	1.573581E-1	0.3332

The temperature range for the correlation is between 1027 -1255 K and for pressures between 5.75- 23.75 bar. The ratio oxygen/inlet carbon must be in the range of 0.148-0.343 and the ratio steam/inlet carbon between 0.24-1.97 (Dutta & Phillips, 2009). The gases leaving the gasifier are cleaned from solids in two cyclones, the first one to remove the char and the second one to remove the ashes (Zhu et al., 2008).

b.1.1.3 *Direct gasification with Air/Steam*

The direct gasifier with air and steam uses a configuration similar to the direct gasifier with oxygen/steam. However, the oxygen is replaced by air or an enriched air with up to an oxygen molar fraction of 0.4. A surrogate model based on correlations has been developed in this work. The data for these correlations have been taken from the experiments carried out in a gasification pilot plant (Campoy et al., 2008; Campoy et al., 2009). The data used to develop the correlations employed wood pellets as raw material with an empirical formula of $CH_{1.4}O_{0.64}$ (dry and ash free) calculated based on the ultimate analysis of the biomass. The gasifier operated adiabatically. The working pressure was atmospheric. With these data, the yield (Y_i) for H_2, CO, CO_2, CH_4 and Char was correlated as a function of four variables:

Table B.3: Correlations to model the Air/Steam direct gasifier

	H_2	CO	CO_2	CH_4	Char
a0	236.134724	-758.768571	36651.3912	1625.70807	1356.79816
a1	-0.59246955	2.87931869	-91.0013798	-3.92738663	-3.60847944
a2	0.00035217	-0.00197877	0.0593536	0.00251846	0.00230493
a3	168.079598	-9.99925439	-6141.40211	-141.574346	549.840001
a4	-257.915778	817.985898	11151.9862	210.792784	-1090.38656
a5	37.8323438	-103.235783	319.997157	-31.419258	-30.0839584
a6	-31.9242057	-258.958857	345.997303	50.18269	-1.1476191
a7	3.70003089	380.503236	-1752.95314	63.8403192	214.600153
a8	44.4015283	215.128344	-1008.99174	-133.133672	42.8805991

the Gasifier Temperature (T), the Steam to Biomass ratio (S/B) defined as the mass ratio between the inlet steam flow and the fed biomass (dry and ash free), the oxygen percentage of the enriched air (OP) and the equivalent ratio (ER) defined as the mass ratio between the real inlet oxygen respect to the stoichiometric oxygen required for combustion. This data has been fitted to the following equation:

$$Y_i = a_0 + a_1 T + a_2 T^2 + a_3 ER + a_4 ER^2 + a_5 \frac{S}{B} + a_6 \left(\frac{S}{B}\right)^2 + a_7 OP + a_8 OP^2 \tag{B.3}$$

Where i Y_i is the yield as g/kg dry and ash free (daf) biomass and T the temperature in K. The Table B.3 collects the coefficient for the equation eq.B.3. The correlations have been obtained for the following ranges for the variables: ER, 0.19-0.38, OP, 0.21-0.4, S/B, 0-0.63, T, 1000-1113 K.

Due to the very similar composition between switchgrass and the wood pellets and the fact that a thermochemical process is carried out, it is assumed that the same yields will be achieved if switchgrass is employed instead of the wood pellets.

The following mass balances describe the gasifier performance. The tars composition ($C_6H_6O_2$) is taken from Thunman et al. (2001). The gasifier

is modelled using eq.B.4-eq.B.18 including yield calculations (computed using the correlation eq.B.3), mass balances and some empirical parameters.

$$\begin{aligned}&\text{Biomass} + O_2 + N_2 + H_2O \rightarrow \\ &\quad H_2 + CO + CO_2 + CH_4 + N_2 + O_2 + C_6H_6O_2 + \text{Char}\end{aligned} \tag{B.4}$$

$$fc_i^{out} = Y_i fc_{\text{biomass daf}}^{in} \frac{MW_{\text{biomass daf}}}{MW_i 1000} \quad \forall i \in \{H_2, CO, CO_2, CH_4\} \tag{B.5}$$

$$Y_{\text{Char}} fc_{\text{biomass daf}}^{in} \frac{MW_{\text{biomass daf}}}{1000} = \sum_j n_j^{\text{char}} MW_j \quad \forall j \in \{C, H, O, N, S\} \tag{B.6}$$

$$fc_{\text{biomass daf}}^{in} C_{\text{biomass daf}} = fc_{CO_2}^{out} + fc_{CO}^{out} + fc_{CH_4}^{out} + n_C^{\text{char}} + 6fc_{\text{Tars}}^{out} \tag{B.7}$$

$$2fc_{H_2O}^{in} + fc_{\text{biomass daf}}^{in} H_{\text{biomass daf}} = 2fc_{H_2O}^{out} + 2fc_{H_2}^{out} + n_H^{\text{char}} \tag{B.8}$$

$$fc_{H_2O}^{in} + 4fc_{CH_4}^{in} + 6fc_{\text{Tars}}^{in} + 2fc_{H_2S}^{in} + 3fc_{NH_3}^{in} + fc_{H_2O}^{in} + fc_{\text{biomass daf}}^{in} O_{\text{biomass daf}} + 2fc_{O_2}^{in} = fc_{CO}^{out} + 2fc_{CO_2}^{out} + fc_{H_2O}^{out} + n_O^{\text{char}} + 2fc_{\text{Tars}}^{out} + 2fc_{O_2}^{out} \tag{B.9}$$

$$fc_{N_2}^{in} = 2fc_{N_2}^{out} \tag{B.10}$$

$$fc_{\text{ash}}^{in} = 2fc_{\text{ash}}^{out} \tag{B.11}$$

$$fc_{\text{biomass daf}}^{in} S_{\text{biomass daf}} = fc_{H_2S}^{out} + n_S^{\text{char}} \tag{B.12}$$

$$fc_{\text{biomass daf}}^{in} N_{\text{biomass daf}} + 2fc_{N_2}^{in} = fc_{NH_3}^{out} + 2fc_{N_2}^{out} + n_N^{\text{char}} \tag{B.13}$$

$$X_{\text{Carbon}} = \frac{fc_{\text{biomass daf}}^{in} - n_C^{\text{char}}}{fc_{\text{biomass daf}}^{in}} \tag{B.14}$$

$$0.87 \leq X_{\text{Carbon}} \leq 0.98 \tag{B.15}$$

$$n_O^{\text{char}} = \frac{5}{100} fc_{\text{biomass daf}}^{in} O_{\text{biomass daf}} \tag{B.16}$$

$$n_N^{\text{char}} = \frac{3.36}{100} fc_{\text{biomass daf}}^{in} N_{\text{biomass daf}} \tag{B.17}$$

$$8.45$$

$$S = \frac{}{100} f c_{\text{biomass daf}} S_{\text{biomass daf}} \quad \text{(B.18)}$$

where fc_i is the inlet or outlet molar flow for component i, Y_i is the yield of component i calculated using the equation eq.B.3, MW_i is the molecular weight for each component, X_{Carbon} is the carbon conversion in the gasifier and, finally, $C_{\text{biomass daf}}$, $H_{\text{biomass daf}}$, $O_{\text{biomass daf}}$, $S_{\text{biomass daf}}$, $N_{\text{biomass daf}}$ are the index for each component in the empirical formula of the switchgrass from the ultimate analysis of it presented in Table B.1. The carbon conversion is limited to the interval between 0.87 and 0.98 according to the experimental results (Campoy et al., 2008; Campoy et al., 2009).

The gasification agent (Air/Stream) is heated up before being fed to the gasifier. The inlet temperature is fixed to 673 K (Campoy et al., 2008). The particles leaving the gasifier are removed in a cyclone with an assumed efficiency of 99.99%

b.1.1.4 *Digester*

The digester behaviour is described using the model proposed by León and Martín (2016). The digester operates at 328 K. The model requires experimental data for the treated biomass. The switchgrass properties for digestion are shown below (Massé et al., 2011; Brown et al., 2012; Frigon et al., 2012; Paul & Dutta, 2018):

$$0.289 \leq V_{\text{biogas/SG}} \left(\text{m}^3 \text{ biogas/kg SV}\right) \leq 0.441 \tag{B.19}$$

$$0.367 \leq w_{\text{DM/SG}} \left(\text{kg DM/kg}\right) \leq 0.508 \tag{B.20}$$

$$0.908 \leq w_{\text{VS/SG}} \left(\text{kg VS/kg DM}\right) \leq 0.943 \tag{B.21}$$

$$89.8 \leq R_{\text{C-N/SG}} \leq 92.0 \tag{B.22}$$

$$0.00014 \leq w'_{\text{Nam/SG}} \left(\text{kg N}_{\text{am}}/\text{kg DM}\right) \leq 0.00108 \tag{B.23}$$

$$0.0018 \leq w'_{\text{Norg/SG}} \left(\text{kg N}_{\text{org}}/\text{kg DM}\right) \leq 0.0132 \tag{B.24}$$

$$0.0004 \leq w_{\text{P/SG}} \left(\text{kg P/kg DM}\right) \leq 0.0021 \tag{B.25}$$

$$0.0034 \leq w'_{\text{K/SG}} \left(\text{kg K/kg DM}\right) \leq 0.0222 \tag{B.26}$$

The heat of combustion for the switchgrass is fixed to 17.4 MJ/kg dry biomass (Monti, 2012).

b.1.2 *Gas Clean Up*

The gas leaving the gasifier/digester section contains particles and hydrogen sulphide as main contaminants in the case of gasification (Figure B.1-A) and only hydrogen sulphide in the case of biomass digestion (Figure B.1-B). To remove particles and other small solids contained in the stream, a filter is used. After the filter, a train of compressors is employed to raise the pressure up to 2-3 MPa (Gupta, 2008; Reimert et al., 2011). Intercooling between the compressors takes place to avoid a temperature too high between them improving the performance and reducing energy consumption (Couper et al., 2005). The compressors are modelled as polytrophic with the following equations:

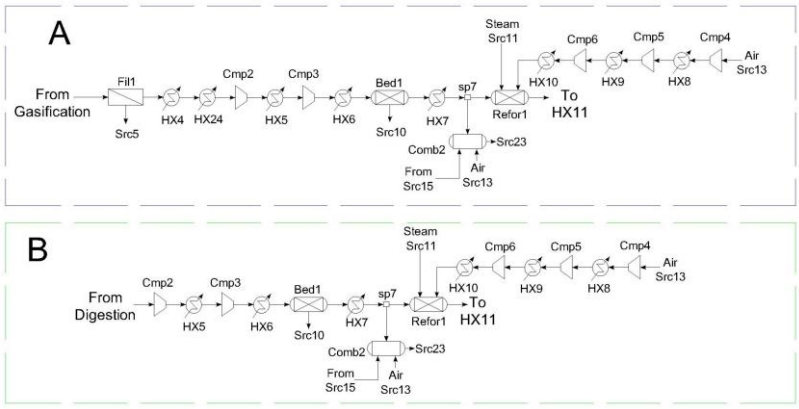

Figure B.1: Gas Clean Up and Reformer Section: A: for gases from gasification, B: for gases from digestion

$$W = \frac{8.314\,\mathrm{F\,k\,(T_{in} + 273.15)}}{\mathrm{MW}(k-1)} \left[\left(\frac{P_{out}}{P_{in}} \right)^{\frac{k-1}{k}} - 1 \right] \frac{1}{\eta_s} \tag{B.27}$$

$$T_{out} = T_{in} + (T_{in} + 273.15) \left[\left(\frac{P_{out}}{P_{in}} \right)^{\frac{k-1}{k}} - 1 \right] \frac{1}{\eta_s} \tag{B.28}$$

T is the temperature in °C, P is the pressure in bar, η_s is the efficiency fixed to 0.85 and k is the polytrophic index equal to 1.4 (Couper et al., 2005).

The cooling between the compressors is modelled, as well as other heat exchanger included in this work, using mass and energy balances:

$$fc_i^{in} = fc_i^{out} \quad \forall i \tag{B.29}$$

$$Q = \sum_i fc_i^{out} h_i^{out} - \sum_i fc_i^{in} h_i^{in} \tag{B.30}$$

where fc_i is the molar flowrate for each component i, h is the specific enthalpy per component and Q is the heat involved in the unit. The specific enthalpy is calculated as follows:

$$h_i = \Delta H_{form,i} + \Delta H_{sen,i} + \Delta H_{latent,i} \tag{B.31}$$

where $\Delta H_{form,i}$ is the heat of formation for component, $\Delta H_{latent,i}$ is the latent heat for component (if it is necessary in the stream involved) and

$\Delta H_{sen,i}$ is the sensible heat for component. The sensible heat can include

two terms: the liquid sensible heat and the gas sensible heat. In both cases, the sensible heat is computed as follows:

$$\Delta H_{sen,i} = \int_{T_1}^{T_2} C_{p,i}(T)dT \tag{B.32}$$

where , $C_{p,i}(T)$ is the heat capacity. In this work, the ideal behaviour is assumed and the heat capacity for the gases only depends on the temperature (Smith et al., 2004; Cengel et al., 2011). The relation between the heat capacity and the temperature follows the subsequent equation (Sinnott, 2014):

$$C_{p,i}(T) = A_i + B_i\,T + C_i\,T^2 + D_i\,T^3 \tag{B.33}$$

For the liquid, a constant value for the heat capacity is assumed.

To remove the hydrogen sulphide, the gas stream passes through a bed of ZnO. Due to low sulphur content in biomass, it is possible to use this technology alone. A removal of 99.9% is considered (Shah, 2015). Only H_2S is removal according to the following reaction:

$$H_2S + ZnO \rightarrow H_2O + ZnS \tag{B.34}$$

A temperature of 473 K is fixed in the bed (Shah, 2015). The removal takes place before the reformer due to the low sulphur tolerance of the ATR catalyst (Reyes Valle et al., 2013).

b.1.3 *Reforming*

In the reforming stage, the methane and the rest of hydrocarbons are transformed into hydrogen, carbon monoxide, carbon dioxide and water. The objective is to increase the amount of hydrogen for the synthesis of ammonia.

Two kinds of reformers have been evaluated: Autothermal Reforming (ATR) and Steam Methane Reforming (SMR). In the first one, air and steam are introduced in the reformer. This one operates adiabatically and the heat necessary for the steam methane reforming reaction is supplied by the combustion with air of a fraction of the fed stream inside the reformer itself. The air used in the reformer is limited by the ratio between the nitrogen and hydrogen in the ammonia synthesis loop. The SMR only introduces steam and the heat necessary comes from the combustion with air of the outlet gases from the PSA system (Bed 2) in a separated chamber and, if it is necessary, a fraction of the gases generated in the gasifier/digester. In the

reformer, the following reactions have been considered (Aasberg-Petersen et al., 2003):

$$C_nH_m + nH_2O \rightarrow nCO + \left(n + \frac{m}{2}\right) H_2 \tag{B.35}$$

$$3H_2 + CO \rightleftharpoons CH_4 + H_2O \tag{B.36}$$

$$CO + H_2O \rightleftharpoons H_2 + CO_2 \tag{B.37}$$

In the first reaction, all high hydrocarbons are converted completely to carbon monoxide and hydrogen. Besides, two equilibria are involved, the decomposition of methane and the Water Gas Shift Reaction (WGSR). The reformer is modelled as an equilibrium reactor. The equilibrium constant for the two last reaction is taken from Roh et al. (2010):

$$k_p = 10^{\left(-\frac{11650}{T(K)} + 13.076\right)} = \frac{P_{CO} P_{H_2}^3}{P_{CH_4} P_{H_2O}} \tag{B.38}$$

$$k_p = 10^{\left(\frac{1910}{T(K)} - 1.784\right)} = \frac{P_{CO_2} P_{H_2}}{P_{CO} P_{H_2O}} \tag{B.39}$$

The molar ratio between oxygen and methane in the ATR lies between 0.25 and 2. In SMR and ATR, the molar ratio between steam and methane could take a maximum value of 20 (Chen et al., 2010). The maximum temperature allowed in the reformer is fixed to 1600 K.

The steam enters the reformer as saturated steam at the same pressure that the stream from the gasifier/digester. The air is compressed from the ambient up to the same pressure that the other two inlet streams in the reformer.

The mass and energy balances in the reformers are formulated as follows:

$$fc^{in}_{CO} + fc^{in}_{CO_2} + fc^{in}_{CH_4} + n fc^{in}_{C_nH_m} = fc^{out}_{CO} + fc^{out}_{CO_2} + fc^{out}_{CH_4} \tag{B.40}$$

$$2\left(fc^{in}_{H_2O} - n fc^{in}_{C_nH_m}\right) + 4 fc^{in}_{CH_4} + 2\left(fc^{in}_{H_2} + \left(n + \frac{m}{2}\right) fc^{in}_{C_nH_m}\right) + 2 fc^{steam}_{H_2O} = 2 fc^{out}_{H_2O} + 2 fc^{out}_{H_2} + 4 fc^{out}_{CH_4} \tag{B.41}$$

$$fc^{in}_{H_2O} + 2 fc^{in}_{H_2O} = 2 fc^{out}_{H_2O} + 2 fc^{out}_{H_2} + 4 fc^{steam}_{CH_4} + H_2O + 2 fc_{CO_2} + fc_{CO} + n fc_{C_nH_m} + 2 fc_{O_2} + fc_{H_2O} + fc^{air}_{H_2O} \tag{B.42}$$

$$fc^{in}_{N_2} + fc^{air}_{N_2} = fc^{out}_{N_2} \tag{B.43}$$

$$y_i^{out} = fc_i \quad \forall i \in \{NH_3, H_2S, Char, Ash, Olivine, Ar\} \tag{B.44}$$

$$y_i^{out} = \frac{fc_i^{out}}{\sum^i fc_i^{out}} \quad \forall i \tag{B.45}$$

$$P_i^{out} = y_i^{out} P \quad \forall i \tag{B.46}$$

$$\sum_i fc_i^{in} h_i^{in} + \sum_i fc_i^{air} h_i^{air} + \sum_i fc_i^{steam} h_i^{steam} = \sum_i fc_i^{out} h_i^{out} \tag{B.47}$$

where fc is the molar flow for each specie i, y_i^{out} is the outlet molar fraction for each component i, P_i^{out} is the partial pressure in the outlet stream of the reformer, P is the total pressure and h_i is the enthalpy for each component.

b.1.4 *WGSR*

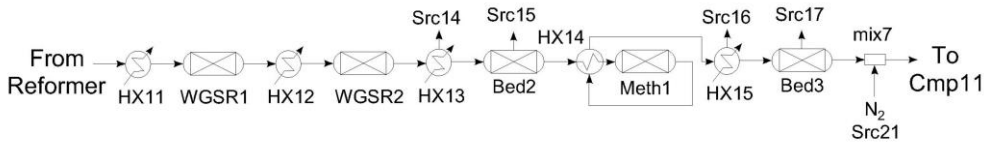

Figure B.2: Shift reaction and methanator section

To reach the hydrogen content required for the synthesis of ammonia, the water gas shift reaction (WGSR) is employed (see Figure B.2). With this, a reduction in the carbon monoxide concentration takes place, another factor interesting for the operation of the ammonia catalyst (see eq.B.37). In this study, a two-step shift conversion is selected, one at high temperature and other at low temperature (Appl, 1999). The first reactor (high temperature) has an outlet temperature in the range of 573-773 K and the second one (low temperature) between 453 K and 533 K (Appl, 1999). Both reactors work as adiabatic. The WGSR reactors are modelled as an equilibrium system. For this purpose, the equation eq.B.39 is used. The heat exchangers before the reactors adapt the inlet temperature to achieve the desired outlet temperature.

The mass and energy balances for the WGS reactors are showed below:

$$fc_{CO}^{in} + fc_{CO_2}^{in} = fc_{CO}^{out} + fc_{CO_2}^{out} \tag{B.48}$$

$$2fc_{H_2O}^{in} + 2fc_{H_2}^{in} = 2fc_{H_2O}^{out} + 2fc_{H_2}^{out} \tag{B.49}$$

$$fc_{H_2O}^{in} \cdot fc_{CO}^{in} + 2fc_{CO_2}^{in} = fc_{H_2O}^{out} + fc_{CO}^{out} + 2fc_{CO_2}^{out} \tag{B.50}$$

$$fc_i^{in} = fc_i^{out} \quad \forall i \in \{CH_4, NH_3, N_2, , H_2S, Char, Ash, Olivine, Ar\} \tag{B.51}$$

$$y_i^{out} = \frac{fc_i^{out}}{\sum^i fc_i^{out}} \quad \forall i \tag{B.52}$$

$$P_i^{out} = y_i^{out} P \quad \forall i \tag{B.53}$$

Table B.4: Fraction of fed stream leaving the adsorption bed (Bed2)

Component	% in the outlet stream (respect to the initial amount)
H_2O	0%
CO_2	0%
CH_4	45%
CO	75%
N_2	80%
H_2	97%

$$\sum_i fc_i^{in} \, h_i^{in} = \sum_i fc_i^{out} \, h_i^{out} \tag{B.54}$$

b.1.5 *Final Syngas Adjust*

After the WGSR section, it is necessary to remove a large fraction of the following species present in the gas: methane, carbon dioxide and carbon monoxide, this last one due to the high poisoned effect on the ammonia catalyst and CO2 because of the production of carbonates.

First, in the Bed2 (see Figure B.2), carbon dioxide is removed from the gases using activated carbon (Lopes et al., 2009). The PSA is designed to separate 100% of CO_2. The other species are removed with different efficiencies according to their different adsorption kinetics (Table B.4) (Lopes et al., 2009). The adsorption temperature is fixed to 343 K.

Due to the high sensitivity of the ammonia catalyst to carbon monoxide, it is necessary to reduce its concentration below 10ppm. To achieve this, the most appropriate method is methanation. In this process, the remained carbon monoxide is transformed into methane that is an inert using methanation. The equilibrium given by eq.B.36 is used. The final temperature in the methanator is limited between 523-623 K. Temperatures over 773 K must be avoided to prevent catalyst damage and below 473 K because of the risk of nickel carbonyl formation (Appl, 1999). The equipment is modelled as an equilibrium and adiabatic reactor. The equilibrium constant is taken from equation eq.B.38. The mass and energy balances for this reactor are as follows:

$$fc_{CO}^{in} + fc_{CH_4}^{in} = fc_{CO}^{out} + fc_{CH_4}^{out} \tag{B.55}$$

Table B.5: Fraction of fed stream leaving the adsorption bed (Bed3)

Component	% in the outlet stream (respect to the initial amount)
H_2O	0%
CH_4	0%
CO	65%
N_2	80%
H_2	97%

$$2fc^{in}_{H_2O} + 2fc^{in}_{H_2} = 2fc^{out}_{H_2O} + 2fc^{out}_{H_2} \tag{B.56}$$

$$fc^{in}_{H_2O} + fc_{CO} = fc_{H_2O} + fc_{CO} \tag{B.57}$$

$$fc^{in}_i = fc_i \quad \forall i \in \{CO_2, NH_3, N_2, , H_2S, Char, Ash, Olivine, Ar\} \tag{B.58}$$

$$y^{out}_i = \frac{fc_i}{\sum^i fc^{out}_i} \quad \forall i \tag{B.59}$$

$$P^{out}_i = y_i \; P \quad \forall i \tag{B.60}$$

$$\sum_i fc^{in}_i \; h_i = \sum_i fc^{out}_i \; h_i \tag{B.61}$$

After the methanator, the methane produced is separated using an activated carbon bed. The temperature is adjusted to 298 K. The amounts of each component captured is shown in the Table B.5 (Lopes et al., 2009).

b.1.6 *Ammonia Synthesis*

The compression of the inlet gas is the first step in the synthesis of ammonia (Figure 5.3). A multistage compression with intercooling is selected according to the rules of thumb (Couper et al., 2005). The final pressure is limited within the range from 125 to 350 bar. After the compression, the inlet gases are fed to the synthesis loop. First at all, the inlet gases are mixed with the recycled gases in a mixer. At the outlet of this equipment, the ratio between hydrogen and nitrogen is limited in the interval of 3-3.2.

The reaction to synthetize the ammonia is shown below:

$$N_2 + 3H_2 \rightleftharpoons 2NH_3 \tag{B.62}$$

Two reactor designs have been considered: multibed reactor with direct

cooling and multibed reactor with indirect cooling. The tubular design is not considered in this study because its use is limited to small scale production (Appl, 1999). Here, only a summary of the modelling is described.

The complete modelling of the ammonia reactor is found in Sánchez and Martín (2018). A three-bed reactor is used in both configurations.

Direct Cooling. In this reactor (Figure 5.3-A), the cooling between the beds, necessary to increase the conversion because of the tight equilibrium, takes places using a fraction of the fed stream. After mixing with the unreacted gases, the inlet stream is split in three fractions, one to each reactor bed. The inlet temperatures are around 673 K for each bed and final temperatures are limited in the range of 733-823 K. A detailed model accounting for mass and energy balances, mass transfer, kinetic expressions, pressure drop, etc. is solved in MATLAB© to provide bounds for the mass and energy balances used in the flowsheet optimization. Before mixing the fresh syngas with the gases leaving the reactor beds, each fraction of the inlet stream could be heated up using the outlet stream from the final bed.

Indirect Cooling. For this configuration (Figure 5.3-B), the cooling in the multibed reactor is carried out using external heat exchangers. The total flow passes through every bed. Due to the high temperature in the gases leaving the reactor beds, it is possible to generate steam. As in the previous reactor, a detailed model is used to set up the bounds for the optimization problem.

Ammonia is recovered by condensation after the reactor. A two stage cooling is carried out: A first step with water as cooling agent. The second one uses a refrigerant. In both cases, to determine the liquid fraction, a surrogate model is developed taking into account the main operating conditions involved (final pressure and temperature) (Sánchez & Martín, 2018).

In the cooling with water, the recovery yield to ammonia is given by:

$$\beta_{NH_3} = 0.025860989 + 0.001428067 \frac{P(mmHg)}{760} \tag{B.63}$$

In the second step with a refrigerant, the yields of each component follow these expressions:

$$\sigma_{NH_3} = 2.063269676 + 0.000163965 \frac{P(mmHg)}{760} - 0.004908159T(K) \tag{B.64}$$

$$\sigma_{H_2} = -0.005616112 + 4.076910^{-6} \frac{P(mmHg)}{760} + 2.2846810^{-5}T(K) \tag{B.65}$$

$$\sigma_{N_2} = -0.008053425 + 9.0875810^{-6} \frac{P(mmHg)}{760} + .4997910^{-5}T(K) \tag{B.66}$$

Table B.6: Parameters to estimate the gasifier capital cost (Sadhukhan et al., 2014)

Technology	Base Cost (MM$)	Base Size (t dry biomass/h)	Scale factor
Indirect gasifier	16.3	68.8	0.65
O_2/Steam direct gasifier	38.4	68.8	0.7

Table B.7: Data for estimating reactors capital cost

	GHSV (h-1)	Catalyst Cost ($/kg)	Annual Replacement	Source
ATR	1780	10.3	25%	(Villanueva Perales et al., 2011)
SMR	5000	25	15%	(Reyes Valle et al., 2013)
WGSR	4000	22.3	50%	(Feedstock, 2006)
Methanation	8000	21	0%	(Bartholomew & Farrauto, 2011)

In the gas stream leaving the gas-liquid separator, a purge is allowed to avoid impurities built-up. In the purge, a membrane to recover, mainly, hydrogen is installed because of the high value of this product. This membrane recovers 85% of hydrogen present in the initial stream and 10% of the other gases (Air Products, 2016; Membrane Technology and Research, 2016).

b.2 cost estimation procedure

Using the results from the optimization, capital and operating costs have been estimated. The procedure for the estimation of the capital cost is based on the factorial method (Sinnott, 2014). To estimate the cost of equipment, the correlations presented inAlmena and Martín (2016) have been employed. To evaluate the investment cost for the gasifier, the modified six-tenth rule is used (see Table B.6). For the air/steam direct gasifier, it is assumed that the cost can be estimated with the same data as the oxygen/steam direct gasifier.

For the digester, an organic loading rate of 15 kg VS/m^3 d is fixed (Brebbia, 2011) and an estimated cost of 365 €/m^3 (Doddapaneni et al., 2018; Taifouris & Martín, 2018). A normalized digester size of 6000 m^3 has been considered (Taifouris & Martín, 2018).

To estimate the investment cost of the reactors, the gas hourly space velocity (GHSV), the catalyst cost and the annual replacement are provided. With the GHSV, it is possible to calculate the volume of the reactor and, therefore, the catalyst amount. In Table B.7, the value of these parameters for the following reactors is presented: ATR, SMR, WGSR and methanation

reactor. The capital cost for the ammonia reactor is computed using the six-tenth rule (Morgan, 2013).

For the adsorption bed, the estimation procedure is the same as in the previous reactors. For the ZnO bed, a GHSV of 10260 h^{-1} is assumed (Hofbauer et al., 2007). The cost is fixed equal to 355 \$/ft^3 (Feedstock, 2006) with an annual replacement. For the activated carbon beds, it is assumed an adsorbent price of 1 \$/lb (Mussatti et al., 2002).

Table B.8: Summary of the operating cost calculations (Sinnott, 2014)

Variable Costs	
Raw materials	from flowsheet optimization
Miscellaneous materials	10% of maintenance
Utilities	from flowsheet optimization
Fixed Costs	
Maintenance	5% of fixed capital
Catalyst	from previous estimation (Table B.7)
Labour	estimated from correlations
Laboratory	20% of labour
Supervision	20% of labour
Plant Overheads	50% of labour
Capital charges	10% of fixed capital
Insurance	1% of fixed capital
Taxes	2% of fixed capital

For the production cost, the method proposed by Sinnott (2014) is employed. In this methodology, the production cost is computed as the sum of two terms: the variable and the fixed costs. In the variable costs, raw materials are included. The cost for the raw materials has been presented in the previous section. In the utilities item, the utilities cost has been computed following the same prices that in the objective function.

The fixed cost items include labour, amortization, insurances, taxes, maintenance and other items. The labour costs are computed using the correlation proposed by Green and Southard (2019). A summary table (Table B.8) with the method to calculate the operating cost is presented.

nomenclature

a, b, c	Coefficients for the indirect gasifier correlation (eq.B.1)
a_{0-8}	Coefficients for the Air/Steam direct gasifier correlation (eq.B.3)
A, B, C, D, E	Coefficients for the O2/Steam direct gasifier correlation (eq.B.2)
$C, H, O, S, N_{\text{biomass daf}}$	Index in the switchgrass empirical formula
$C_{p,i}$	Heat capacity per component (kJ/kmol·K)
ER	Equivalent Ratio
f_i	Variables for the O2/Steam direct gasifier correlation (eq.B.2)
fc_i	Molar flow for component i (kmol/s)
h_i	Specific enthalpy per component i (kJ/kmol)
k_p	Equilibrium constant
k	Polytrophic index
MW_i	Molecular weight for component i (kg/kmol)
n_j^{char}	Molar amount of component j in the char
OP	Oxygen Percentage of the enriched air
P	Pressure (bar)
Q	Heat (kW)
P_i	Partial pressure of component i (bar)
$R_{C-N/SG}$	Carbon to nitrogen ratio in the switchgrass (SG)
S/B	Steam to Biomass Ratio
T	Temperature (K)
W	Compressor power
$V_{\text{biogas/SG}}$	Biogas volume produced

	per mass unit of volatile solids (VS)
	in switchgrass (SG) (m^3/kg)
$w_{DM/SG}$	Dry mass (DM) fraction
	in the switchgrass (SG) (kg/kg)
$w_{VS/SG}$	Fraction of volatile solid (VS) with respect
	to dry mass of switchgrass (SG) (kg/kg)
$w_{Norg/SG}$	N_{org} fraction in the dry mass
	of switchgrass (SG) (kg/kg)
$w_{Nam/SG}$	N_{am} fraction in the dry mass
	of switchgrass (SG) (kg/kg)
$w_{P/SG}$	P fraction in the dry mass
	of switchgrass (SG) (kg/kg)
$w_{P/SG}$	K fraction in the dry mass
	of switchgrass (SG) (kg/kg)
X	Variables for the indirect gasifier
	correlation (eq. B.1)
X_{carbon}	Carbon conversion in the gasifier
Y_i	Yield in the Air/Steam
	direct gasifier (g/kg)
y_i	Molar fraction of component i
η_s	Compressor efficiency
β_{NH_3}	Ammonia separation yield
	in the first heat exchanger HX21
σ_i	Separation yield for each component
	in the heat exchanger HX22
$\Delta H_{form,i}$	Heat of formation
	for component (kJ/kmol)
$\Delta H_{latent,i}$	Latent heat for component (kJ/kmol)
$\Delta H_{sen,i}$	Sensible heat for component (kJ/kmol)

bibliography

Appl, M. (1999). Ammonia: Priciples & industrial practice.

Thunman, H., Niklasson, F., Johnsson, F., & Leckner, B. (2001). Composition of volatile gases and thermochemical properties of wood for mod-

eling of fixed or fluidized beds. *Energy & Fuels*, *15*(6), 1488–1497. https://doi.org/10.1021/ef010097q

Mussatti, D. C., Srivastava, R., Hemmer, P. M., & Strait, R. (2002). Epa air pollution control cost manual. *Air Quality Strategies and Standards Division of the Office of Air Quality Planning and Standards, US Environmental Protection Agency, Research Triangle Park, NC, 27711*.

Aasberg-Petersen, K., Christensen, T. S., Stub Nielsen, C., & Dybkjær, I. (2003). Recent developments in autothermal reforming and pre-reforming for synthesis gas production in gtl applications. *Fuel Processing Technology*, *83*(1), 253–261. https://doi.org/10.1016/S0378-3820(03)00073-0

Di Blasi, C. (2004). Modeling wood gasification in a countercurrent fixed-bed reactor. *AIChE Journal*, *50*(9), 2306–2319. https://doi.org/10.1002/aic.10189

Smith, J. M., Van Ness, H., & Abbott, M. (2004). Introduction to chemical engineering thermodynamics.

Couper, J. R., Penney, W. R., Fair, J. R., & Walas, S. M. (2005). *Chemical process equipment: Selection and design*. Gulf Professional Publishing.

Feedstock, E.-.-W. (2006). Equipment design and cost estimation for small modular biomass systems, synthesis gas cleanup, and oxygen separation equipment. *Nat Renew Energy Lab*.

Hofbauer, H., Rauch, R., & Ripfel-Nitsche, K. (2007). Report on gas cleaning for synthesis applications work package 2e:" gas treatment. *Vienna University of Technology, Austria*.

Phillips, S., Aden, A., Jechura, J., Dayton, D., & Eggeman, T. (2007). *Thermochemical ethanol via indirect gasification and mixed alcohol synthesis of lignocellulosic biomass* (tech. rep.). National Renewable Energy Lab.(NREL), Golden, CO (United States).

Campoy, M., Gómez-Barea, A., Villanueva, A. L., & Ollero, P. (2008). Air-steam gasification of biomass in a fluidized bed under simulated autothermal and adiabatic conditions. *Industrial & Engineering Chemistry Research*, *47*(16), 5957–5965. https://doi.org/10.1021/ie800220t

Gupta, R. B. (2008). *Hydrogen fuel: Production, transport, and storage*. Crc Press.

Zhu, Y., Gerber, M. A., Jones, S. B., & Stevens, D. J. (2008). *Analysis of the effects of compositional and configurational assumptions on product costs for the thermochemical conversion of lignocellulosic biomass to mixed alcohols–fy 2007 progress report* (tech. rep.). Pacific Northwest National Lab.(PNNL), Richland, WA (United States).

Campoy, M., Gómez-Barea, A., Vidal, F. B., & Ollero, P. (2009). Air-steam gasification of biomass in a fluidised bed: Process optimisation

by enriched air. *Fuel Processing Technology*, *90*(5), 677–685. https://doi.org/10.1016/j.fuproc.2008.12.007

Dutta, A., & Phillips, S. D. (2009). *Thermochemical ethanol via direct gasification and mixed alcohol synthesis of lignocellulosic biomass* (tech. rep.). National Renewable Energy Lab.(NREL), Golden, CO (United States).

Lopes, F. V. S., Grande, C. A., Ribeiro, A. M., Loureiro, J. M., Evaggelos, O., Nikolakis, V., & Rodrigues, A. E. (2009). Adsorption of h2, co2, ch4, co, n2 and h2o in activated carbon and zeolite for hydrogen production. *Separation Science and Technology*, *44*(5), 1045–1073. https://doi.org/10.1080/01496390902729130

Chen, W.-H., Lin, M.-R., Lu, J.-J., Chao, Y., & Leu, T.-S. (2010). Thermodynamic analysis of hydrogen production from methane via autothermal reforming and partial oxidation followed by water gas shift reaction. *International Journal of Hydrogen Energy*, *35*(21), 11787–11797. https://doi.org/10.1016/j.ijhydene.2010.08.126

Roh, H.-S., Lee, D. K., Koo, K. Y., Jung, U. H., & Yoon, W. L. (2010). Natural gas steam reforming for hydrogen production over metal monolith catalyst with efficient heat-transfer. *International Journal of Hydrogen Energy*, *35*(4), 1613–1619. https://doi.org/10.1016/j.ijhydene.2009.12.051

Bartholomew, C. H., & Farrauto, R. J. (2011). *Fundamentals of industrial catalytic processes*. John Wiley & Sons.

Brebbia, C. A. (2011). *The sustainable world* (Vol. 142). WIT Press.

Cengel, Y. A., Boles, M. A., & Kanoglu, M. (2011). *Thermodynamics: An engineering approach* (Vol. 5). McGraw-hill New York.

Martín, M., & Grossmann, I. E. (2011). Energy optimization of hydrogen production from lignocellulosic biomass. *Computers & Chemical Engineering*, *35*(9), 1798–1806. https://doi.org/10.1016/j.compchemeng.2011.03.002

Massé, D., Gilbert, Y., Savoie, P., Bélanger, G., Parent, G., & Babineau, D. (2011). Methane yield from switchgrass and reed canarygrass grown in eastern canada. *Bioresource Technology*, *102*(22), 10286–10292. https://doi.org/10.1016/j.biortech.2011.08.087

Reimert, R., Marschner, F., Renner, H.-J., Boll, W., Supp, E., Brejc, M., Liebner, W., & Schaub, G. (2011). Gas production, 2. processes. *Ullmann's encyclopedia of industrial chemistry*.

Villanueva Perales, A., Reyes Valle, C., Ollero, P., & Gómez-Barea, A. (2011). Technoeconomic assessment of ethanol production via thermochemical conversion of biomass by entrained flow gasification. *Energy*, *36*(7), 4097–4108. https://doi.org/10.1016/j.energy.2011.04.037

Brown, D., Shi, J., & Li, Y. (2012). Comparison of solid-state to liquid anaerobic digestion of lignocellulosic feedstocks for biogas production.

Bioresource Technology, *124*, 379–386. https://doi.org/10.1016/j.biortech.2012.08.051

Frigon, J.-C., Mehta, P., & Guiot, S. R. (2012). Impact of mechanical, chemical and enzymatic pre-treatments on the methane yield from the anaerobic digestion of switchgrass. *Biomass and Bioenergy*, *36*, 1–11. https://doi.org/10.1016/j.biombioe.2011.02.013

Monti, A. (2012). *Switchgrass: A valuable biomass crop for energy*. Springer Science & Business Media.

Morgan, E. R. (2013). *Techno-economic feasibility study of ammonia plants powered by offshore wind*. University of Massachusetts Amherst.

Reyes Valle, C., Villanueva Perales, A., Vidal-Barrero, F., & Gómez-Barea, A. (2013). Techno-economic assessment of biomass-to-ethanol by indirect fluidized bed gasification: Impact of reforming technologies and comparison with entrained flow gasification. *Applied Energy*, *109*, 254–266. https://doi.org/10.1016/j.apenergy.2013.04.024

Sadhukhan, J., Ng, K. S., & Hernandez, E. M. (2014). *Biorefineries and chemical processes: Design, integration and sustainability analysis*. John Wiley & Sons.

Sinnott, R. (2014). *Chemical engineering design* (Vol. 6). Elsevier.

Shah, Y. T. (2015). *Energy and fuel systems integration*. CRC Press.

Air Products. (2016). Prism® membrane systems for ammonia plants... tell me more. Retrieved May 7, 2017, from https://www.airproducts.no/wp-content/uploads/2016/06/Membrane-Systems-For-Ammonia-Plants.pdf

Almena, A., & Martín, M. (2016). Technoeconomic analysis of the production of epichlorohydrin from glycerol. *Industrial & Engineering Chemistry Research*, *55*(12), 3226–3238. https://doi.org/10.1021/acs.iecr.5b02555

León, E., & Martín, M. (2016). Optimal production of power in a combined cycle from manure based biogas. *Energy Conversion and Management*, *114*, 89–99. https://doi.org/10.1016/j.enconman.2016.02.002

Membrane Technology and Research. (2016). Hydrogen recovery from ammonia plant purge gas. Retrieved May 7, 2017, from www.mtrinc.com/pdf_print/refinery_and_syngas/MTR_Brochure_Hydrogen_Recovery_from_Ammonia_Plant_Purge_Gas.pdf

Doddapaneni, T. R. K. C., Praveenkumar, R., Tolvanen, H., Rintala, J., & Konttinen, J. (2018). Techno-economic evaluation of integrating torrefaction with anaerobic digestion. *Applied Energy*, *213*, 272–284. https://doi.org/10.1016/j.apenergy.2018.01.045

Paul, S., & Dutta, A. (2018). Challenges and opportunities of lignocellulosic biomass for anaerobic digestion. *Resources, Conservation and Recycling*, *130*, 164–174. https://doi.org/10.1016/j.resconrec.2017.12.005

Sánchez, A., & Martín, M. (2018). Optimal renewable production of ammonia from water and air. *Journal of Cleaner Production*, *178*, 325–342. https://doi.org/10.1016/j.jclepro.2017.12.279

Taifouris, M. R., & Martín, M. (2018). Multiscale scheme for the optimal use of residues for the production of biogas across castile and leon. *Journal of Cleaner Production*, *185*, 239–251. https://doi.org/10.1016/j.jclepro.2018.03.018

Green, D. W., & Southard, M. Z. (2019). *Perry's chemical engineers' handbook*. McGraw-Hill Education.

C

APPENDIX C: SUPPLEMENTARY INFORMATION OF CHAPTER 6

c.1 membrane reactor model

In the decomposition membrane reactor, ammonia is converted to nitrogen and hydrogen, according to the reaction C.1, and this component passes through the membrane and is separated in situ.

$$NH_3 \rightarrow \frac{1}{2}N_2 + \frac{3}{2}H_2 \tag{C.1}$$

The catalyst used in the decomposition section is Ni/Al_2O_3 and a Pd-Ag supported membrane is installed to recover the hydrogen from the decomposition of ammonia. The kinetics expression of the ammonia decomposition reaction is adapted from the Temkin expression (Dyson & Simon, 1968; Kim et al., 2018):

$$r = 3k_{reac}\left[K^2 a_N \left(\frac{a_{H_2}^{3\alpha}}{p^2}\right) - \left(\frac{a_{NH_3}^2}{a_{H_2}^3}\right)^{(1-\alpha)}\right]\Phi\Omega \tag{C.2}$$

where k_{reac} is the kinetic constant of the reaction, K_p is the equilibrium constant, a_i is the activity of component i, Φ is the effectiveness factor, Ω is the catalytic activity and α is a kinetic parameter. To describe the permeation through the membrane, the following expression C.3 is introduced using the gradient of pressure on both sides of the membrane as driving force (Abashar, 2018).

$$J_{H_2} = \frac{28.84 \cdot 10^{-5}}{\delta} \exp\left(\frac{-1888.381}{T}\right)\left(\sqrt{P_{H_2}^{p}} - \sqrt{P_{H_2}^{p}}\right) \tag{C.3}$$

where δ is the thickness of the membrane, T is the reactor temperature and $p_{H_2}^{i}$ is the partial pressure of hydrogen on both sides of the membrane. The total pressure in the permeate side is set at 1 bar. In this work, an isotherm plug flow reactor is assumed to model this unit. The set of differential

equations to describe the mass balances is as follows (C.4- C.6) (Sánchez & Martín, 2018):

$$\frac{dF_{NH_3}}{dz} = -Ar_{NH_3} \tag{C.4}$$

$$\frac{dF_{N_2}}{dz} = \frac{1}{2}Ar_{NH_3} \tag{C.5}$$

$$\frac{dF_{H_2}}{dz} = \frac{3}{2}Ar_{NH_3} - L_{cir}r^{p}_{H_2} \tag{C.6}$$

where A is the cross-sectional area of the reactor, L_{cir} is the cross-sectional length of the membrane and F_i is the molar flowrate of component i. The activity of each species is computed using the expression C.7.

$$a_i = y_i \gamma_i P \tag{C.7}$$

The fugacity coefficients (γ_i) are calculated as a function of pressure and temperature using the correlations proposed by Dyson and Simon (1968). The kinetic constant (k_{reac}) is expressed as a function of the temperature according to equation C.8.

$$k_{reac} = 8.849 \cdot 10^{14}\exp\left(\frac{-40765}{1.988T}\right) \tag{C.8}$$

The thermodynamic equilibrium constant is also computed as a function of the temperature of the reactor (Martín, 2016):

$$log_{10}(K_p) = \frac{2250.322}{T} - 0.85430 - 1.51049\log_{10}(T) \tag{C.9}$$

$$-2.58987 \cdot 10^{-4}T + 1.48961 \cdot 10^{-7}T^2$$

The initial velocity is an input parameter of this model. Based on this value, the cross-sectional area is calculated:

$$Q^0 = \frac{F_t^0}{\rho^0} \tag{C.10}$$

$$\rho^0 = \frac{P^0}{RT} \tag{C.11}$$

$$A = \frac{Q^0}{v^0} \tag{C.12}$$

Finally, to compute the pressure drop in the catalytic side, the Ergun equation is introduced:

$$\frac{dP}{dz} = -150\frac{(1-\epsilon)^2 \mu v}{\epsilon^3 d_p^2} - 1.75\frac{(1-\epsilon)\rho v^2}{\epsilon^3 d_p} \tag{C.13}$$

Table C.1: Summary of the operating cost calculations (Sinnott, 2014)

Variable Costs	
Raw materials	from flowsheet optimization
Miscellaneous materials	10% of maintenance
Utilities	from flowsheet optimization
Fixed Costs	
Maintenance	5% of fixed capital
Labour	estimated from correlations
Laboratory	20% of labour
Supervision	20% of labour
Plant Overheads	50% of labour
Capital charges	10% of fixed capital
Insurance	1% of fixed capital
Taxes	2% of fixed capital

c.2 cost estimation procedure

With the results obtained in the optimization procedure, the economic analysis is carried out. First, the capital cost is estimated based on the factorial method proposed by Sinnott (2014). The first step consists of calculating the total purchase cost of the major equipment of the facility. For the basic units such as heat exchangers or compressors, the cost is estimated based on the correlations proposed by Almena and Martín (2016). In the ammonia decomposition reactor, the price of Ni/Al2O3 is set at 30€/kg (Jess & Wasserscheid, 2020) and the Pd/Ag supported membrane at 1500€/m^2 (De Falco et al., 2011). The costs of the gas and steam turbines are calculated as a function of the produced power (Caputo et al., 2005). The SCR treatment consists of a fixed bed reactor with a GHSV equal to 8000 h^{-1} (Yu et al., 2010). The catalyst is Pd/Al_2O_3 with a price equal to 2501 €/kg (Pappaterra et al., 2021). With the total purchase cost of the major equipment, a detailed factorial estimation is applied to calculate the

fixed capital of the facility including piping, instrumentation, erection, etc. For a facility working with fluids, the total factor is equal to 1.45.

Operating cost is a sum of two terms: the fixed and variable costs (see Table **??**). The fixed part includes maintenance, labor, capital charges, etc. and is estimated as a percentage of different items, as shown in Table **??**. Labor costs are computed using the correlation proposed by Green and Southard (2019). On the variable side, the costs of the raw materials and utilities are included. The price of ammonia is fixed to 0.5 €/kg (Pfromm, 2017), however, the influence of the variation of this parameter is assessed in this work based on the different ammonia production technologies. The price of argon, nitrogen and hydrogen are set at 0.037 €/kg (Elishav et al., 2017), 0.5 €/kg (Downie, 2007) and 4 €/kg (Matzen et al., 2015), respectively. Finally, the cost of utilities are equal to 2.20 €/GJ for steam (Yang & You, 2018), 4.58 €/kt (Yang & You, 2018) for cooling water and 0.0787 €/kWh (Statista, 2018) for electricity.

C.3 operating conditions of the gas turbine

The inlet and outlet compositions of the combustion chamber in the gas turbine are presented here in terms of molar fraction.

Table C.2: Molar fraction of the inlet/outlet streams in the gas turbine

		A	B	C	D	E	F	G	H	I
Inlet Composition	H_2O	0.0	0.0	0.0	0.0	0.0	0.0	0.0	0.0	0.0
	N_2	39.1	42.6	41.5	45.3	39.2	42.6	41.5	45.3	58.0
	O_2	10.5	11.5	10.6	11.6	10.5	11.5	10.6	11.6	14.9
	Ar	31.7	22.2	29.0	19.1	31.3	22.2	29.0	19.1	0.7
	H_2	5.6	7.1	5.7	7.2	5.7	7.1	5.7	7.2	7.9
	NH_3	13.1	16.6	13.2	16.8	13.3	16.6	13.2	16.8	18.5
	NO_x	0.0	0.0	0.0	0.0	0.0	0.0	0.0	0.0	0.0
Outlet Composition	H_2O	20.5	21.8	20.6	22.0	20.5	21.8	20.6	22.0	28.6
	N_2	44.5	48.4	46.9	51.0	44.6	48.4	46.9	51.0	64.9
	O_2	0.0	0.0	0.0	0.0	0.0	0.0	0.0	0.0	0.0
	Ar	30.9	21.1	28.2	18.1	30.5	21.1	28.2	18.1	0.7
	H_2	4.1	8.7	4.2	8.8	4.4	8.7	4.2	8.8	5.8
	NH_3	0.0	0.0	0.0	0.0	0.0	0.0	0.0	0.0	0.0
	NO_x	0.0	0.0	0.0	0.0	0.0	0.0	0.0	0.0	0.0

c.4 operating conditions of the rankine cycle

In this section, the input/output pressures and temperatures of the different sections of the steam turbine are collected. This information complements that provided in Table 6.1 of the manuscript.

Table C.3: Operating conditions of the different sections of the steam turbine

		A	B	C	D	E	F	G	H	I
High Pressure	Inlet P (bar)	125.0	125.0	125.0	125.0	125.0	125.0	125.0	125.0	125.0
	Inlet T (K)	782.0	991.6	785.9	785.9	782.7	991.6	785.9	782.7	785.9
	Outlet P (bar)	35.0	35.0	35.0	35.0	35.0	35.0	35.0	35.0	35.0
	Outlet T (K)	564.0	745.7	567.1	567.1	564.0	745.7	567.1	564.0	567.1
Intermediate Pressure	Inlet P (bar)	35.0	35.0	35.0	35.0	35.0	35.0	35.0	35.0	35.0
	Inlet T (K)	564.0	745.7	567.1	567.1	564.0	745.7	567.1	564.0	567.1
	Outlet P (bar)	5.0	9.5	9.5	9.5	5.0	9.5	9.5	5.0	9.5
	Outlet T (K)	425.5	621.6	451.3	451.3	425.5	621.6	451.3	425.5	451.3
Low Pressure	Inlet P (bar)	5.0	9.5	9.5	9.5	5.0	9.5	9.5	5.0	9.5
	Inlet T (K)	425.5	621.6	451.3	451.3	425.5	621.6	451.3	425.5	451.3
	Outlet P (bar)	0.1	0.1	0.1	0.1	0.1	0.1	0.1	0.1	0.1
	Outlet T (K)	399.1	569.3	401.8	401.8	399.1	569.3	401.8	399.1	401.8

bibliography

Dyson, D. C., & Simon, J. M. (1968). Kinetic expression with diffusion correction for ammonia synthesis on industrial catalyst. *Industrial & Engineering Chemistry Fundamentals*, *7*(4), 605–610. https://doi.org/10.1021/i160028a013

Caputo, A. C., Palumbo, M., Pelagagge, P. M., & Scacchia, F. (2005). Economics of biomass energy utilization in combustion and gasification plants: Effects of logistic variables. *Biomass and Bioenergy*, *28*(1), 35–51. https://doi.org/10.1016/j.biombioe.2004.04.009

Downie, N. A. (2007). *Industrial gases*. Springer Science & Business Media.

Yu, Q., Kong, F., Li, L., Wu, G., & Guan, N. (2010). Fast catalytic reduction of nox by h2 over pd-based catalysts. *Chinese Journal of Catalysis*, *31*(3), 261–263. https://doi.org/10.1016/S1872-2067(09)60045-0

De Falco, M., Marrelli, L., & Iaquaniello, G. (2011). Membrane reactors for hydrogen production processes.

Sinnott, R. (2014). *Chemical engineering design* (Vol. 6). Elsevier.

Matzen, M., Alhajji, M., & Demirel, Y. (2015). Chemical storage of wind energy by renewable methanol production: Feasibility analysis using a multi-criteria decision matrix. *Energy*, *93*, 343–353. https://doi.org/10.1016/j.energy.2015.09.043

Almena, A., & Martín, M. (2016). Technoeconomic analysis of the production of epichlorohydrin from glycerol. *Industrial & Engineering Chemistry Research*, *55*(12), 3226–3238. https://doi.org/10.1021/acs.iecr.5b02555

Martín, M. M. (2016). *Industrial chemical process analysis and design*. Elsevier.

Elishav, O., Tvil, G., Mosevitzky, B., Lewin, D., Shter, G. E., & Grader, G. S. (2017). The nitrogen economy: The feasibility of using nitrogen-based alternative fuels. *Energy Procedia*, *135*, 3–13. https://doi.org/10.1016/j.egypro.2017.09.482

Pfromm, P. H. (2017). Towards sustainable agriculture: Fossil-free ammonia. *Journal of Renewable and Sustainable Energy*, *9*(3), 034702. https://doi.org/10.1063/1.4985090

Abashar, M. (2018). Ultra-clean hydrogen production by ammonia decomposition. *Journal of King Saud University - Engineering Sciences*, *30*(1), 2–11. https://doi.org/10.1016/j.jksues.2016.01.002

Kim, S., Song, J., & Lim, H. (2018). Conceptual feasibility studies of a co x-free hydrogen production from ammonia decomposition in a membrane reactor for pem fuel cells. *Korean Journal of Chemical Engineering*, *35*(7), 1509–1516.

Sánchez, A., & Martín, M. (2018). Optimal renewable production of ammonia from water and air. *Journal of Cleaner Production*, *178*, 325–342. https://doi.org/10.1016/j.jclepro.2017.12.279

Statista. (2018). Prices of electricity for the industry in spain from 2008 to 2017 (in euro cents per kilowatt hour). Retrieved May 7, 2020, from https://www.statista.com/statistics/595813/electricity-industry-price-spain/

Yang, M., & You, F. (2018). Modular methanol manufacturing from shale gas: Techno-economic and environmental analyses of conventional large-scale production versus small-scale distributed, modular processing. *AIChE Journal*, *64*(2), 495–510. https://doi.org/10.1002/aic.15958

Green, D. W., & Southard, M. Z. (2019). *Perry's chemical engineers' handbook*. McGraw-Hill Education.

Jess, A., & Wasserscheid, P. (2020). *Chemical technology: From principles to products*. John Wiley & Sons.

Pappaterra, M., Xu, P., van der Meer, W., Faria, J. A., & Fernandez Rivas, D. (2021). Cavitation intensifying bags improve ultrasonic advanced oxidation with pd/al2o3 catalyst. *Ultrasonics Sonochemistry*, *70*, 105324. https://doi.org/10.1016/j.ultsonch.2020.105324

D

APPENDIX D: SUPPLEMENTARY INFORMATION OF CHAPTER 7

d.1 modelling issues

Some modelling details are included in this section to deepen the information given in the main text.

d.1.1 *Vapour-Liquid Equilibrium (VLE) in urea synthesis*

Vapour-Liquid Equilibrium (VLE) is used in the urea synthesis section to describe the performance of the system in spite of the conditions are supercritical (Piotrowski et al., 1998; Zhang et al., 2005; Meessen, 2014). The equation to implement this VLE are as eq.D.1. The main equation that describes the VLE is (Piotrowski et al., 1998):

$$P y_i \phi_i = f_i^0 x_i \gamma_i \tag{D.1}$$

where P is the total pressure, y_i is the molar fraction per component i, ϕ_i is the fugacity coefficient, f_i^0 is the fugacity, x_i is the liquid molar fraction, and γ_i is the activity coefficient.

For the most ideal case, the following assumptions hold:

$$\phi_i = 1 \quad ; \quad \gamma_i = 1 \; ; \quad f_i^0 = P_i^0 \tag{D.2}$$

where P_i^0 is the vapour pressure for each component. The vapour pressures for the species involved in the system were computed using Antoine equations from the literature (Sinnott, 2014) or fitting experimental data or from rigorous simulation to an equation in the same form that the Antoine equation.

Therefore, the VLE equation takes the following form:

$$K = \frac{y_i}{x_i} = \frac{P_i^0}{P} \tag{D.3}$$

where K is the VL equilibrium constant. This relationship is joined to the mass balances to compute the vapour and liquid fraction depends on the operating conditions (pressure, temperature and composition).

$$F = L + V \tag{D.4}$$

$$Fz_i = Lx_i + Vy_i \tag{D.5}$$

$$\sum_i y_i = 1 \tag{D.6}$$

$$\sum_i x_i = 1 \tag{D.7}$$

d.1.2 *Urea Reactor*

The urea reactor is modelled based on the correlation for the conversion presented in eq.7.3. The mass and energy balances that with the conversion modelled this unit are as follow (based on reactions eq.7.1-7.2):

$$fc^{out}_{\text{Carbamate}} = fc^{in}_{CO_2} + fc^{in}_{\text{Carbamate}} - \left(fc^{out}_{\text{Urea}} - fc^{in}_{\text{Urea}}\right) \tag{D.8}$$

$$fc^{out}_{\text{Urea}} = X\left(fc^{in}_{\text{Urea}} + fc^{in}_{CO_2} + fc^{in}_{\text{Carbamate}}\right) \tag{D.9}$$

$$fc^{out}_{H_2O} = fc^{in}_{H_2O} + \left(fc^{out}_{\text{Urea}} - fc^{in}_{\text{Urea}}\right) \tag{D.10}$$

$$fc^{out}_{NH_3} = fc^{in}_{NH_3} - 2fc^{in}_{CO_2} \tag{D.11}$$

$$\sum_i fc^{in}_i h_i + \Delta H_{reac1} fc^{in}_{CO_2} = \sum_i fc^{out}_i h_i + \Delta H_{reac2}\left(fc^{out}_{\text{Urea}} - fc^{in}_{\text{Urea}}\right) \tag{D.12}$$

where fc_i is the molar flow per component i, X is the conversion of the second urea reaction, h_i is the enthalpy for each component, ΔH_{reac1} is the heat of reaction for the first urea reaction (-159 kJ/kmol of carbamate), and ΔH_{reac2} is the heat of reaction for the second urea reaction (31.4 kJ/kmol of urea).

d.1.3 *Urea stripper*

The urea stripper is modelled based on a surrogate model that compute

the liquid yield for each specie involved (see section 7.3.1.2 in the main text). The yields are calculated with the following equations:

—

$$
\begin{aligned}
R_{\text{Urea}} = {} & -518.215028200482 - 0.284950725834463P \\
& + 2.95476072757198T + 1.80131942015766 \frac{Q}{U} \\
& - 217.645482840702 \frac{U}{\text{NH}_3} + 144.322612155776 \frac{U}{\text{H}_2\text{O}} \\
& - 23.4997562338943 \frac{U}{\text{CO}} - 18.6482710341462 \frac{U}{\text{CO}_{2in}} \\
& - 0.000625187050143106P^2 - 0.00358947384425963T^2 \\
& - 0.00159480074579542 \left(\frac{Q}{U}\right)^2 - 43.6916212334017 \left(\frac{U}{\text{NH}_3}\right)^2 \\
& + 0.000883129727668199PT + 0.123968437321115P \frac{U}{\text{NH}_3} \\
& - 0.00357027639984928T \frac{Q}{U} + 0.508817144975195T \frac{U}{\text{NH}_3} \\
& - 0.33575712211849T \frac{U}{\text{H}_2\text{O}} + 0.0559892272569286T \frac{U}{\text{CO}_2} \\
& + 0.04413818470365 54T \frac{U}{\text{CO}_{2in}} \\
& - 0.280993398880857 \frac{Q}{U} \frac{U}{\text{H}_2\text{O}} \\
& + 23.8479014645434 \frac{U}{\text{NH}_3} \frac{U}{\text{H}_2\text{O}}
\end{aligned}
\tag{D.13}
$$

$$
\begin{aligned}
R_{\text{NH}_3} = {} & 363.421008053347 + 1.02283207923837P \\
& - 1.68658498168 83T - 1.42886596581643 \frac{Q}{U} \\
& + 1.89678432914491 \frac{U}{\text{NH}_3} - 173.541185790149 \frac{U}{\text{H}_2\text{O}} \\
& + 2.13291242076277 \frac{U}{\text{CO}_2} + 80.6413084986838 \frac{U}{\text{CO}_{2in}} \\
& + 0.001911154989014 65T^2 + 61.2980445456304 \left(\frac{U}{\text{H}_2\text{O}}\right)^2 \\
& - 0.00195433955988442PT - 0.00213399216789 27P \frac{Q}{U}
\end{aligned}
\tag{D.14}
$$

$$- 0.192442657544106P \frac{U}{H_2O} + 0.122348143496973P \frac{U}{CO_{2in}}$$

$$+ 0.003698275284848878T \frac{Q}{U} + 0.2805083921937047 \frac{U}{H_2O}$$

$$- 0.170925026271615T \frac{U}{CO_{2in}} + 0.247064145229264 \frac{Q}{U} \frac{U}{H_2O}$$

$$- 0.183712997636469 \frac{Q}{U} \frac{U}{CO_{2in}}$$

$$- 14.8974151859256 \frac{U}{H_2O} \frac{U}{CO_{2in}}$$

$$
\begin{aligned}
R_{CO_2} = {} & -24.6820636152254 + 0.222380812733441P \\
& + 0.177196824184314T - 0.0141855991019543 \frac{Q}{U} \\
& - 59.1242003629388 \frac{U}{NH_3} - 15.4525458485839 \frac{U}{H_2O} \\
& - 9.03647006314354 \frac{U}{CO_2} - 0.854264129513543 \frac{U}{CO_{2in}} \\
& - 0.000219146793932474T^2 + 19.3825862013371 \left(\frac{U}{CO_2}\right)^2 \\
& - 3.05683312723582 \left(\frac{U}{CO_{2in}}\right)^2 - 0.00046188239342957 7PT \\
& - 0.0880742901622562P \frac{U}{H_2O} + 0.0539665938430128P \frac{U}{CO_2} \\
& + 0.0559983482606198P \frac{U}{CO_{2in}} + 0.124371549409968T \frac{U}{NH_3} \\
& + 0.0896301599303116 \frac{Q}{U} \frac{U}{NH_3} \\
& - 0.0612997203229086 \frac{Q}{U} \frac{U}{CO_{2in}} \\
& + 5.12639174859366 \frac{U}{CO_2} \frac{U}{CO_{2in}}
\end{aligned}
\tag{D.15}
$$

$$
\begin{aligned}
R_{H_2O} = {} & 415.656146379107 - 1.40951201488907P \\
& - 0.806726309737707T + 3.5522739160318 \frac{Q}{U} \\
& - 268.1249557368 \frac{U}{NH_3} + 237.93460634717 \frac{U}{H_2O} \\
& + 7.65189731042131 \frac{U}{CO_2} + 8.66265209434843 \frac{U}{CO_{2in}} \\
& + 0.00317313232439402PT - 0.00764567556523745T \frac{Q}{U} \\
& + 0.669844549831203T \frac{U}{NH_3} - 0.548994997976013T \frac{U}{H_2O} \\
& \frac{Q}{U} \frac{U}{}
\end{aligned}
\tag{D.16}
$$

$$-0.680329653858759 \quad \overline{\overline{U}} \quad \overline{\overline{H_2O}}$$

$$\overline{}$$

$$
\begin{aligned}
T_{\text{liquid}}^{out} &= 180.074822916299 - 1.29647750539426P \\
&+ 0.537306963368549T + 3.30253577898588 \frac{Q}{U} \\
&+ 635.378632760966 \frac{U}{NH_3} - 1.4887132676095 \frac{U}{H_2O} \\
&- 9.08774528270758 \frac{U}{CO_2} - 211.483091694472 \frac{U}{CO_{2in}} \\
&+ 0.00243789836116356PT + 0.440497648476484P \frac{U}{NH_3} \\
&- 0.00460841793394988T \frac{Q}{U} - 1.42689653407166T \frac{U}{NH_3} \\
&+ 0.502790812183236T \frac{U}{CO_{2in}} + 1.45095567309948 \frac{Q}{U} \frac{U}{H_2O} \\
&- 0.0256532339924944 \frac{Q}{U} \frac{U}{CO_2}
\end{aligned}
\tag{D.17}
$$

$$
\begin{aligned}
T_{\text{gas}}^{out} &= 56.6201838288691 + 0.0000150301463124054P \\
&+ 0.864243130532875T - 1.71036819173564 \frac{Q}{U} \\
&+ 93.7078150219783 \frac{U}{NH_3} - 111.514440146262 \frac{U}{H_2O} \\
&- 2.25327122002595 \frac{U}{CO} + 6.51724015832229 \frac{U}{CO} \\
&+ 0.00398684220198224T^2 \frac{Q}{U} - 0.207737654112389T^{2in} \frac{U}{NH_3} \\
&+ 0.219116462750508T \frac{U}{H_2O} + 0.76534937413338 \frac{Q}{U} \frac{U}{NH_3} \\
&+ 0.509782670009266 \frac{Q}{U} \frac{U}{H_2O} \\
&- 0.165851633915337 \frac{Q}{U} \frac{U}{CO_{2in}}
\end{aligned}
\tag{D.18}
$$

The surrogate models have been developed for the following operating ranges:

$$140 \le P(\text{bar}) \le 200 \tag{D.19}$$

$$443 \le T(\text{K}) \le 493 \tag{D.20}$$

$$20 \le \frac{Q}{U} \quad \frac{\text{MJ}}{\text{kmol}} \le 50 \tag{D.21}$$

$$0.2 \le \frac{U}{\text{NH}_3} \quad \frac{\text{kmol}}{\text{kmol}} \le 0.5 \tag{D.22}$$

$$0.4 \le \frac{U}{\text{H}_2\text{O}} \quad \frac{\text{kmol}}{\text{kmol}} \le 0.7 \tag{D.23}$$

$$0.9 \le \frac{U}{\text{CO}_2} \quad \frac{\text{kmol}}{\text{kmol}} \le 1.4 \tag{D.24}$$

$$0.9 \le \frac{U}{\text{CO}_{2in}} \quad \frac{\text{kmol}}{\text{kmol}} \le 1.4 \tag{D.25}$$

The total mass balances in the stripper unit are as follow:

$$fc^{liq}_{\text{Urea}} = \frac{R_{\text{Urea}}}{100} fc^{in}_{\text{Urea}} \tag{D.26}$$

$$fc^{in}_{\text{Urea}} = fc^{liq}_{\text{Urea}} + fc^{gas}_{\text{Urea}} \tag{D.27}$$

$$fc^{liq}_{\text{NH}_3} = \frac{R_{\text{NH}_3}}{100} fc^{in}_{\text{NH}_3} + 2fc^{in}_{\text{Carbamate}} \tag{D.28}$$

$$fc^{in}_{\text{NH}_3} + 2fc^{in}_{\text{Carbamate}} = fc^{liq}_{\text{NH}_3} + fc^{gas}_{\text{NH}_3} \tag{D.29}$$

$$fc^{liq}_{\text{CO}_2} = \frac{R_{\text{CO}_2}}{100} fc^{in}_{\text{CO}_2} + fc^{in}_{\text{Carbamate}_2} \tag{D.30}$$

$$fc^{in}_{\text{CO}_2} + fc^{in}_{\text{Carbamate}} = fc^{liq}_{\text{CO}_2} + fc^{gas}_{\text{CO}_2} \tag{D.31}$$

$$fc^{liq}_{\text{H}_2\text{O}} = \frac{R_{\text{H}_2\text{O}}}{100} fc^{in}_{\text{H}_2\text{O}} \tag{D.32}$$

$$fc^{in}_{\text{H}_2\text{O}} = fc^{liq}_{\text{H}_2\text{O}} + fc^{gas}_{\text{H}_2\text{O}} \tag{D.33}$$

d.1.4 *Urea Condenser*

In the urea condenser, the reaction that forms ammonium carbamate takes place. The reaction is controlled by the heat removed in this unit. The

conversion is limited by the heat balances in the urea reactor. The following mass and energy balances described the urea condenser performance:

$$fc_{\text{Urea}}^{in/mix2} = fc_{\text{Urea}}^{out} \tag{D.34}$$

$$fc_{H_2O}^{in/mix1} + fc_{H_2O}^{in/mix2} = fc_{H_2O}^{out} \tag{D.35}$$

$$fc_{CO_2}^{in/mix1} + fc_{CO_2}^{in/mix2} = fc_{\text{Car}}^{out} \tag{D.36}$$

$$fc_{NH_3}^{in/mix1} + fc_{NH_3}^{in/mix2} = fc_{\text{NHbamate}}^{out} + fc_{CO_2} + 2fc_{\text{Carbamate}}^{out} \tag{D.37}$$

$$\sum_i fc_i^{in/mix1} h_i^{in/mix1} + \sum_i fc_i^{in/mix2} h_i^{in/mix2} = \sum_i fc_i^{out} h_i^{out} + \Delta H_{reac1} fc_{\text{Carbamate}}^{out} \tag{D.38}$$

d.1.5 *First DMC reactor*

The first DMC reactor (Reac2) is modelled considering a conversion equal to 100% and an isotherm and isobaric system. The pressure is fixed to 20 bar and the temperature to 423K (de Groot et al., 2014). The mass and energy balances are as follows:

$$fc_{NH_3}^{in} + fc_{\text{Urea}}^{out} = fc_{NH_3}^{out} \tag{D.39}$$

$$fc_{\text{Urea}}^{in} = fc_{\text{MC}}^{out} \tag{D.40}$$

$$fc_{\text{MeOH}}^{in} - fc_{\text{Urea}}^{out} = fc_{\text{MeOH}}^{out} \tag{D.41}$$

$$fc_{H_2O}^{in} = fc_{H_2O}^{out} \tag{D.42}$$

$$Q_{reac2} = \sum_i fc_i^{out} h_i^{out} + \Delta H_{reac3} fc_{\text{MC}}^{out} - \sum_i fc_i^{in} h_i^{in} \tag{D.43}$$

$$\sum_i fc_i^{out} h_i^{out} + \Delta H_{reac3} fc_{\text{MC}}^{out} - \sum_i fc_i^{in} h_i^{in} \tag{D.44}$$

where ΔH_{reac3} is the heat of reaction for the methyl carbamate (MC) formation (-10310 kJ/kmol MC).

d.1.6 *Second DMC Reactor*

The second DMC reactor is modelled based on the experimental yield from the equation eq.7.10. In this reactor, two reactions are involved: the DMC formation and the NMMC formation. The NNMC reaction is

undesirable. The yields with the mass and energy balances determined the reactor performance:

$$fc^{out}_{DMC} = fc^{in}_{DMC} + Y_{DMC} fc^{in}_{MC} \quad (D.45)$$

$$fc^{out}_{NMMC} = fc^{in}_{NMMC} + Y_{NMMC} fc^{in}_{MC} \quad (D.46)$$

$$fc^{out}_{NH_3} = fc^{in}_{NH_3} + Y_{DMC} fc^{in}_{MC} + Y_{NMMC} fc^{in}_{MC} \quad (D.47)$$

$$fc^{in}_{CO_2} = Y_{NMMC} fc^{in}_{MC} \quad (D.48)$$

$$fc^{out}_{MeOH} = fc^{in}_{MeOH} - Y_{DMC} fc^{in}_{MC} \quad (D.49)$$

$$fc^{out}_{MC} = fc^{in}_{MC} - Y_{DMC} fc^{in}_{MC} - 2\, Y_{NMMC} fc^{in}_{MC} \quad (D.50)$$

$$fc^{in}_{H_2O} = fc^{out}_{H_2O} \quad (D.51)$$

d.1.7 *Distillation column: Fenske-Underwood-Gilliland (FUG) method*

To describe the operation of distillation columns, the shortcut method of Fenske-Underwood-Gilliland (FUG) is used (Geankopolis, 2005). The fed stream enters in the column as saturated liquid and, therefore, at its bubble temperature. The distillate and the bottom stream are also saturated liquid. The following equations hold in a saturated liquid:

$$\sum_i K_i x_i = 1 \quad (D.52)$$

$$K_i = \frac{P^i_{vap}}{P} \quad (D.53)$$

In the saturated vapour streams hold the following relation:

$$\sum_i \frac{y_i}{K_i} = 1 \quad (D.54)$$

The minimum number of stages is calculated using the Fenske equation:

$$N_m = \frac{\log\left(\frac{x_{LD,D}}{x_{HD,D}} \cdot \frac{x_{HW,W}}{x_{LW,W}}\right)}{\log\left(\alpha_{L,av}\right)} \quad (D.55)$$

Where LD is the key light component in the distillate, HD is the key heavy component in the distillate, HW is the key heavy component in the bottom and LW is the light key component in the bottom. $\alpha_{L,av}$ is the average value of the relative volatility calculated as follow:

$$\alpha_{L,av} = \sqrt{\alpha_{LD}\, \alpha_{LW}} \quad (D.56)$$

The minimum reflux ratio is calculated with the two Underwood equations:

$$1 - q = \sum_i \frac{\alpha_i x_{iF}}{\alpha_i - \theta} \tag{D.57}$$

$$R_m + 1 = \sum_i \frac{\alpha_i x_{iD}}{\alpha_i - \theta} \tag{D.58}$$

Where q is the feed condition, θ is the underwood parameter and the volatility is calculated based on the average temperature in the column. To calculate the real reflux ratio, the following rule of thumb is used (Couper et al., 2005):

$$R = 1.2R_m \tag{D.59}$$

The number of stages is calculated, for instance, with the empirical correlation of Erbar and Maddox (Geankopolis, 2005).

nomenclature

fc	Molar flow
f_i^0	Fugacity
F	Feed molar flow
h	Enthalpy
K	Equilibrium constant
L	Liquid molar flow
N_m	Minimum number of stages
P	Pressure
p_i^0	Vapor pressure
q	Feed condition
R_i	Stripper yield
R_m	Minimum reflux ratio
R	Reflux ratio
V	Molar vapor flow
x_i	Molar fraction
X	Conversion
y_i	Molar fraction
Y_i	Reaction yield in Reac3

z_i Feed molar flow

ϕ_i Fugacity coefficient

γ_i Activity coefficient

ΔH Heat of reaction

α Volatility

bibliography

Piotrowski, J., Kozak, R., & Kujawska, M. (1998). Thermodynamic model of chemical and phase equilibrium in the urea synthesis process. *Chemical Engineering Science*, *53*(1), 183–186. https://doi.org/10.1016/S0009-2509(97)00271-6

Couper, J. R., Penney, W. R., Fair, J. R., & Walas, S. M. (2005). *Chemical process equipment: Selection and design*. Gulf Professional Publishing.

Geankopolis, C. J. (2005). *Transport processes and unit operations*. Prentice-Hall.

Zhang, X., Zhang, S., Yao, P., & Yuan, Y. (2005). Modeling and simulation of high-pressure urea synthesis loop. *Computers & Chemical Engineering*, *29*(5), 983–992. https://doi.org/10.1016/j.compchemeng.2004.10.004

de Groot, F. F., Lammerink, R., Heidemann, C., van der Werff, M. P., Garcia, T. C., Van Der Ham, L., & van den Berg, H. (2014). The industrial production of dimethyl carbonate from methanol and carbon dioxide. *Chemical engineering transactions*, *39*, 1561–1566. https://doi.org/10.3303/CET1439261

Meessen, J. (2014). Urea synthesis. *Chemie Ingenieur Technik*, *86*(12), 2180–2189. https://doi.org/10.1002/cite.201400064

Sinnott, R. (2014). *Chemical engineering design* (Vol. 6). Elsevier.

E

APPENDIX E: SUPPLEMENTARY INFORMATION OF CHAPTER 8

e.1 modeling parameters

Parameter $\rho_{i,j}$

Process	Resource	Yield (kW/kW or kg/kW)
PV	Solar production	-1
PV	Power	1
WT	Wind production	-1
WT	Power	1
EL	Water	-4.48263608e-5
EL	H_2	5.12612885e-6
EL	O_2	4.12998750e-5
EL	Power	-1
AS (Distillation)	Air	-1.21682195e-3
AS (Distillation)	N_2	9.06520023e-4
AS (Distillation)	O_2	2.94648710e-4
AS (Distillation)	Power	-1
AS (PSA)	Air	-3.80407220e-3
AS (PSA)	N_2	8.99459261e-4
AS (PSA)	Power	-1
AS (Membrane)	Air	-2.49476770e-3
AS (Membrane)	N_2	6.59397172e-4
AS (Membrane)	Power	-1
DM	H_2	-3.29085182e-3
DM	CO_2	-2.41201209e-2

DM	DME	1.26069367e-2
DM	Power	-1
CH	H_2	-1.26639437e-3
CH	CO_2	-6.96619528e-3
CH	CH_4	2.74830155e-3
CH	Power	1
ME	H_2	-2.68866125e-4
ME	CO_2	-1.97126317e-3
ME	MeOH	1.43374179e-3
ME	Power	-1
NH	H_2	-7.90036943e-5
NH	N_2	-8.52418111e-4
NH	NH_3	3.19096482e-4
NH	Power	-1
GT	Power	1
GT	CH_4	-3.0644e-5

Maximum process capacity C_i^{max}

Process	C_i^{max} (kW)
PV	5% of total area of the sub-region
WT	5% of total area of the sub-region
EL	495110.46
ASU (distillation)	25250.41
ASU (PSA)	5541.84
ASU (Membrane)	4813.67
DM	625.37
CH	1461.63
ME	487.21
NH	32125.08
GT	200000.00

Maxi um storage capacity $\overline{C}_i^{max}$

Resource	$\overline{C}_i^{max}$ (kg)
N_2	50000
H_2	50000
DME	5e6
CH_4	5e6
MeOH	5e6
NH_3	5e6

Transportation cost Γ_{jd}

Mode of transportation	($/km t)
Truck (liquids)	0.034
Truck (gases)	0.035
Train	0.025
CH_4 pipeline	0.021

Process capital cost δ_i, γ_i

Resource	δ_i (MM$)	γ_i
PV	0.01	1.69650602e-4
WT	0.01	5.33333333e-4
EL	18.61182898	0.00208263
ASU (distillation)	1.26183952e1	4.56887900e-3
ASU (PSA)	3.00697981e-1	6.06296004e-3
ASU (Membrane)	1.89366268e-1	8.33085712e-3
DM	2.09620435e1	7.03176498e-1
CH	3.06292520e-1	2.22428080e-2
ME	5.61429083	5.61666595e-3
NH	1.14249824e1	9.25374128e-3
GT	0	0.882e-3

Storage capital cost α_i, β_i

Resource	α_i (MM$)	β_i
N_2	0.079	9.036e-5
H_2	0.079	0.00125695
DME	0.079	1.6866e-7
CH_4	0.079	0.000172256
MeOH	0.079	1.427e-7
NH_3	0.079	1.856e-7

Piece-wise linear approximation $\hat{P}_{iml}$, $\hat{J}_{iml}$

Resource	(kW)	(MM$/year)
PV	0	0
PV	5e6	0
WT	0	0
WT	5e6	0
EL	0	0.320
EL	16503.68	-0.177
EL	990220.91	-25.321
ASU (distillation)	0	0.374
ASU (distillation)	1010.02	0.236
ASU (distillation)	4040.07	-0.187
ASU (distillation)	60600.98	-10.433
ASU (PSA)	0	0.218
ASU (PSA)	46.18	0.235
ASU (PSA)	277.09	0.328
ASU (PSA)	738.91	0.403
ASU (PSA)	2124.37	0.510

ASU (PSA)	11083.68	0.761
ASU (Membrane)	0	0.161
ASU (Membrane)	17.19	0.174
ASU (Membrane)	103.15	0.246
ASU (Membrane)	343.83	0.318
ASU (Membrane)	1375.33	0.431
ASU (Membrane)	8595.84	0.665
DM	0	0.395
DM	15.63	1.298
DM	1876.11	119.926
CH	0	0.236
CH	48.72	0.284
CH	194.88	0.390
CH	487.21	0.488
CH	3897.68	0.917
ME	0	1.577
ME	474.21	2.190
ME	33194.96	32.229
NH	0	0.163
NH	53.54	0.179
NH	1070.84	0.329
NH	5354.18	0.410
NH	10708.36	0.410
NH	85666.88	-0.567
GT	0	0
GT	200000	2.6

F

APPENDIX F: SUPPLEMENTARY INFORMATION OF CHAPTER 9

f.1 model formulation

f.1.1 *Mass balances*

The general equation for the mass balance of the different processes for a given facility is as follows:

$$\overline{Q}_{jht} = \overline{Q}_{jht-1} + B_{jht} - S_{jht} + \sum_i \rho_{ij} P_{iht} + \qquad \forall j, h, t \in \overline{T}_h \tag{F.1}$$

In this equation, the amount of resource j stored at time t of season h is represented by $\overline{Q}_{rjht}$. B_{rjht} and S_{rjht} denote the amounts of consumed or discharged resource at each location. The amount of reference resource produced or consumed is denoted by P_{riht}. Finally, the parameter ρ_{ij} denotes the conversion factor between resource j and the reference resource of process i.

The production of the reference resource in each process i is limited by the plant capacity:

$$P_{iht} = \eta_{iht} C_i \quad \forall i \in \{PV, WT\}, h, t \in T_h \tag{F.2}$$

$$P_{iht} \leq \eta_{iht} C_i \quad \forall i \in I \setminus \{PV, WT\}, h, t \in T_h \tag{F.3}$$

The plant capacity is denoted by C_i. The parameter η_{ikt} is used to represent the time-varying process capacity, for instance, wind or solar generation, where the capacity is not only a function of the plant size but also of the wind/solar availability. This parameter is calculated using the solar irradiance/ambient (Sánchez & Martín, 2018a; Hlal et al., 2019) temperature or the wind velocity (de la Cruz & Martín, 2016) for each time period and location.

The storage capacity $\overline{C}_j$ is an upper bound for the inventory level in those resources with associated storage.

$$\overline{Q}_{jht} \leq \overline{C}_j \quad \forall j \in \hat{S}, h, t \in \overline{T}_h \tag{F.4}$$

$$\overline{Q}_{jht} = 0 \quad \forall j \notin \hat{S}, h, t \in \overline{T}_h \tag{F.5}$$

The set $\hat{S}$ consists of all resources that can be stored (battery power, hydrogen and methane/ammonia in this particular analyzed facilities).

For the specific case of the battery, a minimum level is imposed to avoid problems in the performance and durability of the unit. In this case, a 15% of the capacity is set as minimum level of storage.

$$\overline{Q}_{jht} \geq 0.15\overline{C}_j \qquad \forall j \in \{\text{Battery}\}, h, t \in \overline{T_h} \tag{F.6}$$

There is a maximum value for the capacity ($C_i^{\max}$)for each process involved in the network. The binary variable x_i indicates whether process i is selected in the process network.

$$C_i \leq C_i^{\max} x_i \qquad \forall i \tag{F.7}$$

In this particular case, the process capacities of the battery charge and discharge must be the same (both are determined by the battery specifications):

$$C_{BC} = C_{BD} \tag{F.8}$$

Similarly, there is also a maximum value for the storage capacity denoted by $\overline{C}_j^{\max}$. The binary variable $\overline{x}_j$ is equal to 1 if a storage facility for product j is selected.

$$\overline{C}_j \leq \overline{C}_j^{\max} \overline{x}_j \qquad \forall j \tag{F.9}$$

The resource availability is also limited for those resources used as raw materials in the proposed network (indicated by the set $\hat{B}$).

$$B_{jht} \leq B_{jht}^{\max} \qquad \forall j \in \hat{B}, h, t \in \overline{T_h} \tag{F.10}$$

$$B_{jht} = 0 \qquad \forall j \notin \hat{B}, h, t \in \overline{T_h} \tag{F.11}$$

Some resources (includes in the set $\tilde{B}$) could have a maximum annual consumption not to be exceeded. In this particular case, biomass is included in this set with a maximum availability depending of the region.

$$\sum_h \sum_t B_{jht} = \overline{B}_j^{max} \qquad \forall j \in \tilde{B} \tag{F.12}$$

Some resources of the network do not have an associated demand (i.e., they are not in the set $\hat{J}$). Therefore, the outlet flowrate of these species is fixed to 0:

$$S_{jht} = 0 \qquad \forall j \notin \hat{J}, h, t \in \overline{T_h} \tag{F.13}$$

F.1.2 *Mode-based operation*

Each of the processes involved can operate in four different operating modes: off, startup, on and shutdown. The binary variable y_{imht} indicates if a process i is operating in a certain mode m. If a process is selected, one of the operating modes must be assigned:

$$\sum_{m \in M_i} y_{imht} = x_i \quad \forall i, h, t \in \overline{T_h} \tag{F.14}$$

The set M_i denotes the set of allowed operating modes for process i.

In the particular case of the battery charge and discharge processes, only one of the two could be in on mode at the same time (it is not possible to charge and discharge the battery simultaneously):

$$\sum_{i \in \{BC,BD\}} y_{imht} \leq 1 \quad \forall m \in \{ON\}, h, t \in \overline{T_h} \tag{F.15}$$

The amount of reference resource consumed or produced by process i, P_{iht}, must be produced or consumed in one of the different operating modes. The variable P_{imht} denotes the quantity of reference resource consumed or produced in mode m:

$$P_{iht} = \sum_{m \in M_i} \overline{P}_{imht} \quad \forall i, h, t \in \overline{T_h} \tag{F.16}$$

A maximum ($\overline{P}_{im}^{max}$) and minimum ($\overline{P}_{im}^{min}$) value for the amount of reference resource produced or consumed for each mode is introduced:

$$\overline{P}_{im}^{min} y_{imht} \leq \overline{P}_{imht} \leq \overline{P}_{im}^{max} y_{imht} \quad \forall i, m \in M_i, h, t \in \overline{T_h} \tag{F.17}$$

The following constraints are related to the transition between operating modes for the same process unit. The maximum rate of change within a mode is limited by an upper bound ($\overline{\Delta}_{im}^{max}$):

$$\begin{aligned} &-\overline{\Delta}_{im}^{max} - \overline{M}(2 - y_{imht} - y_{imh,t-1}) \leq \overline{P}_{imht} - \overline{P}_{imh,t-1} \\ &\leq \overline{\Delta}_{im}^{max} + \overline{M}(2 - y_{imht} - y_{imh,t-1}) \quad \forall i, m \in M_i, h, t \in \overline{T_h} \end{aligned} \tag{F.18}$$

The binary variable $z_{im'mht}$ is introduced to indicate that process i switches from mode m to mode m' at time t. The possible transitions are defined by the following equation:

$$\sum_{m' \in TR_{im}} z_{im'mh,t-1} - \sum_{m' \in TR_{im}} z_{imm'h,t-1} = y_{imht} - y_{imh,t-1} \tag{F.19}$$

$$\forall i, m \in M_i, h, t \in T_h$$

where the set TR_i includes all the possible mode-to-mode transitions for the process i, and $\overline{TR}_{im} = \{m' : (m', m) \in TR_i\}$ and $TR_{im} = \{m' : (m, m') \in TR_i\}$.

A process i must remain for a certain minimum number of time periods ($\theta_{imm'}$) in an operating mode m before switching to another mode m':

$$y_{im'ht} \geq \sum_{k=1}^{\theta_{im}^{m'}} z_{imm'h,t-k} \qquad \forall i, (m, m') \in TR_i, h, t \in \overline{T}_h \tag{F.20}$$

Finally, predefined sequences of modes (from mode m to mode m' to mode m'') for a process i can be defined, establishing a fixed stay time for each of the modes involved in the sequence.

$$z_{imm'h,t-\bar{\theta}_{imm'm''}} = z_{im'm''ht} \qquad \forall i, (m, m', m'') \in SQ_i, h, t \in \overline{T}_h \tag{F.21}$$

The set SQ_i denotes the set of predefined sequences for process i and $\theta_{imm'm''}$ is the fixed stay time in mode m' in the predefined sequence.

F.1.3 *Continuity constraints*

Continuity constraints ensure the feasible transition between seasons. A cyclic schedule is imposed; therefore, the initial mode of a season must be the same as the final one.

$$y_{imh,0} = y_{imh,|\overline{T}_h|} \qquad \forall i, m \in M_i, h \tag{F.22}$$

$$z_{imm'ht} = z_{imm'h,t+|\overline{T}_h|} \qquad \forall i, (m, m') \in TR_i, h, -\theta_i^{\max} + 1 \leq t \leq -1 \tag{F.23}$$

For the transitions between seasons, the state at the final time of one season and at the initial time of the next season must be the same.

$$y_{imh,|\overline{T}_h|} = y_{im,h+1,0} \qquad \forall i, m \in M_i, h \in H \setminus |H| \tag{F.24}$$

$$z_{imm'h,t+|\overline{T}_h|} = z_{imm',h+1,t} \qquad \forall i, (m, m') \in TR_i, h \in H \setminus |H|, -\theta_i^{\max} + 1 \leq t \leq -1. \tag{F.25}$$

The storage is allowed between seasons. The following equations determine the change in inventory levels from one season to the next.

$$\hat{Q}_{jh} = \overline{Q}_{jh,|\overline{T}_h|} - \overline{Q}_{jh,0} \qquad \forall j \in \hat{S}, h \tag{F.26}$$

$$\overline{Q}_{jh,0} + n_h \hat{Q}_{jh} = \overline{Q}_{j,h+1,0} \qquad \forall j, h \in H \setminus |H| \tag{F.27}$$

$$\overline{Q}_{j,|H|,0} + n_{|H|}\hat{Q}_{j,|H|} = \overline{Q_{j,1,0}} \qquad \forall j \tag{F.28}$$

f.1.4 *Objective function*

The objective of this work is to meet a given power demand $D_{power,h,t}$ using the different proposed technologies (including storage).

$$S_{jht} = D_{jht} \quad \forall j \in \hat{J}, h, t \in \overline{T_h} \tag{F.29}$$

The goal is to minimize the following objective function:

$$OC = \sum_i \sum_{m \in M_i} \sum_h \sum_t J_{imht} + \sum_i \sigma_i (\delta_i x_i + \gamma_i C_i) + \sum_{j \in \hat{S}} (\alpha_j \bar{x}_j + \beta_j C_j) + \sum_i \sum_j \sum_h \sum_t \xi_{ij} \rho_{ij} P_{iht} + \sum_h \sum_t \phi_{CO_2} B_{CO_2,ht} \tag{F.30}$$

which comprises the costs of production and storage.

The piece-wise linear approximation used to compute the first term of equation (F.30), J_{imht}, is as follows:

$$P_{imht} = \sum_{l \in L_i} (\lambda_{imhtl} (\hat{P}_{im,l-1} - \hat{P}_{im,l}) + \hat{P}_{iml} \omega_{imhtl}) \quad \forall i, m \in M_{ri}, h, t \tag{F.31}$$

$$J_{imht} = \sum_{l \in L_i} (\lambda_{imhtl} (\hat{J}_{im,l-1} - \hat{J}_{im,l}) + \hat{J}_{iml} \omega_{imhtl}) \quad \forall i, m \in M_{ri}, h, t \tag{F.32}$$

$$\lambda_{imhtl} \leq \omega_{imhtl} \quad \forall i, m \in M_i, h, t, l \in L_i \tag{F.33}$$

$$\sum_{l \in L_i} \omega_{iktl} = y_{ikt} \quad \forall i, m \in M_i, h, t \tag{F.34}$$

f.2 modeling parameters

The values for the parameters in the biomass process changes between the different regions according to the biomass selected following the procedure explained in the manuscript. In this section, the biomass parameters for the province of Almeria are presented as example. The sources from the different data are:

1. **Wind Turbines (WT):** de la Cruz and Martín (2016).
2. **Photovoltaic (PV):** Sánchez and Martín (2018a) and Hlal et al. (2019).
3. **Biomass gasifier/gas turbine (BIO)** León and Martín (2016) and Sánchez et al. (2019).
4. **Battery charge (BC):** Gonzalez-Castellanos et al. (2020).

5. **Battery discharge (BD)** Gonzalez-Castellanos et al. (2020).
6. **Water electrolysis (EL):** Sánchez and Martín (2018a).
7. **Hydrogen fuel cell (FC):** Kashefi Kaviani et al. (2009) and Palys and Daoutidis (2020).
8. **Methane production (CH):** Davis and Martín (2014).
9. **Methane gas turbine (CHGT):** León and Martín (2016).
10. **Air separation (AS):** Sánchez and Martín (2018b).
11. **Ammonia synthesis (NH):** Sánchez and Martín (2018a).
12. **Ammonia based power production (NHGT):** Sánchez et al. (2021).

Parameter $\rho_{i,j}$

Process	Resource	Yield (kW/kW or kg/kW)	Process	Resource	Yield (kW/kW or kg/kW)
PV	Solar	-1	CH	Power	-1
PV	Power	1	CH	H_2	-1.26639437E-01
WT	Wind	-1	CH	CO_2	-6.96619528E-01
WT	Power	1	CH	CH_4	2.40758605E-01
BIO	Power	1	CHGT	Power	1
BIO	Biomass	-1.317336E-04	CHGT	CH_4	-3.0644E-05
BIO	O_2	-1.541830E-05	CHGT	CO_2	8.4271E-05
BC	Power	-1	AS	Power	-1
BC	Battery power	0.97	AS	N_2	9.06520023E-04
BD	Power	1	NH	Power	-1
BD	Battery power	-1.1494	NH	H_2	-7.90036943E-05
EL	Power	-1	NH	N_2	-8.5248111E-04
EL	Water	-4.48263608E-05	NH	NH_3	3.19096482E-04
EL	H_2	5.12612885E-06	NHGT	Power	1
FC	Power	1	NHGT	N_2	8.1258E-04
FC	H_2	-5.5556E-06	NHGT	NH_3	-1.58344E-04

Maximum process capacity C_i^{max}

Process	C_i^{max} (area or kW)	Process	C_i^{max} (area or kW)
PV	5% of total area of the sub-region	FC	100000
WT	5% of total area of the sub-region	CH	14.6
BIO	68050	CHGT	200000
BC	3000	AS	60601
BD	3000	NH	85667
EL	495110.46	NHGT	200000

M ximum storage capacity $\overline{C}_i^{max}$

Resource	$\overline{C}_i^{max}$ (kJ or kg)
Battery	1.08e8
H_2	18000
N_2	650000
CH_4	2e7
NH_3	7e7

Storage capital cost α_i, β_i

Resource	α_i (MM$)	β_i (MM$/kJ or
Battery	0	0.07111
H_2	0.0001	500
N_2	0.0001	12.5
CH_4	0.0001	3.26
NH_3	0.0001	3.1

Process capital cost δ_i, γ_i

Resource	δ_i (MM$)	γ_i (MM$ / area or
PV	0.0001	1.60865979e-4
WT	0.0001	4.91e-4
BIO	1.495353e1	2.398390e-3
BC	0	0
BD	0	0
EL	17.72062345	0.00161936
FC	9.4377e-2	1.9593e-3
CH	0.0001	2.327738
CHGT	0.0001	0.882e-3
AS	1.26183952e1	4.568879e-3
NH	1.14249824e1	9.25374128e-3
NHGT	5.2878893e1	0.003882

Storage O&M cost ξ_j

Resource	ξ_j ($/kJ or $/kg)
Battery	83.3333 e-9
H_2	0
N_2	0
CH_4	0.225
NH_3	0

Piece-wise linear approximation $\hat{P}_{iml}$, $\hat{J}_{iml}$

Resource	(kW)	(MM$/year)	Resource	(kW)	(MM$/year)
PV	0	0	FC	100000	17.5
PV	5.00E+09	0	CH	0	0.25
WT	0	0	CH	3.41	0.44
WT	5.00E+09	0	CH	14.6163	0.66
BIO	0	0.2394925	CHGT	0	0
BIO	69762.321	3.66814385	CHGT	200000	2.6
BC	0	0	AS	0	0
BC	3500	0	AS	60600.98	-10.4334063
BD	0	0	NH	0	0.25
BD	3500	0	NH	5354.18	0.409
EL	0	0	NH	85666.88	0.351
EL	16503.9	-0.17744678	NHGT	0	0
EL	990220.9	-25.3211135	NHGT	600000	-114.0064
FC	0	0			

f.3 operating results

The scheduling results for the location of Asturias and Almeria are shown in this section complementing those presented in the manuscript. Therefore, Figure F.1 shows the scheduling results for scenario 1 in the province of Almeria, Figure F.2 the results for scenario 2 in the region of Asturias, and, finally, Figure F.3 the results for scenario 3 in the province of Almeria.

The process capacity results for all the studied regions have been included in Table F.1 for scenario 1. Table F.2 includes the capacities for scenario 2, in which biomass is introduced. Finally, Table F.3 presents the process capacities for scenario 3.

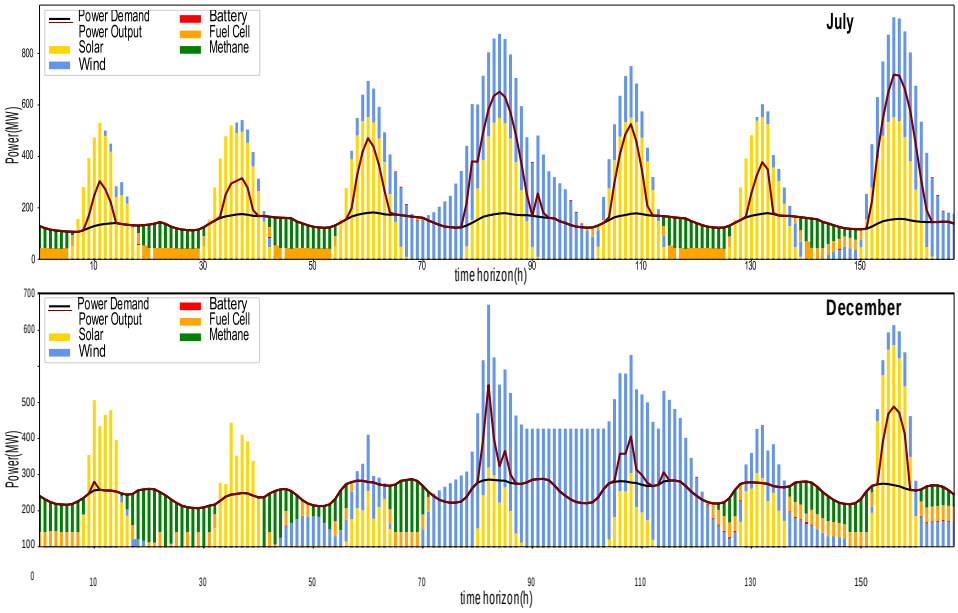

Figure F.1: Scheduling results for the Scenario 1 in Almeria

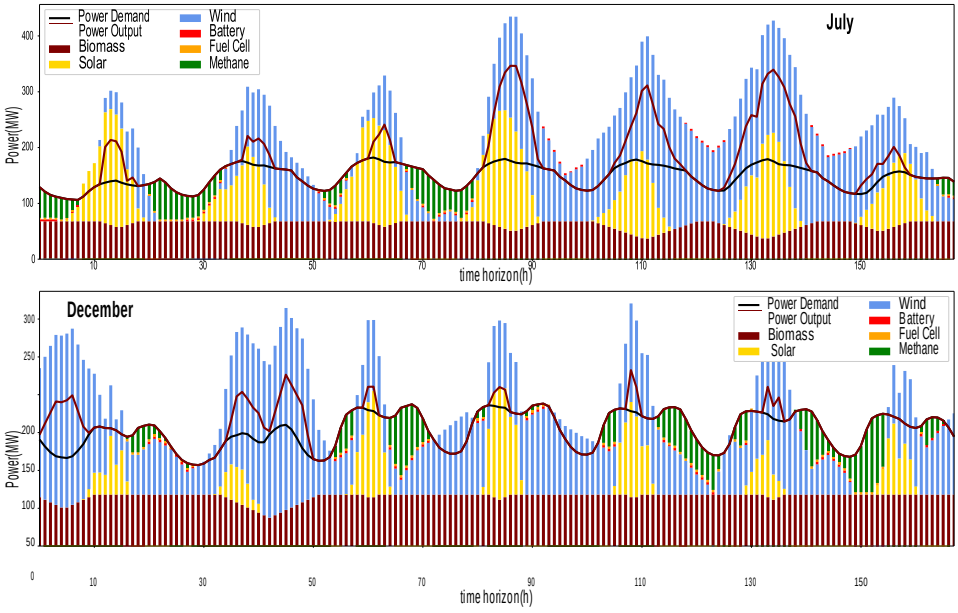

Figure F.2: Scheduling results for the Scenario 2 in Asturias

f.4 social index

First, in Table F.4, all required data to calculate the social index are presented. The data for this particular case study have been obtained from these sources:

1. **Lost installed capacity:** Wikipedia contributors (2021).

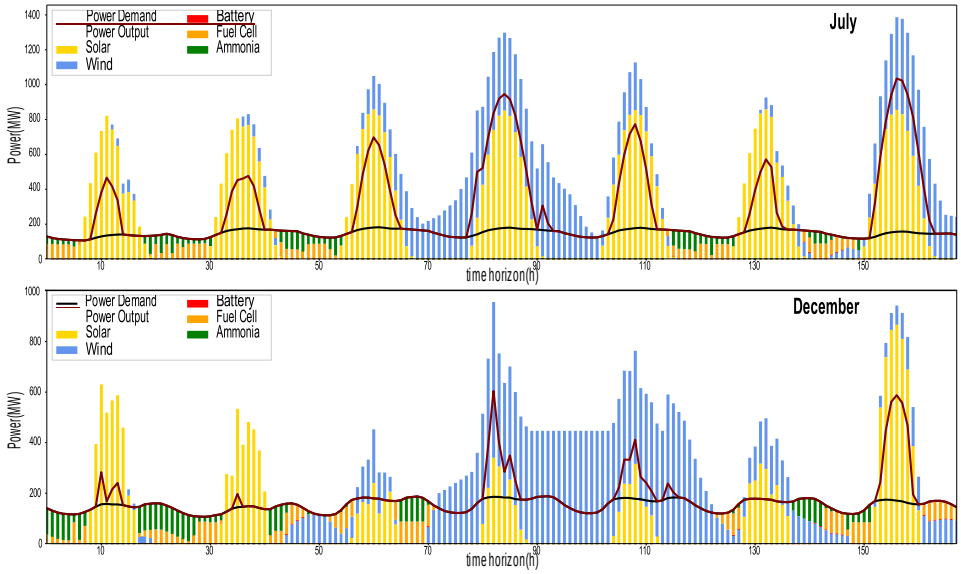

Figure F.3: Scheduling results for the Scenario 3 in Almeria

Table F.1: Process capacities for the scenario 1

	Asturias	Almeria	Badajoz	Teruel	Leon	Coruña	Cordoba	Ciudad Real	Sevilla	Zaragoza	Burgos	Navarra	Soria	Salamanca
Solar (ha)	193.18	282.87	525.90	281.30	378.33	188.53	667.06	508.22	333.82	232.04	298.11	216.15	288.94	392.37
Wind (ha)	107.55	98.22	134.35	96.88	115.08	101.89	165.09	134.66	117.36	102.55	101.04	106.59	102.70	117.46
Battery (MW)	3.00	3.00	3.00	3.00	3.00	3.00	3.00	3.00	3.00	3.00	3.00	3.00	3.00	3.00
Electrolysis (MW)	173.76	223.08	223.08	221.34	223.08	150.56	223.08	223.08	223.08	201.03	221.88	183.41	223.08	223.08
Fuel Cell (MW)	14.16	40.65	56.32	43.25	49.94	11.79	65.62	56.83	49.03	27.84	43.47	18.39	45.71	49.91
CH_4 production (kW)	6.64	7.90	8.67	7.89	8.45	5.71	8.75	8.81	8.34	7.48	8.04	6.82	8.14	8.68
CH_4 Turbine (MW)	174.55	148.06	144.17	146.43	139.74	177.00	134.87	140.44	140.50	159.50	146.21	170.31	143.97	147.36
Biomass (MW)	0	0	0	0	0	0	0	0	0	0	0	0	0	0
ASU (MW)	0	0	0	0	0	0	0	0	0	0	0	0	0	0
NH_3 (MW)	0	0	0	0	0	0	0	0	0	0	0	0	0	0
NH_3 power production (MW)	0	0	0	0	0	0	0	0	0	0	0	0	0	0

Table F.2: Process capacities for the scenario 2

	Asturias	Almeria	Badajoz	Teruel	Leon	Coruña	Cordoba	Ciudad Real	Sevilla	Zaragoza	Burgos	Navarra	Soria	Salamanca
Solar (ha)	103.59	158.03	254.72	155.79	240.79	104.68	259.25	277.53	188.44	129.70	195.67	126.04	187.44	285.63
Wind (ha)	59.09	48.17	37.71	47.45	57.05	56.32	28.62	46.94	40.38	54.83	58.90	61.78	57.73	58.36
Battery (MW)	3.00	3.00	3.00	3.00	3.00	3.00	3.00	3.00	3.00	3.00	3.00	3.00	3.00	3.00
Electrolysis (MW)	85.16	118.81	160.46	112.57	149.89	74.97	162.42	179.59	129.01	102.96	132.41	98.62	137.87	150.05
Fuel Cell (MW)	3.14	18.81	43.44	22.91	38.35	0.00	44.36	45.40	34.64	8.30	32.53	9.34	33.50	37.91
CH_4 production (kW)	3.10	3.69	3.57	3.62	4.54	2.64	3.04	4.25	3.24	3.57	4.46	3.40	4.42	4.00
CH_4 Turbine (MW)	117.52	101.85	95.43	98.72	98.44	120.75	88.08	98.98	86.84	111.00	104.26	118.06	103.30	106.48
Biomass (MW)	68.05	68.05	61.63	68.05	52.88	68.05	68.05	52.88	68.05	68.05	52.88	61.30	52.88	52.88
ASU (MW)	0	0	0	0	0	0	0	0	0	0	0	0	0	0
NH_3 (MW)	0	0	0	0	0	0	0	0	0	0	0	0	0	0
NH_3 power production (MW)	0	0	0	0	0	0	0	0	0	0	0	0	0	0

2. **Loss of jobs:** Ministerio para la Transicion Ecologica y el Reto Demografico (2021), El Comercio (2017), La Voz de Asturias (2018), Diario de Pontevedra (2019), Diario de Burgos (2017).

Table F.3: Process capacities for the scenario 3

	Asturias	Almeria	Badajoz	Teruel	Leon	Coruña	Cordoba	Ciudad Real	Sevilla	Zaragoza	Burgos	Navarra	Soria	Salamanca
Solar (ha)	317.52	438.76	702.26	454.45	520.08	320.60	817.36	659.43	442.59	414.62	511.56	338.84	395.48	684.40
Eolica (ha)	127.51	134.02	202.79	132.19	162.66	121.03	270.22	202.63	162.77	133.00	131.85	127.32	154.92	157.87
Bateria (MW)	3.00	3.00	3.00	3.00	3.00	3.00	3.00	3.00	3.00	3.00	3.00	3.00	3.00	3.00
Electrolisis (MW)	195.07	321.43	440.39	319.87	354.76	167.41	446.17	430.76	332.89	246.86	310.74	196.57	304.09	373.14
Fuel Cell (MW)	78.29	85.17	95.09	79.02	81.42	84.64	95.98	90.19	81.35	76.52	78.90	91.99	84.13	84.78
CH4 (kW)	0	0	0	0	0	0	0	0	0	0	0	0	0	0
CH4GT (MW)	0	0	0	0	0	0	0	0	0	0	0	0	0	0
Biomass (MW)	0	0	0	0	0	0	0	0	0	0	0	0	0	0
ASU (MW)	9.18	13.18	23.11	14.96	17.39	7.43	29.36	23.38	13.20	11.54	14.86	8.59	14.75	19.92
NH3 (MW)	10.94	17.13	27.82	17.54	21.13	9.14	30.02	27.12	17.98	14.12	17.22	10.65	17.61	22.27
NH3GT (MW)	111.27	104.39	106.26	111.52	109.12	106.07	105.37	107.93	109.03	111.68	111.64	97.58	108.16	113.35

3. **GDP:** Instituto Nacional de Estadistica (2020)
4. **Active population:** Instituto Nacional de Estadistica (2021c)
5. **Unemployment rate:** Instituto Nacional de Estadistica (2021d)
6. **Population decline:** Instituto Nacional de Estadistica (2021f)
7. **Aging index:** Instituto Nacional de Estadistica (2021a)
8. **Total population:** Instituto Nacional de Estadistica (2021e)
9. **Area:** Ministerio para la Transicion Ecologica y el Reto Demografico (2005)
10. **Youth migration:** Instituto Nacional de Estadistica (2021b)

With this data, the index is calculation following the instructions explained in the manuscript. The first three items, related to the energy transition, are collected in Table F.5. The last items of the index are included in Table F.6.

In the manuscript, the Figure with the trade off between economic and social issues is presented for scenario 1. In this supplementary information, the figures for scenario 2 (Figure F.4) and scenario 3 (Figure F.5) are included.

Table F.4: Data for the social index calculation

	Lost installed capacity (MW)	Loss of jobs	GDP (million €)	Active population	Unemployment rate (%)	Population decline (20 years) (%)	Aging index	Total population	Area(km2)	Youth migration (10 years)
Asturias	2162.7	2390	23258.67	447.4	14.09	-5.37	224.57	1018784	10604	-6.194
Teruel	1101	504	3367.24	61.6	10.6	-1.68	175.91	134176	14797	-1896
Leon	2025	960	10006.59	193.7	14.12	-9.10	241.01	456439	15570	-5850
Coruña	2895	436	26682.18	507.8	12.7	1.21	193.56	1121815	7950	-756
Almeria	1159	269	13979.83	358.8	17.14	40.47	84.56	727945	8775	-2835
Cordoba	324	129	14534.33	371.6	20.07	1.59	124.93	781451	13771	-10573
Badajoz	0	0	12423.26	308.9	21.47	1.55	129.37	672137	21766	-8080
Ciudad Real	0	0	10689.03	228	19.99	3.86	134.42	495045	19813	-9299
Sevilla	0	0	39535.35	922.4	23.81	12.41	95.38	1950219	14036	-7452
Zaragoza	0	0	27348.81	475.6	12.97	14.68	139.41	972528	17274	49
Burgos	466	440	10505.02	171.4	9.88	3.00	175.56	357650	14022	-3707
Navarra	0	0	20047.45	313.6	11.45	21.60	121.58	661197	9801	2525
Soria	0	0	2380.73	42.1	9.73	-2.23	194.89	88884	10303	-1056
Salamanca	0	0	7048.64	148.2	16.24	-5.86	215.81	329245	12349	-6097

Table F.5: First items of the social index related to the energy transition

	Loss of installed capacity in the region vs. total capacity lost			Loss of jobs related to energy transition vs. total employment in the region				Loss of installed capacity vs. total GDP of the region				
	Lost installed capacity (MW)	MW (%)	Index Contribution	Loss of jobs	Active Population	% lost	Index Contribution	Lost installed capacity (MW)	GDP (millions €)	MW/M€	multicolumn1c	Index Contribution
Asturias	2162.70	19.48	7.47	2390	447400	0.534	6.53	2162.7	23258.67	0.0930	2.84	
Teruel	1101.00	9.92	3.80	504	61600	0.818	10.00	1101	3367.24	0.3270	10.00	
Leon	2025.00	18.24	6.99	960	193700	0.496	6.06	2025	10006.59	0.2024	6.19	
Coruña	2895.00	26.08	10.00	436	507800	0.086	1.05	2895	26682.18	0.1085	3.32	
Almeria	1159.00	10.44	4.00	269	358800	0.075	0.92	1159	13979.83	0.0829	2.54	
Cordoba	324.00	2.92	1.12	129	371600	0.035	0.42	324	14534.33	0.0223	0.68	
Badajoz	0.00	0.00	0.00	0	308900	0.000	0.00	0	12423.26	0.0000	0.00	
Ciudad Real	0.00	0.00	0.00	0	228000	0.000	0.00	0	10689.03	0.0000	0.00	
Sevilla	0.00	0.00	0.00	0	922400	0.000	0.00	0	39535.35	0.0000	0.00	
Zaragoza	0.00	0.00	0.00	0	475600	0.000	0.00	0	27348.81	0.0000	0.00	
Burgos	466.00	4.20	1.61	440	171400	0.257	3.14	466	10505.02	0.0444	1.36	
Navarra	0.00	0.00	0.00	0	313600	0.000	0.00	0	20047.45	0.0000	0.00	
Soria	0.00	0.00	0.00	0	42100	0.000	0.00	0	2380.73	0.0000	0.00	
Salamanca	0.00	0.00	0.00	0	148200	0.000	0.00	0	7048.64	0.0000	0.00	

Table F.6: Last items of the social index related to the general social environment

	GDP of the region vs. total GDP of the country			Unemployment rate		Population decline over the last 20 years		Aging Index		Population density		Youth migration				GDP per capita	
	GDP (millions €)	% GDP	Index Contr.	Unempl. rate	Index Contr.	Population decline (%)	Index Contr.	Aging index	Index Contr.	Pop. density (/km²)	Index Contr.	Youth migration	Total population	Ratio	Index Contr.	GDP per cap. (€/person)	Index Contr.
Asturias	23258673	10.49	4.38	14.09	3.10	-5.37	9.25	224.57	8.95	96.08	3.40	-6194	1018784	-0.61	4.38	22829.84	8.95
Teruel	3367236	1.52	9.73	10.60	0.62	-1.68	8.50	175.91	5.84	9.07	9.97	-1896	134176	-1.41	7.94	25095.67	5.84
Leon	10006588	4.51	7.95	14.12	3.12	-9.10	10.00	241.01	10.00	29.32	8.44	-5850	456439	-1.28	7.36	21923.17	10.00
Coruña	26682181	12.03	3.46	12.70	2.11	1.21	7.92	193.56	6.97	141.11	0.00	-756	1121815	-0.07	1.99	23784.83	6.97
Almeria	13979829	6.30	6.88	17.14	5.26	40.47	0.00	84.56	0.00	82.96	4.39	-2835	727945	-0.39	3.41	19204.51	0.00
Cordoba	14534325	6.55	6.73	20.07	7.34	1.59	7.84	124.93	2.58	56.75	6.37	-10573	781451	-1.35	7.68	18599.15	2.58
Badajoz	12423261	5.60	7.30	21.47	8.34	1.55	7.85	129.37	2.86	30.88	8.32	-8080	672137	-1.20	7.01	18483.23	2.86
Ciudad Real	10689033	4.82	7.76	19.99	7.29	3.86	7.38	134.42	3.19	24.99	8.77	-9299	495045	-1.88	10.00	21592.04	3.19
Sevilla	39535345	17.82	0.00	23.81	10.00	12.41	5.66	95.38	0.69	138.94	0.16	-7452	1950219	-0.38	3.38	20272.26	0.69
Zaragoza	27348811	12.33	3.28	12.97	2.30	14.68	5.20	139.41	3.51	56.30	6.40	49	972528	0.01	1.67	28121.36	3.51
Burgos	10505020	4.74	7.81	9.88	0.11	3.00	7.56	175.56	5.82	25.51	8.73	-3707	357650	-1.04	6.28	29372.35	5.82
Navarra	20047454	9.04	5.25	11.45	1.22	21.60	3.81	121.58	2.37	67.46	5.56	2525	661197	0.38	0.00	30319.94	2.37
Soria	2380731	1.07	10.00	9.73	0.00	-2.23	8.61	194.89	7.05	8.63	10.00	-1056	88884	-1.19	6.95	26784.70	7.05
Salamanca	7048640	3.18	8.74	16.24	4.62	-5.86	9.35	215.81	8.39	26.66	8.64	-6097	329245	-1.85	9.88	21408.50	8.39

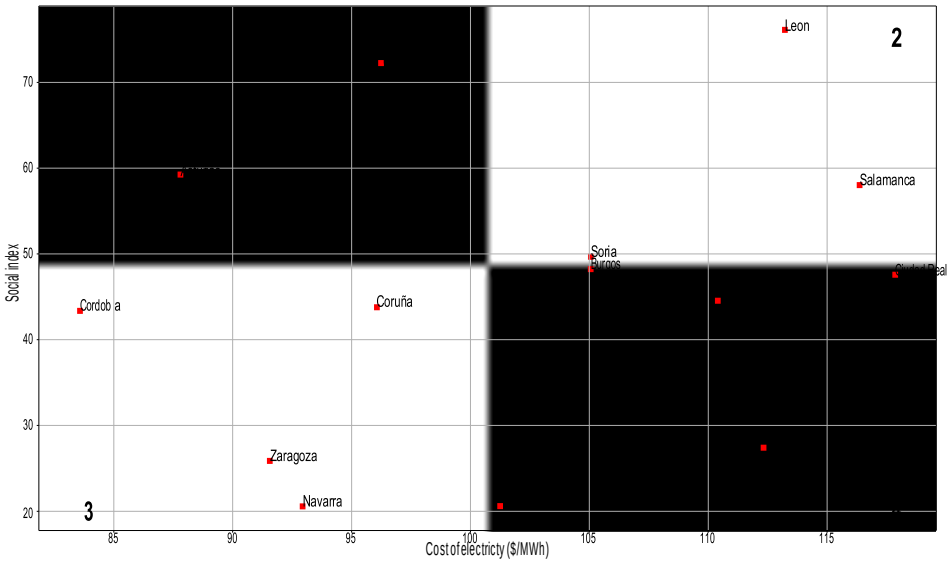

Figure F.4: Social and economic results for scenario 2

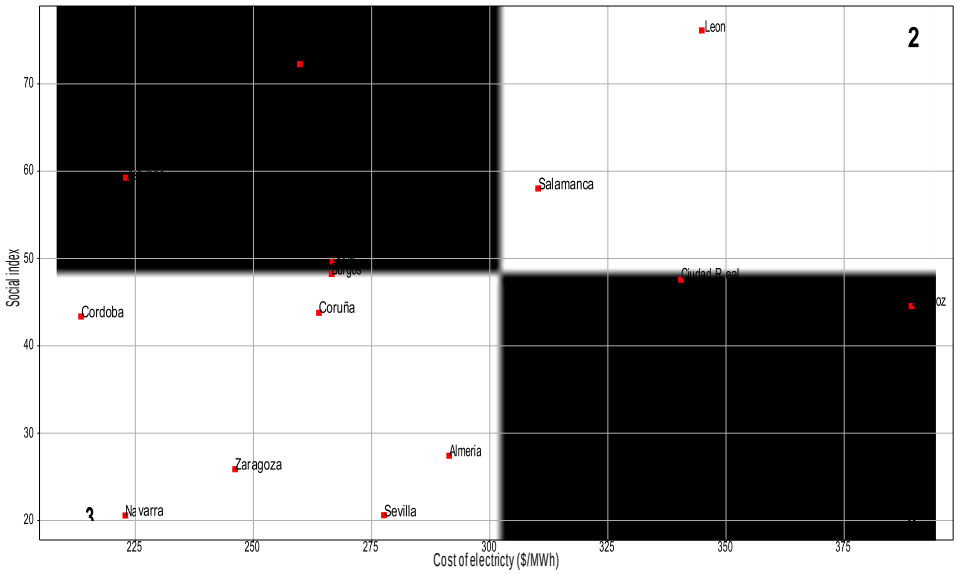

Figure F.5: Social and economic results for scenario 3

nomenclature

Indices / sets/ subsets

$\hat{B}$	resources use as raw material of the network
$\tilde{B}$	resources with a maximum annual availability
$h \in H$	seasons in the multiscale time representation
$i \in I$	processes evaluated in the power to fuel network
$j \in J$	resources involved in the network
$\hat{J}$	product with associated demand
$l \in L$	segments in operating cost
	piecewise-linear approximations
L_i	segments in piecewise-linear approximation
$m \in M$	operating modes for each of the process
M_i	operating modes for a process
$\hat{S}$	resources that could be stored
$t \in T$	time periods in the multiscale time representation
$\overline{T}_h$	time periods in season h
$\overline{TR}_{im}$	mode transitions to reach mode m
TR_{im}	mode transtions to progress from mode m
TR_i	predefined sequences of mode transitions

Parameters

B_{jht}^{max}	maximum resource that can be consumed
$\overline{B}_j^{max}$	maximum annual resource than can be consumed
C_i^{max}	maximum production capacity
$\overline{C}_i^{max}$	maximum storage capacity
$\overline{\mathcal{O}}_{im}^{max}$	maximum production in a given mode
$\underline{\mathcal{O}}_{im}^{min}$	minimum production in a given mode
$D_{power,h,t}$	power demand
$\hat{J}_{iml}$	operating cost for piecewise-linear approximation
$\overline{M}$	big-M parameter
n_h	number of repetition of the horizon
	scheduling for a season
$\hat{P}_{iml}$	production level for piecewise-linear approximation
ρ_{ij}	conversion factor of the different products
	with respect to the reference resource

η_{iht}	availability of production capacity for wind/solar
$\overline{\Lambda}_{im}^{\max}$	maximum rate of change
$\theta_{imm'}$	minimum stay time in a certain mode
$\theta_{imm'm''}$	fixed stay time for a predefined sequence
$\theta^{\max}$	stay time in a mode
σ_i	conversion factor between capital and operating cost for a process
δ_i	fixed capital cost coefficient
γ_i	unit capital cost coefficient
α_j	annualized fixed capital cost for storing
β_j	annualized unit capital cost for storing
Δt	length of one time period
λ_{imhtl}	coefficient for piecewise-linear approximation
ξ_j	O&M cost for storing
ϕ_{CO_2}	Cost of captured carbon dioxide

Variables

B_{jht}	amount of resource consumed
C_i	production capacity for different processes
$\overline{C}_j$	storage capacity for different resources
J_{imht}	process operating cost not related to capital cost
OC	Operating cost
P_{iht}	amount of reference resource produced
$\overline{P}_{imht}$	reference resource produced in certain mode
$\overline{Q}_{jht}$	inventory level
$\hat{Q}_{jh}$	net inventory in a season
S_{jht}	amount of resource release
x_i	binary variable to select process units
$\overline{x}_i$	binary variable to select storage units
y_{imht}	binary variable to select a mode for a specific process
$z_{imm'ht}$	binary variable for mode transitions
w_{rimhtl}	binary variable for piecewise-linear aproximation

bibliography

Ministerio para la Transicion Ecologica y el Reto Demografico. (2005). Anuario de estadistica forestal. distribucion de la superficie por provincias y comunidades autonomas. Retrieved June 7, 2020, from https://www.miteco.gob.es/es/biodiversidad/estadisticas/1_tcm30-132670.pdf

Kashefi Kaviani, A., Riahy, G., & Kouhsari, S. (2009). Optimal design of a reliable hydrogen-based stand-alone wind/pv generating system, considering component outages. *Renewable Energy*, *34*(11), 2380–2390. https://doi.org/10.1016/j.renene.2009.03.020

Davis, W., & Martín, M. (2014). Optimal year-round operation for methane production from co2 and water using wind and/or solar energy. *Journal of Cleaner Production*, *80*, 252–261. https://doi.org/10.1016/j.jclepro.2014.05.077

de la Cruz, V., & Martín, M. (2016). Characterization and optimal site matching of wind turbines: Effects on the economics of synthetic methane production. *Journal of Cleaner Production*, *133*, 1302–1311. https://doi.org/10.1016/j.jclepro.2016.06.019

León, E., & Martín, M. (2016). Optimal production of power in a combined cycle from manure based biogas. *Energy Conversion and Management*, *114*, 89–99. https://doi.org/10.1016/j.enconman.2016.02.002

Diario de Burgos. (2017). Garoña ha perdido 280 trabajadores. Retrieved August 8, 2020, from https://www.diariodeburgos.es/noticia/z56f23ec3-e4bb-fcd2-a06d88d0afe80e57/garona-ha-perdido-280-trabajadores

El Comercio. (2017). Cuatro térmicas y casi 600 empleos. Retrieved August 8, 2021, from https://www.elcomercio.es/economia/cuatro-termicas-empleos-20171029011631-ntvo.html

La Voz de Asturias. (2018). ¿peligran 60.000 empleos por la descarbonización en asturias? Retrieved August 8, 2021, from https://www.lavozdeasturias.es/noticia/asturias/2018/09/13/peligran-60000-empleos-descarbonizacion-asturias/000315368584976153221 54.htm

Sánchez, A., & Martín, M. (2018a). Optimal renewable production of ammonia from water and air. *Journal of Cleaner Production*, *178*, 325–342. https://doi.org/10.1016/j.jclepro.2017.12.279

Sánchez, A., & Martín, M. (2018b). Scale up and scale down issues of renewable ammonia plants: Towards modular design. *Sustainable Production and Consumption*, *16*, 176–192. https://doi.org/10.1016/j.spc.2018.08.001

Diario de Pontevedra. (2019). Endesa mantendrá los contratos de las auxiliares de as pontes al menos hasta final de año. Retrieved August

8, 2020, from https://www.diariodepontevedra.es/articulo/galicia/endesa-mantendra-contratos-auxiliares-pontes-menos-final-ano/20191014175955105 6305.html

Hlal, M. I., Ramachandaramurthy, V. K., Sarhan, A., Pouryekta, A., & Subramaniam, U. (2019). Optimum battery depth of discharge for off-grid solar pv/battery system. *Journal of Energy Storage*, *26*, 100999. https://doi.org/10.1016/j.est.2019.100999

Sánchez, A., Martín, M., & Vega, P. (2019). Biomass based sustainable ammonia production: Digestion vs gasification. *ACS Sustainable Chemistry & Engineering*, *7*(11), 9995–10007. https://doi.org/10.1021/acssuschemeng.9b01158

Gonzalez-Castellanos, A., Pozo, D., & Bischi, A. (2020). Detailed li-ion battery characterization model for economic operation. *International Journal of Electrical Power & Energy Systems*, *116*, 105561. https://doi.org/10.1016/j.ijepes.2019.105561

Instituto Nacional de Estadistica. (2020). Contabilidad regional de españa. resultados. Retrieved August 8, 2020, from https://www.ine.es/dyngs/INEbase/es/operacion.htm?c=Estadistica_C&cid=1254736167628&menu=resultados&idp=1254735576581

Palys, M. J., & Daoutidis, P. (2020). Using hydrogen and ammonia for renewable energy storage: A geographically comprehensive techno-economic study. *Computers & Chemical Engineering*, *136*, 106785. https://doi.org/10.1016/j.compchemeng.2020.106785

Instituto Nacional de Estadistica. (2021a). Demografia y poblacion. indicadores de estructura de poblacion. indice de envejecimiento por provincia. Retrieved August 8, 2020, from https://www.ine.es/jaxiT3/Tabla.htm?t=1489

Instituto Nacional de Estadistica. (2021b). Demografia y poblacion. migraciones interiores. saldo migratorio interprovincial por semestre, provincia, sexo y generación. Retrieved August 8, 2020, from https://www.ine.es/jaxiT3/Tabla.htm?t=24449&L=0

Instituto Nacional de Estadistica. (2021c). Encuesta de poblacion activa. resultados provinciales. activos por grupo de edad y provincia. Retrieved August 8, 2020, from https://www.ine.es/jaxiT3/Tabla.htm?t=3989&L=0

Instituto Nacional de Estadistica. (2021d). Encuesta de poblacion activa. resultados provinciales. tasas de actividad, paro y empleo por provincias. Retrieved August 8, 2020, from https://www.ine.es/jaxiT3/Tabla.htm?t=3996

Instituto Nacional de Estadistica. (2021e). Padron. poblacion por municipios. poblacion por provincias y sexo. Retrieved August 8, 2020, from https://www.ine.es/jaxiT3/Tabla.htm?t=2852

Instituto Nacional de Estadistica. (2021f). Padron. poblacion por municipios. variacion anual en la poblacion por provincias. Retrieved August 8, 2020, from https://www.ine.es/jaxiT3/Tabla.htm?t=2918&L=0

Ministerio para la Transicion Ecologica y el Reto Demografico. (2021). Transicion justa. Retrieved May 8, 2021, from https://www.miteco.gob.es/es/transicion-justa/default.aspx

Sánchez, A., Castellano, E., Martín, M., & Vega, P. (2021). Evaluating ammonia as green fuel for power generation: A thermo-chemical perspective. *Applied Energy*, *293*, 116956. https://doi.org/10.1016/j.apenergy.2021.116956

Wikipedia contributors. (2021). Anexo:centrales térmicas en españa [[Online; accessed 11-August-2021]]. https://es.wikipedia.org/wiki/Anexo:Centrales_t%C3%A9rmicas_en_Espa%C3%B1a